DISSERTATION

THE CONTRIBUTION OF $H_2^{18}O$, ^2HHO, AND Cl^- TO THE MODELING OF WATER MOVEMENT IN THE UNSATURATED ZONE

by

Abdel-Rahman M. Shurbaji

Hydrology Program, Geoscience Department

Submitted in partial fulfillment of the requirements

for the degree of Doctor of Philosophy

New Mexico Institute of Mining and Technology

Socorro, New Mexico

April, 1994

ABSTRACT

Vertical profiles of $H_2{}^{18}O$ and ^2HHO concentrations have proven to yield useful information on the evaporation process in soils. However, interpretation of such profiles has been limited by the restrictions inherent in the quasi-steady-state and transient analytical models available to describe the physical processes. In this study a flexible numerical model that simulates transient fluxes of heat, liquid water, water vapor, and isotopic species is presented. A single equation is used to describe isotope transport throughout the profile, in contrast to previous solutions which applied separate equations above and below an evaporation plane where a sharp transition in phase takes place for the heavy isotopic species and the light water molecules. Relaxation of the sharp transition assumption produces broad isotope enrichment peaks that model data from relatively dry soils more realistically. The model is capable of simulating both infiltration and evaporation under fluctuating meteorological conditions, and soils ranging from saturated to dry and thus should be useful in investigating water movement in the shallow unsaturated zone and interpreting field isotope profiles.

The constituent blocks of the numerical model were tested against available analytical solutions. A controlled field experiment was designed and conducted to study the development of isotope profiles under natural conditions and their dependence on moisture and temperature distributions. This field experiment also provided a basis for further testing of the model. Comparison between model predictions of the measurable state variables (moisture content, temperature, and isotopic enrichment) and the corresponding experimental observations shows a good agreement and illustrates that the

model satisfactorily simulates the main processes involved in water evaporation and infiltration in the shallow unsaturated zone. The isotope profile development in the soil is influenced by the average daily conditions of relative humidity and temperature at the surface and not by the daily fluctuations.

Field and experimental observations showed that, for a given soil, the maximum isotopic enrichment occurs at a unique value of the moisture content, specifically the moisture content at liquid discontinuity. This value is needed for vapor flow in dry soils and is used in the model to locate the evaporation front in the soil profile. Field depth distributions of moisture content, chloride concentration, and isotope enrichment from two different areas in New Mexico (an arid region) were utilized based on the developed theory and knowledge gained from simulations of the controlled field experiment data to explain water movement in the unsaturated zone. The chloride mass balance model was used to estimate the local recharge rate in dune sand at the WIPP site in southeastern New Mexico. Analysis using a bimodal flow and transport model provided evidence for preferential flow through the root zone. This simple method should be valuable for long-term estimation of recharge rates and, together with the moisture distribution, gives us a basis for long-term estimate of recharge rate and an insight into recharge systematics in the unsaturated zone. The isotope profile completes the picture of water movement in soil by providing a basis for evaporation estimation and insight into vapor flow in the shallow unsaturated zone.

ACKNOWLEDGEMENTS

Many people deserve thanks for their contributions to this dissertation. I am grateful to my advisor Dr. Fred Phillips for his encouragement, support, and guidance in all aspects of this research. I thank Dr. John Wilson for his assistance in the numerical aspects of this research and for the many modeling ideas I have learned from him through his hydrology classes. Thanks are rendered to Dr. Andrew Campbell for his invaluable assistance in completing the isotope experimental portion of this study with his students Chris Wolf, Scott Douglass, James Corboy, and Russell Vanlandingham. I wish to thank Dr. Jan Hendrickx who provided me with valuable guidance in earlier stages of this effort. Thanks also goes to Dr. Robert Knowlton who lately joined my Ph.D committee with valuable ideas.

I gratefully acknowledge the financial support I have received from Sandia National Laboratories, Albuquerque, New Mexico, and the U.S. Department of Energy through the New Mexico Waste-Management Education and Research Consortium.

Finally, I express my undying appreciation to my wife, Basema S. Yousef, for her faith and perseverance.

Table of Contents

List of Tables

List of Figures

List of Symbols

Symbol	First Use	Description With Units
C, C_d	(H-3,4)	Heat capacity of moist and dry soil (cal g^{-1} $°K^{-1}$)
C_l	(H-4)	Specific heat of liquid water (cal g^{-1} $°K^{-1}$)
C_v	(H-4)	Specific heat of water vapor (cal g^{-1} $°K^{-1}$)
°C		Degrees centigrade
D_i^*, D_i^{v*}	(I-2,5)	Effective diffusion coefficient of isotopic species i in liquid and vapor phases of the soil water (cm^2 s^{-1})
D_i^l	(I-2)	Molecular diffusion coefficient of isotopic species i in liquid water (cm^2 s^{-1})
D^{v*}	(M-1)	Effective diffusion coefficient of water vapor in soil (cm^2 s^{-1})
D_{TV}	(M-13)	Thermal vapor diffusion coefficient (cm $°C^{-1}$ s^{-1})
D_v^{atm}	(M-2)	Diffusion coefficient of water vapor in free atmosphere air (cm^2 s^{-1})
E^v, E^l E	(M-23,20,23)	Upward volumetric flux of water in vapor, liquid and total (cm s^{-1})
g	(M-6)	Acceleration of gravity (cm s^{-2})
h	(M-5)	Relative humidity
K	(M-20)	Hydraulic conductivity (cm s^{-1})
°K		Degrees Kelvin
$K_{\Psi V}$	(M-14)	Isothermal conductivity for water vapor (cm s^{-1})
L	(H-2)	Latent heat of evaporation (cal g^{-1})
n	(M-26)	Porosity

Symbol	First Use	Description With Units
I^v, I^l	(I-1,5)	Volume flux of isotopic species in vapor and liquid water (cm s^{-1})
I	(I-17)	Total volume flux of isotopic species (cm s^{-1})
R^e		Recharge rate (cm s^{-1})
R_i, R_i^v	(I-1,8)	Isotope ratio in liquid and vapor phases
R_v	(M-4)	Ideal gas constant (cm^2 s^{-2} K^{-1})
S_h	(H-3)	Heat content (cal cm^{-3})
s		Second
T, T_a	(M-4,19)	Temperature of soil and soil air (°C or °K)
t	(M-24)	Time (s)
z		Vertical coordinate and depth below surface (cm); positive downward.
α_i^*	(I-8)	Equilibrium fractionation factor of isotopic species i between vapor and liquid phases
γ	(I-2)	Pore geometry factor
δ_i	(I-22)	Relative isotopic enrichment
θ, θ_a	(M-17,12)	Volumetric water content and air content in soil
θ_{wk}, θ_{aK}	(M-16)	Volumetric water content and air content at liquid discontinuity
θ_m, θ_o	(H-5)	Volumetric content of mineral matter and organic matter
λ	(H-1)	Thermal conductivity (cal cm^{-1} s^{-1} $°C^{-1}$)
ρ, ρ_v, ρ_{vs}	(M-13,1,5)	Liquid water, water vapor, and saturated vapor densities (g cm^{-3})

Symbol	First Use	Description With Units
σ_i^v	(I-6)	Kinetic fractionation factor for isotopic species i in vapor phase
τ^l, τ^v	(I-3,M-2)	Tortuosity factor for liquid and vapor
ϕ	(M-19)	Hydraulic (total)head (cm)
ψ	(M-6)	Pressure head (cm)
∇	(M-1)	Gradient operator (cm^{-1}) = $\partial/\partial z$ for 1-D problem
∂	(M-7)	Partial derivative operator
$\approx$	(I-14)	Approximately equals.

1. Introduction

Loss of water from soil by evaporation is difficult to measure because it is subject to the vagaries of climate and water potential. Such loss can be a dominating parameter in the water balance of arid or semiarid regions. Understanding the evaporation process and the estimation of the rate of evaporation from the soil might be necessary for evaluation of groundwater recharge and discharge from shallow groundwater. In such arid areas where water resources are scarce, reliable recharge estimates are needed for wise management of groundwater. Evaluating recharge at arid sites is also important for siting waste disposal facilities. In this study which deals with water movement in desert soils, the environmental traces, $H_2{}^{18}O$, ^2HHO, and Cl^- were used for quantifying the evaporation and infiltration processes involved.

The stable isotopes deuterium(^2H) and oxygen-18 ($^{18}0$) can be found in nature with an abundance of 0.015% and 0.205%, respectively [Sheppard,C.W., 1962]. The use of isotopically-labeled water molecules for tracing water movement in a soil undergoing evaporation stems from the fact that they have similar physical and chemical behavior to bulk water molecules and differential behavior during hydrological processes such as evaporation [Dincer and Davis, 1984]. During evaporation (transfer of water from the liquid to the vapor phase) the ordinary 'light' water molecules ($H_2{}^{16}O$) are preferentially transferred into water vapor (equilibrium isotope fractionation). Moreover, the light molecules diffuse faster than the heavy ones (kinetic fractionation). Their different behavior during evaporation from soil produces the isotope enrichment profile which constitutes the key for studying and quantifying evaporation from desert soils.

The isotope method is more robust than the other traditional methods for

estimating evaporation for two reasons. First, the diffusivities of the heavy isotopic species of water in liquid or gas vary slowly with water content (in contrast to the extreme variation of the soil water diffusivity or hydraulic conductivity with water content) thereby giving greater confidence in the isotope data than the hydrologic data. Second, measurements of isotope concentration can be made very accurately with a mass spectrometer, thereby minimizing uncertainty in the isotope data for studying evaporation.

The depth profile of deuterium enrichment resulting from evaporation of water from a saturated sand in the laboratory was first measured by Zimmermann et al. [1967]. They showed that, for steady-state evaporation where the deuterium profile is also stable, a balance is established between the upward liquid evaporative flux of deuterium and the downward diffusion of deuterium in water. This work was extended to unsaturated soils by Munnich et al. [1980]. Barnes and Allison [1983] established a theoretical basis for the scenario of steady-state evaporative uptake through the vadose zone above a shallow groundwater aquifer. They hypothesized that, at steady-state, a balance is established between the upward liquid evaporative flux, the downward liquid-phase diffusive flux, and vapor flux of the heavy isotopic species in water. This theory was used to obtain evaporation rates in the field for systems showing steady evaporation from a water table [Allison and Barnes, 1983, 1985; Fontes et al., 1986; Christmann and Sonntag, 1987]. Barnes and Allison [1984] included the effect of temperature gradients in the model. However, in the field, it is the exception rather than the rule that evaporation rate is constant with time since, even where a high-water-table condition exists, water table

depths (as well as external meteorological conditions such as radiation, wind, and air humidity) seldom remain constant for very long.

After a soil profile is wetted by infiltration, for example from a rainfall event, it will typically drain fairly rapidly to field capacity and more slowly thereafter. While the soil is wet and sufficiently conductive to supply water to the surface in response to steepening evaporation-induced gradients, the evaporation rate is limited by -and hence largely controlled by- the external meteorological conditions rather than by the properties of the soil profile. The evaporation rate at this first stage would be constant if the external meteorological conditions were not changing. The end of the first stage of evaporation is reached when this rate can no longer be matched by the flux of liquid from below due to reduction of hydraulic conductivity resulting from drying. In a dry climate (which is the case with this study), this first stage of evaporation is brief and may last from a few hours to a few days.

Most of the isotope studies in arid regions concentrate on the second stage of evaporation, as does this study. During the second stage, the top of the zone moist enough to transmit water by liquid flow will be separated from the soil surface by a very dry layer through which the water moves by vapor transport. At this stage, the atmospheric relative humidity and air surface temperature are the main meteorological conditions that affect the evaporation rate. During this second stage of evaporation, the evaporation rate will decrease progressively as the drying front gets deeper in the soil.

Walker et al. [1988] and Barnes and Walker [1989] have extended the steady-state model to nonsteady isothermal evaporation from a soil with an initially uniform water

content. However, their nonsteady-state model is analytical and is strictly applicable for ideal (laboratory) conditions where the initial and boundary conditions of the experiment are controlled. Field situations involve variable meteorological conditions and a nonsteady thermal regime in the shallow unsaturated zone due to diurnal and seasonal temperature change. Incorporating isotopic data in a combined isotopic and hydrologic model to study nonsteady nonisothermal evaporation/infiltration from natural desert soils is a primary goal of this research. This requires a mathematical formulation of water, isotope, and heat flow with a numerical solution which will simulate water (vapor and liquid) movement in the shallow unsaturated zone under nonisothermal conditions. Such a model should provide a more realistic understanding of the development of isotope profiles under natural conditions.

The model developed was limited to a one-dimensional form because heat and water flows are predominantly unidirectional in a soil undergoing evaporation. Upon testing of the model and validation of its application to the experiment designed for this study, the model and the theory behind it were used to investigate the following issues::

1. Effect of diurnal fluctuations in temperature and relative humidity on the isotope profile, moisture distribution and temperature distribution.
2. Effect of summer temperature gradients on vapor flow and isotope profiles.
3. Development of isotope profiles under natural conditions where infiltration and evaporation are intermittent.
4. Use of the developed theory to interpret the field observed depth distributions of moisture content, chloride concentration, and isotope enrichment.

2. Theory and Model Development

Modeling water movement in unsaturated soils is much more complicated than modeling saturated flow. Soils contain solid particles (which are usually disordered) and pore spaces (which are filled with gas and water) that form tortuous interconnected pathways. Water can be transported by vapor diffusion, Knudsen diffusion, internal evaporation and condensation, liquid flow due to capillary forces or gravity, and liquid and vapor flow due to differences in total pressure [Bruin and Luyben, 1980]. Often, there is a mixture of various transport mechanisms; and the contributions of different mechanisms to total transport vary from place to place and change with water content. Knudsen diffusion, which occurs in very small pores and in near-vacuum conditions [Bruin and Luyben, 1980; Clifford and Hillel, 1986], is neglected here. In the model we develop, it is considered that liquid water flows due to capillary pressure gradients as well as gravity. Water vapor is considered to diffuse through a stagnant gas phase due to vapor concentration differences created by temperature and water content gradients.

Many processes contribute to heat flow in the unsaturated soil. Continuous water films and the interconnected skeleton of solid particles can transfer heat by conduction and mass flow (sensible heat transport). For a stagnant gas phase, radiation and latent heat transport (distillation) are the primary mechanisms for heat transfer. Radiation is usually small [Whitaker, 1980] so it will be neglected in this study. The effects of bulk mass flow (sensible heat) were discussed by O'Neil [1978] and Sophocleous [1979]. Sophocleous found that, in the wet soils examined, sensible heat accounted for up to 8% of the total heat flow. In our modeling study heat transfer by conduction, latent heat

transfer and mass flow were considered .

The heavy isotopic species, ^2HHO and $H_2{}^{18}O$, used to trace water movement are considered to be solutes moving in the liquid phase by advection and diffusion and by diffusion in the vapor phase.

In the derivations below, the following sign convention is used:

1. Depth z is positive downward.
2. Heat flux is positive downward.
3. Evaporation volumetric fluxes E for liquid and vapor phases as well as isotopic volumetric fluxes (I) are positive upward.

2.1 *Water vapor Flow*

Water vapor transport is diffusive in nature. Previous investigators modeling vapor transport used Fick's law of diffusion [e.g., Rollins et al., 1954]

$$E^v = \frac{D_v^*}{\rho} \nabla \rho_v \qquad \text{(M-1)}$$

where E^v is volumetric vapor flux (cm s^{-1}), D_v^* is the effective diffusion coefficient of water vapor in soil ($cm^2\ s^{-1}$), ρ_v is the mass of water vapor per volume of gas phase (g cm^{-3}), and ∇ is the gradient operator ($\partial/\partial z$ for one-dimensional flow).

This equation states that water vapor molecules diffuse through a stagnant gas phase in the direction of decreasing vapor density (or concentration). This equation was called "the simple theory of diffusion" for vapor transfer by Philip and de Vries [1957].

The proportionally constant D_v^* used by Phillip and de Vries is given by the Penman equation

$$D_v^* = D_v^{atm} \tau^v \theta_a \qquad \text{(M-2)}$$

where D_v^{atm} is the diffusion coefficient of water vapor in free atmosphere air ($cm^2\ s^{-1}$), τ^v is a tortuosity factor which is defined as the ratio between the straight line path length and the actual pore path length, and θ_a is the volumetric air content of the medium. The factors "τ^v" and "θ_a" account for the reduced ability of vapor to diffuse through sinuous gas-filled pores. The volumetric air content ($\theta_a = n-\theta$) ranges from zero at saturation to n when the soil is completely dry (where n is porosity and θ is volumetric water content).

This "simple theory" has proved successful for isothermal vapor [Philip, 1958a] flow but underpredicted the amount of water vapor transported under the influence of temperature gradients in soil [Gurr et al., 1952; Taylor and Cary, 1954; Rollins et al., 1954]. Phillip and de Vries made a significant contribution toward reconciling the discrepancy between theory and experiments by suggesting two enhancement mechanisms to account for accelerated vapor transport under thermal gradients in the soil. The first mechanism they suggested was that vapor flow is enhanced by the presence of "liquid islands" in the soil. They pictured the interaction between vapor flow and liquid islands in dry soils as being a series of evaporation and condensation steps coupled with flow through liquid islands. The term "dry" soil is intended to imply a soil so dry that liquid continuity does not exist ($\theta \leq \theta_{wk}$ or $\theta_a \geq \theta_{ak}$ where θ_{wk} is the value of θ when the liquid phase is nearly continuous, and $\theta_{ak} = n-\theta_{wk}$). The remaining liquid is adsorbed

to given surfaces, filling small pores and forming bridges or islands between pores at the points of contact between soil particles (see Figure 2-1). When a temperature gradient is applied across this soil, some water will evaporate at the warm side of the pores and diffuse toward the lower vapor density at the cool side.

Liquid islands randomly distributed throughout the soil serve as one-way valves for water transport. Condensation on the upstream (warmer) side of an island and evaporation from the downstream (cooler) side alter the originally equal meniscus curvatures to the dotted lines shown. The upstream meniscus curvature decreases while the downstream meniscus curvature increases. Condensation and evaporation continue and the difference in curvature increases until capillary flow through an island equals the rate of condensation (and evaporation). Water transport toward the cold side increases due to this short circuit in the vapor diffusion process.

Thus, the physical model advanced by Philip and de Vries gives an improved picture of the process. Water transfer under temperature gradients in a soil with poor liquid continuity is regarded as a series-parallel process of flow through regions of vapor and liquid. The vapor flux is determined by the vapor-pressure gradients across air-filled pores; the flux through liquid islands adjusts itself to equal this vapor flux. In this physical model, the presence of liquid islands decreases the diffusion path length (or increases the value of the tortuosity factor) and increases the cross-sectional area available for diffusion. As a result, they suggested some approximate corrections to the "simple theory". They eliminated the tortuosity (=0.66), thereby increasing E^v by a factor of 1.5. In Equation (2-3), they also replaced the area available for diffusion θ_a by n (total

porosity) for dry soils and by ($\theta_a + \theta\ \theta_a/\theta_{ak}$) for soils which have a continuous liquid phase. This later correction for wet soils is not as obvious as the case for dry soil where total porosity was used for diffusion. According to Philip and de Vries, for wet soil, the liquid phase becomes continuous and vapor flow becomes less important due to a reduction in the number of islands and in the air-filled porosity and to a growth in the size of remaining islands. Enlargements of the islands decreases the curvature of the menisci to the point where the islands no longer automatically adjust to the vapor flux. Since all liquid islands contribute to overall vapor flow at the point of liquid discontinuity, θ_{wk} and there are no islands at saturation, Philip and de Vries proposed a linear decrease as θ increases from θ_{wk} to n in the flow enhancement by liquid islands. Hence, their choice of air porosity: $\theta_a + (\theta\ \theta_a/\theta_{ak})$.

The second enhancement mechanism suggested by Philip and de Vries was that the local temperature gradient present within air-filled pores was higher than the over-all macroscopic gradient of the porous medium because the thermal conductivity of the water vapor is significantly lower than the thermal conductivity of the liquid and solid phases of the composite porous medium. This Philip and de Vries mechanism would also increase the predicted vapor flux in nonisothermal conditions. An empirical thermal conductivity model developed by de Vries [1952] assumes that the temperature gradients across air-filled pores could be as much as double the mean temperature gradient in the medium as a whole (Figure 2-2). Since de Vries' model works very well for soils, they suggested that the temperature gradient in the gas phase is higher than that in the solid and liquid phases. This proposed difference in temperature gradients is significant

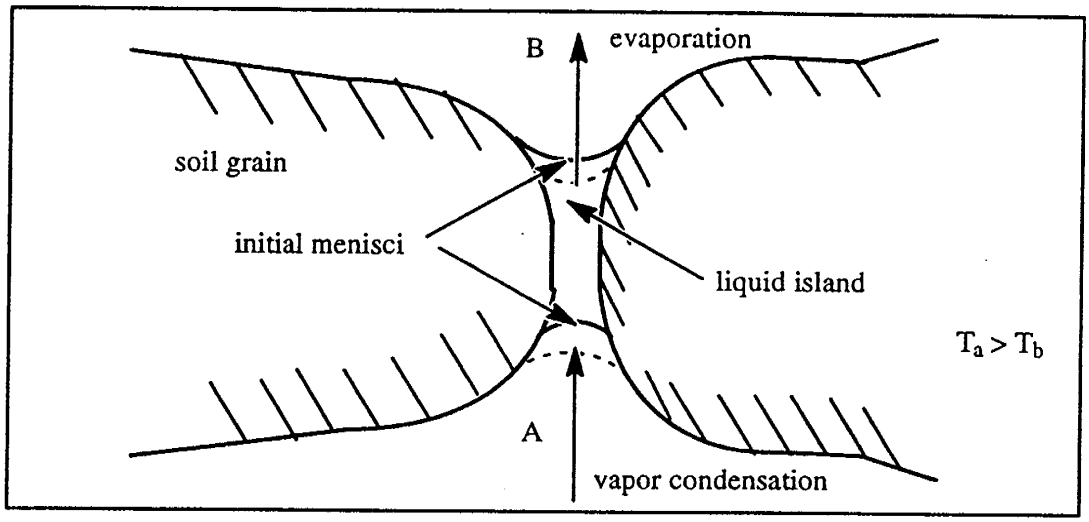

Figure 2–1. Moisture transfer through a liquid island.
Arrows indicate directions of transfer (Phillips and de Vries, 1957)

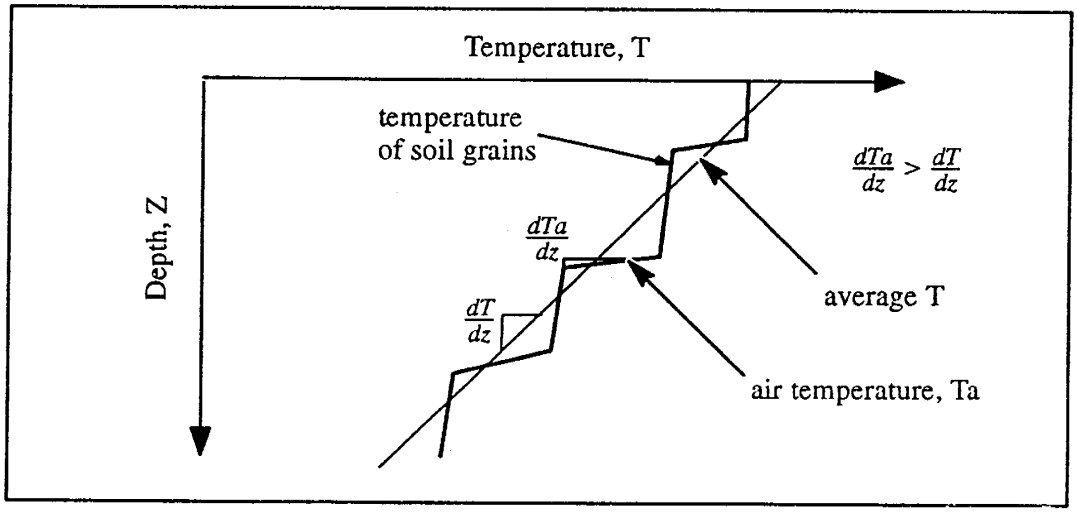

Figure 2–2. Suggested temperature distribution in air and soil grains in response to imposed temperature gradient.

because vapor diffusion is presumably caused by the temperature gradient in the gas phase (and by the vapor density boundary conditions along the pore), while the liquid islands are assumed to automatically transmit the vapor they intercept. Therefore, thermally-induced vapor flow would increase by $\nabla T_a/\nabla T$, the ratio of the temperature gradient in the air phase to the overall gradient. Later, de Vries and Philip [1959] showed that this ratio could not exceed (but was close to) the inverse of the air-filled porosity, $1/\theta_a$. Generally, values of $\nabla T_a/\nabla T$ calculated as Philip and de Vries showed are close to 1/n for the entire range of water content. Hence, $\nabla T_a/\nabla T$ would be around 3 for sand and less than 2 for clay soils.

The supposition that the temperature gradient varies among phases seems plausible because the thermal conductivities of the air, liquid, and solid differ by orders of magnitude. Since air has a lower thermal conductivity than the other phases, (even when allowing for the transfer of latent heat by water vapor distillation) it appears possible that the temperature gradient in the gas phase is greater than the overall temperature gradient imposed on the soil.

The vapor density ρ_v is linked to the partial pressure P_v by the ideal gas law

$$P_v = \rho_v R_v T \qquad \text{(M-3)}$$

where P_v is the partial pressure of water vapor(g cm^{-1} s^{-2}), ρ_v is the vapor density (g cm^{-3}), R_v is the ideal gas constant = 4.6199 x 10^6 cm^2 s^{-2} K^{-1}, and T is temperature (°K).

The water vapor density ρ_v is estimated as

$$\rho_v = h\ \rho_{vs} \qquad \text{(M-4)}$$

where ρ_{vs} is the saturated vapor density, a function of T (refer to Appendix A), and h is the relative humidity.

When a local equilibrium exists between the liquid and vapor phases, their free energies are equal and the relative humidity is given by the Kelvin equation [Edlefson and Anderson, 1943, p. 145]

$$h(\psi, T) = \exp\left(\frac{\psi\, g}{R_v\, T}\right) \qquad \text{(M-5)}$$

where ψ is the matric head (cm), and g is the gravitational acceleration (cm s^{-2}). In this relation, the osmotic head was neglected because it is very small(-0.67 cm for Cl concentration of 50 ppm) compared to the matric head.

Using the chain rule, $\nabla\rho_v$ given in Fick's Law (M-1) can be expanded in terms of ∇T and $\nabla\Psi$

$$\nabla \rho_v = \frac{\partial\, \rho_v}{\partial\, T}\, \nabla\, T + \frac{\partial\, \rho_v}{\partial\, \psi}\, \nabla\, \psi \qquad \text{(M-6)}$$

Using (M-4) $\partial\rho_v/\partial T$ can be written as

$$\begin{aligned} \frac{\partial \rho_v}{\partial\, T} &= h\, \frac{d\rho_{vs}}{dT} + \rho_{vs}\, \frac{\partial h}{\partial T} \\ &= h\, \frac{d\rho_{vs}}{dT} - \rho_v\, \frac{\psi\, g}{R_v\, T^2} \end{aligned} \qquad \text{(M-7)}$$

in which the second term is very small and can be neglected [de Vries,1975] giving

$$\frac{\partial \rho_v}{\partial T} = h \frac{d\rho_{vs}}{dT} \qquad \text{(M-8)}$$

Using the chain rule, $\partial\rho_v/\partial\psi$ can be written as

$$\frac{\partial \rho_v}{\partial \psi} = \rho_v \frac{g}{R_v T} \qquad \text{(M-9)}$$

Substituting (M-8) and (M-9) into (M-6) gives

$$\nabla \rho_v = \left(h \frac{d\rho_{vs}}{dT}\right) \nabla T + \left(\frac{\rho_v g}{R_v T}\right) \nabla \psi \qquad \text{(M-10)}$$

Substituting (M-2) and (M-10), into (M-1) yields

$$E^v = \frac{D_v^{atm}}{\rho} \tau^v \theta_a \left[h \frac{d\rho_{vs}}{dT} \nabla T + \frac{\rho_v g}{R_v T} \nabla \psi\right] \qquad \text{(M-11)}$$

or

$$E^v = D_{TV} \nabla T + K_{\psi v} \nabla \psi \qquad \text{(M-12)}$$

where

$$D_{TV} = \frac{D_v^{atm} \tau^v \theta_a}{\rho} h \frac{d\rho_{vs}}{dT} \qquad \text{(M-13)}$$

$$K_{\psi v} = \frac{D_v^{atm} \tau^v \theta_a}{\rho} \frac{\rho_v g}{R_v T} \qquad \text{(M-14)}$$

According to Philip [1958], the coefficient of $\nabla\Psi$ in (M-12) accurately predicts isothermal vapor flow, while the coefficient of ∇T under-predicts thermally-induced vapor flow. Philip and de Vries suggested several modifications to the term $\tau^v\theta_a$ in eqn. (M-13). First, the fraction of soil volume through which vapor diffuses should not be θ_a

since vapor flow in effect is occurring through both vapor and liquid-filled portions of the soil, but rather $\theta_a + f(\theta_a)\theta$ where

$$f(\theta_a) = 1 \qquad \theta_a \geq \theta_{ak}$$
$$= \frac{\theta_a}{\theta_{ak}} \qquad 0 \leq \theta_a \leq \theta_{ak} \qquad \text{(M-15)}$$

in which $\theta_{ak} = n\text{-}\theta_{wk}$. Hence the coefficient of ∇T should accordingly be changed to $\theta_a + f(\theta_a)\theta$. Second, because the temperature gradient across an air-filled pore is greater than the mean temperature gradient, Philip and de Vries suggested multiplying ∇T by $(\nabla T)_a/\nabla T$,thereby, hoping to get the actual value of ∇T in the air phase. Also the tortuosity factor τ^v which appears in D_{TV} can be eliminated since Philip and de Vries claimed this is taken into account in the average $(\nabla T)_a$. Thus $\theta_a\tau^v$ in (M-13) becomes $(\theta_a + f(\theta_a)\theta)[(\nabla T)_a/\nabla T]$. Fundamentally, the reason for all the above modifications was that experimental data showed that theory grossly under-predicted the thermally-induced vapor flux.

Making the above noted changes to D_{TV} gives

$$D_{TV} = \frac{D_v^{atm}\, h\, [\theta_a + f(\theta_a)\,\theta]}{\rho} \frac{(\nabla T)_a}{\nabla T} \frac{d\,\rho_{vs}}{dT} \qquad \text{(M-16)}$$

in which $(\nabla T)_a/\nabla T$ can be replaced by 1/n as suggested by Philip and de Vries.

The water vapor diffusion coefficient D_v^{atm} depends on temperature as given in Appendix A [Kimball et al., 1976].

2.2 *Water liquid Flow*

Darcy's Law describes the liquid flow as

$$E^l = K \nabla\phi \qquad \text{(M-17)}$$

where E^l is the volumetric liquid flux (cm s^{-1}), $K = K(\theta)$ is the hydraulic conductivity of the medium (cm s^{-1}), Φ is the total hydraulic head (cm) made up of a gravitational component '-z' (cm) and soil-water matric head component Ψ (cm)($\Phi = \Psi - z$).

Equation (M-17) can be rewritten

$$E^l = K \nabla\psi - K \qquad \text{(M-18)}$$

The hydraulic conductivity K should be corrected for the effect of temperature on viscosity and density using the relationship

$$K(T) = K(T_{ref}) \ (\mu/\rho)_{Tref} \ (\rho/\mu)_T \qquad \text{(M-19)}$$

where T_{ref} is the laboratory temperature under which the $K(\Theta)$ experimental measurement is performed. Also, the matric potential should be corrected for temperature (see Appendix A).

2.3 *Transient Water Flow Equation*

Total water flux can be obtained by summing the liquid and vapor fluxes

$$E = K_\psi \ \nabla\psi + D_{TV} \nabla T - K \qquad \text{(M-20)}$$

where $K_\psi = K_{\psi_v} + K$ is the total isothermal conductivity.

The moisture content θ is the summation of liquid moisture content θ_l and moisture content θ_v which would result if water vapor was condensed. This vapor moisture content θ_v is given by

$$\theta_v = \frac{\rho_v^{sat} h (n-\theta_l)}{\rho} \qquad \text{(M-21)}$$

where n is the soil porosity. The value of $\theta_v(\approx 1 \times 10^{-6})$ is negligible compared to θ_l. In the following formulations, θ will be used for the liquid moisture content.

The transient equation for water flow can be obtained from mass balance on moisture in a small element, i.e.,

$$\frac{\partial \theta}{\partial t} = \frac{\partial E}{\partial z} \qquad \text{(M-22)}$$

which can be rewritten as

$$F\frac{\partial \psi}{\partial t} = \frac{\partial E}{\partial z} \qquad \text{(M-23)}$$

in which the soil water capacity F is given by

$$F = \frac{\partial \theta}{\partial \psi} \qquad \text{(M-24)}$$

Equation (M-23) describes the one dimensional governing equation for water flow.

2.4 *Heat Transfer*

The thermal regime of the soil profile is a primary concern of this study where the effect of temperature is important in water vapor flow as well as in isotope

movement. In order to formulate an equation that describes the temperature distribution with depth and time, the heat flux equation and energy balance are presented first.

In this study, as mentioned earlier, heat flow is considered to be by conduction through the soil, the latent heat transfer, and the sensible heat with mass flow. Thus, after de Vries [1958], the total heat flux is given by

$$H = -\lambda \nabla T - D_l \nabla \psi - C_l \rho (T-T_0)E \qquad \text{(H-1)}$$

where λ is the thermal conductivity (cal cm^{-1} s^{-1} $°C^{-1}$) which depends mainly on moisture content, T is the temperature (°C), C_l is the specific heat of liquid water (cal g^{-1} $°C^{-1}$), T_0 is an arbitrary reference temperature (°C), and D_l is the coupling coefficient for vapor induced heat transfer given by

$$D_l = \rho L K_{\psi v} \qquad \text{(H-2)}$$

in which L is the latent heat of evaporation (cal g^{-1}), a coefficient that depends on temperature (see Appendix A).

The first term in (H-1) represents heat conduction through the moist medium. The second term represents the transfer of latent heat by vapor movement induced by moisture gradients and the third term represents the transfer of heat with mass flow.

The bulk volumetric heat content of the porous medium S_h is

$$\begin{aligned} S_h &= C(T-T_0) + L_0 \rho_v \theta_a \\ &\approx C(T-T_0) \end{aligned} \qquad \text{(H-3)}$$

where C is the heat capacity (cal cm^{-3} $°K^{-1}$), and L_0 is the value of L at T_0 (cal g^{-1}).

The validity of (H-3) rests on the condition of local thermal equilibrium among

the soil particles, the water, and the air. The assumption that a unique temperature can be defined locally is thus the counterpart of eqn. (M-5).

De Vries [1963] presented a simple expression for the heat capacity

$$\begin{aligned} C &= C_d + C_l\rho\theta + C_v\rho_v(n-\theta) \\ &\approx C_d + C_l\rho\theta \end{aligned} \qquad \text{(H-4)}$$

where C_d is the volumetric heat capacity of the porous medium when dry (cal $cm^{-3}°K^{-1}$), C_l is the specific heat of liquid water (cal g^{-1} $°K^{-1}$) ; and C_v is the specific heat of water vapor (cal g^{-1} $°K^{-1}$).

De Vries gave ρ and C_l the values of 1.0 which is an excellent approximation for C_l since it varies by less than 1% over 0 to 100 °C. However, ρ varies by 4% over that range. He divided the solid phase into mineral and organic fractions since they have different densities and specific heats. Therefore, C_d can be written as

$$C_d = \rho_m C_m \theta_m + \rho_o C_o \theta_o \qquad \text{(H-5)}$$

where ρ_m (or ρ_o) is density (g cm^{-3}), C_m (or C_o) is specific heat (cal g^{-1} $°K^{-1}$), and θ_m (or θ_o) is the volumetric content. The subscripts m and o are for mineral and organic matter, respectively.

De Vries found the coefficients preceding θ_o and θ_m to be 0.6 and 0.46 cal cm^{-3} $°K^{-1}$, respectively. Using these numbers in Equation (H-5) and substituting in (H-4) gives

$$C = 0.46\ \theta_m + 0.6\ \theta_o + C_l\ \rho\ \theta \qquad \text{(H-6)}$$

From (H-6) the relation between θ and C can be found as

$$\frac{\partial C}{\partial \theta} = C_l \rho \tag{H-7}$$

Equating the change in stored energy S_h given by (H-3) to the divergence of the heat flux (principle of heat conservation) and considering the one-dimensional form gives

$$\frac{\partial S_h}{\partial t} = - \frac{\partial H}{\partial z} \tag{H-8}$$

Substituting (H-1) and (H-3) into (H-8), (H-8) can be rewritten as

$$\frac{\partial [C(T-T_o)]}{\partial t} = \frac{\partial}{\partial z}\left(\lambda \frac{\partial T}{\partial z} + D_l \frac{\partial \Psi}{\partial z} + C_l \rho E \frac{\partial T}{\partial z}\right) \tag{H-9}$$

Expanding both sides of eqn. (H-9) it can be rewritten as

$$C\frac{\partial T}{\partial t} + \left[(T-T_o)\frac{\partial C}{\partial \theta}\right]\frac{\partial \theta}{\partial t} = \frac{\partial}{\partial z}\left[\lambda \frac{\partial T}{\partial z} + D_l \frac{\partial \psi}{\partial z}\right] + C_l \rho \left[E\frac{\partial T}{\partial z} + (T-T_o)\frac{\partial E}{\partial z}\right] \tag{H-10}$$

Combining (H-7) and (M-22) with this equation, (H-10) it can be rewritten as

$$C\frac{\partial T}{\partial t} = \frac{\partial}{\partial z}\left[\lambda \frac{\partial T}{\partial z} + D_l \frac{\partial \psi}{\partial z}\right] + C_l \rho E \frac{\partial T}{\partial z} \tag{H-11}$$

This is the transient heat equation that describes the thermal regime of the soil profile. The heat capacity C and apparent thermal conductivity λ are functions of water content. Measurement and prediction of thermal conductivity are discussed at length in Walker et al. [1981].

2.5 *Stable Isotope Transport*

The stable-isotope composition of soil water is measured as the ratio of the heavy (and minor) to the light (and major) isotope ($^{18}O/^{16}O$ or $^{2}H/H$), or in other words the ratio between isotopic species of hydrogen and oxygen in the water molecule, ($H_2{}^{18}O/H_2{}^{16}O$) or ($^{2}HHO/H_2{}^{16}O$).

2.5.1 *Isotope Transport in Liquid Phase*

The flux of the minor isotope (henceforth denoted by subscript i) in the liquid phase can be written as [Barnes and Allison, 1984]

$$I^l = E^l R_i + D_i^* \nabla R_i \qquad \text{(I-1)}$$

where R_i is the isotope ratio in the liquid phase, and D_i^* is the effective diffusion coefficient of species i in liquid water ($cm^2\ s^{-1}$). The first term in this equation describes flow by advection, and the second term describes flow by diffusion.

The effective diffusion coefficient D_i^* is given by

$$D_i^* = \gamma\ D_i^l \qquad \text{(I-2)}$$

where γ is a pore geometry factor given by

$$\gamma = \tau^l\ \theta \qquad \text{(I-3)}$$

where τ^l is the liquid tortuosity factor, which is a product of a constant parameter τ^{l*} and $(1\text{-}XF_v)$, where XF_v is the ratio of the absolute value of vapor flux to the sum of absolute values of vapor and liquid fluxes. The use of such relationship for tortuosity assures having a continuous function for geometry factor for all moisture content and not a sudden drop to zero at liquid discontinuity. For wet soils where the liquid film on the soil grains is continuous and flow is liquid dominant ($XF_v=0$), the pore geometry factor

reduces to the product of moisture content and tortuosity. For dry soil, where the liquid film is discontinuous (the moisture is in the form of liquid islands surrounded by water vapor) and water flow is predominantly in vapor phase ($XF_v = 1$) the pore geometry factor will be zero since no diffusion of isotopes in the liquid phase is possible between the isolated liquid islands. D_i^l in eqn. (I-2) is the diffusion coefficient of isotopic species i in liquid water. The temperature dependence of the diffusion coefficient is given by Wang et al. [1953] and Longsworth, L.G. [1954] (refer to Appendix A).

2.5.2 *Isotope Transport in Vapor Phase*

To develop a vapor flow equation for the minor isotope consistent with the modified diffusion equation obtained for the major water flow, Fick's law is given by

$$\rho I^v = D_i^{v*} \nabla(R_i^v \rho_v) \qquad \text{(I-4)}$$

where D_i^{v*} is the effective vapor diffusion coefficient of the isotopic species ($cm^2 s^{-1}$), R_i^v is the isotope ratio of the water vapor, and I^v is the upward isotope flux in the vapor phase ($cm\ s^{-1}$). D_i^{v*} is related to the water vapor diffusion coefficient D^{v*} through the kinetic fractionation factor σ_i^v , i.e.,

$$\sigma_i^v = \frac{D^{v*}}{D_i^{v*}} \qquad \text{(I-5)}$$

The value of this factor for deuterium and oxygen-18 in the water molecule are 1.0251 and 1.0285, respectively [Merlivat, 1978]. Equation (I-4) can be expanded as

$$\rho I^v = D_i^{v*}[R_i^v \nabla \rho_v + \rho_v \nabla R_i^v] \qquad \text{(I-6)}$$

Assuming that vapor pressure equilibrium between the phases of water is maintained, R_i^v can be obtained from

$$R_i^v = \alpha_i^* R_l \qquad \text{(I-7)}$$

where α_i^* is the equilibrium fractionation factor of isotope i. This parameter has a value less than, but close to, unity. Majoube [1971] gives the following temperature dependence relations for deuterium and oxygen-18 (T is in K):

Deuterium

$$10^3 \ln\left(\frac{1}{\alpha_i^*}\right) = 24.844\left(\frac{10^6}{T^2}\right) - 76.248\left(\frac{10^3}{T}\right) + 52.612 \qquad \text{(I-8)}$$

Oxygen-18

$$10^3 \ln\left(\frac{1}{\alpha_i^*}\right) = 1.137\left(\frac{10^6}{T^2}\right) - 0.4156\left(\frac{10^3}{T}\right) - 2.0667 \qquad \text{(I-9)}$$

Substituting (I-5) and (I-7) into (I-6) gives

$$\rho I^v = \frac{D^{v*}}{\sigma_i^v}\left[\alpha_i^* R_i \nabla\rho_v + \rho_v \nabla(\alpha_i^* R_i)\right] \qquad \text{(I-10)}$$

Expanding the second term on the right hand side and rearranging gives

$$\rho I^v = \frac{\alpha_i^*}{\sigma_i^v} R_i [D^{v*} \nabla \rho_v] + \frac{D^{v*} \rho_v}{\sigma_i^v} \left(\alpha_i^* \nabla R_i + R_i \frac{\partial \alpha_i^*}{\partial T} \nabla T \right) \quad \text{(I-11)}$$

The term $D^{v*} \nabla \rho_v$ is equivalent to ρE^v in eqn. (M-1). Thus eqn. (I-11) can be written as

$$I^v = R_i \frac{\alpha_i^*}{\sigma_i^v} E^v + D_i^{RV} \nabla R_i \quad \text{(I-12)}$$

where

$$D_i^{RV} = \frac{h \rho_{vs}}{\rho} \frac{\alpha_i^*}{\sigma_i^v} D^{v*} \quad \text{(I-13)}$$

2.5.3 *Transient Isotope Flow Equation*

The total isotope flux I is the sum of I^v and I^l. Combining (I-1) and (I-12) yields

$$I = R_i \left(\frac{\alpha_i^*}{\sigma_i^v} E^v + E^l \right) + D_i \nabla R_i \quad \text{(I-14)}$$

where the total diffusion coefficient of the isotopic species D_i is given by

$$D_i = D_i^* + D_i^{RV} \quad \text{(I-15)}$$

Eqn. (I-14) can be rewritten as

$$I = E\,\xi\,R_i + D_i\,\nabla R_i \qquad \text{(I-16)}$$

in which ξ is given by

$$\xi = 1 - F_v\left(1 - \frac{\alpha_i^*}{\sigma_i^v}\right) \qquad \text{(I-17)}$$

in which F_v is the fraction of vapor to total water flow

$$F_v = \frac{E^v}{E} \qquad \text{(I-18)}$$

The factor ξ given in eqn. (I-17) will be called the transition factor because its value changes in the transition zone located between the liquid dominant zone and the vapor dominant zone. For saturated and for fairly wet soil where vapor flow is insignificant ($F_v=0$), ξ is equal to unity; while for dry soil, where flow is predominantly in vapor phase ($F_v=1$), the transition factor ξ reduces to α_i^*/σ_i^v which equals 0.899 for deuterium at 20 °C temperature. In a two-zone model where a sharp change in phase of water (from liquid to vapor) occurs at the evaporation front, the transition factor drops suddenly from 1 to the ratio between the equilibrium fractionation factor and the kinetic fractionation factor α_i^*/σ_i^v. In a more realistic model of a drying soil profile the change in phase of water occurs gradually from liquid to combined liquid and vapor (regardless how narrow this zone is) and finally vapor. Therefore, the transition factor changes gradually from 1 at depth where the soil is wet to α_i^*/σ_i^v in the top dry layer. The rapid change in the value of transition factor happens in the zone where both liquid flow and vapor flow coexist in comparable amounts. For nonvolatile solutes, the transition factor

is the fraction of liquid flow to total water flow.

Mass balance on the isotope can be done by equating the time rate of change of the isotopic mass content in the soil with the divergence of the isotope mass flux at each point in the medium, i.e.,

$$\frac{\partial}{\partial t}(\theta\ \rho\ R_i) = \nabla\cdot(\rho\ I) \qquad \text{(I-19)}$$

Substituting the isotope flux I given by eqn. (I-16) into this equation, considering the one dimensional form, and eliminating the liquid density from both sides gives

$$\frac{\partial}{\partial t}(R_i\ \theta) = \frac{\partial}{\partial z}\left[E\ \xi\ R_i\right] + \frac{\partial}{\partial z}\left[D_i\ \frac{\partial R_i}{\partial z}\right] \qquad \text{(I-20)}$$

As the variability of isotope ratio R_i is small, it is more appropriate to use the dimensionless ratio δ_i which essentially has higher variability. δ_i is the concentration of isotope species in the soil water above that in reference water with known isotopic composition. This reference water can be the standard mean ocean water (SMOW) or the rain water at the site under consideration. Using δ_i will minimize the machine-associated errors included in measurements of R. $\delta_{i\text{-}REF}$ is given by

$$\delta_{i\text{-}REF} = \frac{R_i}{R_{REF}} - 1 \qquad \text{(I-21)}$$

where R_{REF} is the isotope ratio for the reference water. Changing the value of δ_i from the SMOW scale to local scale (for example, using rain water as a reference) can be accomplished using the relation

$$\delta_{X\text{-}REF} = \delta_{X\text{-}SMOW} + \delta_{SMOW\text{-}REF} + \delta_{X\text{-}SMOW} * \delta_{SMOW\text{-}REF} \qquad \text{(I-22)}$$

where $\delta_{SMOW\text{-}REF}$ is obtained using (I-21).

Using the definition of δ_i in eqn. (I-21), eqn. (I-20) can be expanded and rewritten as

$$(1 + \delta_i)\frac{\partial \theta}{\partial t} + \theta\frac{\partial \delta_i}{\partial t} = \frac{\partial}{\partial z}\left[\xi\ E\ (\delta_i + 1)\right] + \frac{\partial}{\partial z}\left(D_i \frac{\partial \delta_i}{\partial z}\right) \qquad \text{(I-23)}$$

Using the mass balance equation (M-22), (I-23) can be further expanded to

$$\theta\frac{\partial \delta_i}{\partial t} = \xi E\frac{\partial \delta_i}{\partial z} + \frac{\partial}{\partial z}\left(D_i \frac{\partial \delta_i}{\partial z}\right) + (1+\delta_i)\left[(\xi - 1)\frac{\partial E}{\partial z} + E\frac{\partial \xi}{\partial z}\right] \qquad \text{(I-24)}$$

This is the governing equation for the transient movement of a stable isotope (^2H or $^{18}0$) in water. The left hand side of eqn.(I-24) represents the rate of increase of δ_i. The right hand side does not express an explicit separation between advection and fractionation since both processes were included in the transition factor ξ which appears in the first and third terms. Diffusion (in both liquid and vapor phases) is represented by the second term. This is a general equation that can be used for a soil ranging from saturated to dry. The transition factor in eqn. (I-24) facilitates obtaining the typical shape of the isotope profile (bulge at the evaporation zone) numerically using only one equation,(I-24).

For isotope transport in a wet soil where liquid flow dominates ($\xi = 1$) under a hydraulic steady-state flow ($\partial E/\partial z = 0$), eqn (I-24) reduces to

$$\theta\frac{\partial \delta_i}{\partial t} = E\frac{\partial \delta_i}{\partial z} + \frac{\partial}{\partial z}\left(D_i \frac{\partial \delta_i}{\partial z}\right) \qquad \text{(I-25)}$$

Considering a hydraulic steady-state ($\partial E/\partial z=0$) and isotopic steady-state ($\partial \delta_i/\partial t=0$), the governing equation describing isotope transport (eqn. I-24) can be reduced to

$$-\xi\ E\ \frac{\partial \delta_i}{\partial z} = \frac{\partial}{\partial z}\left(D_i\ \frac{\partial \delta_i}{\partial z}\right) + (1+\delta_i)E\ \frac{\partial \xi}{\partial z} \qquad \text{(I-26)}$$

2.5.4 *Relation to Previous Work through the Transition Factor*

Walker et al. [1989] assumed a hydraulic quasi-steady-state and effectively used a value of unity for ξ when they used an equation that is similar to eqn. (I-25). For an isotopic steady-state condition, which also necessarily implies a hydraulic steady-state condition, the upward isotope flux I is constant. Deep in the profile, where there is no gradient in the isotope ratio R_i and ξ equals unity, the isotope flux from eqn. (I-16) reduces to

$$I = E\ R_{res} \qquad \text{(I-27)}$$

where R_{res} is the isotopic ratio at the reservoir water (e.g., groundwater).

Along the upward evaporative flowing water pathway the value of the transition factor decreases slowly as the vapor flow component increases and in the evaporation zone, where the vapor flow component of the water flux becomes significant and of comparable magnitude to the coexisting liquid flow, the transition factor decreases strongly until it reaches its lowest value (α_i^*/σ_i^v) in the zone of dominant vapor flow (the top part of the soil profile). At the isotope profile maximum, $\partial R_i/\partial z = 0$ [Barnes and Allison, 1984] and the isotope flux I reduces to

$$I = E\,\xi_p\,R_p \qquad \text{(I-28)}$$

where ξ_p is the transition factor at the depth of the isotope profile maxima (peak), and R_p is the corresponding isotopic ratio. Equating the right hand sides of equations (I-27) and (I-28) and using the definition of δ_i, given by eqn.(I-21), yields,

$$\xi_p = \frac{(\delta_{res}+1)}{(\delta_p+1)} \qquad \text{(I-29)}$$

This equation describes the relation between the maximum relative enrichment (at the isotope profile peak) δ_p and the corresponding value of the transition factor for a steady-state condition.

Barnes and Allison [1983], in their steady-state model for unsaturated soil divided the soil profile into two zones, an upper one in which water movement is by vapor diffusion and a lower one in which liquid flux is dominant. The change in the phase of the water flux from liquid to vapor (i.e., evaporation) takes place at the dividing plane. This sharp dividing plane may be called the "evaporation plane" to distinguish it from the more general and realistic case where evaporation is taking place in a zone, or "evaporation zone". Barnes and Allison [1983] refer to the evaporation plane as the "evaporation front". The steady-state governing equation (for the liquid dominant zone below the evaporation plane) applicable to Barnes and Allison's [1983] analysis is a special case of eqn.(I-26), i.e.,

$$-E\frac{d\delta_i}{dz} = \frac{d}{dz}\left(D_i\,\frac{\partial\delta_i}{\partial z}\right) \qquad \text{(I-30)}$$

Comparison of eqn.(I-30) with eqn.(I-26), indicates that the analysis of Barnes and

Allison [1983] has assumed a value of unity for ξ below the evaporation front. This implies no bulk water vapor flow, even though D_i is accounting for the diffusion of isotopes in the vapor phase below the evaporation front. Their conceptual model followed Zimmerman et al. [1967] for evaporation from saturated soil where ξ clearly has a value of unity. A typical solution for eqn.(I-30) is exponential [Barnes and Allison, 1988], i.e.,

$$\delta(z) = \delta_{res} + (\delta_{ef} - \delta_{res}) \exp\left[-\int_{z_{ef}}^{z} \frac{1}{D_i/E} dz\right] \qquad z \geq z_{ef} \qquad \text{(I-31)}$$

where δ_{res} is the relative isotopic enrichment of the reservoir water (e.g., groundwater), δ_{ef} is the relative isotopic enrichment at the evaporation front (or isotope profile maxima), and z_{ef} is the depth of the evaporation front.

To complete their description of the isotope profile, Barnes and Allison [1983, 1984] used Fick's law of diffusion to find the isotopic composition at the evaporation front δ_{ef} based on vapor diffusion above the evaporation front. They used this value in eqn.(I-31) which describes the isotope concentration in the zone below the evaporation front. In order to relate our model to that of Barnes and Allison it is shown below how the isotopic composition in the vapor dominant zone above the evaporation front can be obtained for this two-zone model.

Evaporation rate at any depth $z < z_{ef}$ can be calculated using Fick's law of diffusion

$$E^v = \frac{D^{v*}}{\rho}\left(\frac{h(z)\rho_{vs}(z) - h_a\rho_{vs}(0)}{z}\right) \qquad \text{(I-32)}$$

For the steady-state condition, the evaporation flux E is constant and, above the evaporation front, equals E^v. The isotope flux in the vapor phase above the evaporation

front is given by

$$I^v = \frac{D_i^{v*}}{\rho}\left(\frac{h(z)R_i^v(z)\rho_{vs}(z) - h_a R_a \rho_{vs}(0)}{z}\right) \qquad \text{(I-33)}$$

Using the relations (I-5), (I-7), and (I-32), eqn.(I-33) can be rewritten as

$$I^v = \frac{1}{\sigma_i^v} E\left(\frac{h(z)\alpha_i^*(z)R_i(z)\ \rho_{vs}(z) - h_a R_a \rho_{vs}(0)}{h(z)\rho_{vs}(z) - h_a \rho_{vs}(0)}\right) \qquad \text{(I-34)}$$

From which the value of isotopic composition of soil water above the evaporation front is given by

$$R_i(z) = \frac{\sigma_i^v[h(z)\rho_{vs}(z) - h_a\rho_{vs}(0)]R_{res} + h_a R_a \rho_{vs}(0)}{\alpha_i^*(z)\ h(z)\ \rho_{vs}(z)} \qquad \text{(I-35)}$$

For isothermal conditions, this reduces to

$$R_i(z) = \frac{1}{\alpha_i^* h(z)}\left(\sigma_i^v R_{res}[h(z) - h_a] + h_a R_a\right) \qquad \text{(I-36)}$$

from which the value of R at the evaporation front (h=1) is given by

$$R_{i,ef} = \frac{1}{\alpha_i^*}\left[\sigma_i^v R_{res}(1-h_a) + h_a R_a\right] \qquad \text{(I-37)}$$

This is identical to equation (5) of Barnes and Allison [1983], which was obtained using identical assumptions. Using δ notation, eqn.(I-37) can be rewritten as

When the physical model of Barnes and Allison (1983) is followed, the following relations are implicitly assumed.

$$\delta_{ef} = \frac{1}{\alpha_i^*}\left[\sigma_i^v\ (\delta_{res}+1)(1-h_a)+h_a(\delta_a+1)\right]-1 \qquad \text{(I-38)}$$

Above the "evaporation front":

$$\begin{aligned} F_v &= 1 \\ D_i &= D_i^{RV} \\ h(z) &= h_a + z/z_{ef}(1-h_a) \end{aligned} \qquad \text{(I-39)}$$

in which h_a is the relative humidity of the atmospheric air at the surface;

and below the "evaporation front":

$$\begin{aligned} F_v &= 0 \\ D_i &= D_i^{RV} + D_i^* \\ h &= 1 \end{aligned} \qquad \text{(I-40)}$$

Inherent in these two equations is the implicit assumption that, at the evaporation front, liquid continuity breaks apart. These two equations were used with a numerical finite difference solution of eqn.(I-26) to produce the isotope profile that is shown in Figure 2-3. Data used for this example are identical to those used in Figure 1 of Barnes and Allison [1983]. The top part of the numerically-calculated profile matches the analytical solution given by eqn.(I-36) after considering the change in notation from R to δ; the bottom part matches the analytical solution of eqn.(I-31). At the evaporation front (isotope profile maxima), ξ_{ef} was calculated via eqn.(I-29). This assures obtaining a value of δ_i at the evaporation front which is identical to the value calculated via eqn.(I-38). In this two-zone approach there is a jump in the value of the transition factor from 1 below the evaporation front to about 0.899 above the evaporation front. For the numerical model the value of transition factor at the depth of evaporation front ξ_{ef} is needed. The value of

Figure 2-3. Typical isotopic and hydraulic relations for the evaporation plane model under steady state condition

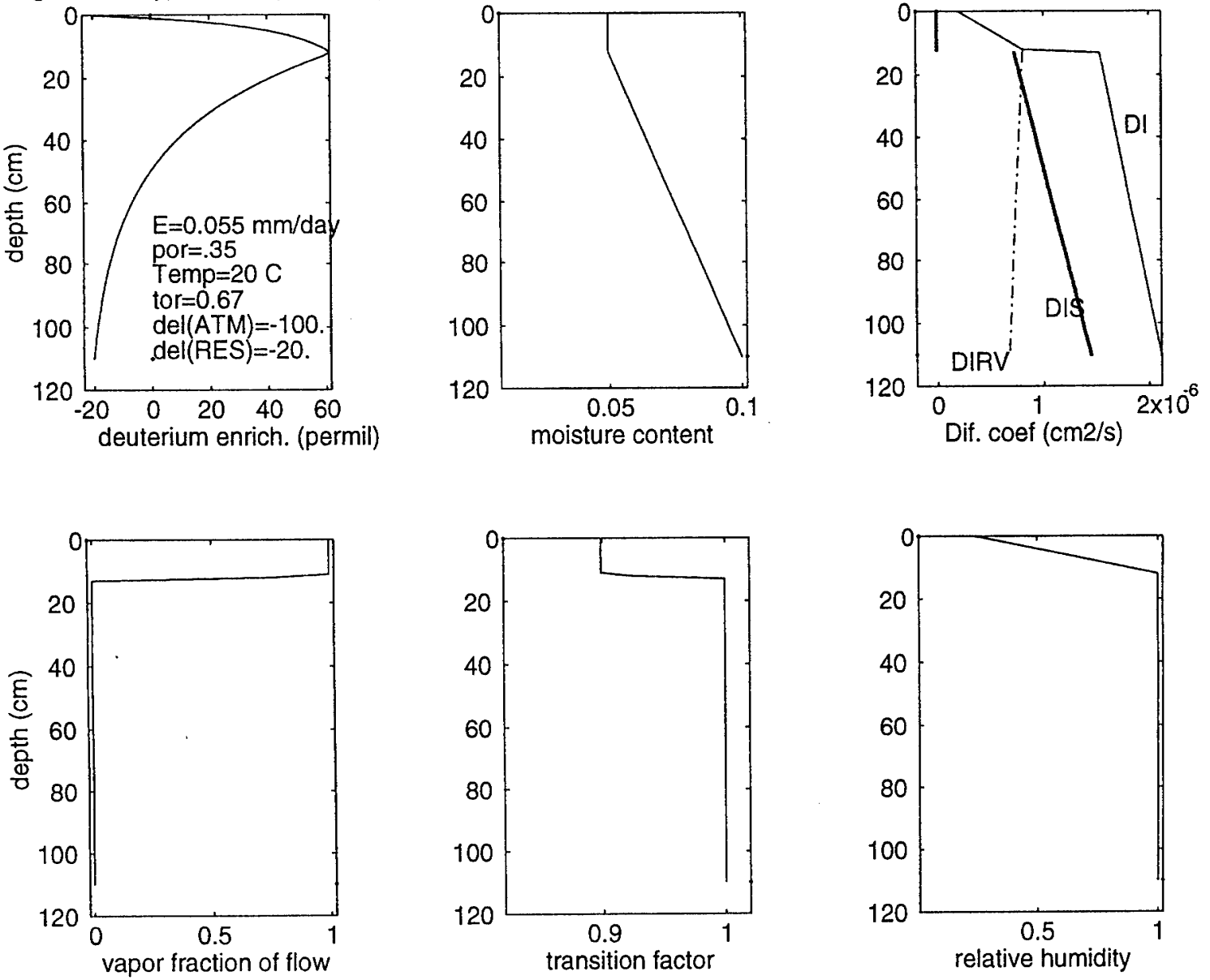

ξ_{ef} calculated --via eqn.(I-29)-- is 0.9231 which corresponds to a value of 0.762 for F_v.

In Figure 2-4, another case was considered for dry dune sand. The relative humidity h in this case is computed via eqn. (M-5) where relative humidity depends on the water potential, which is related to the moisture content through the retention curve of the soil. The effective diffusion coefficient of isotope in the liquid phase D_i^* was modeled as continuous in space (see eqn.(I-3)) unlike that shown in Figure 2-3, which followed the model of Barnes and Allison. This reflects the fact that liquid continuity does not break suddenly but gradually. This results in a smooth peak for the isotope profile unlike the sharp peak of Figure 2-3. The hydraulic conductivity K was calculated via van Genuchten model [Van Genuchten, 1978] based on the retention curve data and the measured saturated hydraulic conductivity. The isothermal water vapor conductivity $K_{\psi v}$ was calculated from eqn.(M-14). The calculated F_v distribution shows that the upward water flux changes phase from liquid dominated to combined vapor and liquid and finally vapor. This change in phase is similarly seen in the transition factor ξ distribution. Consequently, the peak of the profile is broad, unlike that in Figure 2-3. A broad peak is most often seen in drying soil profiles, although the peak will be depressed for nonsteady-state isotope profiles. The evaporation rate used to produce the isotope profile was 0.02 mm/day. If the depth of the isotope peak (15 cm) was used to estimate the evaporation rate -via eqn.(I-32)- then the value estimated would be 0.06 mm/day. As the zone that combines both phases of water gets narrower (which is the case for fairly wet soil), the use of the isotope maxima depth for estimating the instantaneous evaporation rate becomes more satisfactory.

Figure 2-4. Typical isotopic and hydraulic relations for the evaporation zone model under steady state condition

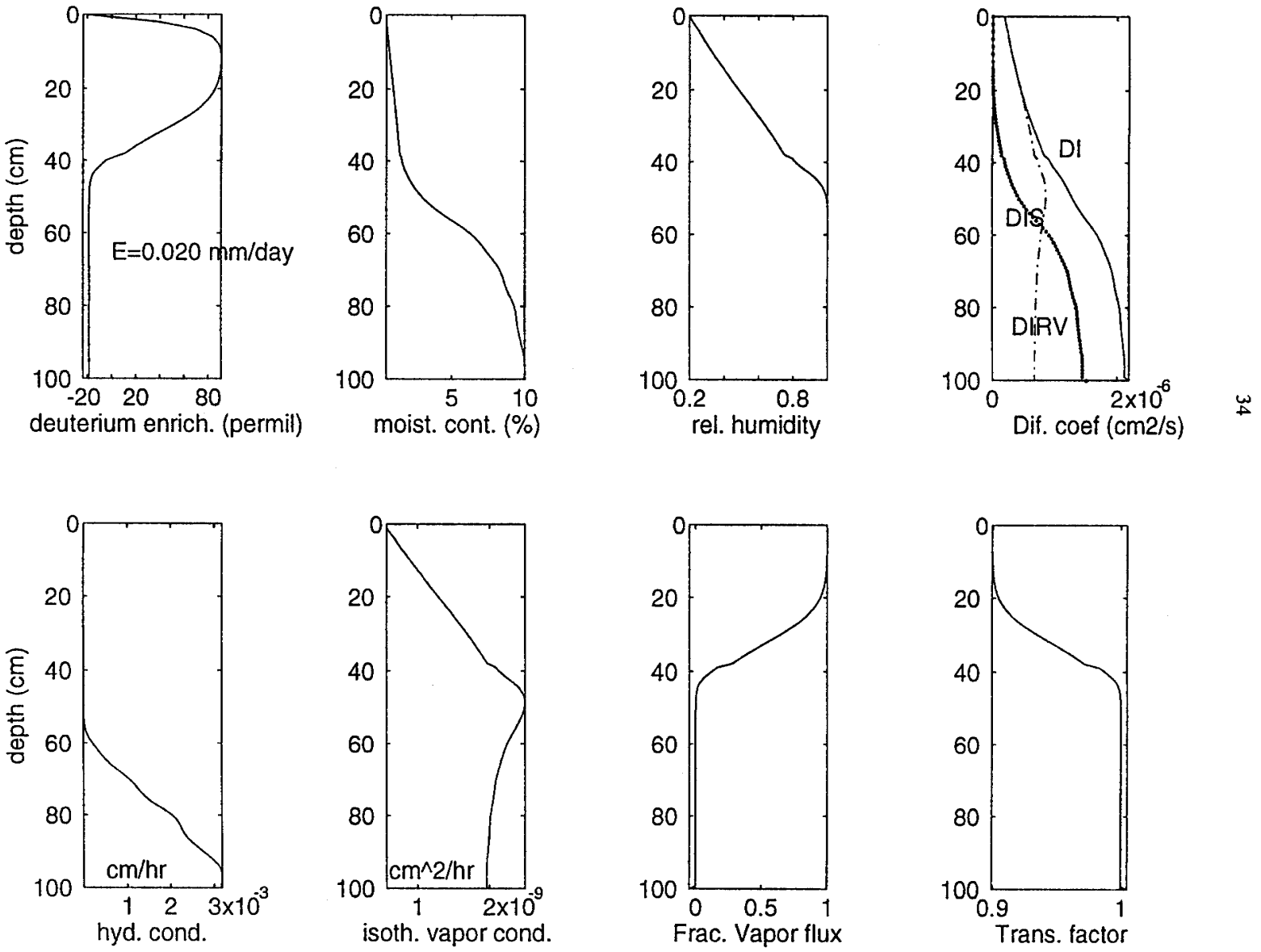

Figure 2-5 shows the transient development of the deuterium profile together with the moisture distribution history for previously published results from experimental soil columns [Allison et al., 1983]. The upper plots (Figure 2-5a) are for bare soil and the shape of the profile is more-or-less similar to Figure 2-3. A hydraulic quasi-steady-state condition was reached by day 182 as it was noticed from the insignificant change in the moisture distribution and depth of isotope maxima during the last 54 days. The isotope profile, however, is still changing slowly toward the final isotope steady-state profile. Allison et al. [1983] have measured the final evaporation rate from weight loss of the bare soil pots as 0.06 mm/day. The estimated evaporation rate from the depth of evaporation front was also 0.06 mm/day. The evaporation rate used in Figure 2-1 was 0.055 mm/day. Similarity in the atmospheric conditions (h_a, δ_a), temperature and isotopic composition of reservoir water (δ_{res}) between the assumed values for Figure 2-1 and the experimental values of Figure 2-5a suggest that the enrichment at the evaporation front should be close to that of Figure 2-3 if an isotopic steady-state profile is reached.

The planted soil (Figure 2-5b) is drier than the bare soil (Figure 2-5a) as it can be seen from the lower average moisture content. The moisture distribution for the planted soil is similar to that in Figure 2-4. The peak of the isotope profile is broad, as in Figure 2-4. For drier soils, the model of sharp transfer from liquid-dominated flow to vapor-dominated flow begins to break down and an evaporation zone model such as that used for Figure 2-4 gives a more realistic results. By comparing the maximum enrichment of the isotope profile in the planted soil with that in Figure 2-4 it is concluded that the isotopic steady-state composition probably was not achieved.

Figure 2-5. Development of deuterium and moisture distributions in bare and planted soils [Reproduced from Allison et al.,1983a]

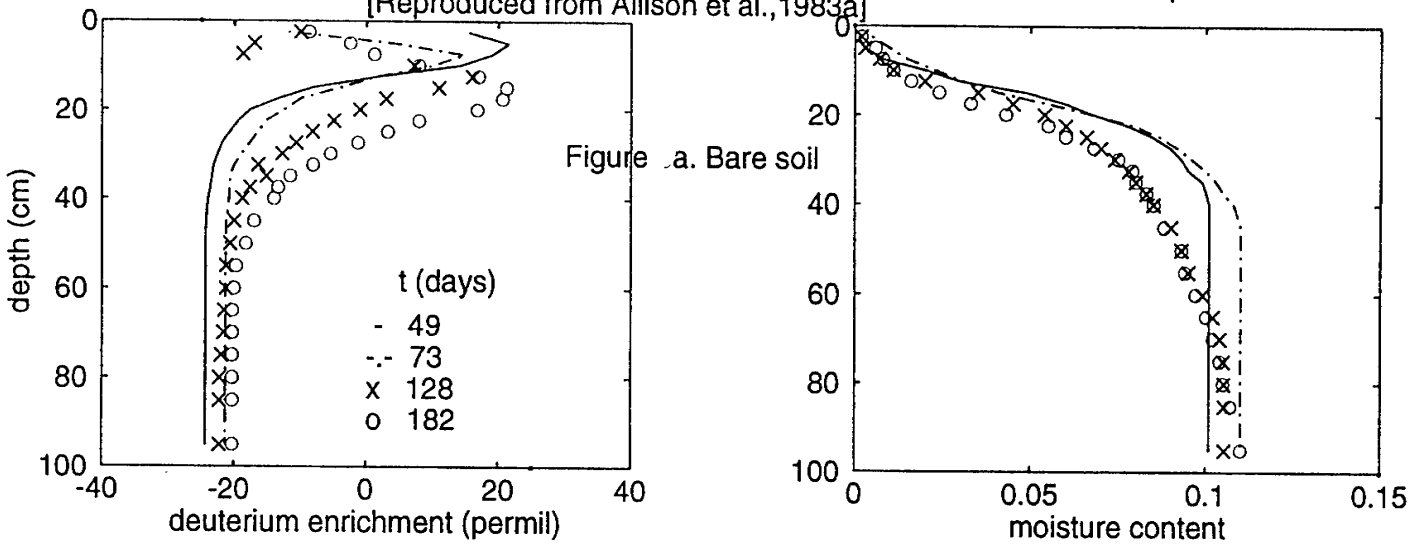

Figure a. Bare soil

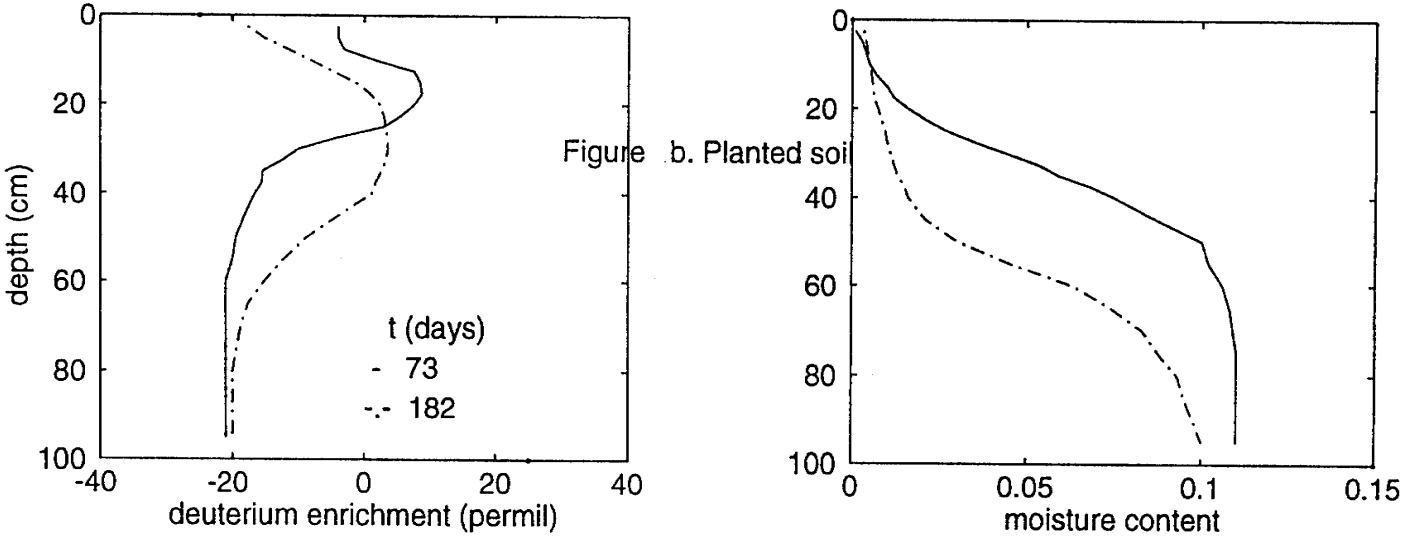

Figure b. Planted soil

Many field isotope profiles show shapes that are similar to Figure 2-5a. In this case, estimation of instantaneous evaporation rate from the depth of the isotope profile peak (via eqn. (I-32)) should be satisfactory. The instantaneous evaporation rate should be equal to the average evaporation rate for a soil profile that has reached a hydraulic quasi steady-state condition. Moreover, Allison et al. [1983] used eqn. (I-31) in an inverse approach to calculate evaporation rate from the same isotope profiles. In both cases, the calculated values of the evaporation rate were higher than those based on the depth of evaporation front. Excessive evaporation estimates result from the use of eqn.(I-31), which was derived using the isotopic steady-state assumption, to match the measured isotope profiles that have not reached an isotopic steady-state condition. Attainment of the isotopic steady-state condition could take as much as one year, even after hydraulic steady-state is achieved.

For later stages of the evaporation process where hydraulic quasi-steady-state is achieved and the moisture distribution is known, the transient isotope equation (eqn. I-24) should be sufficient for predicting the later developments in the isotope profile. However, simulation of the isotope profile for the experimental results shown in Figure 2-5 during the early stage where the moisture distribution is also changing is not possible without knowledge of the history of moisture distribution development. The numerical model presented here simulates water flow, heat transfer, and isotope transport and is capable of predicting changes in the isotope profile for this case and for the more general case of natural conditions where intermittent evaporation and infiltration are contributing in shaping the isotope profile. The need for such a linked thermal, hydraulic, and isotopic

model was anticipated by Barnes et al. [1988].

2.6 *Governing Equations and Boundary Conditions of the Numerical Model*

The governing system of differential equations is

$$F\frac{\partial \psi}{\partial t} = \frac{\partial E}{\partial z} \tag{M-23}$$

$$C\frac{\partial T}{\partial t} = \frac{\partial}{\partial z}\left(\lambda \frac{\partial T}{\partial z} + D_l \frac{\partial \psi}{\partial z}\right) + C_l \rho E \frac{\partial T}{\partial z} \tag{H-11}$$

$$\theta\frac{\partial \delta_i}{\partial t} = \xi E\frac{\partial \delta_i}{\partial z} + \frac{\partial}{\partial z}\left(D_i \frac{\partial \delta_i}{\partial z}\right) + (1+\delta_i)\left[(\xi - 1)\frac{\partial E}{\partial z} + E \frac{\partial \xi}{\partial z}\right] \tag{I-24}$$

where E is given by Equation (M-20)

The three governing equations (M-23), (H-11), and (I-24) contain three state variables: the soil temperature T, the matric potential for soil water Ψ, and (for the isotope under consideration, either ^{18}O or ^{2}H) the concentration δ_i . The moisture content and matric potential are related to one another through the retention relation. The function F can be obtained from the retention relation. Solution of this set of equations requires specification of two boundary conditions and one initial condition each for T, δ, and θ. Initial and boundary conditions proposed for monotonically drying soil are given in Table 1. The top boundary conditions consist of a transient soil surface temperature specification

for the heat flux equation, a transient temperature and humidity (based on which together with the depth of the evaporation front the evaporation rate E is calculated) for the water flow equation, and a constant isotopic composition for the atmospheric water vapor. The bottom boundary conditions consist of a prescribed downward water flux or zero matric head gradient (gravity drainage) for the water flow equation, prescribed heat flux for the heat flow equation, and zero concentration gradient for the isotope transport equation. It is worth mentioning that these boundary conditions can be changed according to the application and the data under consideration. The finite difference method will be used for solving the governing differential equations.

This numerical model can be viewed as being composed of two blocks: (1) an independent hydrologic block which includes the two coupled equations for water and heat flows, (M-23) and (H-11) , and (2) an isotopic block , of one equation (I-24), which depends on the hydrologic block.

Table 1. Initial and Boundary Conditions*

State Variable f(t,z)	Initial Conditions t = 0, z ≥ 0	Boundary Conditions	
		Top Boundary t ≥ 0 , z = 0	Bottom Boundary t ≥ 0, z = L_b
Ψ	$\Psi(0,z) = \Psi_{initial}(z)$	$E = 1/\rho\ D_v^* \partial\rho_v/\partial z$ is calculated through the surface dry layer based on the measured T(t,0), h(t,0) at the surface and the depth of the evaporation front.	$-K_\Psi\ \partial\Psi/\partial z + K$ $-D_{TV}\ \partial T/\partial z = R$ or $\partial\Psi/\partial z = 0$
T	$T(0,z) = T_{initial}(z)$	$T(t,0) = T_{top}(t)$ (measured)	$-\lambda\partial T/\partial z = Q_h$
δ_i	$\delta_i(0,z) = \delta_{i,initial}(z)$	$\delta_i(t,0) =$ $[1/\alpha^*_i(T(t,0))]*(\delta_i^{VA}+1.0)-1.0$ (δ_i^{VA} is measured)	$\partial\delta_i/\partial z = 0$

* see List of Symbols for description of parameters

2.7 *Chloride Transport*

Equation (I-25), which is a special case of eqn. (I-24) where liquid flow dominates, is also applicable to the transport of nonvolatile solutes in which case $\alpha_i^*=0$ and $D_i^{RV}=0$ (from eqn. I-13) and consequently $D_i=D_i^*$. Thus, eqn. (I-25) reduces to

$$\theta\frac{\partial \delta_i}{\partial t} = E\frac{\partial \delta_i}{\partial z} + \frac{\partial}{\partial z}\left(D_i^* \frac{\partial \delta_i}{\partial z}\right) \qquad \text{(I-41)}$$

which can be written for the steady state condition as

$$0 = E\frac{\partial \delta_i}{\partial z} + \frac{\partial}{\partial z}\left(D_i^* \frac{\partial \delta_i}{\partial z}\right) \qquad \text{(I-42)}$$

In cases where the diffusion process can be neglected ($D_i=0$ or $\partial\delta/\partial z=0$) and using zero concentration for reference, δ reduces to C_s. Integrating eqn. (I-42) for this case of negligible diffusion, it can be written as

$$E\ C_s = constant \qquad \text{(I-43)}$$

Using R^e ($R^e = -E$) and considering a long-term downward movement of environmental chloride in soil and average atmospheric input of chloride, eqn. (I-43) can be written as

$$R^e\ C_s = P\ C_o \qquad \text{(I-44)}$$

where

R^e =average drainage (recharge) rate (mm/yr)
C_s =average chloride concentration in soil water (mg/l)
P =precipitation rate (mm/yr)
C_o =average atmospheric input chloride concentration (mg/l)

Equation (I-44) is the well-known chloride mass balance equation for estimating long-term local drainage (recharge) rates [Sharma and Hughes, 1985]. This simple tracer method should be valuable in arid and semiarid regions where all chloride comes from atmospheric sources, where precipitation is the only source of recharge water, where water loss by evapotranspiration is high, and consequently where recharge rates are minimal. Small recharge rates are difficult to estimate based on water balance methods or using Darcian-flux calculations based on measured tension gradients and estimated unsaturated hydraulic conductivity [Gee and Hillel, 1988].

3. Numerical Implementation

In this chapter, the governing equations and boundary conditions will be written in the finite difference form. Our discretization of the solution domain is depicted in figure 3-1. A general scheme of the finite difference method is used for time, and central difference is used for space [Peaceman, D.W., 1977].

In the formulations which follow, the subscript i denotes the spatial node and the superscript j denotes the time level.

3.1 *Water Flow*

Upward water flux E at node i and time level j is given by (see eqn. M-20)

$$E_i^j = K_{\psi_i}^j \frac{\psi_{i+1}^j - \psi_{i-1}^j}{2\Delta z} - K_i^j + D_{TV_i}^j \frac{T_{i+1}^j - T_{i-1}^j}{2\Delta z} \tag{3-1}$$

The differential equation describing mass flow (M-23) can be written in the finite difference form as (fully implicit for time)

$$\begin{aligned} F_i^j \frac{\psi_i^j - \psi_i^{j-1}}{\Delta t} = \frac{1}{\Delta Z}\Big(&K_{\psi_{i+1/2}}^j \frac{\psi_{i+1}^j - \psi_i^j}{\Delta z} - K_{i+1/2}^j \\ &+ D_{TV_{i+1/2}}^j \frac{T_{i+1}^j - T_i^j}{\Delta z} \\ &- K_{\psi_{i-1/2}}^j \frac{\psi_i^j - \psi_{i-1}^j}{\Delta z} + K_{i-1/2}^j \\ &- D_{TV_{i-1/2}}^j \frac{T_i^j - T_{i-1}^j}{\Delta z}\Big) \end{aligned} \tag{3-2}$$

The explicit finite difference form of (M-23) is given by

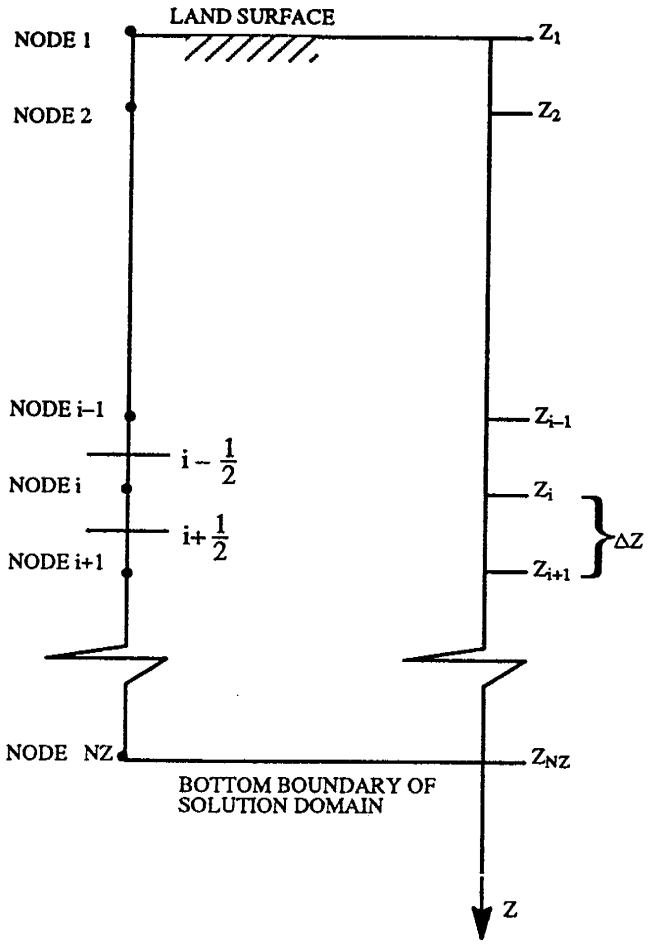

Fig 3–1. Discretization and coordinate system for the one–dimensional numerical model

$$F_i^{j-1}\frac{\psi_i^j - \psi_i^{j-1}}{\Delta t} = \frac{1}{\Delta Z}\left(K_{\psi_{i+1/2}}^{j-1}\frac{\psi_{i+1}^{j-1} - \psi_i^{j-1}}{\Delta z} - K_{i+1/2}^{j-1} + D_{TV_{i+1/2}}^{j-1}\frac{T_{i+1}^{j-1} - T_i^{j-1}}{\Delta z} - K_{\psi_{i-1/2}}^{j-1}\frac{\psi_i^{j-1} - \psi_{i-1}^{j-1}}{\Delta z} + K_{i-1/2}^{j-1} - D_{TV_{i-1/2}}^{j-1}\frac{T_i^{j-1} - T_{i-1}^{j-1}}{\Delta z}\right) \tag{3-3}$$

Multiplying eqn. (3-2) by ω_1 and (3-3) by $(1-\omega_1)$ where $0 \le \omega_1 \le 1$, adding (3-2) to (3-3), and rearranging

$$\begin{aligned}
&\left[-\omega_1 K_{\psi_{i-1/2}}^{j}\right]\psi_{i-1}^{j} + \left[\frac{F_i^*}{r} + \omega_1 K_{\psi_{i-1/2}}^{j} + \omega_1 K_{\psi_{i+1/2}}^{j}\right]\psi_i^j - \left[\omega_1 K_{\psi_{i+1/2}}^{j}\right]\psi_{i+1}^{j} \\
&- \left[\omega_1 D_{TV_{i-1/2}}^{j}\right]T_{i-1}^{j} + \left[\omega_1 D_{TV_{i-1/2}}^{j} + \omega_1 D_{TV_{i+1/2}}^{j}\right]T_i^j - \left[\omega_1 D_{TV_{i+1/2}}^{j}\right]T_{i+1}^{j} \\
&= \left[(1-\omega_1)K_{\psi_{i-1/2}}^{j-1}\right]\psi_{i-1}^{j-1} - \left[-\frac{F_i^*}{r} + (1-\omega_1)K_{\psi_{i-1/2}}^{j-1} + (1-\omega_1)K_{\psi_{i+1/2}}^{j-1}\right]\psi_i^{j-1} \\
&+ \left[(1-\omega_1)K_{\psi_{i+1/2}}^{j-1}\right]\psi_{i+1}^{j-1} + \left[(1-\omega_1]D_{TV_{i-1/2}}^{j-1}\right]T_{i-1}^{j-1} \\
&- \left[(1-\omega_1)D_{TV_{i-1/2}}^{j-1} + (1-\omega_1)D_{TV_{i+1/2}}^{j-1}\right]T_i^{j-1} + \left[(1-\omega_1)D_{TV_{i+1/2}}^{j-1}\right]T_{i+1}^{j-1} \\
&-(1-\omega_1)\Delta Z\left[K_{i+1/2}^{j-1} - K_{i-1/2}^{j-1}\right] - \omega_1\Delta Z\left[K_{i+1/2}^{j} - K_{i-1/2}^{j}\right]
\end{aligned} \tag{3-4}$$

where the ratio r is given by

$$r = \frac{\Delta t}{(\Delta z)^2} \tag{3-5}$$

and the soil water capacity F_i^* is given by

$$F_i^* = \omega_1 F_i^j + (1-\omega_1) F_i^{j-1} \tag{3-6}$$

Average values of K, K_ψ, and D_{TV} at half distance between nodes are given by

the geometric mean. For example, at half the distance between nodes i and i+1 and for time level j, the values of K and D_{TV} are give by

$$K^j_{i+1/2} = \sqrt{K^j_i \; K^j_{i+1}} \tag{3-7}$$

$$D^j_{TV_{i+1/2}} = \sqrt{D^j_{TV_i} \; D^j_{TV_{i+1}}} \tag{3-8}$$

The top boundary condition is a prescribed evaporation rate as calculated from the difference in vapor density between nodes 1 and 2. At i=2 (second node from the surface and first node solved for) the appropriate equation corresponding to (3-4) is

$$\begin{aligned} &\left[\frac{F^*_i}{r} + \omega_1 K^j_{\psi_{i+1/2}}\right] \psi^j_i - \left[\omega_1 K^j_{\psi_{i+1/2}}\right] \psi^j_{i+1} \\ &+\left[\omega_1 D^j_{TV_{i+1/2}}\right] T^j_i - \left[\omega_1 D^j_{TV_{i+1/2}}\right] T^j_{i+1} \\ = &-\left[-\frac{F^*_i}{r} + (1-\omega_1) K^{j-1}_{\psi_{i+1/2}}\right] \psi^{j-1}_i + \left[(1-\omega_1) K^{j-1}_{\psi_{i+1/2}}\right] \psi^{j-1}_{i+1} \\ &- \left[(1-\omega_1) D^{j-1}_{TV_{i+1/2}}\right] T^{j-1}_i + \left[(1-\omega_1) D^{j-1}_{TV_{i+1/2}}\right] T^{j-1}_{i+1} \\ &-\Delta Z\left[\omega_1 E^j_{i-1/2} + \omega_1 K^j_{i+1/2}\right] - \Delta Z \left[(1-\omega_1) K^{j-1}_{i+1/2} + (1-\omega_1) E^{j-1}_{i-1/2}\right] \end{aligned} \tag{3-9}$$

where

$$E^j_{i-1/2} = D^{*j}_{v\,i-1/2} \left(h^j_i \rho_{vs} - h^j_{i-1} \rho_{vs}\right) \tag{3-10}$$

The bottom boundary condition ($i=N_Z$) can be a prescribed recharge rate, R^e, or zero pressure gradient, in which case the recharge rate is calculated via

$$R^e = K_i - D_{TV_i}\frac{T_{i+1} - T_{i-1}}{2\Delta Z} \tag{3-11}$$

The pressure head at the outside node $i+1=N_Z+1$ is given by

$$\psi^j_{i+1} = \psi_{i-1} + \frac{2\Delta z(K_i - R^e) - D_{TV_i}[T_{i+1} - T_{i-1}]}{K_{\psi_i}} \tag{3-12}$$

3.2 *Heat Transfer*

The differential equation describing heat flow, eqn. (H-11), is written in the finite difference form for fully implicit and explicit schemes in equation (3-13) and (3-14), respectively

$$\begin{aligned} C^j_i \frac{T^j_i - T^{j-1}_i}{\Delta t} = \frac{1}{\Delta z}[&\lambda^j_{i+1/2}\frac{T^j_{i+1} - T^j_i}{\Delta z} + D^j_{l_{i+1/2}}\frac{\psi^j_{i+1} - \psi^j_i}{\Delta z} \\ &- \lambda^j_{i-1/2}\frac{T^j_i - T^j_{i-1}}{\Delta z} - D^j_{l_{i-1/2}}\frac{\psi^j_i - \psi^j_{i-1}}{\Delta z}] \\ &+ C_l\,\rho\,E^j_i\frac{T^j_{i+1} - T^j_{i-1}}{2\Delta z} \end{aligned} \tag{3-13}$$

$$\begin{aligned} C^{j-1}_i \frac{T^j_i - T^{j-1}_i}{\Delta t} = \frac{1}{\Delta z}[&\lambda^{j-1}_{i+1/2}\frac{T^{j-1}_{i+1} - T^{j-1}_i}{\Delta z} + D^{j-1}_{l_{i+1/2}}\frac{\psi^{j-1}_{i+1} - \psi^{j-1}_i}{\Delta z} \\ &- \lambda^{j-1}_{i-1/2}\frac{T^{j-1}_i - T^{j-1}_{i-1}}{\Delta z} - D^{j-1}_{l_{i-1/2}}\frac{\psi^{j-1}_i - \psi^{j-1}_{i-1}}{\Delta z}] \\ &+ C_l\,\rho\,E^{j-1}_i\frac{T^{j-1}_{i+1} - T^{j-1}_{i-1}}{2\Delta z} \end{aligned} \tag{3-14}$$

Multiplying eqn. (3-13) by ω_1 and (3-14) by $(1-\omega_1)$, adding (3-13) to (3-14), and rearranging

$$-\left[\omega_1\lambda^j_{i-1/2} - \omega_1 C_l\,\rho\,E^j_i\,\frac{\Delta z}{2}\right]T^j_{i-1} + \left[\frac{C^*_i}{r} + \omega_1\lambda^j_{i-1/2} + \omega_1\lambda^j_{i+1/2}\right]T^j_i$$
$$- \left[\omega_1\lambda^j_{i+1/2} + \omega_1 C_l\,\rho\,E^j_i\,\frac{\Delta z}{2}\right]T^j_{i+1} - \left[\omega_1 D^j_{l_{i-1/2}}\right]\psi^j_{i-1}$$
$$+ \left[\omega_1 D^j_{l_{i-1/2}} + \omega_1 D^j_{l_{i+1/2}}\right]\psi^j_i - \left[\omega_1 D^j_{l_{i+1/2}}\right]\psi^j_{i+1} \qquad (3\text{-}15)$$
$$= \left[(1-\omega_1)\lambda^{j-1}_{i-1/2} - (1-\omega_1)C_l\,\rho\,E^{j-1}_i\,\frac{\Delta z}{2}\right]T^{j-1}_{i-1}$$
$$-\left[-\frac{C^*_i}{r} + (1-\omega_1)\lambda^{j-1}_{i-1/2} + (1-\omega_1)\lambda^{j-1}_{i+1/2}\right]T^{j-1}_i$$
$$+\left[(1-\omega_1)\lambda^{j-1}_{i+1/2} + (1-\omega_1)C_l\,\rho\,E^{j-1}_i\,\frac{\Delta z}{2}\right]T^{j-1}_{i+1} + \left[(1-\omega_1)D^{j-1}_{l_{i-1/2}}\right]\psi^{j-1}_{i-1}$$
$$- \left[(1-\omega_1)D^{j-1}_{l_{i-1/2}} + [1-\omega_1]D^{j-1}_{l_{i+1/2}}\right]\psi^{j-1}_i + \left[(1-\omega_1)D^{j-1}_{l_{i+1/2}}\right]\psi^{j-1}_{i+1}$$

Average values of λ and D_l at the midpoint between nodes are given by the geometric mean. For example, at half the distance between nodes i and i+1 and for time level j, the values of λ and D_l are given by

$$\lambda^j_{i+1/2} = \sqrt{\lambda^j_i\,\lambda^j_{i+1}} \qquad (3\text{-}16)$$

$$D^j_{l_{i+1/2}} = \sqrt{D^j_{l_i}\,D^j_{l_{i+1}}} \qquad (3\text{-}17)$$

and the heat capacity of the soil C_i^* is given by

$$C^*_i = \omega_1\,C^j_i + (1-\omega_1)C^{j-1}_i \qquad (3\text{-}18)$$

For the top boundary (i=1) the temperature is prescribed, and in equation (3-15) for i=2

$$\lambda_{i-1/2} = \lambda_i \tag{3-19}$$

The bottom boundary condition (prescribed heat flux Q_h, $i=N_Z$) is given by

$$T_{i+1} = T_{i-1} - \frac{2\Delta Z}{\lambda_i}\left[Q_h + C_l \rho E_i (T_i - T_o) + D_{l_i}\frac{\Psi_{i+1}-\Psi_{i-1}}{2\Delta Z}\right] \tag{3-20}$$

where T_o is the reference temperature.

3.3 *Isotope transport*

The subscript i that stands for isotopic parameters will be dropped and here i will be used for the node index. The differential equation (I-25) describing the isotope movement is given in the finite difference form using a fully implicit scheme and explicit scheme for time in equations (3-21) and (3-22)

$$\begin{aligned}
\theta_i^j \frac{\delta_i^j - \delta_i^{j-1}}{\Delta t} &= \\
\xi_i^j E_i^j \left(\frac{\delta_{i+1}^j - \delta_{i-1}^j}{2\Delta z}\right) & \\
+\frac{1}{\Delta z}\left(D_{i+1/2}^j \frac{\delta_{i+1}^j - \delta_i^j}{\Delta z} - D_{i-1/2}^j \frac{\delta_i^j - \delta_{i-1}^j}{\Delta z}\right) & \\
+\left(1+\delta_i^j\right)\left((\xi_i^j - 1)\frac{E_{i+1}^j - E_{i-1}^j}{2\Delta z} + E_i^j \frac{\xi_{i+1}^j - \xi_{i-1}^j}{2\Delta z}\right) &
\end{aligned} \tag{3-21}$$

$$\theta_i^{j-1}\,\frac{\delta_i^j - \delta_i^{j-1}}{\Delta t} =$$

$$\xi_i^{j-1}\,E_i^{j-1}\,\left(\frac{\delta_{i+1}^{j-1} - \delta_{i-1}^{j-1}}{2\Delta z}\right)$$

$$+\frac{1}{\Delta z}\left(D_{i+1/2}^{j-1}\frac{\delta_{i+1}^{j-1} - \delta_i^{j-1}}{\Delta z} - D_{i-1/2}^{j-1}\frac{\delta_i^{j-1} - \delta_{i-1}^{j-1}}{\Delta z}\right) \qquad (3\text{-}22)$$

$$+\left(1+\delta_i^{j-1}\right)\left((\xi_i^{j-1}-1)\frac{E_{i+1}^{j-1} - E_{i-1}^{j-1}}{2\Delta z} + E_i^{j-1}\,\frac{\xi_{i+1}^{j-1} - \xi_{i-1}^{j-1}}{2\Delta z}\right)$$

Multiplying eqn. (3-21) by ω_2 and (3-22) by $(1-\omega_2)$ where $0\le\omega_2\le1$, adding (3-21) to (3-22), and rearranging

$$-\left[\omega_2 D_{i-1/2}^j - \omega_2\xi_i^j\,E_i^j\,\frac{\Delta z}{2}\right]\delta_{i-1}^j$$

$$+\left[\frac{\theta_i^*}{r} + \omega_2 D_{i-1/2}^j + \omega_2 D_{i+1/2}^j - \omega_2 f_i^j\,\frac{\Delta z}{2}\right]\delta_i^j$$

$$-\left[\omega_2 D_{i+1/2}^j + \omega_2\xi_i^j\,E_i^j\,\frac{\Delta z}{2}\right]\delta_{i+1}^j$$

$$=\left[(1-\omega_2)D_{i-1/2}^{j-1} - (1-\omega_2)\xi_i^{j-1}E_i^{j-1}\frac{\Delta z}{2}\right]\delta_{i-1}^{j-1} \qquad (3\text{-}23)$$

$$-\left[-\frac{\theta_i^*}{r} + (1-\omega_2)D_{i-1/2}^{j-1} + (1-\omega_2)D_{i+1/2}^{j-1} - (1-\omega_2)f_i^{j-1}\frac{\Delta z}{2}\right]\delta_i^{j-1}$$

$$+\left[(1-\omega_2)D_{i+1/2}^{j-1} + (1-\omega_2)\xi_i^{j-1}E_i^{j-1}\frac{\Delta Z}{2}\right]\delta_{i+1}^{j-1}$$

$$+\omega_2 f_i^j\frac{\Delta Z}{2} + (1-\omega_2)f_i^{j-1}\frac{\Delta Z}{2}$$

where f_i is given by

$$f_i^j = \left[\xi_i^j - 1\right]\left(E_{i+1}^j - E_{i-1}^j\right) + E_i^j\left(\xi_{i+1}^j - \xi_{i-1}^j\right) \qquad (3\text{-}24)$$

Average values of D at half distance between nodes is given by the geometric mean. For example, at half the distance between nodes i and i+1 and at time level j, the value of D is given by

$$D^j_{i+1/2} = \sqrt{D^j_i \; D^j_{i+1}} \tag{3-25}$$

The value of θ^* is given by

$$\theta^*_i = \omega_2 \; \theta^j_i + (1-\omega_2)\theta^{j-1}_i \tag{3-26}$$

At the top boundary (i=1) the isotopic composition of atmospheric vapor δ^{VA}, is prescribed and the isotopic composition of the soil water is given by

$$\delta_i = \frac{1}{\alpha_i} * \left(\delta^{VA}_i + 1.0\right) - 1 \tag{3-27}$$

The bottom boundary condition (zero gradient in isotopic composition of soil water δ; i=number of nodes) is given by

$$\delta_{i+1} = \delta_i \tag{3-28}$$

3.4 *Numerical Solution Algorithm*

The coefficients F, K, K_ψ and D_{TV}, on the left side of eqn. (3-4), are highly nonlinear functions of the state variables θ(or Ψ) and/or T. The relation between θ and Ψ is also nonlinear. In eqn. (3-9) λ, C, and D_l are functions of θ and E is calculated based on θ and T distributions. These coefficients and the state variables are to be evaluated at the new time level, so the system is nonlinear.

For the water flow, a tridiagonal coefficient matrix G is built of the coefficients of

Ψ^j in the left side of eqn. (3-9), for node 2, and of the coefficients of Ψ^j in the left side of eqn. (3-4) for nodes 3 through N_Z. Another tridiagonal coefficient matrix W is built of the coefficients of T^j in the left side of eqn. (3-9), for node 2, and of the coefficients of T^j in the left side of eqn. (3-4) for nodes 3 through N_Z. Similarly for the heat transfer, a tridiagonal coefficient matrix D is built of the coefficients of T^j in the left side of eqn. (3-15), for nodes 2 through N_Z. Another tridiagonal coefficient matrix E is built of the coefficients of Ψ^j in the left side of eqn. (3-15), for node 2 through N_Z. The two equations which are solved simultaneously are given by

$$\{\Psi\}^j = [G]^{-1}\{U\} \qquad \text{where} \qquad \{U\} = \{HM\}^{j-1} - [W]^j \{T\}^j \tag{3-29}$$

$$\{T\}^j = [D]^{-1}\{V\} \qquad \text{where} \qquad \{V\} = \{HH\}^{j-1} - [E]^j \{\Psi\}^j \tag{3-30}$$

The vector {HM} is filled from the right hand side of eqn. (3-9) for node 2 and the right hand side of eqn. (3-4) for nodes 3 through N_Z. The vector {HH} is filled from the right hand side of eqn. (3-15) for nodes 2 through N_Z .

The solution procedure used consists of alternate solution of eqn. (3-29) and eqn. (3-30) for Ψ^j and T^j, respectively, updating the coefficient matrices, G, W, D, and E, each iteration until a desired degree of convergence is obtained each for T and Ψ. An advantage of such a procedure is that the matrix equation to be solved is always tridiagonal, a feature that makes it relatively easy to solve.

4. Code Testing

No exact analytical solutions are presently available for the coupled problem of nonisothermal nonsteady evaporation/infiltration and the associated nonsteady isotope equation. However, to test the validity of the constituent code blocks (water, heat, and isotope blocks), the performance of each block was compared with available analytical solutions for certain artificial cases. Having established the validity of the code for simulating various processes independently, it will be assumed that the code may be used with confidence for more complex situations (such as studying soil profiles undergoing evaporation under natural conditions).

4.1 *Water Flow*

A comparison was made between infiltration profiles (θ vs. Z for different times) as calculated with the water flow equation (M-23) and as calculated with the quasi-analytical solution of Philip [1958b] using the sandy soil described by Havercamp et al. [1977]. The comparison was done for liquid flow under isothermal conditions. This reduces the water flow equation to the well-known Richard's equation

$$F\,\frac{\partial \psi}{\partial t} = \frac{\partial}{\partial z}\left(K\frac{\partial \psi}{\partial z} - K\right) \tag{4-1}$$

Philip solved Equation (4-1) subject to the conditions

$$\begin{array}{lll} t \le 0 & Z \ge 0 & \psi = \psi_n \\ t \ge 0 & Z = 0 & \psi = \psi_o \end{array} \tag{4-2}$$

Havercamp et al. [1977] used Philip's quasi-analytical solutions assuming $\theta_n = 0.1 (\Psi_n = -61.5$ cm) and $\theta_o = 0.2675 (\Psi_o = -20.73$ cm) for sandy soil. They described

the retention curve and conductivity function by the two analytical expressions

$$\theta = \frac{\alpha\ (\theta_s - \theta_r)}{\alpha + |\psi|^{\beta}} + \theta_r \tag{4-3}$$

where θ_s=0.287, θ_r=0.075, α=1.611x10^6, and β=3.96; and

$$K = K_s \frac{A}{A + |\psi|^{B}} \tag{4-4}$$

where K_s=34 cm/hr = 9.44x10^{-3} cm/sec, A=1.175x10^6, and B=4.74

Comparison between Philip's solution as given by Haverkamp et al. [1977] and the numerical solution of the one-dimensional water flow block ODW is given in Figure 4-1. In the numerical solution, a Crank-Nicholson scheme for time is used (ω_1=0.5). The values used for time increment (Δt) and depth increment (Δz) were 0.001 hr and 1.0 cm respectively. The numerical and analytical solutions agree closely.

4.2 *Heat Transfer*

To test the numerical solution of the heat flow equation, a hypothetical horizontal soil column of homogeneous moisture content was considered. This means no water potential difference ($\partial\Psi/\partial z$=0) and no flow (E=0), including no flow caused by gravity effects. Thus the transient heat flow equation (H-11) can be rearranged and written as

$$\frac{\partial T}{\partial t} = \frac{\lambda}{C} \frac{\partial^2 T}{\partial Z^2} \tag{4-5}$$

If temperature at one end (z=0) is given by

$$T(0,t) = T_{ave} + T_o \sin(wt) \tag{4-6}$$

in which T_o is amplitude of surface temperature variation, and w is the angular frequency

Figure 4-1. Comparison between Philip analytical solution (1958) and the ODW results

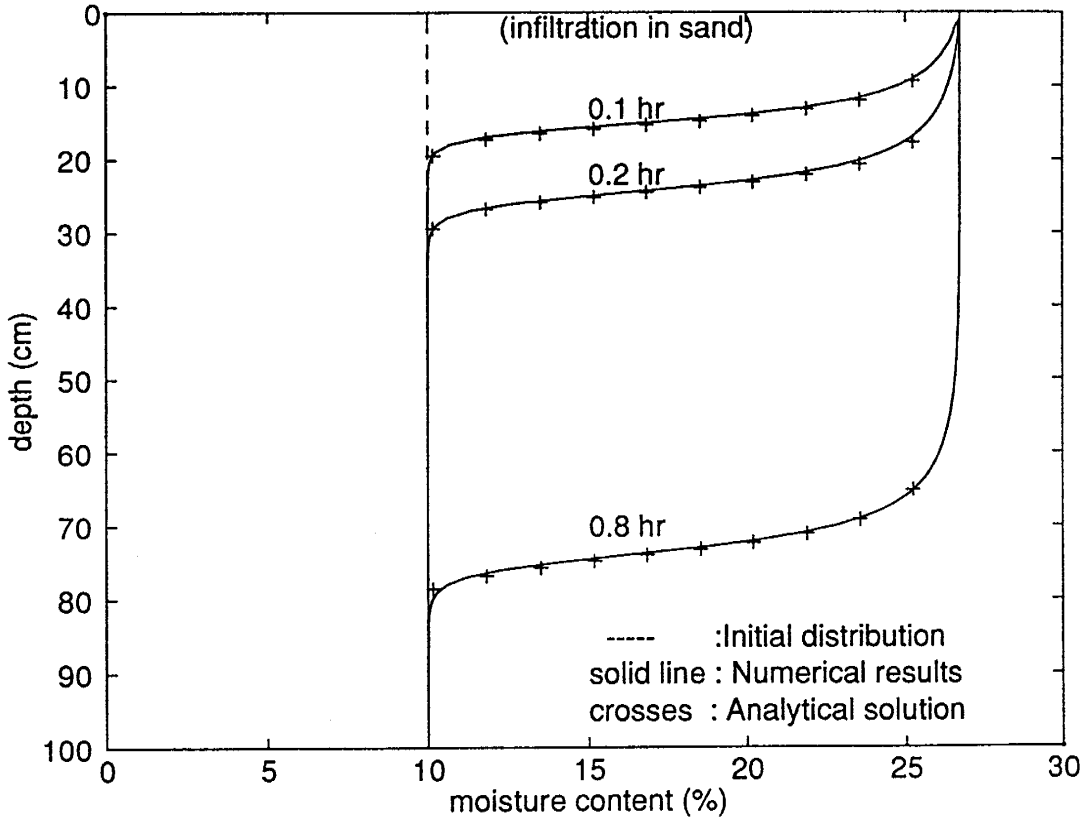

of variation ($2\ \pi/t_c$) where t_c is the period of temperature fluctuation, then a typical solution of Equation (5-5) is

$$T(Z,t) = T_{ave} + T_o \exp(-Z/d)\ \sin(wt\ -\ Z/d) \qquad (4\text{-}7)$$

where the damping depth d is given by

$$d = \left(\frac{2\ \lambda}{w\ C}\right)^{1/2} \qquad (4\text{-}8)$$

This analytical solution is valid for a semi-infinite medium subject to the boundary condition given by eqn. (4-6) above.

Comparison between the analytical solution (i.e., Equation 4-7) and the numerical solution of the one-dimensional heat block ODH is given in Figure 4-2. In the numerical solution, a Crank-Nicholson scheme for time (ω_1=0.5) was used. Values used for this example were: T_{ave}=0.0 °C; T_o=10 °C; t_c= 24 hr; λ=2x10^{-3} cal/(cm sec °C); C=0.56 cal/(cm^3 °C); time increment (Δt)=0.01 hr; depth increment (Δz)=0.5 cm. The numerical and analytical solutions agree closely.

4.3 *Isotope Transport*

It has been shown earlier (Figure 2-3) that eqn.(I-26) which is the steady-state version of eqn.(I-24), matched the analytical solution of Barnes and Allison [1983]. To solve the transient isotope equation (I-24), it should be connected to the hydrologic block. For such case, there is no known analytical solution. Barnes and Walker [1989] considered the isothermal condition and neglected gravity to find an approximate analytical solution for a uniform moisture profile that dries only above a sharp evaporation front. In that case, the soil had two different values of moisture content: one

Figure 4-2. Comparison between analytical heat solution and the ODH results

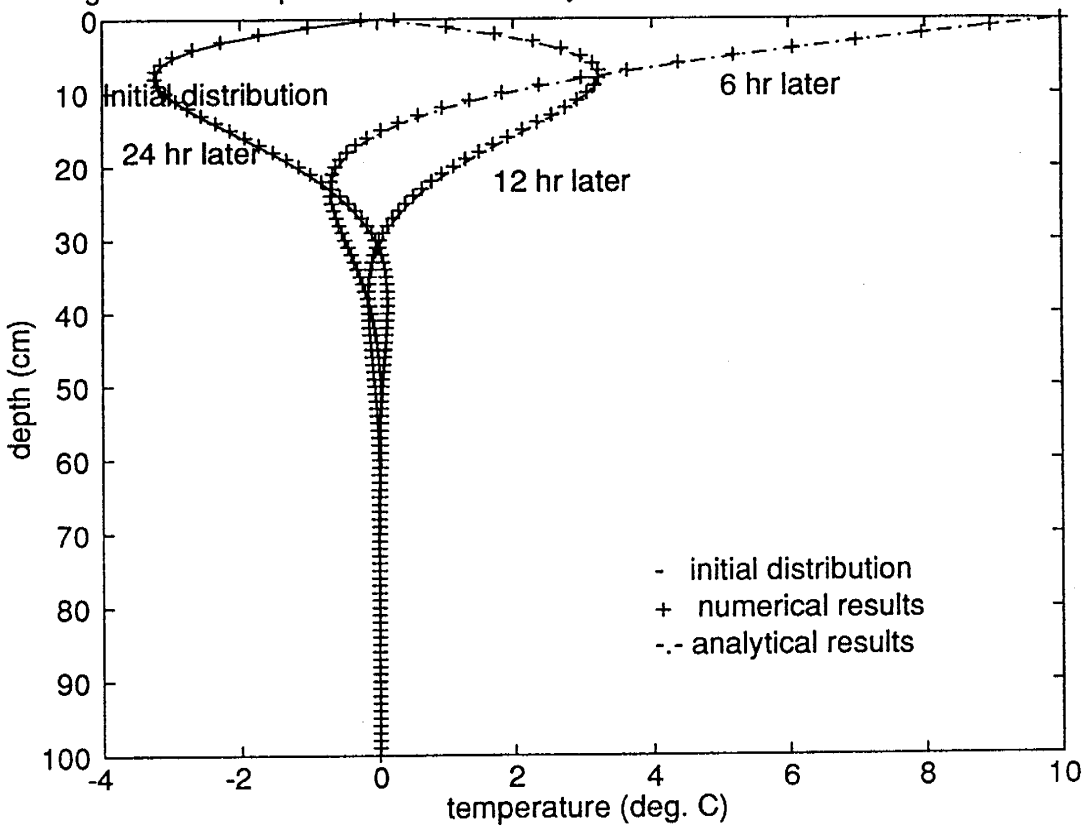

low value above the evaporation front, and another high value below the evaporation front. This physical model is realistic only as an approximation since water would actually flow downward under a gravitational gradient in the case of a uniform moisture content.

To test the performance of the one-dimensional isotope block ODI under nonsteady-state conditions the two-zone model was considered. Similar to Figure 2-3 a case was considered in which the moisture content above the evaporation front has uniform value θ_o and below the evaporation front the distribution is linear in all times, i.e.,

$$\begin{aligned} \theta(z,t) &= \theta_o && z<z_{ef} \\ &= \theta_o + S(z-z_{ef}(t)) && z \geq z_{ef} \end{aligned} \qquad (4\text{-}9)$$

where S is the slope of the moisture linear distribution given by

$$S = \frac{\theta_b^i - \theta_o}{z_b - z_{ef}^i} \qquad (4\text{-}10)$$

In which θ_b^i is the initial moisture content at the bottom of the solution domain, and z_{ef}^i is the initial depth of the sharp evaporation front.

In the following example, $\theta_b^i = 0.1051$, $\theta_o = 0.05$, $z_b = 110.0$ cm, and $Z_{ef}^i = 2.0$ cm. This will result in a value of $\theta_b = 0.1$ when $z_{ef} = 12.0$ cm, which is the moisture distribution used in Figure 2-3 and the final distribution the model should achieve if the final steady-state evaporation rate is similar to that used in Figure 2-3. The initial isotope profile was determined using the steady-state isotope code which was used to produce Figure 2-3. The hydraulic parameters used here are the same as those used in the simulation shown in Figure 2-3. In order to obtain a final steady-state evaporation rate

similar to that used for Figure 2-3, the evaporation rate was assumed to decrease according to

$$E_{ef}(t) = \left(E_{ef}^{i} - E_{ef}^{f}\right)\exp(-\Lambda t) + E_{ef}^{f} \qquad (4\text{-}11)$$

where E_{ef}^{i} is the initial steady-state evaporation rate, E_{ef}^{f} is the final steady-state evaporation rate, and Λ is a decay factor. The values used for these parameters were 0.2908 mm/day, 0.055 mm/day, and 0.0449/day respectively.

The net evaporation rate at any time t is defined as the difference between the evaporation rate at the evaporation front and the upward liquid flux at the bottom of the solution domain, i.e.,

$$E_{net}(t) = E_{ef}(t) - E(z_b,t) \qquad (4\text{-}12)$$

The upward water flux at the bottom of the profile $E(Z_b,t)$ is assumed to equal E^{f}_{ef}. Thus, eqn.(4-12) after substituting eqn.(4-11) can be rewritten as

$$E_{net}(t) = \left(E_{ef}^{i} - E_{ef}^{f}\right)\exp(-\Lambda t) \qquad (4\text{-}13)$$

From eqn.(4-9)

$$\frac{d\theta}{dt} = -S^{i}\frac{dz_{ef}}{dt} \qquad z \geq z_{ef} \qquad (4\text{-}14)$$

Combining eqn.(M-22) and eqn.(4-14)

$$\frac{dE}{dz} = -S^{i}\frac{dz_{ef}}{dt} \qquad z \geq z_{ef} \qquad (4\text{-}15)$$

The upward water flux E at any depth is given by

$$\begin{aligned} E(z,t) &= E_{ef}(t) && z<z_{ef}(t) \\ &= E_{ef}(t)+\frac{dE}{dz}\left[z-z_{ef}(t)\right] && z\geq z_{ef}(t) \end{aligned} \tag{4-16}$$

From which the net evaporation rate, as defined by eqn.(4-12) can be written as

$$E_{net}(t) = -\frac{dE}{dz}\left[z_b - z_{ef}(t)\right] \tag{4-17}$$

The downward progress of the evaporation front Δz_{ef} (after time increment Δt) can be determined by equating the right hand sides of equations (4-13) and (4-17) and then substituting (4-15) for *dE/dz*, i.e.,

$$(E_{ef}^{i} - E_{ef}^{f})\exp(-\Lambda\, t) = S^{i}\left[z_b - z_{ef}(t)\right]\frac{\Delta z_{ef}}{\Delta t} \tag{4-18}$$

This equation can be solved explicitly for Δz_{ef}. The new value for the depth of the evaporation front is determined by incrementing the current value by Δz_{ef}.

Figure 4-3 shows the history of the evaporation rate, as calculated using eqn.(4-11), and the corresponding relation obtained for the depth of evaporation front, as calculated numerically by eqn.(4-18). The isotope enrichment was calculated via eqn (23) (in Chapter 3) using $\omega_2=0.5$, which is the weight factor for Crank-Nicholson scheme. The isotope profiles as well as the moisture distributions are depicted in Figure 4-4 for times 10 days, 25 days, 83 days, and 417 days. The isotope enrichment maximum recedes deeper in the profile with time until a hydraulic steady-state moisture distribution is achieved. Penetration of the evaporation front and change in the moisture distribution is

Figure 4-3. History of evaporation rate and evaporation front depth

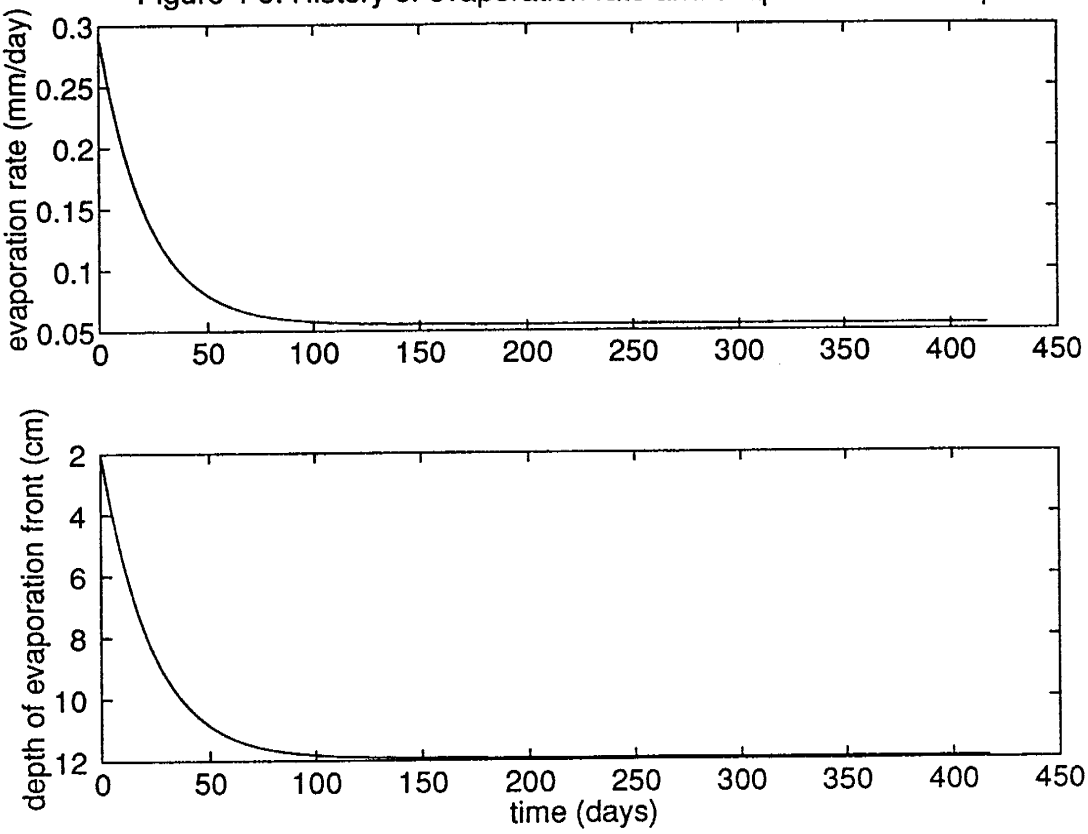

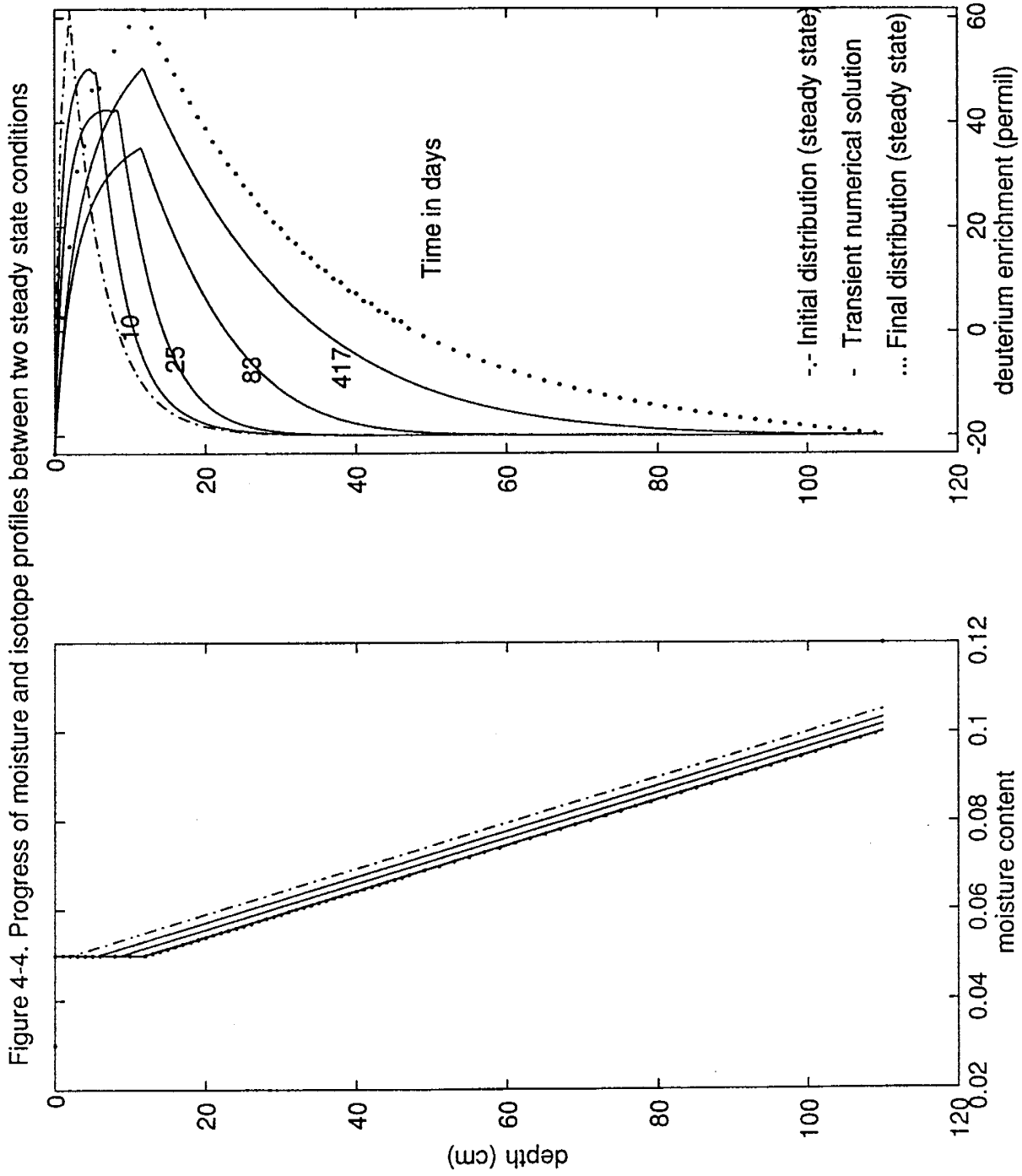
Figure 4-4. Progress of moisture and isotope profiles between two steady state conditions
depth (cm)
moisture content
deuterium enrichment (permil)
Time in days
10
25
88
417
-.- Initial distribution (steady state)
- Transient numerical solution
... Final distribution (steady state)

very minimal after 83 days. The assumption of a hydraulic steady-state condition is therefore justified after this time. The isotope profile at 83 days is, however, still very different from the final steady-state isotope profile. The isotope peak is less enriched than the final evaporation front enrichment (which should be similar to the initial value for this example of constant atmospheric parameters). At 417 days, more enrichment is seen and the profile is more shifted toward the final steady-state profile. The progression of the isotope profile and eventual matching of the appropriate steady-state condition suggests that the transient isotope block is working properly and can be applied to the study of changes in isotope profiles during nonsteady-state conditions. Following is another test of the isotope block for its performance in simulating solute transport under saturated conditions.

4.4 *Nonvolatile Solute Transport*

For saturated flow, $D^{v^*} = 0$ (see eqn. M-2) , and consequently $D_i^{RV} = 0$ (see eqn. I-13). Thus, the total isotope diffusion coefficient reduces to the diffusion coefficient in the liquid phase, i.e., $D_i = D_i^*$. For saturated flow, the moisture content θ equals the porosity n and thus D_i^* is constant and eqn. (I-25) reduces to

$$\frac{\partial \delta}{\partial t} = - v \frac{\partial \delta}{\partial z} + D \frac{\partial^2 \delta}{\partial z^2} \qquad (4\text{-}19)$$

where $v = -E/n$ and $D = D_i^*/n$. The subscript i for the isotopic species in δ was dropped for convenience and δ can be the concentration or the relative concentration of the solute such as the relative isotopic enrichment. This equation is the well-known advection-diffusion equation which describes the transient solute concentration distribution in a soil

column where water flow is in steady state condition [Van Genuchten and Wierenga, 1986]. Lapidus and Amundson [1952] presented analytical solution for the following conditions:

Initial condition: $\delta(0,z) = \delta_\varepsilon$

Boundary conditions: $\delta(t,0) = \delta_0$ and $\partial\delta/\partial z \,|_{z=L} = 0$

Peclet number $P = vL/D$ is large (i.e., $P > 10$) where L is the length of the soil column.

Their analytical solution is

$$\delta(t,z) = \delta_\epsilon + (\delta_o - \delta_\epsilon)\left(\frac{1}{2}\ erfc\left[\frac{z-vt}{2(Dt)^{1/2}}\right] + \frac{1}{2}\ \exp\left(\frac{vz}{D}\right)\ erfc\left[\frac{z+vt}{2(Dt)^{1/2}}\right]\right) \qquad (4\text{-}20)$$

Comparison between the analytical solution, given by eqn. (4-20), and the numerical solution given by the one-dimensional isotope block for the advection-dispersion equation, (4-19), is given in Figure 4-5. In the numerical solution, a Crank-Nicholson scheme for time was used ($\omega_2 = 0.5$). The values used for time increment Δt, depth increment Δz were .05 hr and .05 cm, respectively. The values used for velocity v, and porosity n were 0.0891 cm s^{-1} and 0.35, respectively. This corresponds to $E = -0.0312$ cm s^{-1} where 0.0312 is a reasonable value for the saturated hydraulic conductivity. The value used for the diffusion coefficient D was 2×10^{-5} $cm^2\ s^{-1}$ which corresponds to $D_i^* = 7 \times 10^{-6}$ $cm^2\ s^{-1}$ which is reasonable for oxygen-18. The length of the soil columns L is 10 cm giving a peclet number of 4.4×10^4. The numerical and analytical solutions agree closely.

Figure 4-5. Comparison between ODI numerical results and the analytical solution for the advection-dispersion equation

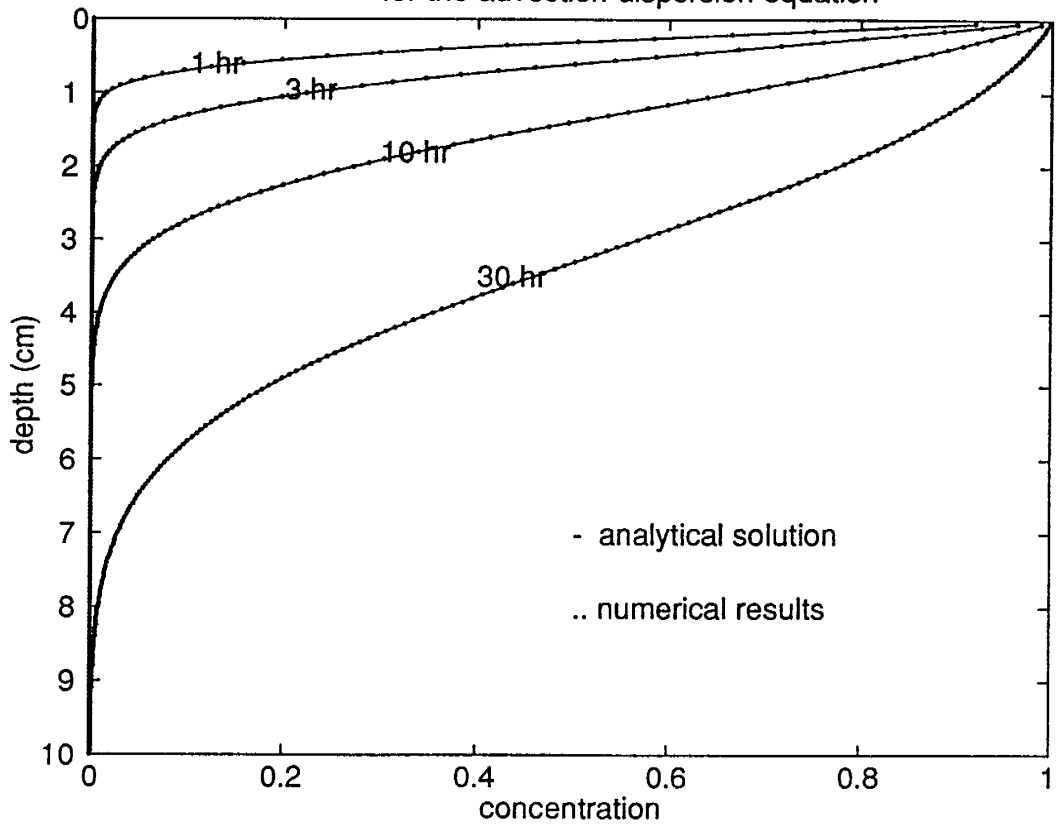

5. Methods

5.1 *Data Requirements for the Transient Model*

Collection and analysis of a comprehensive set of field data is important for this study, both to provide a basis for verifying the accuracy of the simulation model and to provide the physically accurate and defensible data needed to evaluate flow mechanisms. Experimentally-determined input data required for the simulation model include temperature and relative humidity values at the surface, the initial depth distributions of temperature, moisture content, and isotopic enrichment. For further testing of the computer code in predicting the depth distributions of temperature, moisture content, and isotopic enrichment at the end of any simulation period, the values of these variables as observed at the end of the simulation period are required. A controlled field experiment was designed and conducted to provide the data basis for further testing of the numerical model. The simulations carried in this study focus on the top 1 m of the soil which represents the depth of soil most affected by daily variation in temperature and is also the active zone in terms of evaporation and the associated isotopic enrichment. The parameters required for the model are porosity and moisture content at liquid discontinuity. The relations required are retention relation, unsaturated hydraulic conductivity function, and thermal conductivity relation.

5.2 *Controlled Field Experiment*

Sevilleta dune sand (taken from the Sevilleta National Wildlife Refuge 20 km north of Socorro, New Mexico) was the porous medium used in this experiment. Eleven PVC columns, each 105 mm in diameter and 2.0 m in length, were packed with air dry soil.

Sand was added in depth intervals of approximately 50 mm and compacted by tapping the base of the column after each addition. Each column had about 100 mm of gravel at the base to allow free drainage of water. The average dry bulk density of sand in columns was 1.550 g/cm^3. In one of these columns, temperature probes were installed at depths of 2.0, 4.0, 10.0, 22.2, 27.7, 42.2, 82.0, and 148.0 cm below the soil surface. About 2.5 pore volumes of tap water, having an isotopic composition of δ^2H=-97.7 permil, $\delta^{18}O$= -11.6 permil vs Standard Mean Ocean Water (SMOW), were run through each of the columns, then the columns were covered and allowed to drain for 24 hours. Thereafter, the columns were sealed from the bottom and each weighed. Tap water was used as the standard instead of SMOW throughout the simulations. The values used for the atmospheric water vapor were δ^2H=-82.2 and $\delta^{18}O$=-15.10 permil vs. tap water. These values were obtained from the minimum soil water isotopic composition at the surface and the fractionation factor at 25 °C .

In the field, a drilling rig was used to auger eleven holes to host the experimental columns. The columns were lowered into the holes (with soil added in the hole assuring that contact was made between the PVC pipe and the native soil) until the depth of soil in the column was similar to that of native soil outside the column. One column was lowered in a hole without a contact with the native soil. If sampled at the same time, comparison between the moisture and isotope profiles in this column and a second column in contact with the native soil would give an idea of the importance of this procedure.

A probe which measures temperature and relative humidity was placed on the ground surface to establish the top boundary condition for the model. All eleven columns

Figure 5-1. Observed relative humidity and temperature at the soil surface

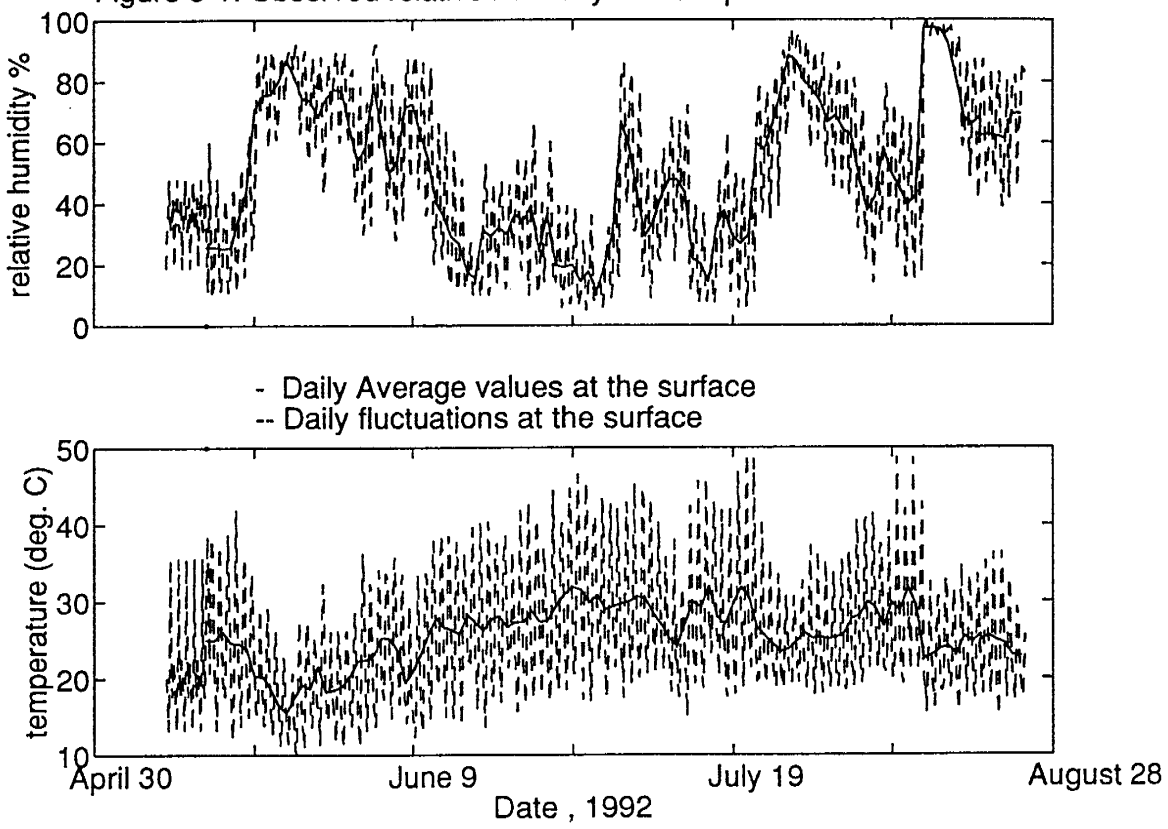

Figure 5-2. Daily average temperature distribution in the soil profile

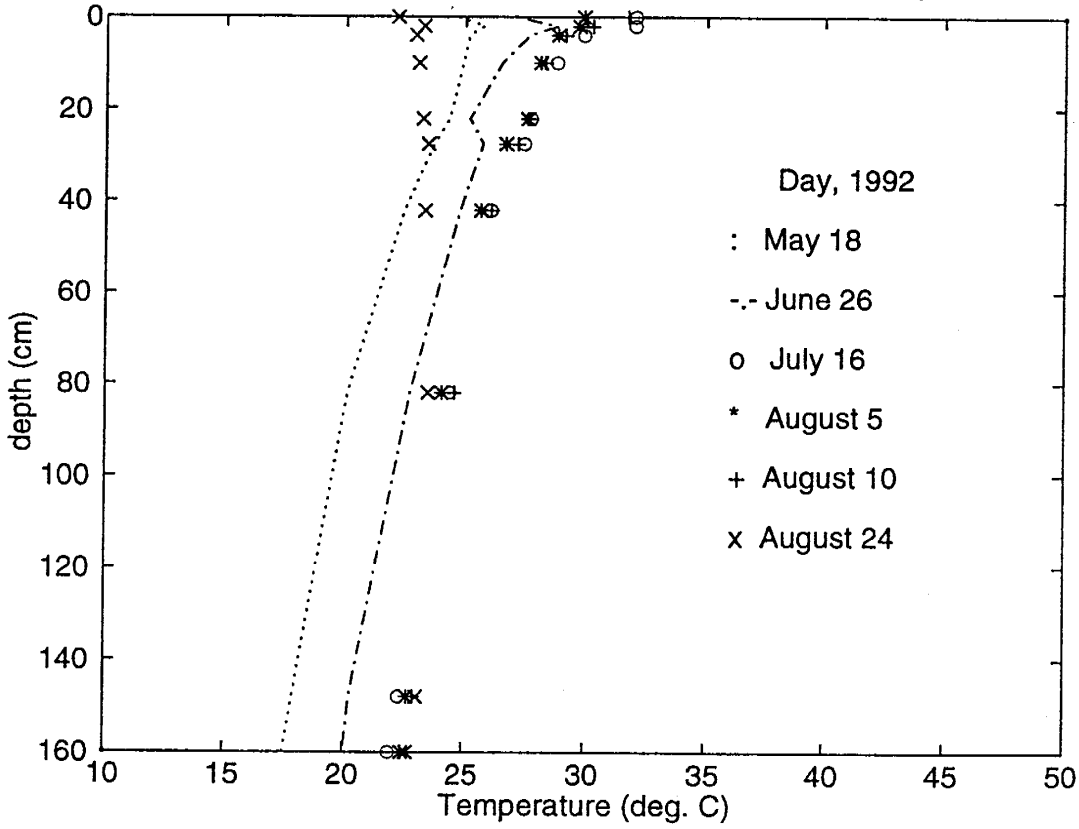

were placed in a line. The temperature probes buried in the soil at different depths were connected to a Campbell CR7 data logger programmed to automatically take readings every 3 hours. Figure 5-1 shows the observed relative humidity and temperature at the soil surface. Figure 5-2 shows the daily average temperature distribution in the soil profile.

A wooden structure carrying a 1.5 m high inclined cover made of fiberglass screen served to keep the soil columns free from any input water (e.g., rain) unaccounted for in the simulation runs. The columns were allowed to evaporate for up to 108 days. At sampling times, a fork lift facilitated pulling the columns from the ground. A column was sampled destructively at each of 1, 10, 49, 69, 89, 94, and 108 days after evaporation started. On day 89 two columns were sampled; one column in contact with the native soil and the column that was left in the open hole (no contact with the native soil) and 81 mm of water was added to the remaining columns. Two columns were sampled 5 and 19 days later. Unfortunately, the last three columns in the ground were flooded with rain water and thus could not be used in the analysis. After a column was removed, samples of soil (for water content and isotopic analysis) were collected by first sectioning the PVC tube into 4 pieces and then taking samples, from the PVC tube pieces, at 20 mm intervals near the surface (where rapid change in the isotopic and moisture profiles was expected) and at 180 mm depth intervals where little change was expected. Soil samples were stored in air-tight jars. Approximately half of each sample was used for soil water extraction for determination of the moisture content and the isotopic composition; the remaining soil in the jar was kept for possible repeat measurements.

5.3 *Laboratory Procedures*

Porosity, dry bulk density, and saturated hydraulic conductivity were measured using standard techniques. The estimated values of these parameters were 0.351, 1.554 g/cm^3, and 0.0132 cm/sec, respectively. The measured retention relation $\Psi(\theta)$ for the soil (Figure 5-3a) was determined by using the filter paper method to determine the matric head for a soil in contact with the filter paper following the procedures of Fawcett and Collis-George [1967]. McCord [1989] used a hanging column apparatus to measure the hysteristic retention relation for the same Sevilleta soil. Based on seven cores he presented the hanging column data given in Figure 5-3a for the average drying retention relation. The hanging column data set and the filter paper data set show very similar trends but the hanging column matric heads are systematically slightly more negative than the filter paper heads. The difference between these two data sets may be attributed to two things. First, in the filter paper method, a disturbed soil sample is used while for the hanging column apparatus a non disturbed sample was used. Second, McCord derived his relation from seven cores while one set of data was used here, for the filter paper method. The moisture content of importance in this study, where the soil profile is drying, is generally lower than the moisture range measure by the hanging column experiment. The filter paper method was employed because it provides a wider range of moisture content for the retention relation.

Using the Van Genuchten fitting parameters from the retention relation and the measured value of the saturated hydraulic conductivity, the unsaturated hydraulic conductivity function $K(\theta)$ was determined (Figure 5-3b) from the Van Genuchten

Figure 5-3a. Retention curve

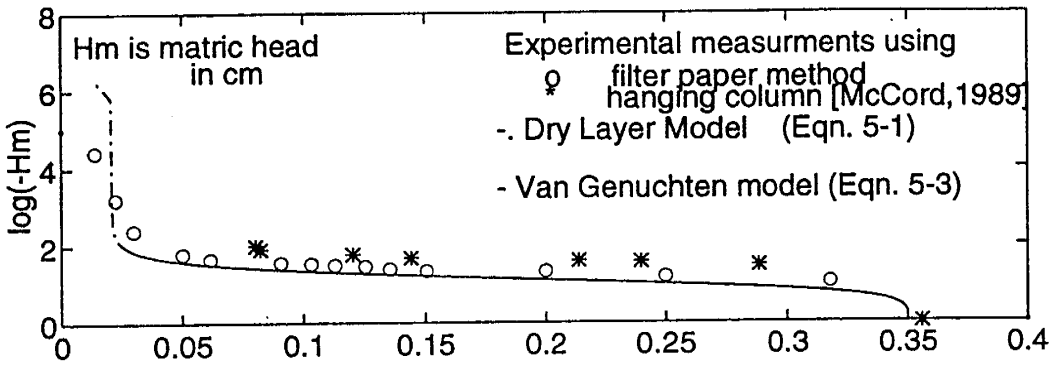

Figure 5-3b. Hydraulic conductivity function

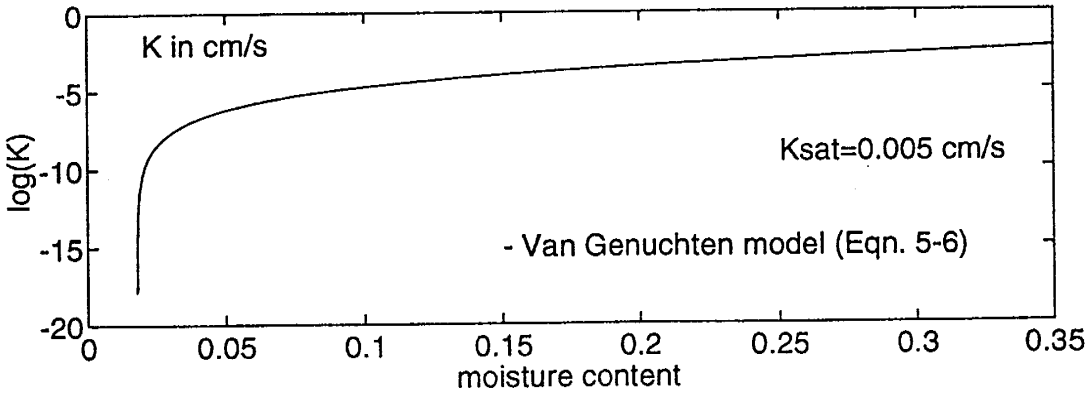

Figure 5-4. Size distribution of soil grains

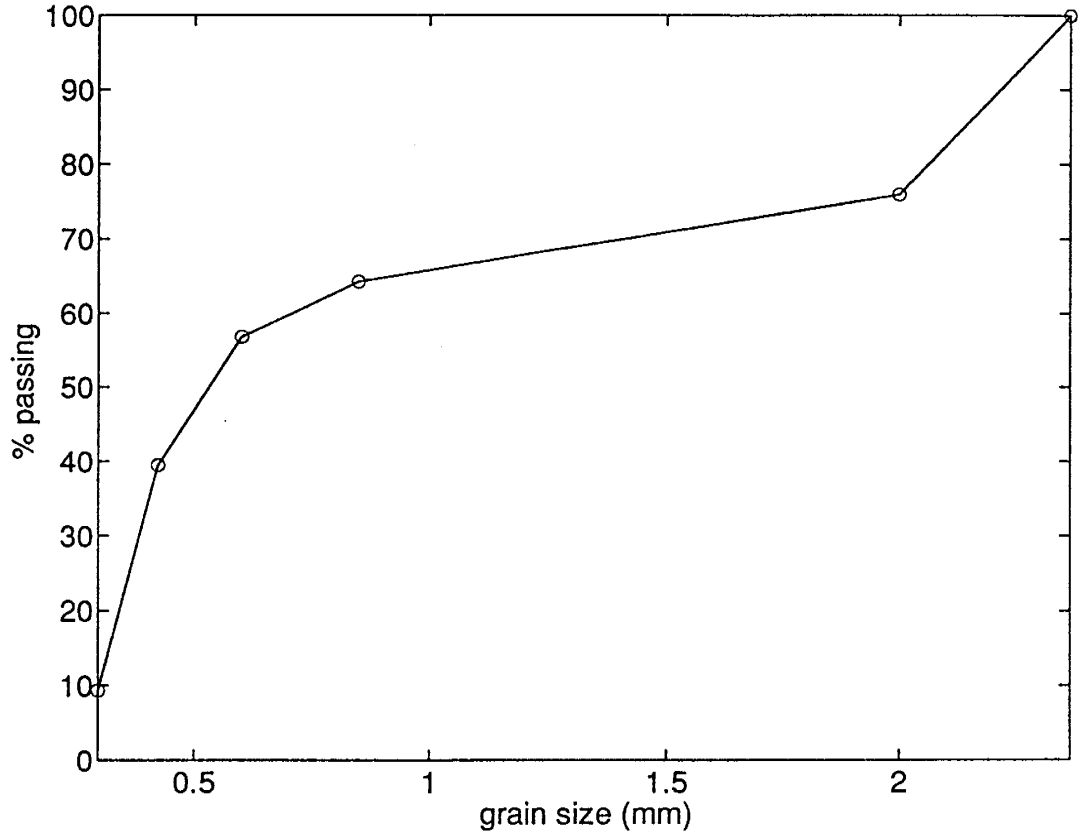

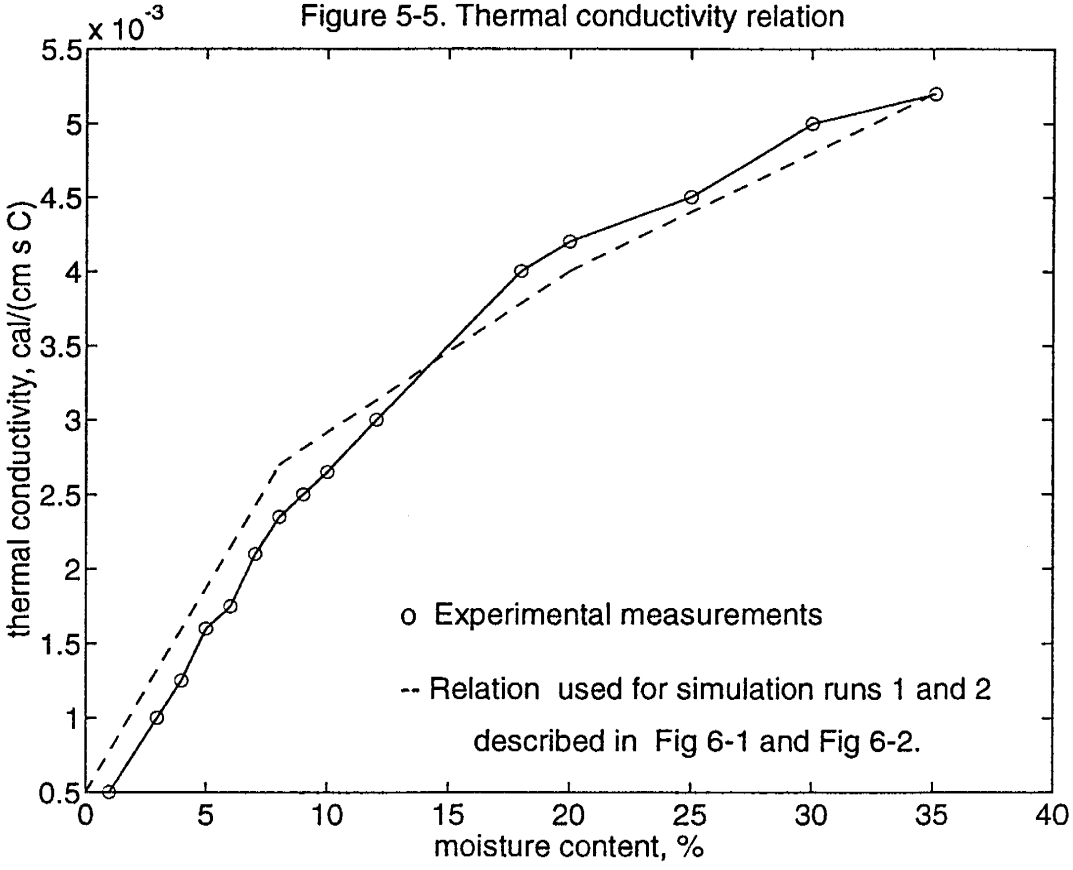

Figure 5-5. Thermal conductivity relation

hydraulic conductivity model. Section 5.5 below describes the mathematical model used for the retention relation and the hydraulic conductivity function which are applicable for soils ranging from air dry to saturated. The particle size distribution was obtained using sieve analysis (Figure 5-4). The soil is a fairly homogeneous, clean, coarse sand. The thermal conductivity relation $\lambda(\theta)$ was adapted from Knowlton [1989] for dune sand taken from the same area (see Figure 5-5). He measured the thermal conductivity for the soil using a cylindrical source thermal conductivity probe following the procedure of De Vries and Peck [1958].

Water from the soil was extracted by vacuum distillation following the procedure described by Knowlton [1989]. Moisture content was determined from weight loss of soil during distillation. To measure the $\delta^{18}O$ value of soil water, 0.5 ml of the distillate was equilibrated with CO_2 gas following the procedure outlined by Roether [1970]. The equilibrated CO_2 gas was analyzed for isotopic composition using a Finnegan-MAT Delta E mass spectrometer. The value of $\delta^{18}O$ (oxygen-18 isotopic composition) of the water was calculated based on mass balance of this isotope in the CO_2-H_2O mixture during equilibration. To determine the δ^2H (deuterium isotopic composition) of the water, a zinc reduction technique was employed to generate hydrogen gas from the water sample [after Kendall and Coplan, 1985; Coleman et al., 1982] which was then analyzed using the mass spectrometer.

Figure 5-6 depicts the development of oxygen-18 isotope profile in all soil columns throughout the evaporation period. Figure 5-7 shows the moisture distribution and oxygen-18 enrichment for the two columns that were sampled 89 days after the start of

the experiment. These two columns were left under different conditions; one column was in contact with the native soil (like all other columns) and the other column was left without contact with the soil.

5.4 *Moisture Content at Liquid Discontinuity*

The moisture content at liquid discontinuity was discussed but never quantified by Philip and de Vries [1957]. Gee [1966] determined the value of this parameter by looking at plots of the moisture distribution in soil columns, and he identified the value where $|\partial\theta/\partial z|$ is maximum as the moisture content at liquid discontinuity. Given the uncertainty involved in the measurement of moisture content at low values this method can be only approximate. In this study a new approach is presented where the isotope profiles instead of moisture distributions are used to determine the value of moisture content at liquid discontinuity. This value is a characteristic property of a given porous medium and should be a constant for this homogeneous soil. For drying soils, liquid discontinuity breaks at the evaporation front. The location of the evaporation front is often determined from the depth of the maximum isotope enrichment in isotope profiles. Figure 5-8 shows the isotope enrichment vs. moisture content for all experimental columns regardless of evaporation period. The maximum enrichment always occurs at the same value of moisture content which is the moisture content at liquid discontinuity as recognized by the theory of Philip and de Vries. Using this figure, the value of moisture content at liquid discontinuity was determined to be 2.4% which is the value corresponding to the maximum isotopic enrichment.

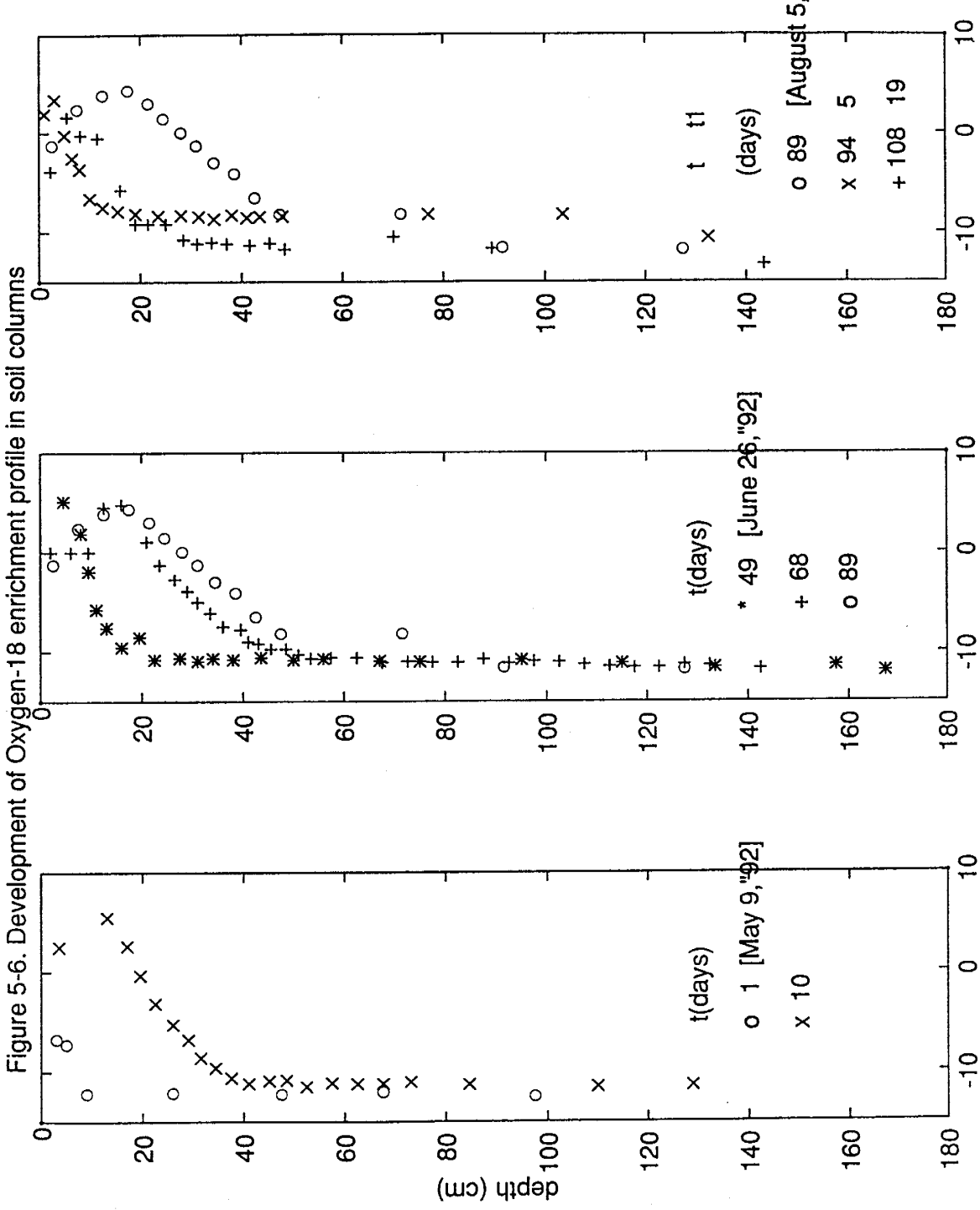

Figure 5-6. Development of Oxygen-18 enrichment profile in soil columns

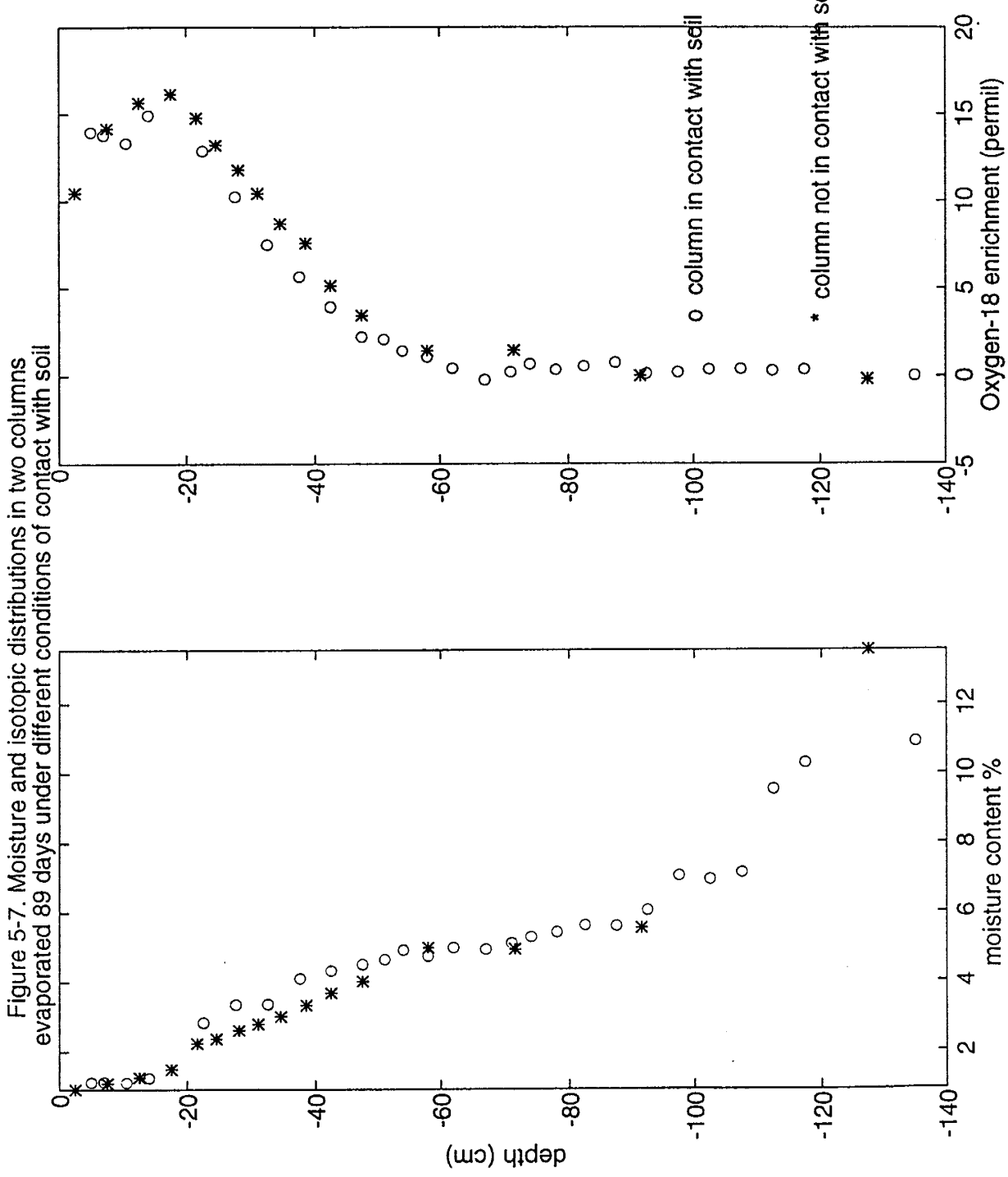

Figure 5-7. Moisture and isotopic distributions in two columns evaporated 89 days under different conditions of contact with soil

Figure 5-8. Oxygen-18 enrichment vs. moisture content

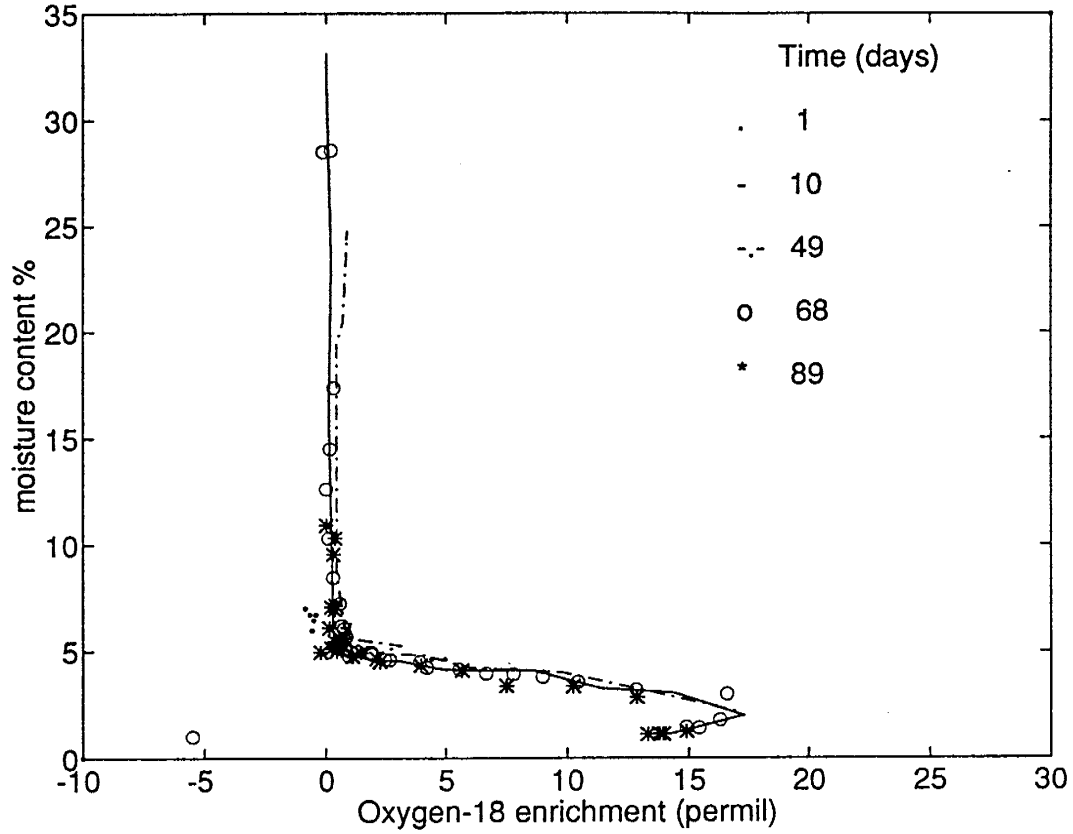

5.5 *Retention Relation and Hydraulic Conductivity Function*

The portion of the retention relation for moisture content less than the moisture content at liquid discontinuity ($\theta_{rl} \leq \theta \leq \theta_{wk}$) should be determined in a way that reflects the fact that it is a zone of vapor diffusion to the atmosphere. The matric head in this zone was calculated using

$$\psi(\theta) = \beta_1 \ln \left[\alpha_1 + S_{el}(h_{wk} - \alpha_1)\right] \tag{5-1}$$

in which β_1 and α_1 are fitting parameters and h_{wk} is the relative humidity of a soil at the depth of the evaporation front (which is located from the moisture content where liquid continuity breaks). The value of h_{wk} (corresponding to $\Psi(\theta_{wk})$ which is calculated from Van Genuchten model, eqn. 5-3 below) is calculated using eqn. (M-5) . In eqn. (5-1), S_{el} is given by

$$S_{el} = \frac{\theta - \theta_{rl}}{\theta_{wk} - \theta_{rl}} \tag{5-2}$$

where θ_{rl} is the minimum moisture content observed at the soil surface under natural conditions. Looking at the similarity between eqn. (5-1) and the Kelvin relation (eqn. M-5) which is the basis for the vapor flow formulations presented earlier in Chapter 2, the value of β_1 should be close to {RT/g} and the value of α_1 should be close to the minimum atmospheric relative humidity in the study area or smaller.

The wet portion of the retention relation ($\theta_{wk} \leq \theta \leq n$) is given by the Van Genuchten model

$$\psi(\theta) = -\frac{1}{\alpha_2}[(S_{e_2})^{-\frac{1}{\gamma}} - 1]^{\frac{1}{\beta}} \tag{5-3}$$

where S_{e2} and γ are given by the relations

$$S_{e2}=\frac{\theta-\theta_{r2}}{n-\theta_{r2}} \tag{5-4}$$

$$\gamma=1-\frac{1}{\beta} \tag{5-5}$$

In the above relations $\theta_{r1} \le \theta_{r2} \le \theta_{wk} \le n$.

The hydraulic conductivity function used is given by

$$\begin{aligned} K &= 0 && \theta<\theta_{wk} \\ K &= K_s\, S_{e2}^{1/2}\left[1-(1-S_{e2}^{1/\gamma})^{\gamma}\right]^2 && \theta>\theta_{wk} \end{aligned} \tag{5-6}$$

where K_s is the saturated hydraulic conductivity. Practically the only fitting parameters in these relations are those of the Van Genuchten model, namely θ_{r2}, α_2, and β_2. Figure 5-3 given earlier shows the experimental retention relation, the retention relation given by the model presented above (as used in the validation runs) and the unsaturated hydraulic conductivity. Values used to produce these relations were $\alpha_1=.2$, $\theta_{r1}=1.3\%$, $\theta_{r2}=2.1\%$, $\theta_{wk}=2.4\%$, $\alpha_2=.09$, $\beta_2=2.75$, and $K_s=.005$ cm/s.

5.6 *WIPP Site Field study*

5.6.1 *Precipitation and Chloride input*

The Waste Isolation Pilot Plant (WIPP) near Carlsbad in southeastern New Mexico

is located at about 32.5 °N and 104.5 °E. From precipitation records at the nearby airport over the years 1970 to 1987, the average annual precipitation was estimated at 380 mm. The average chloride input for this area was not available but this data was available for the surrounding areas. Precipitation chloride input for Las Cruces (32.5°N,105°E) is 0.35 mg/l and that of Socorro (34°N,106.8°E) is 0.375 mg/l [Phillips et al., 1988]. At the Hueco Bolson in West Texas (31°N,105°E), Scanlon reported a value of 0.29 mg/l [Scanlon, 1990]. Based on interpolation of chloride input for these areas, the average chloride input for the WIPP study area was estimated at 0.32 mg/l.

5.6.2 *Field Work and Procedures*

In the course of this project, five cores were hand augured from the WIPP site during the summers of 1991 and 1992. These holes were designated Hole 2 through Hole 6. Soil samples were taken at 5 cm depth intervals and sealed promptly in air tight jars. Preparation and analysis procedures for moisture content and isotopic enrichment are similar to the laboratory procedures for the controlled field experiment. The dry soil remaining after moisture extraction was used for chloride analysis. An ion-specific electrode was used to determine the chloride concentration in ppm.

5.6.3 *Geological Setting of Holes and Soil Profile*

The locations of holes were selected in different settings of the WIPP site. Hole2 2 was located at top of sand dunes. Hole 3 was located in a sink hole. This site was selected because personal observations indicated that large rainfall events leave standing

water at this sink hole. Thus, this site has a potential for high infiltration. Hole 4 was chosen based on well logs which showed unconsolidated sands to be about 20 meters providing the deepest unconsolidated sediments in the area. Hole 5 was chosen in a trough between dunes adjacent to Hole 2. The site of Hole 5 has a potential for infiltration induced by the topography. Hole 6 is typical of the WIPP environment containing grasses and mesquite in close proximity to the hole.

Vegetation in this area consists mostly of mesquite, and many roots were intercepted during auguring. The soil profile consists predominantly of pure medium sand with, in some holes, one or more thin clay layers.

6. Results and Discussion

6.1 *Transient Numerical Simulations*

6.1.1 *Sensitivity Analysis*

The relations and parameters which describe the soil under study are $\Psi(\theta)$, $K(\theta)$, $\lambda(\theta)$, n, τ^v, τ^l, and θ_{wk}. The transient water flow equation is most sensitive to the characteristic retention relation $\Psi(\theta)$ and hydraulic conductivity function $K(\theta)$. The heat transfer equation is sensitive to the thermal conductivity relation $\lambda(\theta)$. The isotope equation is sensitive to the temperature distribution (which depends on the thermal conductivity relation and temperature at the soil surface), to the atmospheric relative humidity, and to the retention relation and hydraulic conductivity function.

It is a common practice to adjust one or more of these relations and parameters, within their uncertainty limits, during simulation runs until a good match is achieved between model predictions and observations. This science and art procedure is often referred to as calibration. Other simulation runs may be used to validate the earlier choice of parameters. As mentioned above the value of θ_{wk} and the retention relation for the dry layer above the evaporation front (given by eqn. 5-1) were obtained from the experimental data and will be left fixed during the simulation exercises. None of the three governing equations is sensitive to porosity or tortuosity.

6.1.2 *Validation Runs*

Two simulation runs were used for validation of the model in its application to the controlled field experiment. The first run was for the 10-day period after the start of the experiment. The second run was for the period between 49 and 69 days after the start of

the field experiment. These runs will be referred to as Run 1 and Run 2, respectively. A linear relation was used for $\lambda(\theta)$ as given in Figure 5-5. A gravity drainage (zero matric head gradient) type of boundary condition was used for the water flow equation at the bottom of the solution domain. This boundary condition is appropriate for the soil columns and is reasonable for natural conditions.

In simulation Run 1, (see Figure 6-1), reasonable match in all measurable state variables of the model (moisture content, temperature, and oxygen-18 enrichment) were achieved by adjusting the thermal conductivity relation $\lambda(\theta)$, and using the hydraulic fitting parameters $\alpha_1 = 0.2$, $\theta_{r1} = 0.013$, $\theta_{r2} = 0.021$, $\theta_{wk} = 0.026$, and $\beta_2 = 2.85$. The observed distributions agree satisfactorily with the model-predicted distributions for moisture content, temperature, and isotope concentration.

In Run 2, the same relations and parameters used in Run 1 were used, and a satisfactory agreement was achieved between the observed distributions and the predicted distributions (see Figure 6-2). These simulation runs completed the model validation, started earlier by code testing, and proved that the model could simulate the main processes involved in water movement in the shallow unsaturated zone and the associated processes of isotope fractionation and transport.

6.1.3 *Development of Depth Distributions*

Figure 6-4 is presented for Run 1 (with 9-day average temperature and humidity at the surface) which shows the development in the depth distributions of moisture, temperature, oxygen-18 enrichment, relative humidity, water vapor flux and liquid flux. The initial distribution was that of a column sampled one day after evaporation started.

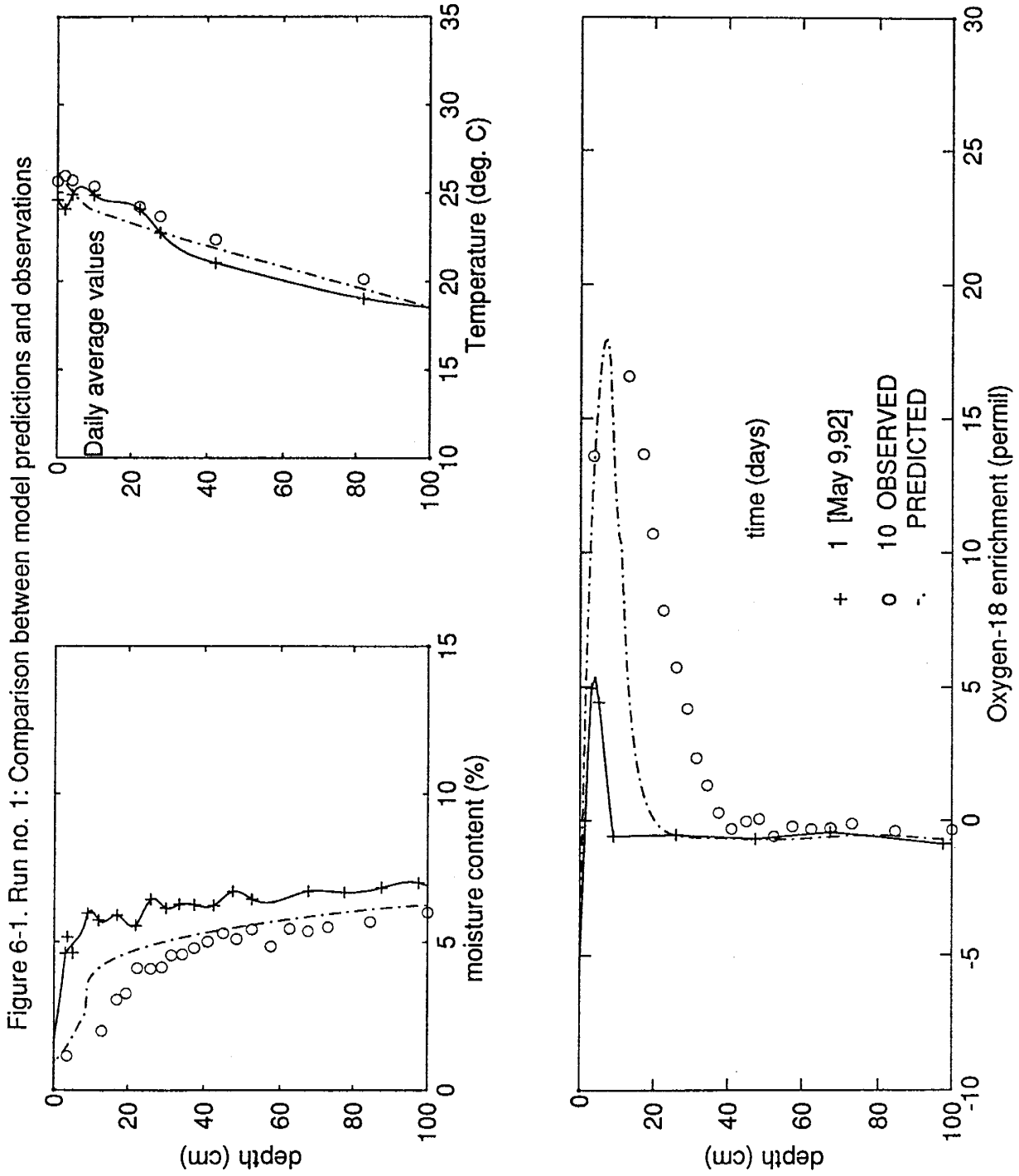

Figure 6-1. Run no. 1: Comparison between model predictions and observations

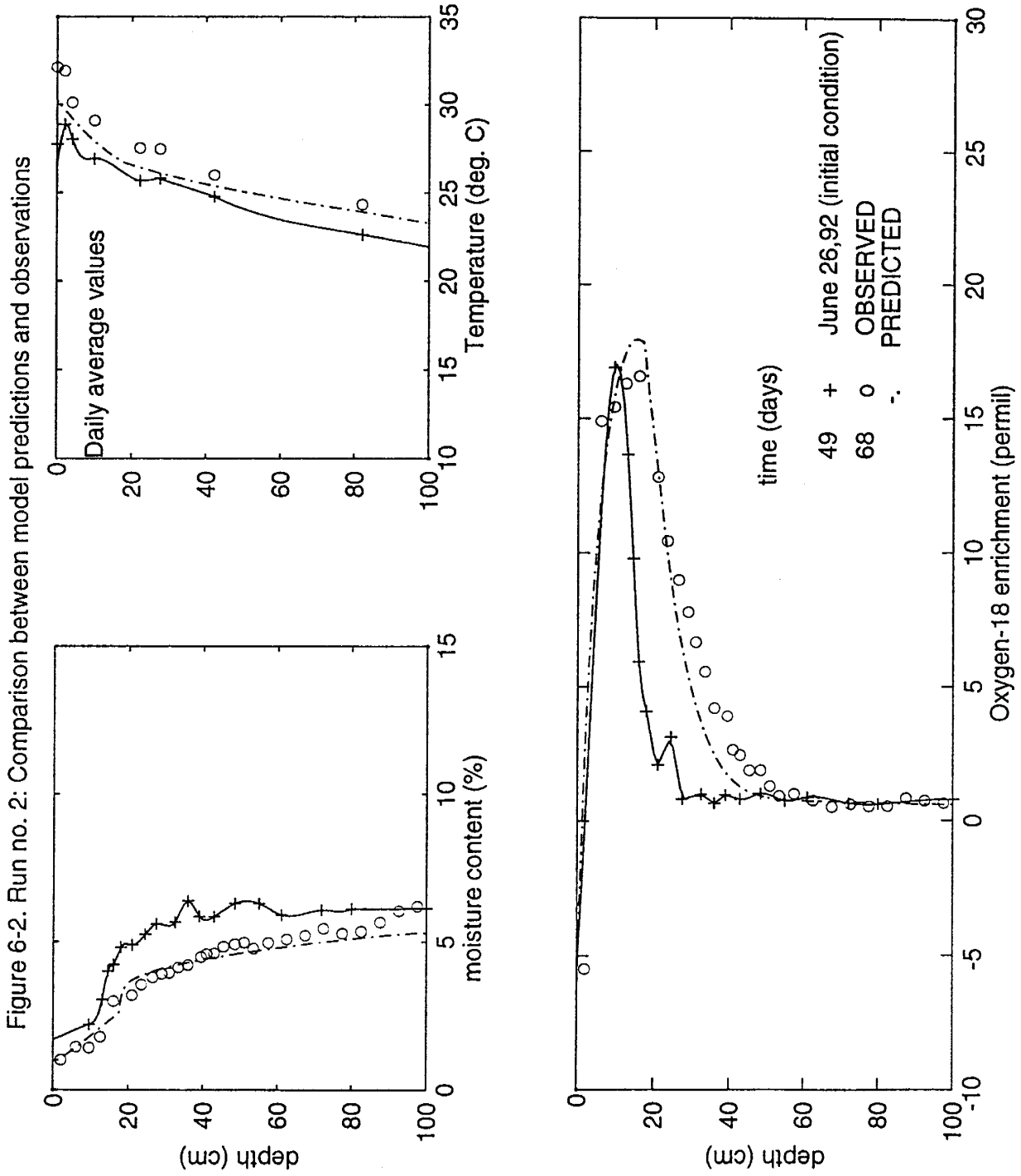

Figure 6-2. Run no. 2: Comparison between model predictions and observations

Figure 6-3. Typical numerical model predictions(.. initial, - after 48 hr, -. after 216 hr).

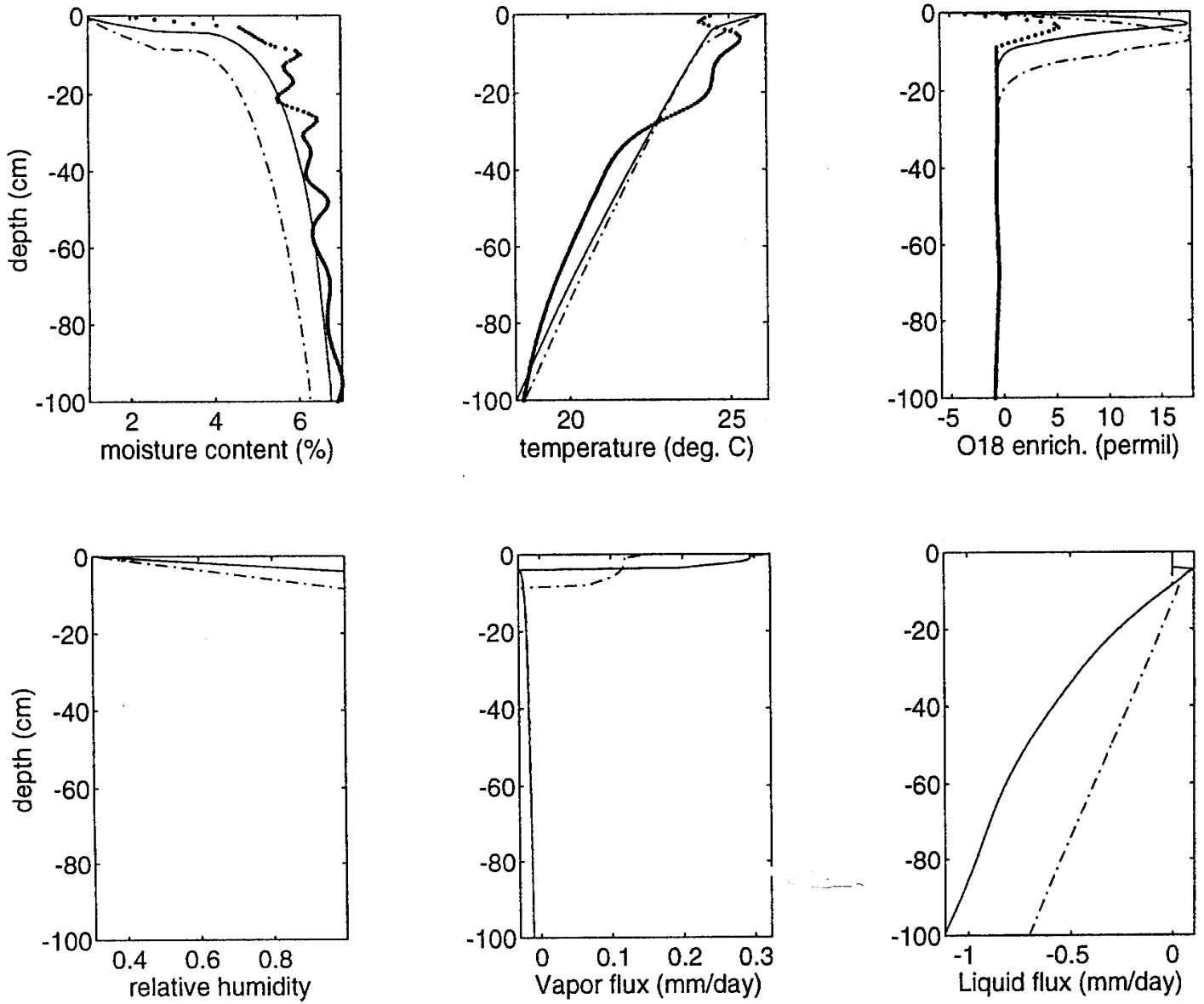

The distributions are given for 3 days later and 10 days after the start of the experiment. At the drying front (evaporation front) water is enriched in the heavy isotopes as a result of water evaporation and the resulting isotopic fractionation. Just below the evaporation front, there is a limited zone of relatively strong upward liquid flux. As time goes on, the drying front gets deeper in the soil profile, the evaporation rate decreases and also the downward liquid flux decreases.

The temperature gradient was 8 °C per meter in the top one meter. This temperature gradient causes part of the evaporated water to move downward below the evaporation front. However the scenario of a constant top boundary condition of temperature and relative humidity should be considered hypothetical. The value of the downward vapor flux is much smaller than the upward water vapor flux. The downward water vapor flux decreases with depth which means that part of this water is condensed on the soil. This downward water vapor movement and the consequent condensation is not sufficient to change the shape of the isotope profile. No local minimum was obtained in the isotope profile as a result of the condensation of the isotopically light water vapor that diffuses downward.

6.1.4 *Effect of Temperature and Humidity Diurnal Fluctuations*

Figure 6-5 shows, for simulation Run 1, the history of the evaporation rate and depth of the evaporation front during the 9-day period. Three different data levels were considered for comparison. In the first case the average temperature and humidity during the 9-day simulation period was used in the simulation. In the second case the record of average daily temperature and relative humidity was used. In the third case the daily

Figure 6-4. History of evaporation rate and depth of evaporation front

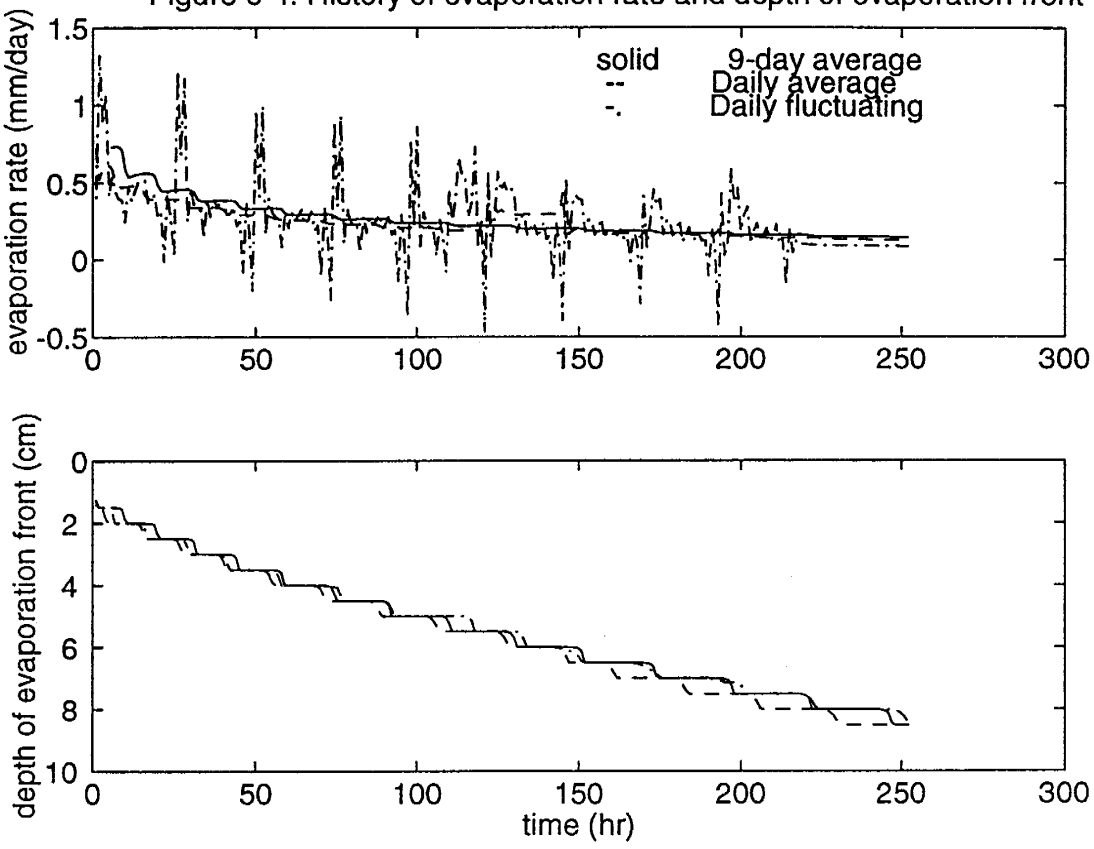

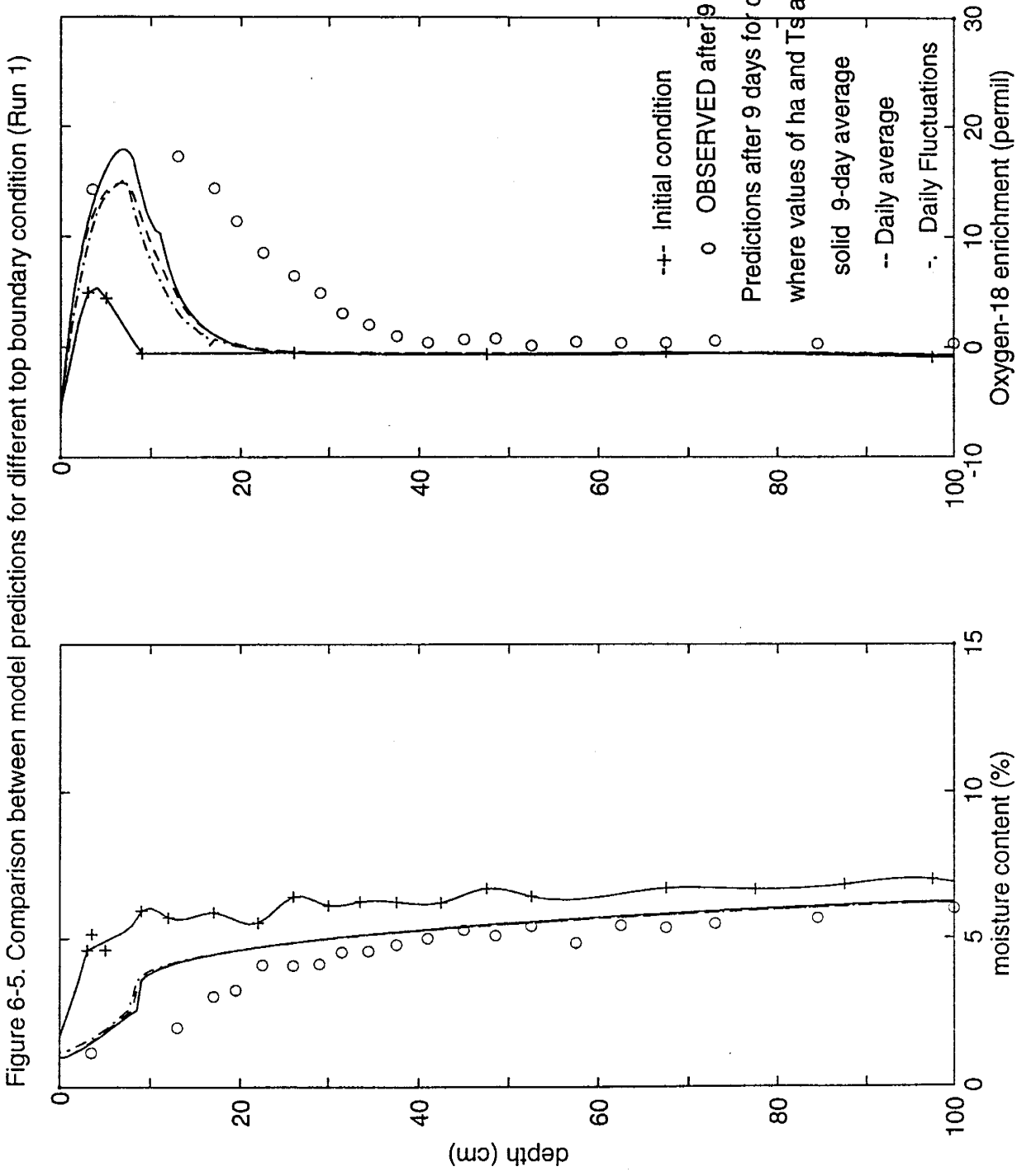

Figure 6-5. Comparison between model predictions for different top boundary condition (Run 1)

might be reasonable for continuous drying periods.

6.2 WIPP Site Profiles

Chloride concentration and isotopic enrichment of soil water and the corresponding volumetric water content of the soil as functions of depth for the WIPP site holes are presented in Figures 6-7 through 6-11. This section contains a discussion of the profiles from each hole in view of the developed theory and the knowledge gained from the simulations of the controlled field experiment.

Hole 2

In Hole 2 (Figure 6-7), the moisture content does not exceed 1.3% which is very low compared to the Sevilletta soil used in the experiment of this study. One reason might be that, in the field, vegetation is present and consequently there is water uptake by the roots and smaller amounts of moisture are left coating the soil grains. The lower moisture content might also be attributed to the grain size and retention characteristics of this soil. WIPP soil grains are smaller that the experimental (Sevilleta) grains. This means that, in WIPP soils, the water liquid continuity breaks apart at a lower moisture content. This is true since the moisture content that corresponds to the evaporation front in WIPP isotope profiles is 0.6% which is lower than the 2.4% observed in the Sevilleta soil. The absence of a clay binder or clay layers in the sand also explains the relatively low moisture content in Hole 2.

A slight bulge is observed in the moisture distribution between depths 25 and 60 cm. Corresponding to this bulge is a local minimum in the deuterium enrichment profile

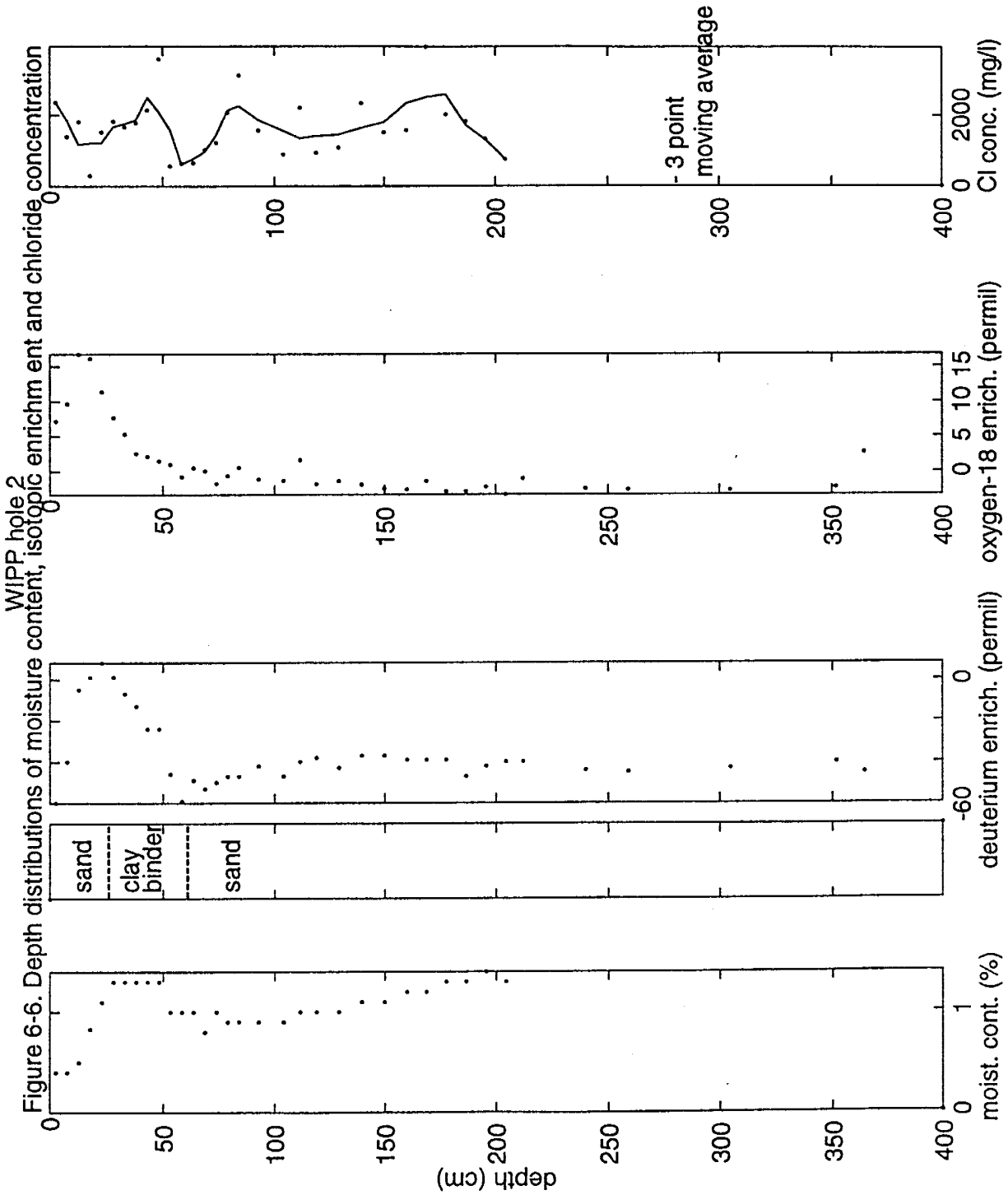

Figure 6-6. Depth distributions of moisture content, isotopic enrichm ent and chloride concentration

and chloride concentration profile. No minimum is observed in the oxygen-18 profile which makes the deuterium minimum questionable, especially that deuterium measurements for other holes were not reliable. The moisture bulge was small and cannot be explained as resulting from a recent rainfall event. The most likely explanation is that some clay binder exists at this depth.

The isotope maximum is obvious at depth 25 cm. During the summer, the atmospheric relative humidity in Socorro (in New Mexico) ranges between 10% and 90% with an average value of 50%. The air temperature at the soil surface ranges between 10°C and 42 °C with an average of 26 °C. Assuming that this is the case for WIPP area and based on Fick's Law of diffusion, the current depth of evaporation front, and the prevailing conditions of temperature and relative humidity, the evaporation rate ranges between 0.0044 mm/day and 0.0396 mm/day with an average value of 0.022 mm/day. This low evaporation rate is limited by the availability of water in the soil and the characteristic relations of the soil such as the retention relation, and the unsaturated hydraulic conductivity. The lower portion of the ^{18}O isotope profile is gradually decreasing with depth and the moisture content (also matric potential) increases with depth. The moisture distribution, with such low values, and isotope profile suggest that water is flowing upward in response to the potential gradient induced by evaporation. Upward water flow rates in the soil profile should be lower than the average evaporation rate for such a drying profile. The scatter in the chloride concentration may be attributed to analysis error. A continuous solid line was shown in the chloride concentration distribution to represent a 3-point moving average that may minimize the error and show

a clear trend in the concentrations.

Hole 3

Chloride concentration, moisture content, and isotope enrichment profiles for Hole 3 are given in Figure 6-8. The moisture content is as high as 3% which is higher than those of Hole 2. At 35 cm depth, some minor clay layer was encountered during drilling. Clay layers hold more water than sand. Therefore, higher moisture content in this soil profile than that for Hole 2 may be attributed to the presence of a clay layer at the bottom of the profile and possibly the presence of a protective clay layer at depth 35 cm, which partially delays the loss of water through the atmosphere by evaporation. The bottom clay (also low conductivity) layer delays downward water drainage and results in more water being available in the profile. The maximum isotopic enrichment, which identifies the evaporation front, occurs at a depth of 27 cm. The corresponding moisture content is 0.6%, similar to Hole 2, which should be the value of moisture content at liquid discontinuity θ_{wk}. Above the evaporation front and for moisture contents lower than θ_{wk}, soil water may be visualized as liquid "islands" linked by a vapor continuum. The relative humidity decreases linearly between the evaporation front and the surface. The lack of a distinct isotope minimum in the relatively high moisture content part of the profile also suggests that the water retained in the moisture content bulge is not from an isotopically light recent rain water but is indicative of a clay layer holding more water than the sand above and below the layer.

The chloride concentration distribution shows some variability, but also a bimodal distribution is identified, i.e., concentrations higher than 1000 mg/l above 2.0 m depth

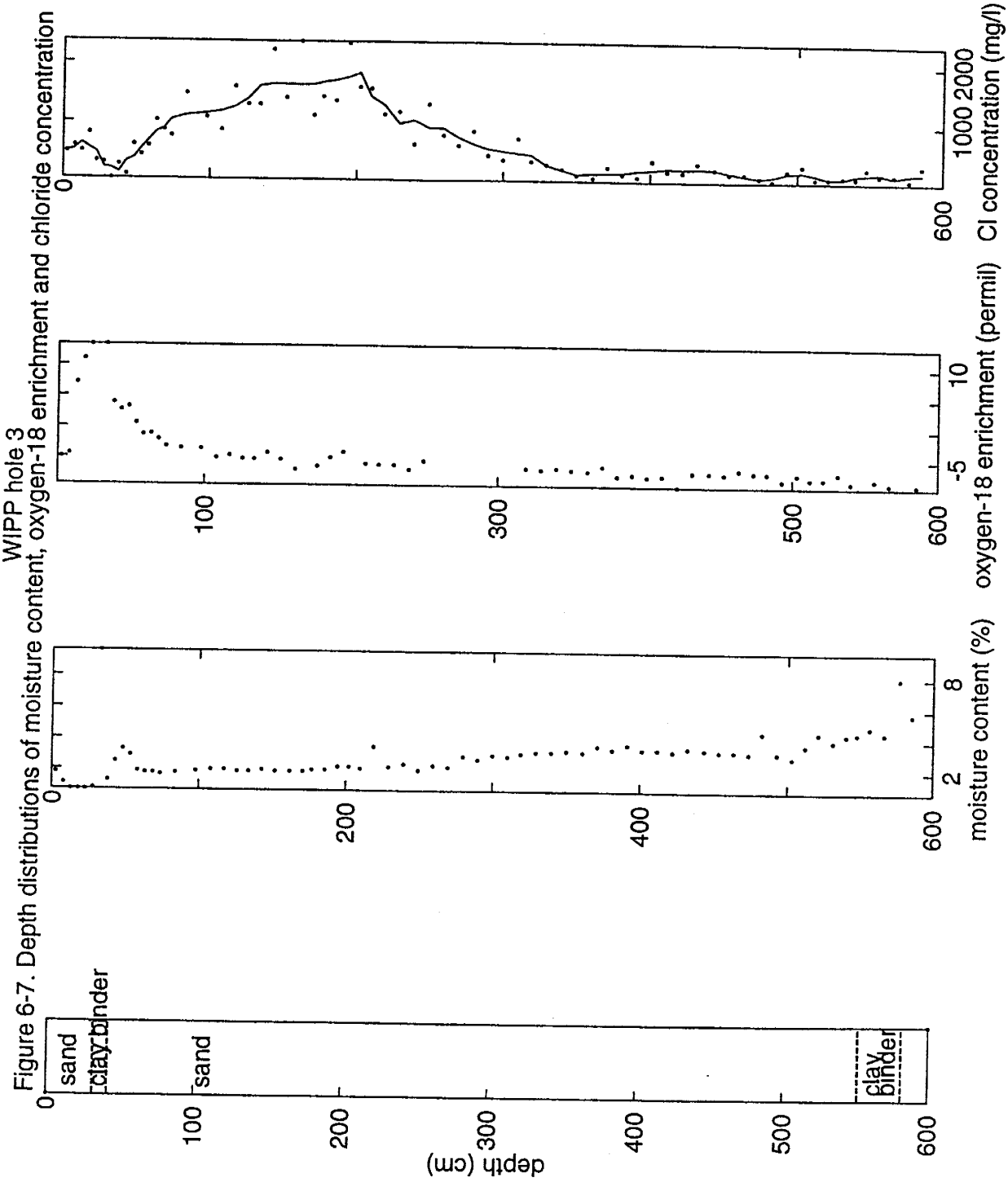

Figure 6-7. Depth distributions of moisture content, oxygen-18 enrichment and chloride concentration

and lower than 250 mg/l below this depth. The variability in the chloride concentration data may be attributed to: (1) analytical error in Cl concentration measurements, (2) unevenly-distributed influence of root water uptake and the questionability of the one-dimensional flow assumption in the root zone, and (3) preferential flow though the root zone and the resulting nonuniformity in leaching the profile. The isotope profile is smoother than the chloride concentration profile. Heavy water molecules diffuse in both the vapor and liquid phases resulting in a smooth isotope profile. The chloride profile is less scattered where moisture contents are higher below the root zone. Obviously, continuous liquid films on the soil grains will increase the effect of diffusion and result in a smoothing of the chloride distribution. The gradual increase in chloride concentration with depth is expected in the root zone and can be explained as follows: when water containing chloride percolates into a soil subject to water loss by transpiration, it is expected that (at steady state and under conditions of piston flow) chloride concentrations in soil water will increase monotonically through the root zone [Gardner, 1967]. That observation can be explained mathematically using eqn. (I-43) where, if R decreases with depth due to water loss by evapotranspiration, C will increase. The chloride peak then corresponds to the maximum depth of abstraction of water by roots. For piston flow, the chloride concentrations should be uniform with depth beneath the bottom of the root zone. Because the chloride concentration below the root zone is lower than the maximum concentration at the bottom of the root zone, the chloride profile observed here suggests that long-term water infiltration at this location cannot be explained by piston flow through the root zone. The most likely explanation is

that infrequent rainfall events of relatively large size (carrying low chloride content) percolates the root zone via preferred pathways to the bottom of the root zone without effectively leaching the soil profile. It is possible that the root channels form part of these fast water-percolating pathways. When the top clay layer at 35 cm dries, it cracks. This is a good environment for preferential flow where water penetrates the profile through these cracks without much interaction with the soil matrix in the root zone.

At depths between 4.0 m and 4.5 m, the profile has almost uniform moisture content (=3 %) implying gravity drainage and also uniform chloride concentration (C=240.0 mg/l) . This condition suggests that quasi-steady-state piston flow can be justifiably assumed and drainage rate can be calculated using the chloride mass balance method. The drainage rate was estimated at 0.5 mm/yr using C=240.0 mg/l, P=380 mm/yr, and C_o=0.32 mg/l. This value of drainage rate has two components in the root zone, water flux through the soil matrix (R_m) and water flux through preferred pathways (R_p). Following Sharma and Hughes [1985] in their bimodal flow model, conservation of mass of water and chloride in this flow system can be represented, respectively, by the two equations

$$R = R_p + R_m \tag{6-1}$$

$$R\,C = R_m\,C_m + R_p\,C_p \tag{6-2}$$

Assuming that the preferred water has a chloride content similar to precipitation and using the concentration at the bottom of the root zone for C_m (1836 mg/l), R (0.5 mm/yr), and C (240 mg/l), the value of R_p is calculated to be 0.43 mm/yr representing

86% of the drainage rate below the root zone. Below a depth of 4m the isotope profile and chloride profile has uniform values supporting the downward movement of water. However, above 4.0 m the moisture distribution and the isotope profile indicate an upward water flow.

Hole 4

The soil profile is relatively high in moisture content (see Figure 6-9). The isotope enrichment profile suggests that rainfall event occurred at least 10 days prior to sampling. The big bulge in the moisture distribution is at the same depth as the bulge in Hole 3 (35 cm) indicating a clay layer although records during drilling are not available. High moisture content at this depth fingerprints a rain fall event (with isotopically light water) that did not penetrate deep in the profile. Sufficient time elapsed before sampling so that no local isotope minimum is apparent. At depth, the soil profile was still draining and did not reach its field capacity. Bulges in the moisture distribution are attributed to thin clay layers available in this soil profile. A caliche layer was encountered at depth 412 cm which has a similar hydraulic effect as the clay layer at the bottom of Hole 3.

Hole 5 (Figure 6-10)

During auguring, a clay layer was encountered between depths 117 cm and 155 cm. At 199 cm, a caliche layer was encountered. The clay layer is the reason for the high moisture content in the bottom of the profile and the bottom caliche layer is delaying the

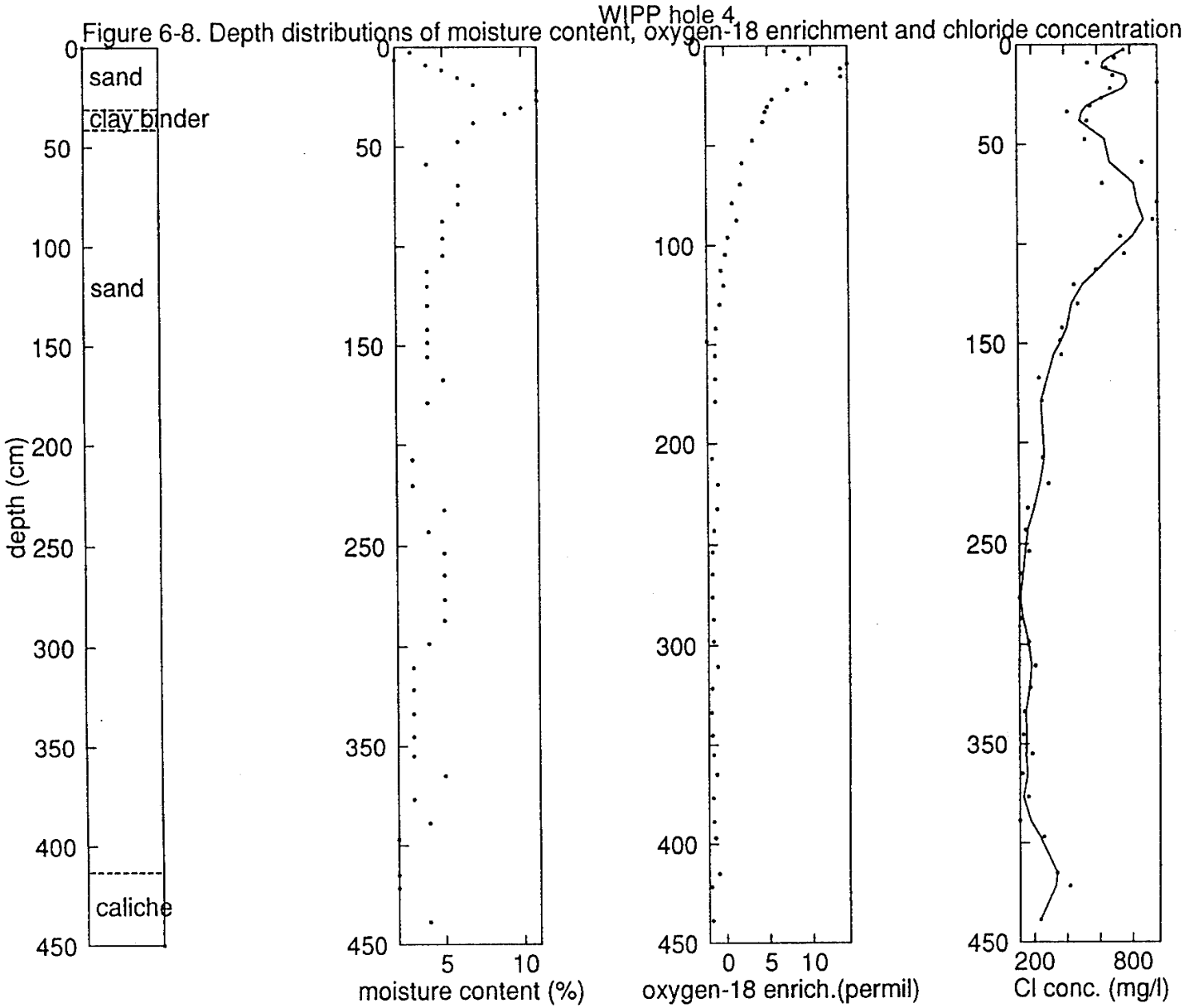

Figure 6-8. Depth distributions of moisture content, oxygen-18 enrichment and chloride concentration

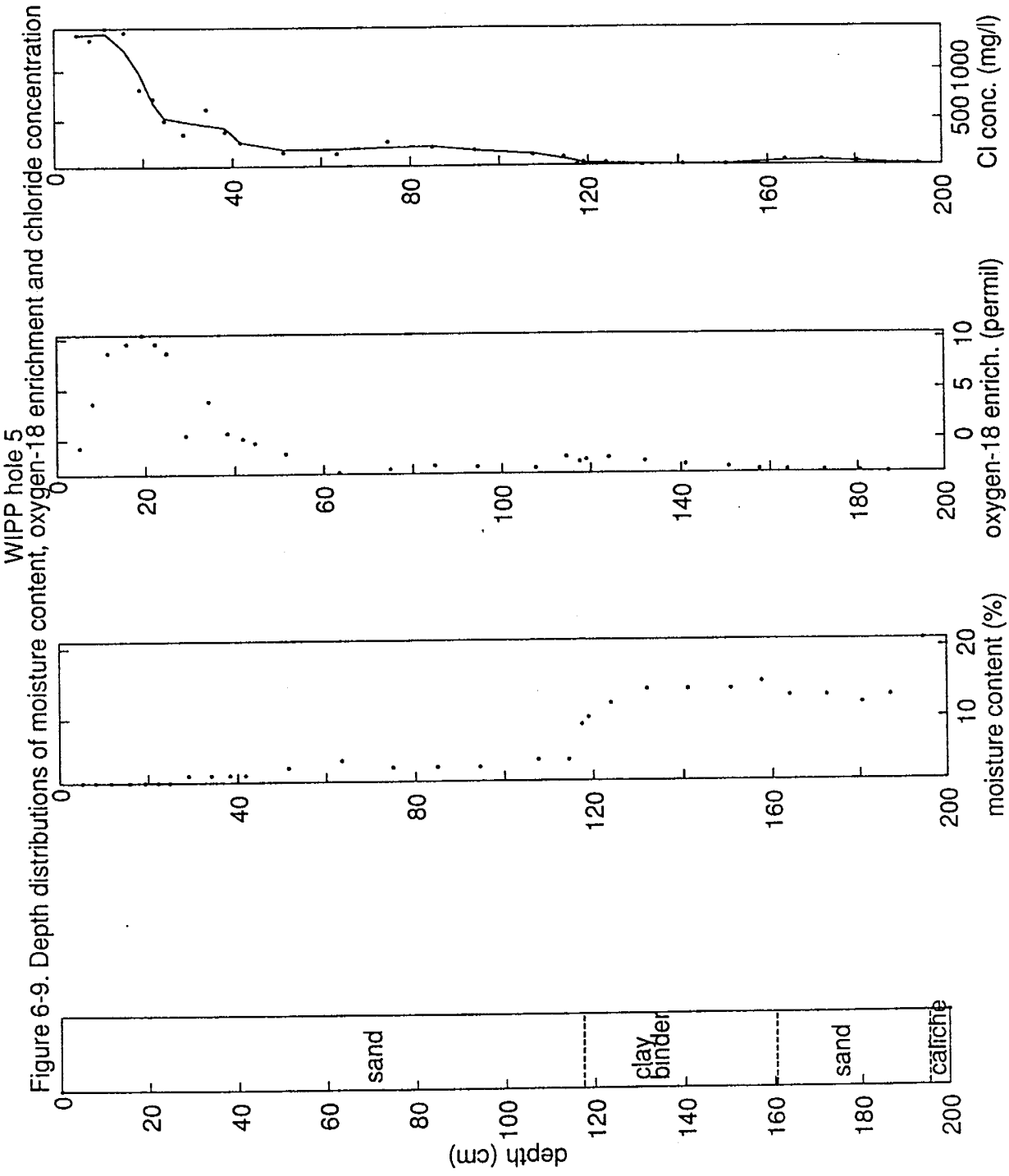

Figure 6-9. Depth distributions of moisture content, oxygen-18 enrichment and chloride concentration

downward water flux further causing a jump in the water content. Above depth 60 cm, the moisture content distribution suggests an upward water flux. The evaporation front is at depth 20 cm. The interesting thing about this hole is the similarity between the isotope profile and chloride profile. There was no sign of a recent rainfall event or a clay layer close to the surface. During auguring, no roots were encountered below 60 cm which explains why the chloride peak is closer to the surface than, for example, Hole 3 and Hole 4. The availability of water in the bottom of the profile makes it easy for water above 60 cm to move upward and isotope and chloride to be smoother than previous holes. The shape of the isotope peak is not sharp but broad. Similar broad isotope peaks were measured by Allison et al. [1983a] in soils planted with wheat. An explanation similar to that for Hole 4 applies to this profile where both vapor and liquid fluxes coexist in a short zone close to the peak (see Figure 2-4).

Hole 6 (Figure 6-11)

Profiles in Hole 6 are similar to those of Hole 5. The only difference is the availability of a bulge in the moisture distribution because of a thin clay layer between depths 60 cm and 80 cm. The availability of grass and mesquite proximal to the hole makes the profile dry above the clay layer and the broad isotope peak is obvious as in Hole 5, suggesting a zone of combined vapor and liquid (see Figure 2-4).

6.3 *Sevilletta Profiles*

The soil here is the same as that used in the controlled field experiment. At this site,

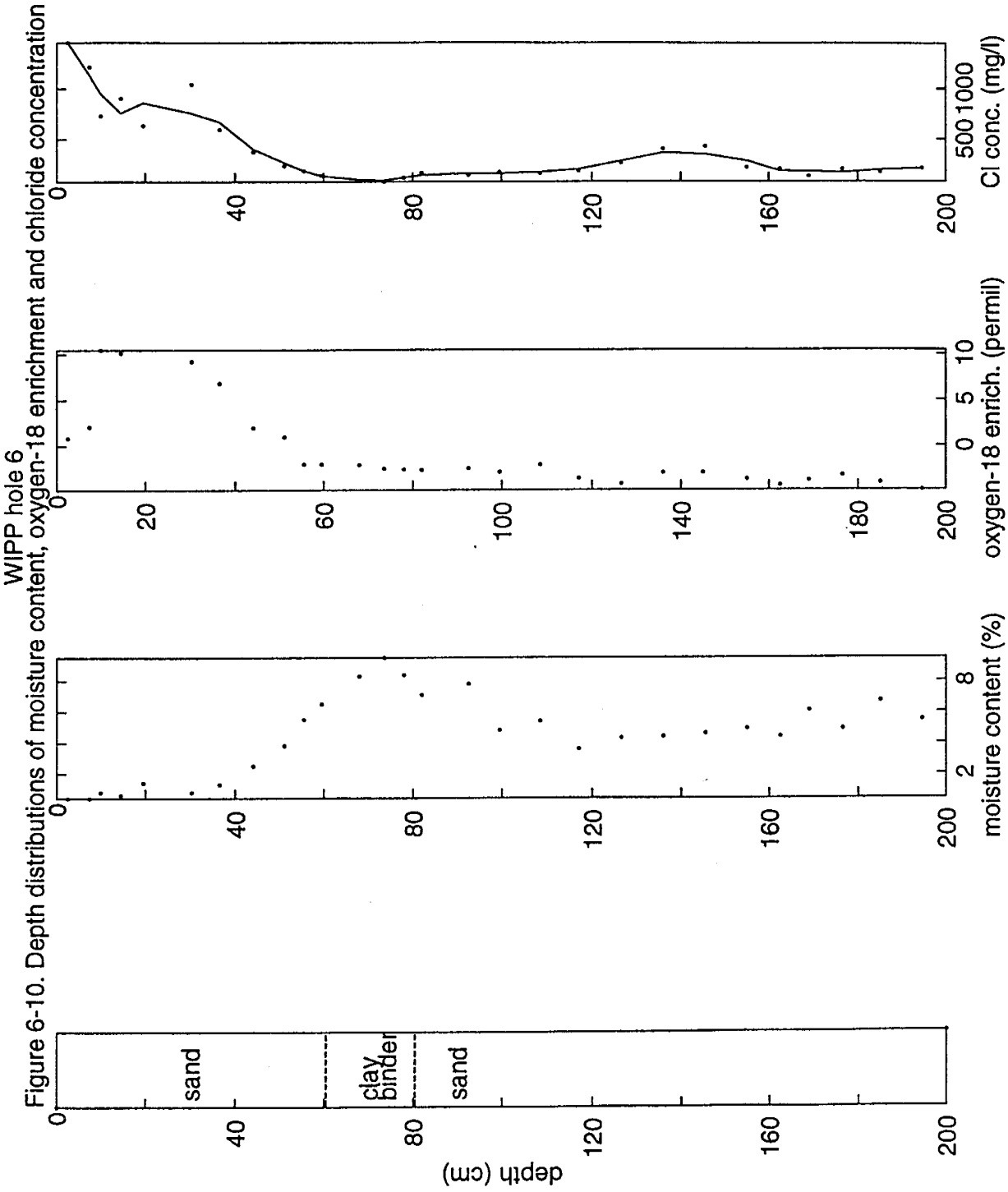

Figure 6-10. Depth distributions of moisture content, oxygen-18 enrichment and chloride concentration

no vegetation was observed in the dunes. Figure 6-12 shows the depth distributions of moisture content and deuterium and oxygen-18 enrichments [Knowlton, 1989]. The moisture distribution has several moisture bulges identifying possibly different soil layers or layers with different clay binder content. Water stored in these higher moisture holding layers must have resulted from a recent rainfall event or several events before the soil profile was sampled. The effect of the light rain water collected in these layers is the production of a smooth minima in the two isotope profiles. During heavy rain, percolating water is more retained in layers having higher clay content. The higher the water content the less the effect of evaporation on isotopic enrichment. The diffusion process of the isotopes in vapor and liquid phases smooth the isotope profiles.

It is quite obvious that the moisture content at the evaporation front is 2.4% which is the value estimated for moisture content at liquid discontinuity, using the experimental isotope profiles. This gives extra evidence that the moisture content at the evaporation front (the moisture content at liquid discontinuity) is a characteristic property of a given soil and supports our approach for estimating the value of this parameter from isotope profiles.

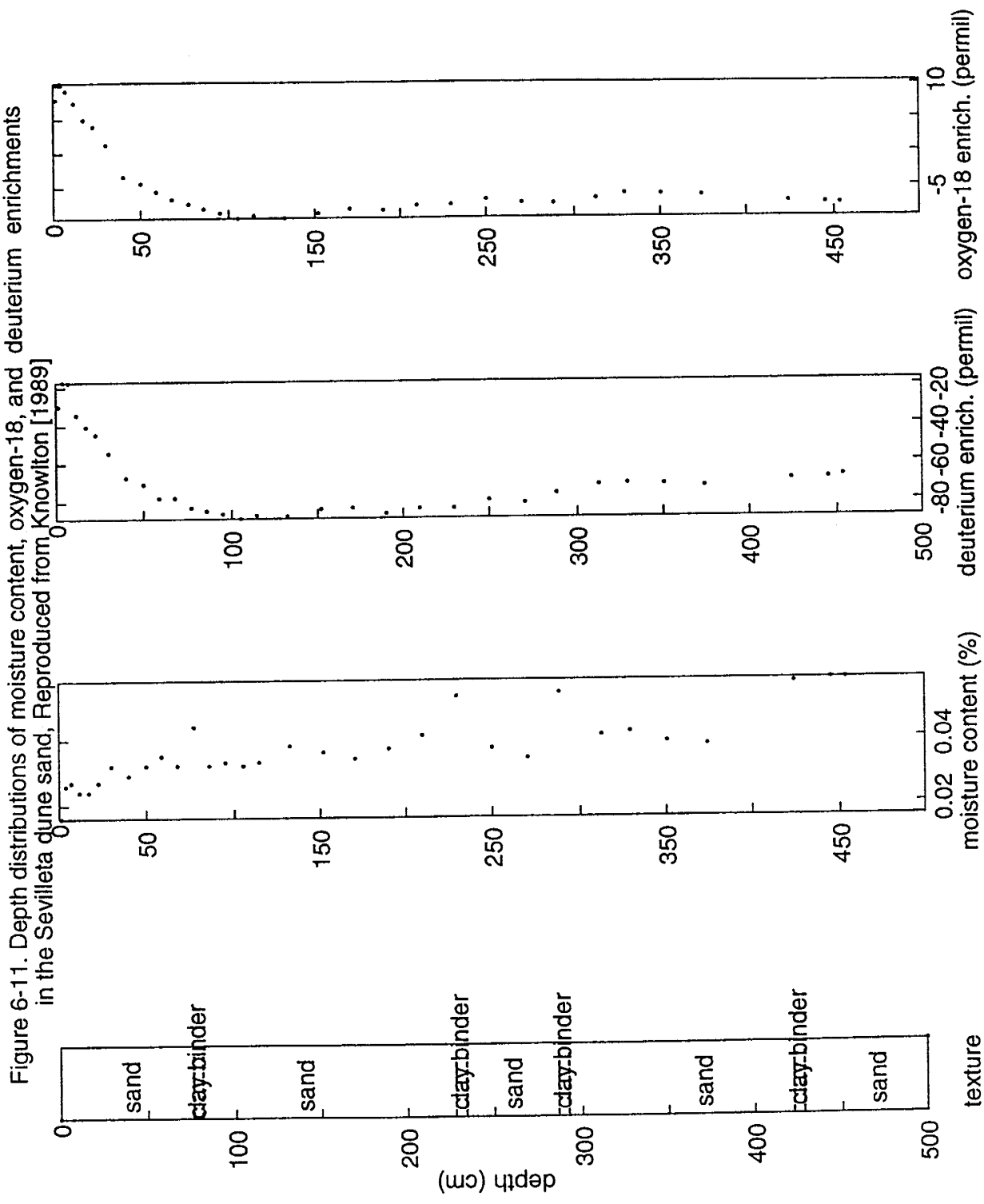

Figure 6-11. Depth distributions of moisture content, oxygen-18, and deuterium enrichments in the Sevilleta dune sand, Reproduced from Knowlton [1989]

7. CONCLUSIONS

A one-dimensional numerical model which simulates water flow, heat transfer, and isotope transport in unsaturated-saturated soils has been developed. This model combines the Philip and de Vries theory for simultaneous heat and moisture transfer in porous media with the stable isotope transport theory. The transport of the stable isotope is modeled similar to that of the solute, but included in the model is the isotope fractionation process and isotope transport in the vapor phase. With this combined hydraulic and isotopic model, water movement in the unsaturated zone can be simulated and changes in isotope profile can be predicted. The isotope profile gives insight into the evaporation process and water movement in the shallow unsaturated zone. Applications of the model includes soils ranging from saturated to very dry, modeling the transport of nonvolatile solutes in soil, and considering the diurnal fluctuations in temperature and relative humidity at the surface.

The model fills a gap in the isotope transport theory by (1) incorporating the theory of Philip and de Vries (for simultaneous moisture and heat transfer) which is necessary for natural conditions where temperature and moisture distributions are often in transient state and (2) being able to model the zone where vapor flow and liquid flow coexist and the isotope transport in vapor and liquid phases throughout the soil profile using a single equation. In this study a single equation was derived for isotope transport under nonsteady-state conditions, based on mass balances for water and for the isotope. A transition factor that reflects the importance of the combined vapor and liquid zone has been introduced. Through use of this factor, earlier work by others was considered as

a special case and the analytical results were reproduced numerically using a single equation. The single equation evaporation-zone approach better simulates the broad stable isotope peaks characteristic of relatively dry soils.

The computer code was tested by comparing its performance in various processes, under certain artificial conditions, with the available analytical solutions. A steady-state version of the isotope equation was tested by comparison with Barnes and Allison's analytical solution [1983]. The results of the numerical model agree well with the analytical solutions. A controlled field experiment provided a basis for further verification of the model. Reasonable agreement between the model-predicted depth distributions of moisture content, temperature and isotopic enrichment and the corresponding experimentally-observed distributions revealed that the developed hydrologic-isotopic model simulates satisfactorily the main processes involved in water movement in the shallow unsaturated zone and the associated isotope transport and fractionation processes.

Hydraulic quasi-steady-state is established much more rapidly than isotopic steady state in soil profiles. Isotope profiles in the field are expected to normally be in a slow transient state. The steady-state assumption must therefore be used cautiously. However, using the isotope maxima as a fingerprint for the evaporation front is useful for determining the instantaneous evaporation rate and the average evaporation rate for soils that are approaching a hydraulic quasi-steady-state condition.

Based on comparison between different levels of humidity and temperature data at the surface, it was found that isotope profiles depend largely on the daily average values of humidity and temperature at the surface and that they do not feel the daily

fluctuations.

The chloride mass balance method was used to estimate the local drainage (recharge) rate below dune sand at the WIPP site. Analysis using a bimodal version of the mass balance model provided evidence for preferential flow through the root zone.

Layers with higher clay content will take longer time to loose water through evaporation and thus to be enriched with isotopes. Such clay layers cause the isotope local minima resulting from rainfall water to stay longer until it disappears as a result of evaporation and isotope diffusion.

Field and experimental observations showed that, for a given soil and regardless of the evaporation period, the maximum isotope enrichment occurs at a unique value of moisture content, which is the moisture content at liquid discontinuity. This value is needed for modeling water vapor flow in dry soils and is used in the model to locate the evaporation front in the soil profile. In the future, we propose to use the isotope profile peaks in soils undergoing evaporation to determine the value of this parameter which is not as accurately determined using other physical methods.

REFERENCES AND SELECTED BIBLIOGRAPHY

Allison, G.B. and C.J. Barnes, 1983. Estimation of evaporation from non-vegetated surfaces using natural deuterium. Nature, 301:143-145.

Allison, G.B., W.J. Stone and M.W. Hughes, 1985. Recharge in karst and dune elements of a semi-arid landscape as indicated by natural isotopes and chloride. J. Hydrology, 76:1-25.

Allison, G.B., C.J. Barnes, M.W. Hughes, and F.W.J. Leaney, 1983a. The effect of climate and vegetation on oxygen-18 and deuterium profiles in soils. Proc. 1983 Int. Symp. Iso. Hydrol. Water Resour. Dev., IAEA, Vienna, No IAEA-SM-270/20.

Allison, G.B., C.J. Barnes, and M.W. Hughes, 1983b. The distribution of deuterium and oxygen-18 in dry soils: II. Experimental. J. Hydrology, 64:377-397.

Barnes, C.J. and G.B. Allison, 1983. The distribution of deuterium and oxygen-18 in dry soils: I. Theory. J. Hydrology, 60:141-156.

Barnes, C.J. and G.B. Allison, 1984. The distribution of deuterium and oxygen-18 in dry soils: III. Theory for non-isothermal water movement. J. Hydrology, 74:119-135.

Barnes,C.J. and G.B. Allison, 1988. Tracing of water movement in the unsaturated zone using stable isotopes of hydrogen and oxygen. J. Hydrology, 100:143-176.

Barnes, C.J. and G.B. Walker, 1989. The distribution of deuterium and oxygen-18 during unsteady evaporation from a dry soil. J. Hydrology, 112:55-67.

Batch, L.B., 1992. Soil water movement in response to temperature gradients: Experimental measurements and model evaluation. Soil Sci Soc. Am. J., 56:37-4

Bruin, S. and K.Ch. Luyben, 1980. Drying of food materials: A review of recent developments. in Advances in Drying, 1:155-215, A.S. Mujumdar, ed., Hemisphere, Washington, D.C.

Campbell,A.R., F.M. Phillips, A.M. Shurbaji and R. Vanlandingham, 1993. Stable isotope study of soil and groundwater, WIPP site, New Mexico: Estimation of recharge to the Rustler aquifers, Technical completion report project No 1-4-23169, New Mexico Waste Management Education and Research Consortium.

Cary, J.W., 1966. Soil moisture transport due to thermal gradients: Practical aspects. Soil Sci. Soc. Am. Proc., 30:428-433.

Cary, J.W., 1979. Soil heat transducers and water vapor flow. Soil Sci. Soc. Am. J., 43:835-839.

Childs, S.W. and G. Malstaff, 1982. Final report: Heat and mass transfer in unsaturated porous media, report PNL-4036/UC-94e. Prepared for Pacific Northwest Lab., Battelle, 173 p.

Coleman, M.L., T.J. Shepherd, J.J. Durham, J.E. Rouse, and G.R. Moore, 1982. Reduction of water with zinc for hydrogen isotope analysis. Analytical Chemistry, 54:993-995.

Connell, L.D. and P.R. Bell, 1993. Modeling moisture movement in revegetating waste heaps: 1. Development of a finite element model for liquid and vapor transport. Water Resources Research, 29:1435-1443.

Christmann, D. and C. Sonntag, 1987. Groundwater evaporation from East-Saharian depressions by means of deuterium and oxygen-18 in soil moisture. Proc. Int. Symp. Use Isot. Tech. Water Resour. Dev., Vienna, Pap. IAEA-SM-99/037.

Clifford, S.M. and D. Hillel, 1986. Knudsen diffusion: the effect of small pore size and low gas pressure on gaseous transport in soil. Soil Science, 141:289-297.

Dahab,M.H., M.A. Mustafa, and H.A. Abdel-Rahman, 1988. Intermittent evaporation, moisture distribution, and salt redistribution through saline-sodic clay soil as affected by irrigation frequency and quantity. Soil Science, 146:168-175.

de Vries, D.A., 1952. The thermal conductivity of granular materials. Annexe 1952-1 Bul., Inst. Intern. du Froid, 115-131.

de Vries, D.A., 1963. Thermal properties of soils. in Physics of Plant Environment, edited by R.W. Van Wijk, p. 210-235, North-Holand Publ. Co., Amsterdam.

de Vries, D.A., 1975. Heat transfer in soils. in Heat and Mass Transfer in the Biosphere, Vol. 1, Transfer processes in the plant environment, D.A. de Vries, N.H. Afgan, ed., Scripta Book Co., Washington, D.C., 1-28.

de Vries,D.A., 1958. Simultanuous transfer of heat and moisture in porous media. Trans. AGU, 39:909-916.

de Vries,D.A. and A.J. Peck, 1958. On the cylindrical probe method of measuring thermal conductivity with special reference to soils, I. Extention of theory and discussion of probe characteristics. Australian J. Physics, 11:255-271.

de Vries, D.A. and J.R. Philip, 1959. Temperature distribution and moisture transfer in porous materials. J. Geophys. Res., 64:386-388.

de Vries, D.A., 1987. The theory of heat and moisture transfer in porous media revisited. Int. J. Heat Mass Transfer, 30:1343-1350.

Dincer, T. and G.H. Davis, 1984. Application of environmental isotope tracers to modeling in Hydrology. J. Hydrology, 68:95-113.

Edlefsen, N.E. and A.B. Anderson, 1943. The thermodynamics of soil moisture. Hilgardia, 15:31-298.

Ewen,J. and H.R. Thomas, 1989. Heating unsaturated medium sand. Geotechnique 39, 3:455-470.

Fawcett,R.G. and N. Collis-George, 1967. A filter paper method for determining soil moisture. J. Exper. Agricul. Animal Husb.. Australia.

Finlayson,B.A., R.W. Nelson, and R.G. Baca, 1978. A preliminary investigation into the theory and techniques of modeling the natural mosure movement in unsaturated sediments, Report RL-47,Rockwell International, Rockwell Hanford Operations, Energy Systems Group, Richland, WA 99352.

Fontes,J. Ch., M. Yousfi, and G.B. Allison, 1986. Estimation of the long term, diffuse groundwater discharge in the Northern Sahara using stable isotope profiles in soil water. J. Hydrology, 86:315-327.

Gardner, W.R., 1967. Water uptake and salt distribution paterns in saline soils. In: Isotope and radiation techniques in soil physics and irrigation studies, Int. Atomic Energy Agency, Vienna pp.335-40.

Gee, G.W. and D. Hillel, 1988. Groundwater recharge in arid regions: Review and ritique of estimation methods. Hydrol. Process., 2:255-266.

Geraminegad,M. and S.K. Saxina, 1985. A solution of coupled heat-moisture transfer in saturated-unsaturated media. Proceedings of fifth international conference on numerical methods in geomechanics, Nagoya, 1-5 April, 1985.

Gurr, C.G., T.J. Marshall, and J.T. Hutton, 1952. Movement of water in soil due to a temperature gradient. Soil Sci., 74:33345.

Hampton,D., 1989. Coupled heat and fluid flow in saturated-unsaturated compresible porous media. Ph.D dissertation. Civil Engineering Dept., Colorado State University, Fort Colins, Colorado, 1989.

Haverkamp,R., M. Vauclin, J. Tomuma, P.J. Wierenga and G. Vachaud, 1977. A comparison of numerical simulation models for one-dimensional infiltration. Soil Science Soc. Am. J.,41:285-293.

Heller, J.P., 1968. The drying through the top surface of a vertical porous column. Soil Sci. Soc. Am. Proc., 32: 778-786.

Hillel,D., 1980. Applications of soil physics. Academic Press, New York.

Jury, W.A. and J. Jr. Letey, 1979. Water vapor movement in soil: Reconciliation of theory and experiment. Soil Sci. Soc. Am. J.,43:823-827.

Kendall,C. and T.B. Coplen, 1985. Multisample conversion of water to hydrogen by zinc for stable isotope determination. Anal. Chem., June 1985, p.1437-1446.

Kimball, B.A., R.D. Jackson, R.J. Reginato, F.S. Nakayama and S.B. Idso, 1976. Comparison of field-measured and calculated soil-heat fluxes. Soil Sci. Soc. Am. Proc., 40:18-25.

Knowlton, R.G., 1989. A stable isotope study of water and chloride movement in natural desert soils. Ph.D dissertation. Geoscience Dept., New Mexico Tech., Socorro, New Mexico.

Knowlton, R.G., F.M. Phillips, and A.R. Campbell, 1989. A stable-isotope investigation of vapor transport during groundwater recharge in New Mexico. Technical Completion Report No. 1345644, New Mexico Water Resources Research Institute, New Mexico State University.

Lapidus, L., and N.R. Amundson, 1952. Mathematics of adsorption in beds. IV. The effects of longitudinal diffusion in ion exchange chromatographic columns. J. Phys. Chem. 56:984-988.

Longsworth, L.G., 1954. Temperature dependence of diffusion in aqueous solutions. J. Phys. Chem., 58, 770-773.

Majoube, M., 1971. Fractionnement en oxygene-18 at en deuterium entre l'eau et sa vapeur. J. Chem. Phys., 68:1423-1436.

Merlivat, L., 1978. Molecular diffusivities of $H_2{}^{16}O$, $HD^{16}O$, and $H_2{}^{18}O$ in gases. J. Chem. Phys., 69: 2864-2871.

McCord,J.T., 1989. Hysterisis and state-dependent anisotropy in variably saturated flow: field, laboratory, and numerical modeling investigation. Ph.D. dissertation, New Mexico Institute of Mining and Technology, Socorro, New Mexico.

Mills, R., 1973. Self diffusion in normal and heavy water in the range 1-45°. J. Phys. Chem., 77:685-688.

Milly,P.C.D., 1988. Advances in modeling of water in the unsaturated zone. Transport in porous media, 3:491-514.

Moldrup,P., D.E. Rolston, and J.A.A. Hansen, 1989. Rapid and numerically stable simulation of one-dimensional, transient water flow in unsaturated layered soils. Soil Sci., 148:219-230.

Munnich, K.O., C. Sonntag, D. Christmann, and D. Thomas, 1980. Isotope fractionation due to evaporation from sand dunes, 2. Mitt Zentralinst. Isot. Stralenforsch, 29:319-332.

O'Neill, K., 1978. An analysis of coupled heat and moisture flow in an unsaturated soil. in Proc. Conf. Modeling of Snow Cover Runoff, S.C. Colbek and M. Ray, eds., USACRREL, Hanover, New Hampshire, 304-309.

Peaceman, D.W., 1977. Fundamentals of Numerical Reservoir Simulation. Elsevier scientific publishing company, New York.

Penman, H.L., 1940. Gas and vapor movements in the soil: I. The diffusion of vapors through porous solids; II. The diffusion of carbon dioxide through porous solids. J. Agric. Sci., 30:437-462, 570-581.

Philip, J.R. and de Vries, D.A., 1957. Moisture movement in porous materials under temperature gradients. Trans. AGU, 38:222-232.

Philip, J.R., 1958a. Simultaneous transfer of heat and moisture in porous media. Trans. AGU, 39:909-916.

Philip, J.R., 1958b. The theory of infiltration 6. Soil Sci. 85:278-286.

Philip, J.R., 1969. Theory of infiltration. Adv. Hydrosci. 5: 215-305. Academic Press, N.Y.

Phillips, F.M., J.L. Mattick, and T.A. Duval, 1988. Chlorine-36 and tritium from nuclear weapons fallout as tracers for long-term liquid movement in desert soils. Water Resour. Res., 24: 1877-1891.

Roether,W., 1970. Water-CO_2 exchange set-up for the routine oxygen-18 assay of natural waters. Int. J. Apll. Rad. and Isot.. 21:379-387.

Rollins, R.L.,M.G. Spangler and D. Kirkham, 1954. Movement of soil moisture under a thermal gradient. Highway Research Board Proc., 33:492-508.

Scanlon,B.R., P.W. Kubik, P. Sharma, B.C. Richter, and H.E. Gove, 1990. Bomb chlorine-36 analysis in the characterization on unsaturated flow at a proposed radioactive waste disposal facility, Chihuahan Desert, Texas. Nucl. Istr. Meth. Phys. Res., 52:489-492.

Smith,G.D., 1985. Numerical solution of partial differential equations: Finite difference methods, 3rd edition. Clarendson Press. Oxford.

Sharma, M.L. and M.W. Hughes, 1985. Groundwater recharge estimation using chloride, deuterium and oxygen-18 profiles in the deep coastal sands of western australia. J. Hydrology, 81:93-109.

Sheppard,C.W., 1962. Principles of the tracer method. John Wiley & Sons, New York.

Shurbaji, A.M. and F.M. Phillips, 1993. A numerical model for the movement of H_2O, $H_2{}^{18}O$, and ^2HHO in the unsaturated zone. J. Hydrology (Submitted).

Sophocleous, M., 1979. Analysis of water and heat flow in unsaturated-saturated porous media. Water Resour. Res., 15:1195-1206.

Taghavi, S.A., M.A. Marino, and D.E. Ralstson, 1985. Infiltration from a trickle source in a hetrogeneous soil medium. J. Hydrology, 78:107-121.

Taylor, S.A. and Cary, J.W., 1964. Linear equations for the simultaneous flow of matter and energy in a continuous soil system. Soil Sci. Soc. Am. Proc., 28:167-172.

Thomas,H.R., 1986. Heat transfer effects on moisture movement in unsaturated soils-A numerical investigation. VI international conference on finite elements in water resources, Lisoa, Portugal.

Thomas,H.R., and J. Ewen, 1989. Heating unsaturated medium sand. Geotechnique, 39:455-470.

Van Genuchten, M.Th. and P.J. Wierenga, 1986. Solute dispersion coefficients and retardation factors. Methods of Soil Analysis, Part 1. Physical and Mineralogical Methods-Agronomy, Monograph no. 9 (2nd Edition).

Van Genuchten, M.T., 1978. Numerical solution of the one dimensional saturated-unsaturated flow equation. Water Resour. Prog., Dept Civ. Eng., Princeton Univ., N.J., Res. Rep. no 78-WR-09.

Vanlandingham, R.J., 1993. Characterization of vertical infiltration near the Waste Isolation Pilot Plant, Carlsbad, New Mexico. M.Sc. thesis, New Mexico Institute of Mining and Technology. 109 pages.

Wang, J.H., C.V. Robinson and I.S. Edelman, 1953. Self-diffusion and structure of liquid water. III Measurement of the self-diffusion of liquid water with H^2,H^3, and O^{18} as tracers. J. Am. Chem. Soc., 75, 466.

Walker, G.R., M.V. Hughes, G.R. Allison, and C.J. Barnes, 1988. The movement of isotopes of water during evaporation from a bare soil surface. J. Hydrology, 97:181-197.

Whitaker, S., 1980. Radiant energy transport in porous media. Ind. Eng. Chem. Fundam., 19:210-218.

Wierenga,P.J., and M.Th. Van Genuchten, 1989. Solute transport through small and large unsaturated soil columns. Ground Water, 27:35-42.

Zimmermann, V., Ehhalt, D. and Munnich, K.O., 1967. Soil-water movement and evapotranspiration: Changes in the isotopic composition of the water. Proc. IAEA Symp. Isotopes in Hydrology, Vienna, 1966, IAEA, pp 567-584.

Appendix A

Empirical relations for water properties

Density of liquid water [g/cm^3] (Finlayson et al., 1978):

$$\rho = 1.00 + 1.45x10^{-5}\,T - 5.15x10^{-6}\,T^2$$

$$0<T<45C$$

Viscosity of water [g/cm/s] (Finlayson et al., 1978):

$$1/\mu = 2.1551(T + \sqrt{8078.4+(T-8.435)^2}) - 138.54$$

Saturated vapor density [g/cm^3] (Childs and Malstaff, 1982):

$$\rho_{vs} = \exp[\frac{17.294\,T}{(T+237.3)}]\;x\;\frac{1323x10^{-6}}{(T+273.16)}$$

Derivative of saturated vapor density with respect to temperature [g/cm^3/C](Childs and Malstaff, 1982) :

$$\eta = \frac{\partial \rho_{vs}}{\partial T} = \rho_{vs}[\frac{-1}{(T+273.16)} + \frac{4104}{(T+237.3)^2}]$$

Latent heat of evaporation coefficient [cal/gm]:

$$L = 597.5 - 0.58\,T$$

$$0<T<120C$$

Diffusion coefficient of atmospheric water vapor [cm^2/s] (Kimball et al., 1976):

$$D_v^{atm} = 0.229(1. + \frac{T}{273.16})^{1.75}$$

Isotopic composition $\delta_{18}^{initial}$ of water:
1. Equilibrium CO_2-H_2O fractionation factor(Roether, 1970):

$$\alpha_{CO_2\text{-}H_2O} = \exp\left(\frac{-21}{T^2} + \frac{17.994}{T} - \frac{19.97}{10^3}\right)$$

2. Final isotopic composition of water δ_{18}^{final}:

$$\delta^{f}_{H_2O} = \frac{\delta^{f}_{CO_2} + 1}{\alpha_{CO_2\text{-}H_2\text{-}O}} - 1$$

3. Initial isotopic composition of water:

$$X\,[\delta^{i}_{H_2O} - \delta^{f}_{H_2O}] = Y\,[\delta^{f}_{CO_2} - \delta^{i}_{CO_2}]$$

which can be rewritten as:

$$\delta^{i}_{H_2O} = \frac{Y}{X}[\delta^{f}_{CO_2} - \delta^{i}_{CO_2}] + \delta^{f}_{H_2O}$$

Diffusion coefficient of ^{2}HHO and $H_2{}^{18}O$ species in liquid water D_i^* [cm^2/s] is given by Figure A-1.(Langsworth,L.G.,1954, Wang et al., 1953):

Kinetic fractionation factor for isotopic species in vapor phase
Deuterium : $\sigma_i^v = 1.0251 +- 0.0009$
Oxygen-18 : $\sigma_i^v = 1.0285 +- 0.0007$

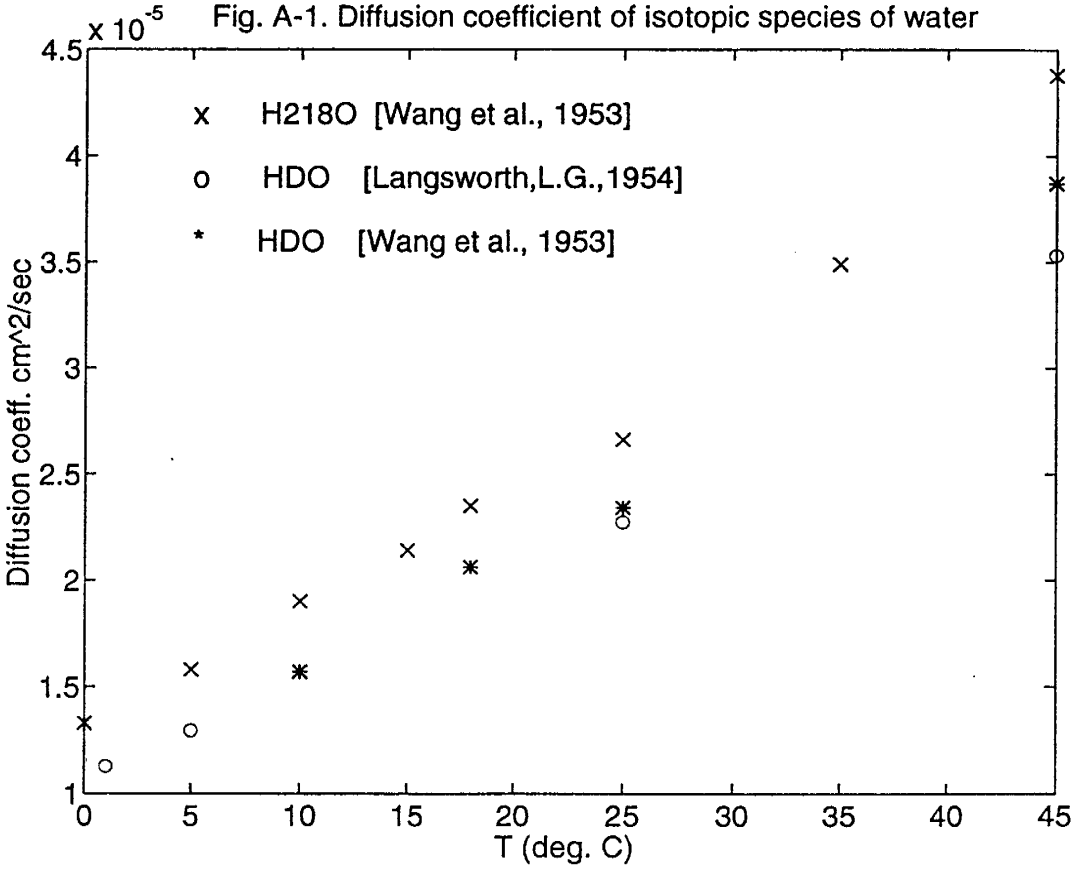

Fig. A-1. Diffusion coefficient of isotopic species of water

Appendix B

Data Files and Computer Codes **Page number**

Julian day 129:

Depth (cm) From	to	moisture content %		(permil) D vs SMOW	O18	D vs TAP water	O18
2.0	4.0	3.0	4.62	-70.121	-6.708	30.565	4.949
4.0	6.0	5.0	4.63	-73.606	-7.235	26.703	4.416
8.0	10.0	9.0	5.96	-93.527	-12.176	4.625	-0.583
24.0	28.0	26.0	6.44	-94.616	-12.124	3.418	-0.530
45.0	50.0	47.5	6.71	-90.194	-12.264	8.319	-0.672
65.0	70.0	67.5	6.72	-90.724	-12.019	7.731	-0.424
95.0	100.0	97.5	7.00	-97.700	-12.466	0.000	-0.876

depth (cm)	Temperature every 3 hours						
0.000	19.840	16.580	12.600	21.540	42.100	39.360	23.840	27.100
2.000	23.670	21.080	16.240	18.480	30.850	37.240	25.540	28.800
4.000	26.220	22.750	20.150	19.380	25.250	32.330	27.910	27.270
10.000	26.570	23.940	22.220	20.460	23.110	27.500	27.530	26.320
22.200	24.550	22.860	24.150	22.360	22.130	20.410	25.450	23.710
27.700	23.040	22.800	22.910	22.360	22.200	21.720	22.880	22.940
42.200	20.540	20.710	21.150	20.850	21.010	20.640	21.480	21.040
82.000	18.790	18.590	18.980	18.750	19.700	19.240	18.680	19.050
148.000	17.130	16.950	17.270	16.980	17.770	17.170	17.090	17.250
160.000	16.740	16.740	16.740	16.740	16.740	16.740	16.740	16.740

Julian day 138:

Depth (cm) From	to	moisture content %		(permil) D vs SMOW	O18	D vs TAP water	O18
0.0	7.0	3.5	1.15	-63.085	2.525	38.363	14.291
10.0	16.0	13.0	2.00	-62.592	5.477	38.909	17.277
16.0	18.0	17.0	3.06	-67.422	2.603	33.556	14.370
18.0	21.0	19.5	3.27	-70.095	-0.335	30.594	11.397
21.0	24.0	22.5	4.12	-85.681	-3.153	13.320	8.546
24.0	28.0	26.0	4.10	-85.388	-5.243	13.645	6.432
28.0	30.0	29.0	4.15	-80.597	-6.767	18.955	4.890
30.0	33.0	31.5	4.55	-91.104	-8.589	7.310	3.046
33.0	36.0	34.4	4.58	-94.637	-9.599	3.395	2.024
36.0	39.0	37.5	4.80	-96.038	-10.610	1.842	1.002
39.0	43.0	41.0	5.02	-98.742	-11.205	-1.155	0.400
43.0	47.0	45.0	5.30	-97.483	-10.928	0.240	0.680
47.0	50.0	48.5	5.11	-96.978	-10.842	0.800	0.767
50.0	55.0	52.5	5.43	-97.042	-11.480	0.729	0.121
55.0	60.0	57.5	4.86	-98.318	-11.120	-0.685	0.486
60.0	65.0	62.5	5.45	-97.734	-11.212	-0.038	0.393
65.0	70.0	67.5	5.37	-96.570	-11.184	1.252	0.421
70.0	76.0	73.0	5.51	-96.882	-11.019	0.907	0.588
81.0	88.0	84.5	5.69	-96.366	-11.292	1.478	0.312
105.0	115.0	110.0	16.10	-96.987	-11.344	.740	0.116
126.0	132.0	129.0	23.44	-97.607	-11.388	0.002	0.214
140.0	150.0	145.0	32.18	-97.700	-11.600	0.000	00
155.0	160.0	157.5	33.12	-97.700	-11.600	0.000	00

depth (cm)	Temperature every 3 hours						
0	20.10	17.80	13.70	21.00	29.00	35.50	35.80	22.80
2	22.67	20.16	17.28	19.10	26.51	37.28	37.40	27.22
4	25.52	22.85	20.75	20.30	24.35	30.11	32.19	28.43
10	26.43	24.36	22.70	21.74	23.25	26.72	29.09	28.08
22.2	25.63	25.08	23.97	24.16	23.25	24.15	24.01	25.15
27.7	24.18	24.18	23.85	23.66	23.20	23.24	23.46	24.10
42.2	22.34	22.37	22.31	22.61	22.53	22.54	22.28	22.42
82.0	20.03	20.09	20.08	20.23	19.98	20.02	20.42	20.31
148	17.87	17.81	17.75	17.96	17.81	17.83	18.05	17.95
160	17.48	17.48	17.48	17.48	17.48	17.48	17.48	17.48

Julian day 177:

Depth (cm) From	to	moisture content %		(permil) D vs SMOW	O18	D vs TAP water	O18
8.00	11.00	9.50	2.21	-51.924	5.115	50.733	16.911
12.00	14.00	13.00	3.05	-56.418	1.913	45.752	13.672
14.00	15.00	14.50	4.02	-65.384	-1.922	35.815	9.792
15.00	17.00	16.00	4.24	-76.873	-5.727	23.082	5.942
17.00	19.00	18.00	4.82	-88.840	-7.562	9.819	4.085
19.00	23.00	21.00	4.90	-84.198	-9.526	14.964	2.098
23.00	26.00	24.50	5.26	???	-8.510	9.781	3.126
25.00	30.00	27.50	5.61	-91.092	-10.777	7.324	0.833
30.00	35.00	32.50	5.67	-89.603	-10.612	8.974	1.000
35.00	37.00	36.00	6.39	-91.062	-10.935	7.357	0.673
37.00	41.00	39.00	5.87	-94.253	-10.639	3.820	0.972
41.00	45.00	43.00	5.86	-89.184	-10.782	9.438	0.828
47.00	50.00	48.50	6.30	-91.735	-10.582	6.611	1.030
53.00	57.00	55.00	6.30	-92.184	-10.836	6.113	0.773
57.00	65.00	61.00	5.92	-89.933	-10.718	8.608	0.892
69.00	75.00	72.00	6.08	-92.220	-10.948	6.073	0.660
75.00	85.00	80.00	6.12	-92.298	-10.988	5.987	0.619
95.00	105.00	100.00	6.13	-94.691	-10.822	3.335	0.787
115.00	125.00	120.00	8.61	-98.995	-11.163	-1.435	0.442
123.00	128.00	125.5	19.43	-95.206	-11.163	-1.435	0.442
135.00	142.00	138.50	20.43	-95.721	-11.587	2.193	0.704
160.00	165.00	162.50	24.77	-93.463	-11.395	4.696	0.885
170.00	175.00	172.50	24.06	-94.533	-10.981	3.510	0.799

depth (cm)	Temperature every 3 hours						
0	22.00	18.10	16.90	20.60	33.00	44.40	35.10	30.20
2	25.62	23.24	22.03	22.46	31.38	40.26	36.51	34.17
4	26.92	24.74	23.31	23.65	28.21	32.97	33.69	31.99
10	27.40	25.66	24.69	24.20	26.01	28.06	29.67	30.47
22.2	27.77	24.61	24.82	24.77	25.39	24.21	24.81	28.56
27.7	26.61	26.02	25.86	25.57	25.23	25.39	25.57	26.51
42.2	25.03	24.71	24.82	25.01	24.84	24.75	24.44	25.22
82.0	22.84	22.43	22.66	22.53	22.53	23.40	22.58	22.66
148	20.46	20.02	20.15	20.26	20.13	20.62	20.11	20.25
160	20.02	20.02	20.02	20.02	20.02	20.02	20.02	20.02

Julian day 197:

Depth (cm) From	to	moisture content %		(permil) D vs SMOW	O18	D vs TAP water	O18
0.0	4.0	2.0	1.01	-102.808	-17.145	-5.662	-5.493
4.0	8.0	6.0	1.45	-66.559	3.127	34.513	14.904
8.0	11.0	9.5	1.42	-65.622	3.651	35.551	15.431
11.0	14.0	12.5	1.79	-64.073	4.514	37.268	16.303
14.0	18.0	16.0	3.00	-63.574	4.792	37.821	16.584
20.0	22.0	21.0	3.20	-67.141	1.084	33.868	12.833
22.0	25.0	23.5	3.56	-75.865	-1.275	24.199	10.446
25.0	28.0	26.5	3.81	-75.234	-2.712	24.899	8.992
28.0	30.0	29.0	3.93	-85.733	-3.900	13.263	7.790
30.0	32.0	31.0	3.96	-81.954	-5.009	17.451	6.668
32.0	35.0	33.5	4.15	-86.085	-6.099	12.873	5.566
35.0	37.0	36.0	4.23	-87.779	-7.450	10.995	4.199
37.0	40.0	39.5	4.50	-88.761	-7.743	9.907	3.902
40.0	42.0	41.0	4.60	-92.941	-8.979	5.274	2.652
42.0	44.0	43.0	4.62	-95.485	-9.173	2.455	2.455
44.0	47.0	45.5	4.85	-92.421	-9.730	5.851	1.892
47.0	50.0	48.5	4.93	-94.519	-9.724	3.525	1.898
50.0	52.0	51.0	4.99	-95.074	-10.306	2.911	1.309
52.0	55.0	53.5	4.78	-95.421	-10.671	2.526	0.940

143	55.0	60.0	57.5	4.98	-95.618	-10.596	2.307	1.016
144	60.0	65.0	62.5	5.10	-95.989	-10.837	1.896	0.772
145	65.0	70.0	67.5	5.22	-96.359	-11.078	1.486	0.528
146	70.0	75.0	72.5	5.46	-98.665	-10.990	1.636	0.617
147	75.0	80.0	77.5	5.29	-99.130	-11.069	.288	0.537
148	80.0	85.0	82.5	5.36	-97.364	-11.064	0.372	0.542
149	85.0	90.0	87.5	5.67	-96.625	-10.771	1.191	0.839
150	90.0	95.0	92.5	6.05	-97.658	-10.863	.840	0.746
151	95.0	100.0	97.5	6.20	-98.691	-10.955	.489	0.653
152	100.0	105.0	102.5	7.23	-99.725	-11.032	-2.244	0.575
153	105.0	110.0	107.5	8.45	-99.051	-11.308	-1.497	0.295
154	110.0	115.0	112.5	10.28	-98.047	-11.505	-0.385	0.096
155	115.0	120.0	117.5	12.60	-98.681	-11.600	-1.087	??
156	120.0	125.0	122.5	14.48	-98.712	-11.443	-1.122	.160
157	125.0	130.0	127.5	17.35	-98.743	-11.285	-1.156	0.319
158	130.0	135.0	132.5	20.56	-98.851	-11.403	-1.276	0.199
159	140.0	145.0	142.5	28.49	-99.156	-11.736	-1.615	-0.138

depth (cm)			Temperature every 3 hours					
0	26.40	27.20	23.30	25.80	38.70	42.80	40.10	31.30
2	28.28	26.71	24.75	25.42	33.31	44.39	41.29	33.21
4	28.30	27.42	26.01	25.23	28.99	36.25	37.12	32.76
10	28.49	27.92	26.99	25.87	27.20	31.35	33.67	32.09
22.2	27.67	29.71	28.57	27.02	25.73	27.20	28.17	29.25
27.7	27.89	28.12	27.79	27.15	26.84	27.03	27.42	28.31
42.2	25.81	26.48	26.40	26.11	25.93	26.15	25.90	26.27
82.0	24.37	24.65	24.38	24.49	24.64	24.22	24.02	24.24
148	22.27	22.56	22.54	22.18	22.36	22.19	21.94	22.09
160	21.89	21.89	21.89	21.89	21.89	21.89	21.89	21.89

Julian day 217:(pvc column in contact with native soil)

Depth (cm) From	to	moisture content %		D vs SMOW	O18	D vs TAP water	O18
4.0	6.0	5.0	1.13	-64.270	3.017		
6.0	8.0	7.0	1.14	-63.819	2.846		
8.0	13.0	10.5	1.12	-63.560	2.363		
13.0	15.0	14.0	1.25	-63.291	3.994		
20.0	25.0	22.5	2.85	-70.591	1.908		
25.0	30.0	27.5	3.37	-75.986	-0.775		
30.0	35.0	32.5	3.38	-81.302	-3.595		
35.0	40.0	37.5	4.12	-84.904	-5.480		
40.0	45.0	42.5	4.34	-88.979	-7.243		
45.0	50.0	47.5	4.52	-89.400	-8.988		
50.0	52.0	51.0	4.66	-87.803	-9.132		
52.0	56.0	54.0	4.93	-94.926	-9.805		
56.0	60.0	58.0	4.75	-96.930	-10.151		
60.0	64.0	62.0	5.00	-93.255	-8.693		
64.0	70.0	67.0	4.95	-89.894	-11.472		
70.0	72.0	71.0	0.00	-88.235	-13.261		
72.0	76.0	74.0	5.31	-90.976	-10.584		
76.0	80.0	78.0	5.45	-93.483	-10.918		
80.0	85.0	82.5	5.65	-92.174	-13.485		
85.0	90.0	87.5	5.63	-88.680	-10.504		
90.0	95.0	92.5	6.08	-96.707	-11.147		
95.0	100.0	97.5	7.97	-95.878	-11.066		
100.0	105.0	102.5	6.96	-95.833	-10.911		
105.0	110.0	107.5	7.15	-92.645	-10.883		
110.0	115.0	112.5	9.54	-97.182	-10.971		
115.0	120.0	117.5	10.30	-94.036	-10.907		
132.0	138.0	135.0	10.91	-101.566	-11.056		

Julian day 217:(pvc column not in contact with native soil)

0.0	5.0	2.5	0.92	-66.796	-0.566
5.0	10.0	7.5	1.10	-62.973	3.229
10.0	15.0	12.5	1.27	-55.795	4.729

214	15.0	20.0	17.5	1.50	-57.708	5.242
215	20.0	23.0	21.5	2.25	-49.151	3.859
216	23.0	26.0	24.5	2.38	-61.136	2.257
217	26.0	30.0	28.0	2.63	-67.702	0.794
218	30.0	32.0	31.0	2.81	-73.767	-0.585
219	32.0	37.0	34.5	3.02	-82.644	-2.354
220	37.0	40.0	38.5	3.35	-83.754	-3.505
221	40.0	45.0	42.5	3.70	-85.331	-6.010
222	45.0	50.0	47.5	4.03	-107.746	-7.748
223	70.0	73.0	71.5	4.96	-101.309	-7.748
224	90.0	93.0	91.5	5.57	-103.581	-11.281
225	125.0	130.0	127.5	13.56	-95.340	-11.482

Julian day 222:

Depth (cm) From	to	moisture content %		D vs SMOW	O18	D vs TAP water	O18
0.0	2.0	1.0	1.06	-43.683	1.967	59.866	13.726
2.0	4.0	3.0	2.06	-39.528	3.419	64.471	15.195
4.0	6.0	5.0	3.37	-52.504	-0.204	50.090	11.530
6.0	7.0	6.5	4.13	-53.647	-2.520	48.823	9.187
7.0	9.0	8.0	5.02	-66.815	-3.649	34.229	8.044
9.0	11.0	10.0	5.11	-75.318	-6.584	24.805	5.075
11.0	14.0	12.5	5.19	-76.778	-7.479	23.187	4.169
14.0	17.0	15.5	5.45	-82.213	-7.853	17.164	3.791
17.0	21.0	19.0	5.68	-87.475	-8.093	11.332	3.548
21.0	26.0	23.5	5.51	-79.715	-8.332	19.932	3.306
26.0	30.0	28.0	5.98	-83.379	-8.273	15.872	3.366
30.0	33.0	31.5	5.44	-78.289	-8.399	21.513	3.239
33.0	36.0	34.5	6.19	-81.373	-8.644	18.095	2.991
36.0	40.0	38.0	6.15	-77.582	-8.232	22.296	3.408
40.0	42.0	41.0	6.35	-76.237	-8.496	23.787	3.140
42.0	45.0	43.5	6.43	-77.644	-8.398	22.228	3.240
45.0	51.0	48.0	6.44	-78.935	-8.385	20.797	3.253
73.0	81.0	77.0	6.72	-73.292	-8.219	27.051	3.423
81.0	87.0	84.0	13.04	??	??	22.144	3.413
95.0	98.0	96.5	11.27	??	??	22.248	3.405
102.0	105.0	103.5	11.60	-77.526	-8.242	22.358	3.397
115.0	120.0	117.5	25.61	??	??	11.388	2.255
122.0	127.0	124.5	22.91	??	??	6.840	1.689
130.0	135.0	132.5	29.44	-96.263	-10.576	1.593	1.036
150.0	155.0	152.5	28.58	??	??	00.15	0.002

depth (cm)			Temperature every 3 hours					
0	26.20	28.10	20.90	24.70	33.50	48.60	40.00	32.50
2	28.52	26.65	25.60	24.89	29.94	38.23	38.02	33.30
4	28.89	27.74	25.62	25.22	28.22	34.03	34.21	32.61
10	29.48	27.97	26.75	26.00	26.59	29.74	31.61	30.95
22.2	29.71	27.43	27.83	28.47	25.51	25.50	28.91	25.95
27.7	27.67	27.34	27.38	27.40	26.42	26.37	27.79	27.06
42.2	26.29	26.05	26.12	26.26	25.79	25.73	26.59	25.55
82.0	24.35	24.31	24.69	24.65	24.50	24.65	24.98	24.42
148	22.93	22.75	22.82	22.97	22.72	22.87	23.28	22.48
160	22.67	22.67	22.67	22.67	22.67	22.67	22.67	22.67

Julian day 236:

Depth (cm) From	to	moisture content %		D vs SMOW	O18	D vs TAP water	O18
1.0	3.5	2.2	1.23	-67.253	-3.851	33.744	7.840
3.5	7.5	5.5	2.18	-39.389	1.644	64.625	13.399
7.5	9.0	8.2	3.38	-48.867	-0.224	54.121	11.510

285	9.0	14.0	11.5	??	-49.456	-.5054	53.468	11.225
286	14.0	18.0	16.0	4.73	-60.396	-5.733	41.343	5.936
287	18.0	20.0	19.0	4.88	-72.909	-9.222	27.475	2.395
288	20.0	23.0	21.5	5.19	-72.824	-9.168	27.570	2.450
289	23.0	27.0	25.0	5.33	-77.153	-10.402	22.772	1.510
290	27.0	30.0	28.5	5.67	-78.765	-10.728	20.985	0.882
291	30.0	32.5	31.2	5.51	-79.677	-11.117	19.975	0.489
292	33.0	35.0	34.0	5.81	-77.224	-10.997	22.693	0.610
293	35.0	39.0	37.0	5.76	-79.983	-11.142	19.635	0.463
294	40.0	43.0	41.5	5.60	-78.682	-11.319	21.077	0.284
295	44.0	47.0	45.5	6.16	-78.083	-11.089	21.741	0.517
296	47.0	50.0	48.5	5.69	-83.073	-11.713	16.211	-0.114
297	68.0	72.0	70.0	5.97	-80.843	-10.442	18.600	1.172
298	80.0	83.0	81.5	21.01	??	??	13.311	0.333
299	83.0	87.0	85.0	21.46	??	??	11.701	0.078
300	95.0	97.0	96.0	26.46	??	??	8.551	-.4231
301	105.0	110.0	107.5	28.22	??	??	6.641	-.727
302	119.0	121.0	120.0	24.60	??	??	4.565	-1.057
303	136.0	139.0	137.5	27.21	??	??	1.659	-1.520
304	142.0	145.0	143.5	20.34	-97.103	-13.259	0.662	-1.678

307	depth (cm)			Temperature every 3 hours				
308	0	19.40	17.40	17.90	19.80	25.50	28.60	26.30	21.10
309	2	22.84	22.30	19.44	19.91	22.58	28.52	27.04	25.14
310	4	23.68	22.37	19.76	20.06	21.48	26.96	25.91	24.55
311	10	24.28	23.13	20.34	20.55	21.65	25.44	25.75	24.92
312	22.2	24.66	23.07	21.05	21.69	22.54	23.75	25.70	23.97
313	27.7	24.94	24.55	21.19	21.52	22.22	24.47	25.17	24.82
314	42.2	24.60	24.40	20.77	21.56	22.51	24.57	24.83	24.49
315	82.0	24.20	24.02	22.52	22.29	22.85	24.10	24.38	24.18
316	148	22.86	22.73	23.25	23.16	23.17	22.83	23.21	22.77
317	160	22.62	22.62	22.62	22.62	22.62	22.62	22.62	22.62

318

319 **********

320

321 WIPP SITE DATA

322

323

324 WIPP hole 2

325

326	depth	Deuterium oxygen-18
327	(cm)	enrichment (permil)
328	2.54	-60 7.14
329	7.62	-40 9.68
330	12.7	-5 16.73
331	17.78	1 16.13
332	22.86	8 11.33
333	27.94	1 7.66
334	33.02	-7 5.35
335	38.1	-13 2.57
336	43.18	-24 2.13
337	48.26	-24 1.46
338	53.34	-46 1.
339	58.42	-59 -0.75
340	63.5	-49 0.49
341	68.58	-53 0.05
342	73.66	-50 -1.75
343	78.74	-47 -0.63
344	83.82	-47 0.53
345	92.71	-42 -1.1
346	104.14	-47 -1.30
347	111.76	-40 1.61
348	119.38	-38 -1.79
349	129.54	-43 -1.4
350	139.7	-37 -1.9
351	149.86	-37 -2.42
352	160.02	-39 -2.55
353	168.91	-39 -1.41
354	177.8	-39 -2.89
355	186.69	-47 -2.87

356	195.58	-42	-2.24
357	204.47	-40	-3.28
358	212.09	-40	-1.04
359	240.03	-44	-2.50
360	259.08	-45	-2.60
361	304.8	-43	-2.703
362	351.79	-40	-2.264
363	364.49	-45	2.706

364

365 Depth/ moisture content/ cl conc./ 3-point moving average

366	2.54	0.004	2352	2352
367	7.62	0.004	1390	1850
368	12.70	0.005	1807	1164
369	17.78	0.083	295	1206
370	22.86	0.011	1516	1210
371	27.94	0.013	1820	1664
372	33.02	0.013	1657	1751
373	38.10	0.013	1777	1856
374	43.18	0.013	2135	2493
375	48.26	0.013	3567	2087
376	53.34	0.010	559	1586
377	58.42	0.010	632	614
378	63.50	0.010	652	769
379	68.58	0.008	1022	964
380	73.66	0.010	1218	1439
381	78.74	0.009	2077	2136
382	83.82	0.009	3112	2253
383	92.71	0.009	1569	1859
384	104.14	0.009	896	1557
385	111.76	0.010	2207	1346
386	119.38	0.010	936	1413
387	129.54	0.010	1096	1455
388	139.70	0.011	2333	1647
389	149.86	0.011	1512	1806
390	160.02	0.012	1572	2337
391	168.91	0.012	3927	2505
392	177.80	0.013	2016	2588
393	186.69	0.013	1822	1719
394	195.58	0.014	1318	1298
395	204.47	0.013	754	754

396

397 **********

398 WIPP hole 3

399

400	depth	oxygen-18 enrichment
401	(cm)	(permil)
402	2.54	-5.00
403	7.62	-4.48
404	12.7	7.11
405	17.78	10.96
406	22.86	13.31
407	33.02	13.36
408	38.10	3.88
409	43.18	2.68
410	48.26	3.25
411	53.34	0.54
412	58.24	-1.28
413	63.50	-1.16
414	68.58	-2.03
415	73.66	-3.17
416	83.82	-3.47
417	97.79	-3.56
418	107.95	-4.97
419	116.84	-4.58
420	125.73	-5.12
421	133.35	-5.21
422	142.24	-4.15
423	151.13	-5.23
424	161.29	-6.84
425	176.53	-6.30
426	185.42	-4.89

427	194.31	-4.02
428	209.55	-5.94
429	218.44	-6.06
430	228.60	-6.07
431	238.76	-6.81
432	248.92	-5.42
433	318.77	-6.54
434	328.93	-6.73
435	339.09	-6.49
436	349.25	-6.78
437	360.68	-7.01
438	370.84	-6.18
439	381.00	-7.73
440	391.16	-7.44
441	401.32	-7.82
442	411.48	-7.66
443	421.64	-9.37
444	431.80	-7.03
445	443.23	-7.06
446	453.39	-7.28
447	463.55	-6.61
448	473.71	-6.99
449	482.60	-7.11
450	492.76	-8.29
451	502.92	-7.29
452	511.81	-7.98
453	520.70	-7.96
454	530.86	-7.11
455	539.75	-8.57
456	556.26	-8.11
457	566.42	-8.80
458	585.47	-8.95
459		
460		
461		

	Depth (cm)	moisture content	cl conc. (mg/l)	3-point moving average conc. (mg/l)
462				
463				
464	2.54	0.018	497.233	497.233
465	7.62	0.011	596.680	535.1177
466	12.7	0.007	511.440	639.3000
467	17.78	0.007	809.780	554.0600
468	22.86	0.007	340.960	489.2400
469	27.94	0.008	316.980	235.8877
470	33.02	0.096	49.723	217.8560
471	38.10	0.013	286.865	149.9857
472	43.18	0.025	113.369	339.8387
473	48.26	0.033	619.282	393.3870
474	53.34	0.029	447.510	554.4907
475	58.24	0.019	596.680	690.6020
476	63.50	0.018	1027.616	831.4847
477	68.58	0.018	870.158	889.9827
478	73.66	0.017	772.174	1041.90
479	83.82	0.018	1483.413	1113.00
480	97.79	0.019	1083.445	1146.50
481	107.95	0.020	872.645	1184.10
482	116.84	0.020	1596.119	1257.30
483	125.73	0.019	1303.275	1400.90
484	133.35	0.019	1303.275	1609.70
485	142.24	0.020	2222.633	1646.40
486	151.13	0.019	1413.189	1639.70
487	161.29	0.019	2363.167	1633.0
488	170.18	0.019	1122.70	1639.30
489	176.53	0.020	1432.03	1675.80
490	185.42	0.020	1372.36	1712.30
491	194.31	0.022	2332.48	1768.30
492	201.93	0.022	1600.19	1836.50
493	209.55	0.021	1576.94	1442.60
494	218.44	0.035	1150.74	1307.00
495	228.60	0.022	1193.36	998.906
496	238.76	0.024	652.62	1057.90
497	248.92	0.020	1327.61	930.3133

498	259.08	0.023	810.71	925.2267
499	269.24	0.022	637.36	774.1700
500	279.40	0.029	874.44	662.310
501	289.56	0.027	475.13	582.4533
502	299.72	0.030	397.79	543.020
503	309.88	0.029	756.14	509.7533
504	318.77	0.031	375.33	484.3733
505	328.93	0.032	321.65	316.233
506	339.09	0.032	251.72	239.3400
507	349.25	0.033	144.65	167.8633
508	360.68	0.032	107.22	180.6400
509	370.84	0.036	290.05	187.9967
510	381.00	0.034	166.72	195.2600
511	391.16	0.037	129.01	231.6600
512	401.32	0.034	399.25	252.1333
513	411.48	0.034	228.14	278.4233
514	421.64	0.033	207.93	266.1133
515	431.80	0.035	362.27	277.8133
516	443.23	0.034	263.24	270.2567
517	453.39	0.033	185.33	211.3000
518	463.55	0.033	185.33	163.9533
519	473.71	0.032	121.20	126.4867
520	482.60	0.045	72.93	145.51
521	492.76	0.032	242.40	213.1300
522	502.92	0.029	324.06	226.4500
523	511.81	0.037	112.89	184.3233
524	520.70	0.045	116.02	122.2967
525	530.86	0.040	137.98	127.6100
526	539.75	0.044	128.83	183.9633
527	547.37	0.045	285.08	198.7433
528	556.26	0.049	182.32	216.5733
529	566.42	0.045	182.32	155.1100
530	576.58	0.080	100.69	203.3800
531	585.47	0.057	327.13	213.9100
532				

533 **********

534 WIPP hole 4

535

	depth (cm)	oxygen-18 enrichment (permil)
536		
537		
538		
539	2.50	6.98
540	6.50	9.65
541	9.00	14.17
542	11.50	13.39
543	15.50	13.44
544	19.00	9.51
545	22.00	7.32
546	27.00	5.51
547	30.75	5.00
548	33.25	4.73
549	38.25	4.45
550	47.50	3.24
551	59.00	2.04
552	69.50	1.82
553	79.00	0.87
554	87.50	1.41
555	96.00	0.38
556	104.50	0.07
557	112.50	-0.47
558	120.00	-0.15
559	130.00	-0.61
560	142.00	-1.07
561	148.50	-2.08
562	155.50	-1.15
563	167.00	-1.17
564	178.5	-1.16
565	207.25	-1.57
566	220.00	-0.93
567	232.25	-1.03
568	243.00	-1.42

```
569   253.50  -1.57
570   264.50  -1.60
571   276.00  -1.63
572   287.00  -1.47
573   298.00  -1.47
574   310.50  -1.03
575   321.50  -1.67
576   333.50  -1.76
577   345.00  -1.68
578   355.00  -1.52
579   365.00  -1.17
580   377.00  -1.61
581   389.00  -1.51
582   397.00  -1.34
583   415.00  -0.90
584   421.50  -1.80
585   438.50  -1.67
586
587   Depth/ moisture content/ cl conc./ 3-point moving average
588     2.50  0.03    762     762
589     6.50  0.02    708     671
590     9.00  0.04    543     636
591    11.50  0.05    656     632
592    15.50  0.06    697     773
593    19.00  0.07    965     781
594    22.00  0.11    681     757
595    27.00  0.11    626     621
596    30.75  0.10    557     537
597    33.75  0.09    419     508
598    38.25  0.07    538     494
599    47.50  0.06    526     645
600    59.00  0.04    872     676
601    69.50  0.06    630     821
602    79.00  0.06    962     842
603    87.50  0.05    935     879
604    96.00  0.05    739     812
605   104.50  0.05    762     697
606   112.50  0.04    589     602
607   120.00  0.04    455     507
608   130.00  0.04    478     438
609   142.00  0.04    381     410
610   148.50  0.04    370     375
611   155.50  0.04    375     328
612   167.00  0.05    239     290
613   178.50  0.04    255     251
614   207.25  0.03    258     268
615   220.00  0.03    292     239
616   232.25  0.05    166     203
617   243.00  0.04    152     164
618   253.50  0.05    173     148
619   264.50  0.05    120     136
620   276.50  0.05    114     119
621   287.00  0.05    123     135
622   298.50  0.04    169     167
623   310.50  0.03    209     186
624   321.50  0.03    179     176
625   333.50  0.03    141     152
626   345.00  0.03    136     155
627   355.00  0.03    187     151
628   365.00  0.05    130     160
629   377.00  0.03    164     136
630   389.00  0.04    115     179
631   397.00  0.02    259     237
632   415.00  0.02    337     338
633   421.50  0.02    417     330
634   438.50  0.04    237     237
635
636   ***************************************************************
637   WIPP hole 5
638
639   depth  oxugen-18 enrichment
```



```
640   (cm)    (permil)
641     5.00  -0.76
642     8.00   3.66
643    11.50   8.66
644    15.75   9.55
645    19.25  10.43
646    22.25   9.54
647    24.75   8.65
648    29.00   0.46
649    34.00   3.82
650    38.25   0.65
651    41.75  0.1025
652    44.50 -0.3277
653    51.50 -1.4228
654    63.50 -3.30
655    75.00 -2.97
656    85.00 -2.64
657    94.50 -2.78
658   107.50 -2.91
659   114.50 -1.80
660   117.50 -2.29
661   119.00 -2.10
662   124.00 -1.91
663   132.00 -2.25
664   141.00 -2.59
665   150.50 -2.88
666   157.50 -3.16
667   164.00 -3.19
668   172.50 -3.21
669   180.50 -3.32
670   187.00 -3.43
671
672
673
674   Depth/ moisture content/ cl conc./ 3-point moving average
675     5.00  0.01    1364    1364
676     8.00  0.01    1317    1371
677    11.50  0.01    1431    1379
678    15.75  0.01    1390    1213
679    19.25  0.01     818     977
680    22.25  0.01     723     681
681    24.75  0.01     501     530
682    29.00  0.02     365     493
683    34.00  0.02     613     455
684    38.25  0.02     388     426
685    41.75  0.02     277     281
686    51.50  0.03     179     206
687    63.50  0.04     163     208
688    75.00  0.03     283     224
689    85.00  0.03     226     235
690    94.50  0.03     196     191
691   107.50  0.04     150     156
692   114.50  0.04     122     107
693   117.50  0.09      49      81
694   119.00  0.10      71      62
695   124.00  0.12      67      59
696   132.00  0.14      40      51
697   141.00  0.14      47      44
698   150.50  0.14      46      47
699   157.50  0.15      48      61
700   164.00  0.13      90      76
701   172.50  0.13      89      84
702   180.50  0.12      72      69
703   187.00  0.13      46      55
704   194.50  0.21      47      47
705
706   ***************************************************************
707   WIPP hole 6
708
709   depth  oxugen-18 enrichment
710   (cm)    (permil)
```

```
711
712      2.50    0.86
713      7.50    2.09
714     10.00   10.49
715     14.50   10.18
716     30.25    9.22
717     36.50    6.82
718     44.00    1.97
719     51.00    0.96
720     55.50   -2.02
721     59.50   -2.02
722     68.00   -2.09
723     73.50   -2.52
724     78.00   -2.59
725     82.00   -2.64
726     92.50   -2.51
727     99.50   -2.90
728    108.50   -2.07
729    117.00    3.56
730    126.50   -4.18
731    136.00   -2.98
732    145.00   -2.98
733    155.00   -3.67
734    162.50   -4.36
735    169.00   -3.80
736    176.50   -3.24
737    185.00   -4.04
738    194.50   -4.83
739
740   Depth/ moisture content/ cl conc./ 3-point moving average
741      2.50  0.004   1460    1460
742      7.50  0.004   1216    1135
743     10.00  0.008    730     950
744     14.50  0.006    903     756
745     19.50  0.014    635     860
746     30.25  0.008   1043     759
747     36.50  0.013    599     672
748     44.00  0.025    373     402
749     51.00  0.038    234     264
750     55.50  0.055    184     185
751     59.50  0.065    137     135
752     68.00  0.083     85      99
753     73.50  0.095     76      92
754     78.00  0.084    116     118
755     82.00  0.071    162     140
756     92.50  0.078    143     160
757     99.50  0.048    174     159
758    108.50  0.054    160     172
759    117.00  0.036    181     200
760    126.50  0.043    259     279
761    136.00  0.044    398     361
762    145.50  0.046    426     347
763    155.00  0.049    218     283
764    162.50  0.044    204     184
765    169.00  0.061    130     178
766    176.50  0.049    199     167
767    185.00  0.067    172     194
768    194.50  0.055    210     210
769
770   ****************************************************
771            SOIL PROPERTIES
772
773
774   Sieve analysis:
775   grain size (mm)  % passing
776            0.300    9.3
777            0.425   39.5
778            0.600   56.8
779            0.850   64.2
780            2.000   76.0
781            2.360  100.0
```



```
782
783   Thermal conductivity of soil
784   moisture content, thermal conductivity(cal/(cm s C)
785   .010 .5E-3
786   .030 1.E-3
787   .040 1.25E-3
788   .050 1.60E-3
789   .06 1.75E-3
790   .07 2.1E-3
791   .08 2.35E-3
792   .09 2.5E-3
793   .10 2.65E-3
794   .12 3.E-3
795   .18 4.E-3
796   .20 4.2E-3
797   .25 4.5E-3
798   .30 5.0E-3
799   .351 5.2E-3
800
801   Retention relation (moisture content, log(-psi) where psi is in cm)
802   from filter paper method
803   .01395      4.41591
804   .02265      3.20531
805   .0300       2.40038
806   .0501       1.79088
807   .0615       1.6599
808   .0906       1.5647
809   .1032       1.53491
810   .1128       1.49986
811   .1251       1.46432
812   .1352       1.39475
813   .1505       1.3444
814   .2001       1.3345
815   .2500       1.1931
816   .3179       1.0453
817
818
819   Retention relation as from Vangenuchton model
820   .0245       3.01000
821   .0263       2.80280
822   .0300       2.40038
823   .0400       2.15000
824   .0547    1.79088
825   .0631    1.6599
826   .0849    1.5647
827   .0948    1.53491
828   .1078    1.49986
829   .1222    1.46432
830   .1532    1.39475
831   .1774    1.3444
832   .1823    1.3345
833   .2498    1.1931
834   .3019    1.0453
835   .3450    0.50000
836   .3500    0.00000
837
838   Retention relation for moisture contents below the moisture content at
839   liquid discontinuity as calculated fron kelvin relation
840   moisture  log(-psi) psi in cm
841   content
842   .0170       6.34020
843   .0175       6.25523
844   .0180       6.17090
845   .0190       6.00320
846   .0200       5.81620
847   .0205       5.70576
848   .0210       5.57390
849   .0214       5.44257
850   .0218       5.26880
851   .0220       5.15300
852   .0223       4.90140
```

```
.0224     4.77204
.0225     4.59300
.02256    4.43604
.0226     4.28870
.02265    3.98610
.02267    3.76365
.02268    3.58730
.02269    3.28592
.0227     3.20531


Hydraulic cond. (cm/s) as calculated from Van Genuchton model
moisture  log(K) where K is in cm/s
content             K (cm/s)
.0215     -12.916   1.2134e-13
.0227     -12.586   2.5942e-13
.0300     -10.580   2.6303e-11
.0331      -9.728   1.8707e-10
.0423      -9.011   9.7499e-10
.0516      -6.991   1.0209e-07
.0609      -5.767  1.7100e-06
.0816      -4.506    3.1189e-05
.1077      -4.065    8.6099e-05
.1392      -3.653    2.2233e-04
.1747      -3.280    5.2481e-04
.2117      -2.955     0.0011
.2468      -2.686     0.0021
.2769      -2.471     0.0034
.3007      -2.308     0.0049
.3180      -2.187     0.0065
.3298      -2.099     0.0080
.3377      -2.036     0.0092
.3427      -1.992     0.0102
.3459      -1.960     0.0110
.3498      -1.909     0.0123
.3503      -1.901     0.0126
.3508      -1.887     0.0130
.3510      -1.879     0.0132


Sutface conditions :
Julian day   Temp(C)  relative humidity %
    129.000 20.0000 19.0000
    129.125 17.2000 31.0000
    129.250 13.2000 37.0000
    129.375 21.3000 48.0000
    129.500 35.6000 34.0000
    129.625 19.3000 31.0000
    129.750 17.6000 34.0000
    129.875 22.4000 42.0000
    130.000 20.0000 19.0000
    130.125 17.2000 31.0000
    130.250 13.2000 37.0000
    130.375 21.3000 48.0000
    130.500 35.6000 34.0000
    130.625 19.3000 31.0000
    130.750 17.6000 34.0000
    130.875 22.4000 42.0000
    131.000 20.0000 19.0000
    131.125 17.2000 31.0000
    131.250 13.2000 37.0000
    131.375 21.3000 48.0000
    131.500 35.6000 34.0000
    131.625 19.3000 31.0000
    131.750 17.6000 34.0000
    131.875 22.4000 42.0000
    132.000 20.0000 19.0000
    132.125 17.2000 31.0000
    132.250 13.2000 37.0000
    132.375 21.3000 48.0000
    132.500 35.6000 34.0000
```



```
    132.625 19.3000 31.0000
    132.750 17.6000 34.0000
    132.875 22.4000 42.0000
    133.000 20.0000 19.0000
    133.125 17.2000 31.0000
    133.250 13.2000 37.0000
    133.375 21.3000 48.0000
    133.500 35.6000 34.0000
    133.625 19.3000 31.0000
    133.750 17.6000 34.0000
    133.875 22.4000 42.0000
    134.000 33.8000 34.0000
    134.125 38.7000 15.0000
    134.250 31.1000 11.0000
    134.375 20.7000 60.0000
    134.500 33.9000 45.0000
    134.625 38.4000 22.0000
    134.750 37.0000 9.00000
    134.875 26.3000 12.0000
    135.000 20.0000 19.0000
    135.125 17.2000 31.0000
    135.250 13.2000 37.0000
    135.375 21.3000 48.0000
    135.500 35.6000 34.0000
    135.625 37.4000 13.0000
    135.750 29.8000 11.0000
    135.875 25.0000 13.0000
    136.000 18.8000 21.0000
    136.125 19.3000 31.0000
    136.250 17.6000 34.0000
    136.375 22.4000 42.0000
    136.500 33.8000 34.0000
    136.625 38.7000 15.0000
    136.750 31.1000 11.0000
    136.875 26.7000 13.0000
    137.000 18.2000 17.0000
    137.125 13.4000 26.0000
    137.250 11.9000 37.0000
    137.375 19.3000 46.0000
    137.500 33.7000 34.0000
    137.625 41.9000 17.0000
    137.750 34.4000 11.0000
    137.875 23.9000 16.0000
    138.000 20.1000 30.0000
    138.125 17.8000 40.0000
    138.250 13.7000 45.0000
    138.375 21.0000 52.0000
    138.500 29.0000 45.0000
    138.625 35.5000 30.0000
    138.750 35.8000 16.0000
    138.875 22.8000 20.0000
    139.000 19.5000 46.0000
    139.125 17.6000 53.0000
    139.250 14.9000 58.0000
    139.375 21.0000 63.0000
    139.500 30.7000 51.0000
    139.625 33.8000 31.0000
    139.750 29.3000 25.0000
    139.875 24.1000 28.0000
    140.000 20.2000 38.0000
    140.125 15.9000 54.0000
    140.250 15.3000 76.0000
    140.375 15.8000 87.0000
    140.500 20.3000 89.0000
    140.625 29.2000 80.0000
    140.750 25.5000 71.0000
    140.875 20.0000 70.0000
    141.000 16.8000 74.0000
    141.125 13.8000 83.0000
    141.250 14.0000 88.0000
    141.375 18.1000 89.0000
```

995	141.500	26.4000	80.0000
996	141.625	29.0000	65.0000
997	141.750	23.9000	58.0000
998	141.875	19.7000	65.0000
999	142.000	15.7000	79.0000
1000	142.125	13.9000	89.0000
1001	142.250	12.8000	86.0000
1002	142.375	17.4000	88.0000
1003	142.500	25.4000	76.0000
1004	142.625	26.0000	62.0000
1005	142.750	21.0000	61.0000
1006	142.875	16.9000	65.0000
1007	143.000	15.5000	71.0000
1008	143.125	13.5000	78.0000
1009	143.250	11.2000	86.0000
1010	143.375	13.6000	89.0000
1011	143.500	18.2000	87.0000
1012	143.625	22.7000	80.0000
1013	143.750	20.9000	74.0000
1014	143.875	16.2000	75.0000
1015	144.000	13.8000	83.0000
1016	144.125	13.0000	88.0000
1017	144.250	11.5000	89.0000
1018	144.375	15.5000	90.0000
1019	144.500	15.4000	88.0000
1020	144.625	17.2000	89.0000
1021	144.750	20.6000	87.0000
1022	144.875	16.6000	84.0000
1023	145.000	12.5000	88.0000
1024	145.125	10.50000	91.0000
1025	145.250	10.10000	92.0000
1026	145.375	15.8000	92.0000
1027	145.500	24.2000	86.0000
1028	145.625	27.6000	73.0000
1029	145.750	22.0000	63.0000
1030	145.875	17.1000	66.0000
1031	146.000	13.8000	79.0000
1032	146.125	13.0000	86.0000
1033	146.250	10.8000	89.0000
1034	146.375	16.9000	90.0000
1035	146.500	26.1000	78.0000
1036	146.625	27.2000	65.0000
1037	146.750	24.9000	54.0000
1038	146.875	20.6000	54.0000
1039	147.000	16.7000	64.0000
1040	147.125	13.8000	76.0000
1041	147.250	13.6000	85.0000
1042	147.375	16.4000	88.0000
1043	147.500	25.4000	79.0000
1044	147.625	25.5000	65.0000
1045	147.750	20.8000	58.0000
1046	147.875	16.9000	75.0000
1047	148.000	15.5000	84.0000
1048	148.125	15.3000	76.0000
1049	148.250	11.3000	82.0000
1050	148.375	17.7000	88.0000
1051	148.500	28.9000	72.0000
1052	148.625	32.3000	56.0000
1053	148.750	30.4000	44.0000
1054	148.875	21.4000	43.0000
1055	149.000	17.5000	61.0000
1056	149.125	14.8000	74.0000
1057	149.250	14.4000	83.0000
1058	149.375	15.7000	86.0000
1059	149.500	21.8000	80.0000
1060	149.625	26.0000	72.0000
1061	149.750	18.7000	63.0000
1062	149.875	17.0000	77.0000
1063	150.000	15.7000	80.0000
1064	150.125	13.9000	86.0000
1065	150.250	11.6000	89.0000

1066	150.375	15.7000	90.0000
1067	150.500	26.1000	85.0000
1068	150.625	24.6000	66.0000
1069	150.750	24.2000	60.0000
1070	150.875	15.8000	62.0000
1071	151.000	13.5000	79.0000
1072	151.125	12.1000	86.0000
1073	151.250	11.0000	89.0000
1074	151.375	18.6000	90.0000
1075	151.500	25.8000	82.0000
1076	151.625	26.1000	65.0000
1077	151.750	23.4000	64.0000
1078	151.875	20.9000	61.0000
1079	152.000	15.8000	72.0000
1080	152.125	14.4000	82.0000
1081	152.250	13.7000	83.0000
1082	152.375	19.0000	84.0000
1083	152.500	26.5000	67.0000
1084	152.625	28.5000	49.0000
1085	152.750	23.8000	40.0000
1086	152.875	20.0000	40.0000
1087	153.000	14.7000	48.0000
1088	153.125	13.2000	66.0000
1089	153.250	11.0000	72.0000
1090	153.375	17.1000	78.0000
1091	153.500	29.1000	62.0000
1092	153.625	36.2000	41.0000
1093	153.750	32.6000	30.0000
1094	153.875	24.1000	33.0000
1095	154.000	16.0000	57.0000
1096	154.125	13.2000	71.0000
1097	154.250	17.5000	73.0000
1098	154.375	23.0000	69.0000
1099	154.500	32.3000	53.0000
1100	154.625	31.7000	34.0000
1101	154.750	26.0000	33.0000
1102	154.875	19.4000	77.0000
1103	155.000	16.2000	89.0000
1104	155.125	14.9000	91.0000
1105	155.250	13.6000	92.0000
1106	155.375	20.0000	92.0000
1107	155.500	29.3000	83.0000
1108	155.625	34.1000	69.0000
1109	155.750	32.6000	58.0000
1110	155.875	23.9000	61.0000
1111	156.000	18.4000	74.0000
1112	156.125	18.5000	83.0000
1113	156.250	17.3000	81.0000
1114	156.375	22.6000	80.0000
1115	156.500	33.6000	63.0000
1116	156.625	33.3000	51.0000
1117	156.750	31.1000	38.0000
1118	156.875	27.7000	43.0000
1119	157.000	21.7000	43.0000
1120	157.125	17.0000	50.0000
1121	157.250	14.8000	69.0000
1122	157.375	21.6000	79.0000
1123	157.500	33.7000	60.0000
1124	157.625	35.7000	41.0000
1125	157.750	31.9000	28.0000
1126	157.875	24.9000	28.0000
1127	158.000	20.4000	49.0000
1128	158.125	19.8000	61.0000
1129	158.250	16.6000	67.0000
1130	158.375	23.1000	73.0000
1131	158.500	32.8000	57.0000
1132	158.625	33.5000	40.0000
1133	158.750	25.3000	34.0000
1134	158.875	17.3000	52.0000
1135	159.000	16.8000	72.0000
1136	159.125	14.2000	81.0000

1137	159.250	14.9000	85.0000
1138	159.375	19.0000	87.0000
1139	159.500	29.5000	76.0000
1140	159.625	25.8000	50.0000
1141	159.750	17.8000	48.0000
1142	159.875	17.1000	73.0000
1143	160.000	14.6000	80.0000
1144	160.125	14.2000	85.0000
1145	160.250	12.3000	87.0000
1146	160.375	16.5000	89.0000
1147	160.500	27.8000	82.0000
1148	160.625	33.5000	58.0000
1149	160.750	27.3000	45.0000
1150	160.875	21.2000	53.0000
1151	161.000	15.8000	63.0000
1152	161.125	13.9000	77.0000
1153	161.250	12.9000	84.0000
1154	161.375	19.0000	86.0000
1155	161.500	31.0000	69.0000
1156	161.625	33.6000	47.0000
1157	161.750	33.4000	36.0000
1158	161.875	25.6000	38.0000
1159	162.000	17.7000	55.0000
1160	162.125	16.7000	73.0000
1161	162.250	14.7000	80.0000
1162	162.375	19.9000	85.0000
1163	162.500	34.3000	66.0000
1164	162.625	37.9000	36.0000
1165	162.750	34.8000	20.0000
1166	162.875	29.4000	21.0000
1167	163.000	23.7000	30.0000
1168	163.125	19.4000	38.0000
1169	163.250	19.0000	53.0000
1170	163.375	22.1000	66.0000
1171	163.500	34.0000	55.0000
1172	163.625	38.8000	36.0000
1173	163.750	37.7000	24.0000
1174	163.875	28.5000	22.0000
1175	164.000	21.0000	30.0000
1176	164.125	17.7000	48.0000
1177	164.250	14.9000	59.0000
1178	164.375	21.8000	64.0000
1179	164.500	34.6000	36.0000
1180	164.625	38.5000	21.0000
1181	164.750	36.6000	13.0000
1182	164.875	27.5000	14.0000
1183	165.000	23.4000	15.0000
1184	165.125	16.1000	27.0000
1185	165.250	14.8000	45.0000
1186	165.375	20.1000	57.0000
1187	165.500	34.3000	45.0000
1188	165.625	37.7000	20.0000
1189	165.750	35.1000	11.0000
1190	165.875	29.1000	12.0000
1191	166.000	22.0000	15.0000
1192	166.125	17.3000	30.0000
1193	166.250	13.7000	38.0000
1194	166.375	20.0000	48.0000
1195	166.500	34.1000	39.0000
1196	166.625	36.3000	20.0000
1197	166.750	32.2000	12.0000
1198	166.875	30.0000	12.0000
1199	167.000	23.0000	15.0000
1200	167.125	22.0000	22.0000
1201	167.250	23.0000	18.0000
1202	167.375	21.3000	24.0000
1203	167.500	33.4000	27.0000
1204	167.625	39.6000	15.0000
1205	167.750	35.5000	10.00000
1206	167.875	28.1000	10.00000
1207	168.000	22.3000	14.0000

1208	168.125	19.5000	16.0000
1209	168.250	15.7000	19.0000
1210	168.375	21.5000	22.0000
1211	168.500	31.6000	19.0000
1212	168.625	40.1000	12.0000
1213	168.750	38.1000	9.00000
1214	168.875	28.9000	13.0000
1215	169.000	19.4000	24.0000
1216	169.125	17.0000	40.0000
1217	169.250	13.6000	45.0000
1218	169.375	18.7000	53.0000
1219	169.500	32.9000	43.0000
1220	169.625	40.3000	24.0000
1221	169.750	38.4000	10.00000
1222	169.875	28.9000	11.0000
1223	170.000	22.8000	25.0000
1224	170.125	17.8000	36.0000
1225	170.250	17.7000	41.0000
1226	170.375	22.4000	47.0000
1227	170.500	35.6000	32.0000
1228	170.625	37.4000	22.0000
1229	170.750	37.5000	13.0000
1230	170.875	30.3000	17.0000
1231	171.000	23.2000	24.0000
1232	171.125	19.4000	39.0000
1233	171.250	16.9000	46.0000
1234	171.375	23.6000	47.0000
1235	171.500	33.4000	40.0000
1236	171.625	38.1000	32.0000
1237	171.750	38.6000	16.0000
1238	171.875	31.3000	12.0000
1239	172.000	24.9000	14.0000
1240	172.125	21.4000	21.0000
1241	172.250	22.6000	38.0000
1242	172.375	24.0000	46.0000
1243	172.500	25.3000	40.0000
1244	172.625	36.6000	29.0000
1245	172.750	32.4000	27.0000
1246	172.875	25.9000	25.0000
1247	173.000	22.3000	35.0000
1248	173.125	18.3000	40.0000
1249	173.250	15.7000	49.0000
1250	173.375	21.8000	56.0000
1251	173.500	35.3000	47.0000
1252	173.625	41.8000	27.0000
1253	173.750	35.8000	19.0000
1254	173.875	27.2000	18.0000
1255	174.000	19.9000	35.0000
1256	174.125	19.1000	43.0000
1257	174.250	16.5000	49.0000
1258	174.375	20.2000	55.0000
1259	174.500	37.1000	43.0000
1260	174.625	42.5000	19.0000
1261	174.750	36.6000	10.00000
1262	174.875	26.1000	17.0000
1263	175.000	21.5000	38.0000
1264	175.125	18.8000	47.0000
1265	175.250	17.3000	58.0000
1266	175.375	21.4000	66.0000
1267	175.500	37.4000	55.0000
1268	175.625	40.7000	26.0000
1269	175.750	38.8000	13.0000
1270	175.875	34.3000	10.00000
1271	176.000	26.6000	14.0000
1272	176.125	21.9000	18.0000
1273	176.250	17.8000	30.0000
1274	176.375	23.9000	40.0000
1275	176.500	37.0000	31.0000
1276	176.625	34.8000	14.0000
1277	176.750	29.5000	22.0000
1278	176.875	27.1000	25.0000

1279	177.000	22.0000	32.0000
1280	177.125	18.1000	45.0000
1281	177.250	16.9000	53.0000
1282	177.375	20.6000	60.0000
1283	177.500	33.0000	47.0000
1284	177.625	44.4000	23.0000
1285	177.750	35.1000	14.0000
1286	177.875	30.2000	16.0000
1287	178.000	26.7000	14.0000
1288	178.125	19.4000	18.0000
1289	178.250	18.5000	27.0000
1290	178.375	21.2000	39.0000
1291	178.500	38.0000	31.0000
1292	178.625	39.9000	13.0000
1293	178.750	40.3000	6.00000
1294	178.875	31.2000	9.00000
1295	179.000	25.1000	13.0000
1296	179.125	20.8000	16.0000
1297	179.250	18.5000	28.0000
1298	179.375	23.2000	39.0000
1299	179.500	40.0000	30.0000
1300	179.625	44.7000	11.0000
1301	179.750	42.0000	7.00000
1302	179.875	33.4000	8.00000
1303	180.000	26.6000	13.0000
1304	180.125	20.7000	23.0000
1305	180.250	20.6000	34.0000
1306	180.375	25.7000	38.0000
1307	180.500	39.4000	27.0000
1308	180.625	46.5000	10.00000
1309	180.750	41.8000	6.00000
1310	180.875	33.6000	8.00000
1311	181.000	31.1000	10.00000
1312	181.125	23.6000	12.0000
1313	181.250	17.2000	17.0000
1314	181.375	23.7000	28.0000
1315	181.500	36.8000	24.0000
1316	181.625	45.5000	9.00000
1317	181.750	43.6000	5.00000
1318	181.875	30.6000	9.00000
1319	182.000	25.6000	13.0000
1320	182.125	19.7000	17.0000
1321	182.250	17.1000	27.0000
1322	182.375	22.7000	36.0000
1323	182.500	39.9000	24.0000
1324	182.625	39.3000	9.00000
1325	182.750	40.7000	7.00000
1326	182.875	33.6000	8.00000
1327	183.000	28.9000	12.0000
1328	183.125	25.0000	12.0000
1329	183.250	22.4000	14.0000
1330	183.375	24.4000	16.0000
1331	183.500	31.3000	13.0000
1332	183.625	43.4000	7.00000
1333	183.750	41.0000	6.00000
1334	183.875	30.3000	9.00000
1335	184.000	22.0000	15.0000
1336	184.125	17.4000	24.0000
1337	184.250	19.0000	24.0000
1338	184.375	23.5000	30.0000
1339	184.500	35.2000	32.0000
1340	184.625	42.6000	16.0000
1341	184.750	39.2000	9.00000
1342	184.875	32.5000	10.00000
1343	185.000	25.0000	15.0000
1344	185.125	25.5000	28.0000
1345	185.250	21.5000	36.0000
1346	185.375	25.3000	43.0000
1347	185.500	42.0000	35.0000
1348	185.625	37.8000	17.0000
1349	185.750	31.5000	16.0000

1350	185.875	26.0000	54.0000
1351	186.000	21.8000	81.0000
1352	186.125	22.6000	83.0000
1353	186.250	17.5000	85.0000
1354	186.375	25.9000	86.0000
1355	186.500	37.0000	71.0000
1356	186.625	42.8000	46.0000
1357	186.750	41.2000	40.0000
1358	186.875	28.6000	42.0000
1359	187.000	24.3000	69.0000
1360	187.125	21.7000	78.0000
1361	187.250	19.1000	80.0000
1362	187.375	25.5000	83.0000
1363	187.500	36.4000	66.0000
1364	187.625	45.3000	31.0000
1365	187.750	37.2000	31.0000
1366	187.875	30.4000	32.0000
1367	188.000	26.1000	36.0000
1368	188.125	20.6000	57.0000
1369	188.250	20.1000	70.0000
1370	188.375	23.5000	77.0000
1371	188.500	35.6000	50.0000
1372	188.625	44.8000	27.0000
1373	188.750	44.4000	16.0000
1374	188.875	29.7000	18.0000
1375	189.000	24.2000	26.0000
1376	189.125	22.0000	37.0000
1377	189.250	20.7000	43.0000
1378	189.375	25.3000	51.0000
1379	189.500	35.8000	38.0000
1380	189.625	43.2000	17.0000
1381	189.750	41.5000	9.00000
1382	189.875	30.2000	12.0000
1383	190.000	24.8000	27.0000
1384	190.125	26.3000	36.0000
1385	190.250	20.8000	43.0000
1386	190.375	25.3000	52.0000
1387	190.500	33.6000	38.0000
1388	190.625	40.2000	23.0000
1389	190.917	27.7000	21.0000
1390	190.875	28.1000	30.0000
1391	191.000	24.7000	34.0000
1392	191.125	23.4000	44.0000
1393	191.250	20.9000	53.0000
1394	191.375	24.5000	58.0000
1395	191.500	35.7000	45.0000
1396	191.625	33.5000	28.0000
1397	191.750	27.8000	37.0000
1398	191.875	25.1000	38.0000
1399	192.000	21.0000	48.0000
1400	192.125	20.6000	58.0000
1401	192.250	18.3000	64.0000
1402	192.375	24.1000	69.0000
1403	192.500	30.0000	60.0000
1404	192.625	38.0000	34.0000
1405	192.750	22.4000	21.0000
1406	192.875	27.1000	29.0000
1407	193.000	21.7000	40.0000
1408	193.125	18.5000	48.0000
1409	193.250	17.6000	59.0000
1410	193.375	21.1000	67.0000
1411	193.500	29.1000	54.0000
1412	193.625	31.8000	32.0000
1413	193.750	29.1000	39.0000
1414	193.875	24.5000	44.0000
1415	194.000	21.6000	54.0000
1416	194.125	18.1000	65.0000
1417	194.250	14.9000	70.0000
1418	194.375	21.8000	72.0000
1419	194.500	31.9000	45.0000
1420	194.625	42.4000	19.0000

1421	194.750	37.9000	11.0000
1422	194.875	29.5000	12.0000
1423	195.000	24.1000	17.0000
1424	195.125	21.6000	28.0000
1425	195.250	19.3000	36.0000
1426	195.375	23.5000	39.0000
1427	195.500	33.5000	27.0000
1428	195.625	45.6000	11.0000
1429	195.750	38.4000	7.00000
1430	195.875	33.5000	9.00000
1431	196.000	24.8000	15.0000
1432	196.125	20.1000	22.0000
1433	196.250	18.8000	29.0000
1434	196.375	22.2000	37.0000
1435	196.500	33.7000	31.0000
1436	196.625	46.0000	10.00000
1437	196.750	36.7000	8.00000
1438	196.875	31.4000	10.00000
1439	197.000	26.4000	16.0000
1440	197.125	27.2000	17.0000
1441	197.250	23.3000	17.0000
1442	197.375	25.8000	23.0000
1443	197.500	38.7000	16.0000
1444	197.625	42.8000	8.00000
1445	197.750	40.1000	7.00000
1446	197.875	31.3000	11.0000
1447	198.000	25.1000	21.0000
1448	198.125	23.6000	32.0000
1449	198.250	20.2000	40.0000
1450	198.375	26.0000	48.0000
1451	198.500	35.3000	39.0000
1452	198.625	41.8000	19.0000
1453	198.750	24.8000	29.0000
1454	198.875	27.3000	32.0000
1455	199.000	22.6000	40.0000
1456	199.125	18.6000	48.0000
1457	199.250	17.6000	53.0000
1458	199.375	20.0000	62.0000
1459	199.500	34.5000	47.0000
1460	199.625	42.5000	25.0000
1461	199.750	32.4000	11.0000
1462	199.875	27.6000	14.0000
1463	200.000	24.2000	21.0000
1464	200.125	20.3000	34.0000
1465	200.250	18.0000	42.0000
1466	200.375	21.1000	50.0000
1467	200.500	32.9000	48.0000
1468	200.625	46.8000	22.0000
1469	200.750	41.5000	6.00000
1470	200.875	32.4000	11.0000
1471	201.000	27.9000	22.0000
1472	201.125	25.8000	33.0000
1473	201.250	18.8000	41.0000
1474	201.375	23.0000	48.0000
1475	201.500	33.9000	37.0000
1476	201.625	45.0000	16.0000
1477	201.750	49.2000	6.00000
1478	201.875	31.1000	11.0000
1479	202.000	24.7000	20.0000
1480	202.125	24.0000	34.0000
1481	202.250	21.5000	40.0000
1482	202.375	28.3000	45.0000
1483	202.500	34.6000	35.0000
1484	202.625	48.5000	18.0000
1485	202.750	37.8000	11.0000
1486	202.875	24.5000	35.0000
1487	203.000	19.6000	64.0000
1488	203.125	21.5000	70.0000
1489	203.250	19.9000	76.0000
1490	203.375	23.2000	80.0000
1491	203.500	31.0000	69.0000

1492	203.625	40.1000	41.0000
1493	203.750	34.9000	37.0000
1494	203.875	22.7000	41.0000
1495	204.000	20.5000	57.0000
1496	204.125	19.1000	67.0000
1497	204.250	22.1000	73.0000
1498	204.375	22.5000	77.0000
1499	204.500	29.5000	64.0000
1500	204.625	35.6000	43.0000
1501	204.750	31.1000	35.0000
1502	204.875	23.4000	47.0000
1503	205.000	21.8000	61.0000
1504	205.125	20.1000	72.0000
1505	205.250	20.3000	78.0000
1506	205.375	19.0000	82.0000
1507	205.500	25.6000	82.0000
1508	205.625	33.5000	61.0000
1509	205.750	32.3000	39.0000
1510	205.875	22.8000	53.0000
1511	206.000	19.7000	69.0000
1512	206.125	21.1000	80.0000
1513	206.250	18.5000	86.0000
1514	206.375	19.5000	90.0000
1515	206.500	27.2000	89.0000
1516	206.625	30.7000	70.0000
1517	206.750	27.1000	62.0000
1518	206.875	24.2000	67.0000
1519	207.000	19.9000	79.0000
1520	207.125	19.5000	94.0000
1521	207.250	19.5000	97.0000
1522	207.375	19.5000	97.0000
1523	207.500	26.5000	94.0000
1524	207.625	30.6000	85.0000
1525	207.750	29.1000	77.0000
1526	207.875	25.8000	85.0000
1527	208.000	21.3000	93.0000
1528	208.125	22.2000	94.0000
1529	208.250	19.5000	95.0000
1530	208.375	21.8000	96.0000
1531	208.500	27.5000	91.0000
1532	208.625	30.4000	81.0000
1533	208.750	32.6000	74.0000
1534	208.875	23.4000	70.0000
1535	209.000	21.1000	84.0000
1536	209.125	20.4000	88.0000
1537	209.250	18.7000	92.0000
1538	209.375	21.4000	93.0000
1539	209.500	27.7000	92.0000
1540	209.625	35.4000	73.0000
1541	209.750	37.2000	58.0000
1542	209.875	25.3000	60.0000
1543	210.000	23.7000	77.0000
1544	210.125	19.8000	79.0000
1545	210.250	17.9000	87.0000
1546	210.375	21.8000	90.0000
1547	210.500	27.2000	85.0000
1548	210.625	36.7000	69.0000
1549	210.750	28.5000	61.0000
1550	210.875	25.8000	70.0000
1551	211.000	23.4000	81.0000
1552	211.125	19.8000	78.0000
1553	211.250	18.1000	85.0000
1554	211.375	20.5000	89.0000
1555	211.500	28.0000	84.0000
1556	211.625	35.4000	65.0000
1557	211.750	31.9000	53.0000
1558	211.875	25.9000	52.0000
1559	212.000	21.6000	65.0000
1560	212.125	20.5000	73.0000
1561	212.250	18.8000	80.0000
1562	212.375	21.8000	83.0000

1563	212.500	28.5000	78.0000
1564	212.625	33.7000	61.0000
1565	212.750	31.5000	46.0000
1566	212.875	24.3000	47.0000
1567	213.000	20.7000	61.0000
1568	213.125	20.2000	76.0000
1569	213.250	18.9000	82.0000
1570	213.375	20.7000	86.0000
1571	213.500	25.1000	85.0000
1572	213.625	33.7000	68.0000
1573	213.750	35.3000	49.0000
1574	213.875	27.5000	45.0000
1575	214.000	21.5000	60.0000
1576	214.125	19.0000	72.0000
1577	214.250	18.5000	76.0000
1578	214.375	20.4000	82.0000
1579	214.500	27.5000	77.0000
1580	214.625	36.5000	58.0000
1581	214.750	33.6000	43.0000
1582	214.875	29.4000	46.0000
1583	215.000	21.6000	63.0000
1584	215.125	21.0000	75.0000
1585	215.250	18.9000	79.0000
1586	215.375	20.7000	81.0000
1587	215.500	29.4000	78.0000
1588	215.625	40.6000	57.0000
1589	215.750	38.2000	34.0000
1590	215.875	31.7000	32.0000
1591	216.000	24.2000	40.0000
1592	216.125	21.0000	54.0000
1593	216.250	19.4000	64.0000
1594	216.375	20.6000	71.0000
1595	216.500	29.4000	69.0000
1596	216.625	40.4000	47.0000
1597	216.750	40.8000	25.0000
1598	216.875	29.1000	21.0000
1599	217.000	25.6000	37.0000
1600	217.125	24.9000	42.0000
1601	217.250	21.4000	48.0000
1602	217.375	24.8000	56.0000
1603	217.500	30.9000	52.0000
1604	217.625	41.4000	35.0000
1605	217.750	40.3000	14.0000
1606	217.875	30.2000	16.0000
1607	218.000	26.1000	31.0000
1608	218.125	24.3000	39.0000
1609	218.250	21.5000	51.0000
1610	218.375	21.8000	62.0000
1611	218.500	36.5000	55.0000
1612	218.625	37.5000	35.0000
1613	218.750	35.9000	30.0000
1614	218.875	28.9000	35.0000
1615	219.000	21.4000	57.0000
1616	219.125	21.2000	68.0000
1617	219.250	20.9000	74.0000
1618	219.375	21.5000	79.0000
1619	219.500	28.8000	74.0000
1620	219.625	40.3000	46.0000
1621	219.750	30.8000	32.0000
1622	219.875	28.9000	38.0000
1623	220.000	22.2000	51.0000
1624	220.125	20.0000	58.0000
1625	220.250	20.9000	66.0000
1626	220.375	23.2000	73.0000
1627	220.500	35.0000	61.0000
1628	220.625	48.7000	34.0000
1629	220.750	36.8000	25.0000
1630	220.875	31.3000	33.0000
1631	221.000	22.0000	45.0000
1632	221.125	23.9000	57.0000
1633	221.250	19.9000	61.0000

1634	221.375	19.3000	69.0000
1635	221.500	31.5000	63.0000
1636	221.625	42.0000	35.0000
1637	221.750	37.8000	16.0000
1638	221.875	33.6000	16.0000
1639	222.000	26.2000	35.0000
1640	222.125	28.1000	48.0000
1641	222.250	20.9000	60.0000
1642	222.375	24.7000	66.0000
1643	222.500	33.5000	50.0000
1644	222.625	48.6000	25.0000
1645	222.750	40.0000	20.0000
1646	222.875	32.5000	14.0000
1647	223.000	25.9000	33.0000
1648	223.125	24.5000	43.0000
1649	223.250	21.0000	55.0000
1650	223.375	24.3000	64.0000
1651	223.500	34.4000	48.0000
1652	223.625	39.2000	29.0000
1653	223.750	42.8000	17.0000
1654	223.875	21.6000	51.0000
1655	224.000	18.7000	98.0000
1656	224.125	18.7000	99.0000
1657	224.250	15.5000	99.0000
1658	224.375	19.0000	100.0000
1659	224.500	24.0000	98.0000
1660	224.625	27.6000	96.0000
1661	224.750	32.5000	94.0000
1662	224.875	24.2000	96.0000
1663	225.000	19.1000	98.0000
1664	225.125	18.5000	99.0000
1665	225.250	16.3000	100.0000
1666	225.375	20.4000	99.0000
1667	225.500	26.4000	97.0000
1668	225.625	30.0000	96.0000
1669	225.750	30.6000	95.0000
1670	225.875	23.3000	97.0000
1671	226.000	18.6000	99.0000
1672	226.125	18.4000	99.0000
1673	226.250	18.5000	99.0000
1674	226.375	19.4000	99.0000
1675	226.500	27.6000	97.0000
1676	226.625	33.2000	95.0000
1677	226.750	32.2000	93.0000
1678	226.875	22.7000	96.0000
1679	227.000	21.4000	97.0000
1680	227.125	19.2000	97.0000
1681	227.250	18.8000	97.0000
1682	227.375	20.9000	98.0000
1683	227.500	27.5000	94.0000
1684	227.625	31.5000	89.0000
1685	227.750	29.7000	86.0000
1686	227.875	23.8000	82.0000
1687	228.000	19.1000	87.0000
1688	228.125	17.1000	91.0000
1689	228.250	15.6000	93.0000
1690	228.375	19.9000	95.0000
1691	228.500	28.6000	87.0000
1692	228.625	34.9000	76.0000
1693	228.750	27.9000	61.0000
1694	228.875	22.2000	59.0000
1695	229.000	22.7000	69.0000
1696	229.125	21.2000	64.0000
1697	229.250	18.1000	79.0000
1698	229.375	21.0000	87.0000
1699	229.500	31.6000	80.0000
1700	229.625	33.4000	61.0000
1701	229.750	30.4000	49.0000
1702	229.875	25.4000	57.0000
1703	230.000	21.8000	66.0000
1704	230.125	18.5000	80.0000

```
1705      230.250 17.5000 86.0000
1706      230.375 20.4000 87.0000
1707      230.500 29.8000 68.0000
1708      230.625 33.5000 54.0000
1709      230.750 31.9000 41.0000
1710      230.875 24.5000 48.0000
1711      231.000 22.1000 69.0000
1712      231.125 18.9000 77.0000
1713      231.250 18.0000 85.0000
1714      231.375 21.5000 87.0000
1715      231.500 30.3000 72.0000
1716      231.625 35.2000 58.0000
1717      231.750 32.7000 47.0000
1718      231.875 26.9000 53.0000
1719      232.000 23.7000 55.0000
1720      232.125 19.9000 65.0000
1721      232.250 17.8000 76.0000
1722      232.375 21.5000 84.0000
1723      232.500 30.7000 71.0000
1724      232.625 36.3000 52.0000
1725      232.750 30.6000 50.0000
1726      232.875 23.8000 49.0000
1727      233.000 18.1000 70.0000
1728      233.125 16.8000 76.0000
1729      233.250 14.9000 80.0000
1730      233.375 21.4000 83.0000
1731      233.500 31.1000 65.0000
1732      233.625 36.4000 46.0000
1733      233.750 33.3000 39.0000
1734      233.875 27.5000 39.0000
1735      234.000 22.1000 54.0000
1736      234.125 20.7000 61.0000
1737      234.250 17.5000 67.0000
1738      234.375 23.3000 80.0000
1739      234.500 31.6000 61.0000
1740      234.625 33.0000 42.0000
1741      234.750 26.3000 55.0000
1742      234.875 21.5000 71.0000
1743      235.000 20.1000 78.0000
1744      235.125 18.9000 77.0000
1745      235.250 17.1000 79.0000
1746      235.375 22.1000 82.0000
1747      235.500 29.2000 65.0000
1748      235.625 28.6000 45.0000
1749      235.750 26.3000 64.0000
1750      235.875 21.2000 65.00
1751      236.000 19.4000 70.0000
1752      236.125 17.4000 81.0000
1753      236.250 17.9000 85.0000
1754      236.375 19.8000 86.0000
1755      236.500 25.5000 83.0000
1756
1757
1758
1759
1760
1761
1762
1763
1764
1765
1766
1767
1768
1769
1770
1771
1772
1773
1774
1775
```

```
*     whi.f
*
cccccccccccccccccccccccccccccccccccccccccccccccccccccccccccccccccccccccccccccccccc
cc
c     ODWISH is a One Dimensional model for simulating Water movement, ISot-
c   ope trasport and heat transfer in the shallow unsaturated zone. This
c   model can describe  evaporation/infiltration from desert soils under
c   non-isothermal conditions using both hydraulic and isotopic parameters.
c   This numerical model considers soil heterogeniety in the soil profiles
c   by accepting more than one layer.
c      Three differential equations describing mass, heat and isotope
c   movement are solved simultaneously using the finite difference method:
c   General (0<W1<1) approach for time and central difference for space.
c      Water(and heavy water isotopic species) movement is considered in
c   the liquid and vapor phases. Heat transfer is considered  by conduction
c   vaporization, and heat transfer with mass flow(sensible heat).
cccccccccccccccccccccccccccccccccccccccccccccccccccccccccccccccccccccccccccccccccc
ccccccccc
c     This code has been developed by AbdelRahman Shurbaji to help in studying
c     the change in isotope profiles with time under natural conditions,
c     and its relation to evaporation rates from soil. Investigating  the
c     interaction between the thermal regime in the top soil and both phases of
c     water(vapor and liquid) flow can be possible with this numerical code.
c     Using this combined hydrologic and isotopic model the isotope profile can
c     be viewed in a  hetrogeneous soil profile and real data from the field
c     can be tested and evaluated.
c
c
c
c     Date: January 18, 1992 :  New Mexico Institute of Mining and Technology
c                                  Hydrology program/Geoscience Department
c     Updated: Nov 12, 1993
c
c

c*************************************************************************
c List of variables
 * CC            volumetric heat capacity of soil (cal/cm^3 C)
 * TS(LT)        ground surface temperature ( C)
 * RHS(LT)        relative humidity of atmospheric air
 * CZ            time in hour after which output is printed
 * CL            specific heat of liquid water (Cal/g)
 * DAWV          moleclular diffusion coefficient of water vapor in air(cm^2/s)
 * DELT          time increment (hr)
 * DELZ          depth increment (cm)
 * D1            coupling coefficient for heat transfer (Cal/cm^2 s)
 * DTV           thermal water vapor diffusivity (cm^2/s C)
 * EPST,EPTH     small positive numbers for T and THETA convergence
 * EVAV          upward vapor flow rate (cm/s)
 * EVAL          upward liquid flow rate (cm/s)
 * EVAT          total upward water(liquid and vapor)flow rate (cm/s)
 * FF            specific water capacity(differential theta with respect to PSI)
 * GR            acceleration of gravity (cm/s^2)
 * HVAP          Cofficient of latent heat of vaporization of water (cal/g)
 * I             index for nodes
 * J             index for time step
 * K             unsaturated hydraulic conductivity (cm/s)
 * KPSI          total water conductivity (cm/s)
 * KPSIV         water vapor conductivity (cm/s)
 * KODEY         =1 IF you want to print THETA,PSI,DTV,KPSIV and K for all nodes
 *               after CZ hours
 * L             index for layer
 * LAMDA         apparant thermal conductivity of moist soil (cal/cm s C)
 * MU            dynamic viscosity of water (g/cm/s)
 * NZ            number of nodes
 * NLAYR         number of layers
 * PSI           pressure head of soil water (cm)
 * R             universal gas constant (cm^2/s^2 C)
 * RECH          recharge rate(cm/s)(positive downward)
 * RO            liquid water density (g/cm^3)
 * SIMT          maximum simulation time (hr)
```



```
 * SRH           soil relative humidity
 * SVD           saturated vapor density (g/cm^3)
 * T             soil temperature ( C)
 * TORV          coefficient of tortuosity for vapor flow
 * THETA         volumetric  moisture content of soil
 * THWK          water content at liquid discontinuity
 * VO            volumetric content of organic matter
 * ZNB(L)        depth at bottom of layer L
 * Z             depth (cm)
 * ZL            total length of soil profile under study (cm)
*****************************************************************
 *   << List of isotope variables >>
 * ALFA          isotopic fractionation factor
 * DAL           isotopic concentration relative to standard mean ocean
 *               water (SMOW)
 * KODEI         numerical input code =1(Deuterium),2(Oxygen-18)
 * DI            total diffusivity of isotopic species
 * DIRV          diffusivity of isotopic species in vapor
 * DIS           diffusivity of isotopic species in liquid water
 * KODEI         numerical input code =1(Deuterium),2(Oxygen-18)
 * TORL          cofficient of tortuosity for liquid flow
*****************************************************************
 * O attachd to the end of the following variables means the value at
 * previous time step: CCO, DLO, DTVO, F, KO, KPSIO, KPSIVO, LAMDAO, PSIO,
 * and THETAO.
*****************************************************************
 * IF YOU HAVE A PROBLEM WITH THIS CODE REPORT IT TO OR ASK
 * ABDEL-RAHMAN SHURBAJI OR FRED PHILLIPS
 * @ Hydrology Department, New Mexico Tech., Socorro, NM 87801
*****************************************************************
       IMPLICIT REAL*8 (A-H,O-Z)
       CHARACTER*12 FIN1,FIN2,FOUT
       LOGICAL OK,EXIST
       PARAMETER(NN=205,NL=4)
       PARAMETER(NLT=1500)
       PARAMETER(LUI1=1,LUI2=2,LUO=3)
       PARAMETER(R=4.6199D+6,GR=980.665D0,TOO=20.0)
       INTEGER NB(0:NL),NT(NLT)

       REAL*8 K(NN),KO(NN),LAMDA(NN),LAMDAO(NN),
      &KPSIV(NN),KPSI(NN),KPSIO(NN),KSAT

       DIMENSION PSI(NN),PSIO(NN),PSII(NN),THETA(NN),THETAO(NN),
      &POR(NN),SRH(NN),DAWV(NN),SVD(NN),T(NN),RO(NN),
      &VO(NN),THETAI(NN),TI(NN),
      &PORL(NL),VOL(NL),FRV(NN),EV(NN),EL(NN),ET(NN),
      &EVAL(NN),TO(NN),CC(NN),CO(NN),DL(NN),DLO(NN),FI(NN),
      &ZNB(NL),EVATO(NN),EVAV(NN),EVAT(NN),
      &DTV(NN),DTVO(NN),
      &TIME(NLT),RHS(NLT),TS(NLT),FF(NN),FO(NN),
      &AMP1(NN),BMP1(NN),CMP1(NN),AMT1(NN),BMT1(NN),CMT1(NN),
      &AMP2(NN),BMP2(NN),CMP2(NN),AMT2(NN),BMT2(NN),CMT2(NN),
      &AHP1(NN),BHP1(NN),CHP1(NN),AHT1(NN),BHT1(NN),Emm(nlt),
      &AHP2(NN),BHP2(NN),CHP2(NN),AHT2(NN),BHT2(NN),ZEFX(nlt),
      &CHT1(NN),HM(NN),HH(NN),DM1(NN),U(NN),V(NN),Z(NN),rnfl(nlt),
      &CHT2(NN),DM2(NN)

       DIMENSION DALO(NN),DAL(NN),DI(NN),DIO(NN),
      &XIET(NN),XIF(NN),XIETO(NN),XIO(NN),
      &AID1(NN),BID1(NN),CID1(NN),HI(NN),FXX(NN),
      &AID2(NN),BID2(NN),CID2(NN),FXO(NN),DID1(NN),DID2(NN)
 C
       DIMENSION A(NN),B(NN),C(NN),X(NN)

       COMMON/TRI/A,B,C,X
       COMMON/THC/ALA,BLA
       COMMON/CCC/CC
       COMMON/TORT/TORV
       COMMON/DTKP/THWK
       COMMON/SATVD/SVD
       COMMON/DIFWV/DAWV
```

```
      COMMON/DNS/RO
      COMMON/PROS/POR
      COMMON/ORG/VO
      COMMON/NDKL/NZ
      COMMON/SOILRH/SRH
      COMMON/ZLED/DELZ
      COMMON/VTD/DTV
      COMMON/VISPK/KPSIV
      COMMON/LD/DL
      COMMON/ISPK/KPSI
      COMMON/FFFF/FF
      COMMON/EVP/EVAV,EVAL,EVAT
      COMMON/FVAP/FRV
      COMMON/ZXY/Z
      COMMON/Nfl/rinfl
      COMMON/thtt/theta
      COMMON/TTT/T
      COMMON/isp/psi
      COMMON/KKK/K
      COMMON/FEZ/ZEF
      COMMON/WK/PSWK
      COMMON/THC/LAMDA
      COMMON/VANGN/AD2,BD2,THR2
      COMMON/XSAT/KSAT
      COMMON/RETD/AD1,THR1,VNU
      COMMON/GAGA/GAMA,GAMA2,BD2X,AD1X
C
      COMMON/ALKDI/KODEI
      COMMON/XIXI/XIF
      COMMON/ID/DI
      COMMON/DIPA/adifO,bdifO,adifD,bdifD
C
C  ... units 1,2 for input files, unit 3 for output file and unit 4 for plot
C       file
      WRITE(*,*)'                Welcome to ODWISH  code       '
      WRITE(*,*)'                          by'
      WRITE(*,*)'                 Abdel-Rahman Shurbaji  '
      WRITE(*,*)'          Hydrology program, New Mexico Tech.  '
      WRITE(*,*)'                          '
    1 WRITE(*,*)'   Enter the name of the INPUT data file ..'
      READ(*,100)FIN1

      INQUIRE(FILE=FIN1,EXIST=EXIST)
      IF(.NOT.EXIST)THEN
         WRITE(*,'(1X,''cannot find file'',A,'',try again.'')')FIN1
         GO TO 1
      ELSE
         OPEN(UNIT=LUI1,FILE=FIN1,STATUS='OLD')
      ENDIF
    2 WRITE(*,*)'Enter the name of the file having soil properties ..'
      READ(*,100)FIN2
      INQUIRE(FILE=FIN2,EXIST=EXIST)
      IF(.NOT.EXIST)THEN
         WRITE(*,'(1X,''cannot find file'',A,'',try again.'')')FIN2
         GO TO 2
      ELSE
         OPEN(UNIT=LUI2,FILE=FIN2,STATUS='OLD')
      ENDIF

    4 WRITE(*,*)'Enter the name of the OUTPUT file '
      READ(*,100)FOUT
      INQUIRE(FILE=FOUT,EXIST=EXIST)
      IF(EXIST)THEN
        WRITE(*,'(1X,''file  '',A,'' exists. Overwrite? (T/F)'')')FOUT
    5   READ(*,'(L1)',ERR=5)OK
        IF (OK)THEN
         OPEN(UNIT=LUO,FILE=FOUT,STATUS='UNKNOWN')
        ELSE
         GO TO 4
```



```
        ENDIF
      ELSE
        OPEN(UNIT=LUO,FILE=FOUT,STATUS='UNKNOWN')
      ENDIF


C     Determine which isotope you will study and the pertinent concentration
C     of atmospheric water vapor
      READ(LUI1,*)KODEI
      READ(LUI1,*)DALAH2,DALAO18
      WRITE(LUO,100)'SOIL PARAM. FILE IS ',FIN2

C   .. read in and print numerical data
      READ(LUI1,*)W1,W2
      READ(LUI1,*)SIMT,DELT,ZL,DELZ,NLAYR,EPST,EPTH,ITERMAX,QH

C    read depth at bottom of each layer(if more than one layer)
      IF(NLAYR.GT.1)THEN
        READ(LUI1,112)(ZNB(L),L=1,NLAYR)
      ELSE
        ZNB(1)=ZL
      ENDIF
      WRITE(LUO,102)SIMT,DELT,ZL,NZ,DELZ,NLAYR,EPTH,EPST

      READ(LUI1,*)KODEY,KODL,KODER
C     Is it zero gradient of psi at bottom BC. This is what koder is about!
      if(koder.ne.1)then
        READ(LUI1,*)RECH
      ENDIF
      READ(LUI1,*)NTIME
      READ(LUI1,*)(TIME(I),TS(I),RHS(I),RNFL(I),I=1,NTIME)
C TIME IN DATA FILE WAS IN DAYS >> CHANGE TO hrs


      READ(LUI1,*)CZ
      NZ=ZL/DELZ+1
      NJ=SIMT/DELT
      KL=NZ+1

      WRITE(LUO,*)'weight factor for time in hydrologic block, w1=',w1
      WRITE(LUO,*)'weight factor for time in isotopic block, w2=',w2

C ..  read in and print out initial conditions

      IF(KODEI.EQ.1)THEN
        DALA=DALAH2
        WRITE(LUO,*)'THE ISOTOPE UNDER STUDY IS DEUTERIUM'
        READ(LUI1,*)(Z(I),THETA(I),DAL(I),xw,T(I),xw,xw,xw,xw,i=2,NZ)
      ELSE
        DALA=DALAO18
        WRITE(LUO,*)'THE ISOTOPE UNDER STUDY IS OXYGEN-18'
        READ(LUI1,*)(Z(I),THETA(I),xw,DAL(I),T(I),xw,xw,xw,xw,i=2,NZ)
      ENDIF


       DO 921 I=1,NZ
        THETA(I)=THETA(I)/100.
        DAL(I)=DAL(I)/1000.
  921  CONTINUE

C     Calculate  ratio 3.6D3*DELT/DELZ**2
      RATIO=3.6D3*DELT/DELZ**2

      CL=1.0

C  .. read and print surface boundary conditions(temperature,relative humidity)
C     Input humidity and temperature at surface is given as histogram.i.e.,
C     TIME(1)=0., temp. at surface TS and atmospheric relative humidity RH
C     are constant between TIME(1) and TIME(2). At TIME(2) change happens,etc.
C     NTIME is the number of data input for surface condition (humidity and
C     temperature)
```

```
      WRITE(LUO,*) ' The surface boudary conditions are :'
      WRITE(LUO,105)

      DO 9 LT=1,NTIME
         XDAL=DALA*1000.
         WRITE(LUO,106)TIME(LT),TS(LT),RHS(LT),XDAL
         RHS(LT)=RHS(LT)/100.
 9    CONTINUE
      do 6 L=1,ntime
         TIME(L)=24*TIME(L)
 6    continue

C     building the continuous values of humidity and surface temperature
C     Time is in Julian day
      DO 8 J=1,NTIME
         DT=TIME(J)-TIME(1)
         NT(J)=DT/DELT+1
 8    CONTINUE

      KODEN=CZ/DELT
      WRITE(LUO,*)' '


C  .. Read soil properties for each layer from 2nd INPUT file
C  .. Tortuosity, prosity, moisture content at liquid discontinuity, and
C     volumetric content of organic mattar. Then,
C     number of data in tables of : LOG(-PSI) vs theta, log(K) vs theta,
C     thermal conductivity vs. theta followed by these tables.
C
      READ(LUI2,*)TORV
      WRITE(LUO,*)'TORV =',TORV
      READ(LUI2,*)AD1,THR1
      READ(LUI2,*)THWK,THR2,KSAT,AD2,BD2
      READ(LUI2,*)adifD,bdifD,adifO,bdifO
      READ(LUI2,*)(PORL(L),VOL(L),L=1,NLAYR)
      WRITE(LUO,*)'   L    PORL        VOL '
      DO 10 L=1,NLAYR
         WRITE(LUO,110)L,PORL(L),VOL(L)
 10   CONTINUE

C thermal cond. relation parameters
      READ(LUI2,*)ALA,BLA

      WRITE(LUO,*)'          '
      WRITE(LUO,*)'ALA=',ALA
      WRITE(LUO,*)'BLA=',BLA


C   Find the characteristic parameters for each NODE
      NB(0)=0
      DO 17 L=1,NLAYR
            NB(L)=ZNB(L)/DELZ+1
            IL=NB(L-1)+1
            DO 16 I=IL,NB(L)
               VO(I)=VOL(L)
               POR(I)=PORL(L)
 16         CONTINUE
 17   CONTINUE


C   Calculate the value of PSI corresponding to THWK
      CALL PSWKS


      WRITE(LUO,*)'  '
      MM=NZ-1
      M2=MM/2+1
      WRITE(LUO,104)CZ
      WRITE(LUO,*)'   '
C    Print initial condition in the soil profile theta and T
      WRITE(LUO,109)
```



```
      TIM1=TIME(1)/24.
      WRITE(LUO,*)'Julian date= ',TIM1
      DO 18 I=2,NZ
         Z(I)=(I-1)*DELZ
         XTHTA=THETA(I)*100.
         XDAL=DAL(I)*1000
         WRITE(LUO,115)Z(I),XTHTA,T(I),XDAL
 18   CONTINUE


C .. Begin incrementing the time
      LT=0
      DO 95 J=1,NJ
         write(*,*)' J= ',J
C        Top boundary conditions
         IF(J.EQ.NT(LT+1))THEN
            LT=LT+1
            SRH(1)=RHS(LT)
            T(1)=TS(LT)
            rinfl=rnfl(lt)
            CALL ALFSUB(ALFA1,T(1))
            DAL(1)=1/ALFA1*(DALA+1.0)-1.0
         ENDIF

C    Calculate liquid density of water
         CALL LDENS

C   Calculate PSI(THETA)
         CALL PSRET


C    Iterate for PSI and T untill get enough convergence
         DO 60 KI=0,ITERMAX


C   ** CALCULATE TRANSPORT COEFFICIENTS ***

C   Calculate relative humidity
         CALL SRHSUB

C   Calculate heat capacity of soil
          CALL HCAPT

C     Calculate unsaturated hydraulic conductivity K corrected to its
C     temperature dependence through MU
          CALL KUNSAT

C     Calculate thermal conductivity LAMDA
          CALL THCOND

C ..    Calculate vapor flow parameters DTV and KPSIV
          CALL DTKPSV

C     Calculate Dl coupling coefficient for latent heat transfer
          CALL DLSUB

C    Calculate total conductivity KPSI
          CALL KTOTL

C  FIND PSI(KL) AND T(KL)
C    Apply the bottom boundary condition
        if(koder.eq.1)then
           CXY1=DTV(NZ)*(T(NZ)-T(MM))
           RECH=K(NZ)-CXY1/DELZ
         endif

          VXY1=-2*DTV(NZ)*(T(NZ)-T(MM))
          VXY2=2*DELZ*(K(NZ)-RECH)
          VXY=VXY1+VXY2
          PSI(KL)=PSI(MM)+VXY/KPSI(NZ)
```

```
425
426             I=NZ
427             EVAV(I)=DTV(I)*(T(I)-T(I-1))/(DELZ)+
428          &KPSIV(I)*(PSI(I)-PSI(I-1))/(2*DELZ)
429             EVAL(I)=K(I)*((PSI(I)-PSI(I-1))/(DELZ)-1.D0)
430             EVAT(I)=EVAV(I)+EVAL(I)
431
432             vxy1=QN+CL*RO(NZ)*EVAT(NZ)*(T(NZ)-TOO)
433             vxy2=DL(NZ)*(PSI(KL)-PSI(MM))/(2*DELZ)
434             VXY=vxy1+vxy2
435             T(KL)=T(MM)-2*DELZ*VXY/LAMDA(NZ)
436
437            if(koder.eq.1)then
438               CXY1=DTV(NZ)*(T(KL)-T(MM))
439               RECH=K(NZ)-CXY1/(2*DELZ)
440             endif
441
442              VXY1=-DTV(NZ)*(T(KL)-T(MM))
443              VXY2=2*DELZ*(K(NZ)-RECH)
444              VXY=VXY1+VXY2
445              PSI(KL)=PSI(MM)+VXY/KPSI(NZ)
446    CCCCCCCCCC FOUND !  CCCCCCCCCCCCCCCCC
447
448    C   Calculate evaporation rate from the top mesh and flow rates at all
449    C   nodes in the profile
450           CALL FLOW
451    C
452           DAL(KL)=DAL(MM)
453    C
454
455    C    Calculate the total isotope diffusivity DI
456           CALL ISOTOPE
457
458    *** END OF TRANSPORT COEFFICIENTS ***
459
460             IF(KI.EQ.0)THEN
461               DO 47 I=2,NZ
462                  THETAO(I)=THETA(I)
463                  TO(I)=T(I)
464                  PSIO(I)=PSI(I)
465                  CO(I)=CC(I)
466                  FO(I)=FF(I)
467                  KPSIO(I)=KPSI(I)
468                  LAMDAO(I)=LAMDA(I)
469                  KO(I)=K(I)
470                  EVATO(I)=EVAT(I)
471                  DLO(I)=DL(I)
472                  DTVO(I)=DTV(I)
473    C
474                  DALO(I)=DAL(I)
475                  DIO(I)=DI(I)
476                  XIO(I)=XIF(I)
477                  XIETO(I)=XIO(I)*EVATO(I)
478     47          CONTINUE
479             DALO(1)=DAL(1)
480             EVATO(1)=EVAT(1)
481             TO(KL)=T(KL)
482             TO(1)=T(1)
483             PSIO(KL)=PSI(KL)
484
485             DALO(KL)=DALO(MM)
486             GO TO 60
487             ENDIF
488    C     Calculate evaporation rate EVAT at half time step
489
490
491    C  Calculate entries of array U=(G)(psi)
492
493    C     Calculate entries of tridiagonal matrices G and W and calculate U
494    C     Where U=(G)(PSI) = HM(I)- [W](T)
495    C     GEOMETRIC  MEAN IS USED FOR CONDUCTIVITY(hydraulic and thermal) AND
```



```
496    C      COEFFICIENTS DTV(thermal vapor diffusivity), KPSIV AND DL(coupling
497    C     coefficient of heat tranfer.
498
499    C     Top node(node # 2)
500           I=2
501              AMP1(I)=0.
502              AMP2(I)=0.
503              CMP1(i)=w1*SQRT(KPSI(I)*KPSI(I+1))
504              CMP2(i)=(1-w1)*SQRT(KPSIO(I)*KPSIO(I+1))
505              FFT=w1*FF(I)+(1-w1)*FO(I)
506              FC=FFT/RATIO
507              BMP1(I)=FC+AMP1(I)+CMP1(I)
508              BMP2(I)=-FC+AMP2(I)+CMP2(I)
509
510              AMT1(I)=0.
511              AMT2(I)=0.
512              CMT1(i)=w1*SQRT(DTV(I)*DTV(I+1))
513              CMT2(i)=(1-w1)*SQRT(DTVO(I)*DTVO(I+1))
514              BMT1(I)=AMT1(I)+CMT1(I)
515              BMT2(I)=AMT2(I)+CMT2(I)
516    C      entries of (DM)
517              DKMINS1=-1*w1*EVAT(1)
518              DKMINS2=-1*(1-w1)*EVATO(1)
519
520              DKPLUS1=w1*SQRT(K(I)*K(I+1))
521              DKPLUS2=(1-w1)*SQRT(KO(I)*KO(I+1))
522
523              DM1(I)=DELZ*(DKPLUS1-DKMINS1)
524              DM2(I)=DELZ*(DKPLUS2-DKMINS2)
525
526
527     24         DO 25 I=3,MM
528    C      entries of [G]
529                AMP1(i)=w1*SQRT(KPSI(I-1)*KPSI(I))
530                AMP2(i)=(1-w1)*SQRT(KPSIO(I-1)*KPSIO(I))
531                CMP1(i)=w1*SQRT(KPSI(I)*KPSI(I+1))
532                CMP2(i)=(1-w1)*SQRT(KPSIO(I)*KPSIO(I+1))
533                FFT=w1*FF(I)+(1-w1)*FO(I)
534                FC=FFT/RATIO
535                BMP1(I)=FC+AMP1(I)+CMP1(I)
536                BMP2(I)=-FC+AMP2(I)+CMP2(I)
537    C      entries of [W]
538                AMT1(i)=w1*SQRT(DTV(I-1)*DTV(I))
539                AMT2(i)=(1-w1)*SQRT(DTVO(I-1)*DTVO(I))
540
541                CMT1(i)=w1*SQRT(DTV(I)*DTV(I+1))
542                CMT2(i)=(1-w1)*SQRT(DTVO(I)*DTVO(I+1))
543
544                BMT1(I)=AMT1(I)+CMT1(I)
545                BMT2(I)=AMT2(I)+CMT2(I)
546    C      entries of (DM)
547                DKMINS1=w1*SQRT(K(I-1)*K(I))
548                DKMINS2=(1-w1)*SQRT(KO(I-1)*KO(I))
549
550                DKPLUS1=w1*SQRT(K(I)*K(I+1))
551                DKPLUS2=(1-w1)*SQRT(KO(I)*KO(I+1))
552
553                DM1(I)=DELZ*(DKPLUS1-DKMINS1)
554                DM2(I)=DELZ*(DKPLUS2-DKMINS2)
555     25       CONTINUE
556
557              I=NZ
558                 AMP1(i)=w1*SQRT(KPSI(I-1)*KPSI(I))
559                 AMP2(i)=(1-w1)*SQRT(KPSIO(I-1)*KPSIO(I))
560                 CMP1(i)=w1*KPSI(I)
561                 CMP2(i)=(1-w1)*KPSIO(I)
562                 FFT=w1*FF(I)+(1-w1)*FO(I)
563                 FC=FFT/RATIO
564                 BMP1(I)=FC+AMP1(I)+CMP1(I)
565                 BMP2(I)=-FC+AMP2(I)+CMP2(I)
566    C      entries of [W]
```

```
567               AMT1(i)=w1*SQRT(DTV(I-1)*DTV(I))
568               AMT2(i)=(1-w1)*SQRT(DTVO(I-1)*DTVO(I))
569
570               CMT1(i)=w1*DTV(I)
571               CMT2(i)=(1-w1)*DTVO(I)
572
573               BMT1(I)=AMT1(I)+CMT1(I)
574               BMT2(I)=AMT2(I)+CMT2(I)
575   C     entries of [DM]
576               DKMINS1=w1*SQRT(K(I-1)*K(I))
577               DKMINS2=(1-w1)*SQRT(KO(I-1)*KO(I))
578
579               DKPLUS1=w1*K(I)
580               DKPLUS2=(1-w1)*KO(I)
581
582               DM1(I)=DELZ*(DKPLUS1-DKMINS1)
583               DM2(I)=DELZ*(DKPLUS2-DKMINS2)
584
585   C   Calculate entries of tridiagonal matrices E and D
586   C   where {V}= [D]{T}={HH}-[E]{psi}
587
588   C   Top node (# 2)
589          I=2
590            HT31=w1*CL*EVAT(I)*DELZ/2.
591              HT32=(1-w1)*CL*EVATO(I)*DELZ/2.
592              AHT1(i)=w1*LAMDA(I)
593              AHT2(i)=(1-w1)*LAMDAO(I)
594              AHT1(I)=AHT1(i)-HT31
595              AHT2(I)=AHT2(i)-HT32
596
597            CHT1(I)=w1*SQRT(LAMDA(I)*LAMDA(I+1))
598              CHT2(i)=(1-w1)*SQRT(LAMDAO(I)*LAMDAO(I+1))
599              CHT1(I)=CHT1(i)+HT31
600              CHT2(I)=CHT2(i)+HT32
601              CCf=W1*CC(I)+(1-W1)*CO(I)
602              CF=CCf/RATIO
603              BHT1(I)=AHT1(I)+CHT1(I)+CF
604              BHT2(I)=AHT2(I)+CHT2(I)-CF
605   C   entries of [E]
606            AHP1(I)=0
607              AHP2(I)=0
608
609            CHP1(I)=0
610              CHP2(I)=0
611
612            BHP1(I)=0
613              BHP2(I)=0
614
615           DO 26 I=3,MM
616   C   entries of [D]
617               HT31=w1*CL*EVAT(I)*DELZ/2.
618               HT32=(1-w1)*CL*EVATO(I)*DELZ/2.
619               AHT1(i)=w1*SQRT(LAMDA(I-1)*LAMDA(I))
620               AHT2(i)=(1-w1)*SQRT(LAMDAO(I-1)*LAMDAO(I))
621               AHT1(I)=AHT1(i)-HT31
622               AHT2(I)=AHT2(i)-HT32
623
624               CHT1(I)=w1*SQRT(LAMDA(I)*LAMDA(I+1))
625               CHT2(i)=(1-w1)*SQRT(LAMDAO(I)*LAMDAO(I+1))
626               CHT1(I)=CHT1(i)+HT31
627               CHT2(I)=CHT2(i)+HT32
628               CCf=W1*CC(I)+(1-W1)*CO(I)
629               CF=CCf/RATIO
630               BHT1(I)=AHT1(I)+CHT1(I)+CF
631               BHT2(I)=AHT2(I)+CHT2(I)-CF
632
633   C   entries of [E]
634               AHP1(i)=W1*SQRT(DL(I-1)*DL(I))
635               AHP2(i)=(1-W1)*SQRT(DLO(I-1)*DLO(I))
636
637               CHP1(I)=W1*SQRT(DL(I)*DL(I+1))
```



```
638               CHP2(I)=(1-W1)*SQRT(DLO(I)*DLO(I+1))
639
640               BHP1(I)=AHP1(I)+CHP1(I)
641               BHP2(I)=AHP2(I)+CHP2(I)
642
643    26     CONTINUE
644   C       Incorporating the 2nd type bottom B.C of T
645   C       in the coefficient matrix
646
647           I=NZ
648               HT31=w1*CL*EVAT(I)*DELZ/2.
649               HT32=(1-w1)*CL*EVATO(I)*DEL2/2.
650               AHT1(i)=w1*SQRT(LAMDA(I-1)*LAMDA(I))
651               AHT2(i)=(1-w1)*SQRT(LAMDAO(I-1)*LAMDAO(I))
652               AHT1(I)=AHT1(i)-HT31
653               AHT2(I)=AHT2(i)-HT32
654
655               CHT1(I)=w1*LAMDA(I)
656               CHT2(i)=(1-w1)*LAMDAO(I)
657               CHT1(I)=CHT1(i)+HT31
658               CHT2(I)=CHT2(i)+HT32
659               CCf=W1*CC(I)+(1-W1)*CO(I)
660               CF=CCf/RATIO
661               BHT1(I)=AHT1(I)+CHT1(I)+CF
662               BHT2(I)=AHT2(I)+CHT2(I)-CF
663   C   entries of [E]
664               AHP1(i)=W1*SQRT(DL(I-1)*DL(I))
665               AHP2(i)=(1-W1)*SQRT(DLO(I-1)*DLO(I))
666
667               CHP1(I)=W1*DL(I)
668               CHP2(I)=(1-W1)*DLO(I)
669
670               BHP1(I)=AHP1(I)+CHP1(I)
671               BHP2(I)=AHP2(I)+CHP2(I)
672
673   C     Calculate elements of HH
674             DO 27 I=2,NZ
675                HH(I)=AMP2(I)*PSIO(I-1)-BMP2(I)*PSIO(I)+
676        &CHP2(I)*PSIO(I+1)+AHT2(I)*TO(I-1)-BHT2(I)*TO(I)+
677        &CHT2(I)*TO(I+1)-DM2(I)
678   C      Calculate elements of HH
679                HH(I)=AHP2(I)*PSIO(I-1)-BHP2(I)*PSIO(I)+
680        &CHP2(I)*PSIO(I+1)+AHT2(I)*TO(I-1)-BHT2(I)*TO(I)+
681        &CHT2(I)*TO(I+1)
682    27       CONTINUE
683
684             DO 28 I=2,NZ
685             U(I-1)=HH(I)-DM1(I)+AMT1(I)*T(I-1)-BMT1(I)*T(I)+
686        &CMT1(I)*T(I+1)
687    28       CONTINUE
688             U(MM)=U(MM)+CMP1(NZ)*PSI(KL)
689   C     Name elements of G in such a way accepted by the TRIDIA solver
690             DO 29 I=1,MM
691                A(I)=-AMP1(I+1)
692                B(I)=BMP1(I+1)
693                C(I)=-CMP1(I+1)
694    29        CONTINUE
695
696
697   C   Solve for PSI
698           CALL  TRIDIA(MM,U)
699
700             DO 30 I=2,NZ
701                PSII(I)=X(I-1)
702    30       CONTINUE
703             if(koder.eq.1)then
704                CXY1=DTV(NZ)*(T(KL)-T(MM))
705                RECH=K(NZ)-CXY1/(2*DELZ)
706             endif
707             VXY2=-DTV(NZ)*(T(KL)-T(MM))
708             VXY3=2*DELZ*(K(NZ)-RECH)
```

```
709           PSII(KL)=PSII(MM)+(VXY2+VXY3)/KPSI(NZ)
710
711
712   C   WHAT ARE THE UPDATED VALUES OF THETA
713           CALL THETRETEN(PSII,THETAI,FI)
714
715         DO 31 I=2,NZ
716           V(I-1)=HH(I)+AHP1(I)*PSII(I-1)-BHP1(I)*PSII(I)+CHP1(I)*PSII(I+1)
717    31           CONTINUE
718           V(MM)=V(MM)+CHT1(NZ)*T(KL)
719           V(1)=V(1)+AHT1(2)*T(1)
720
721   C    Name elements of D in such a way accepted by the solver
722             DO 32 I=1,MM
723               A(I)=-AHT1(I+1)
724               B(I)=BHT1(I+1)
725               C(I)=-CHT1(I+1)
726    32       CONTINUE
727
728   C   Solve for the temperature values T
729           CALL  TRIDIA(MM,V)
730           DO 33 I=2,NZ
731              TI(I)=X(I-1)
732    33       CONTINUE
733
734           vxy1=QH+CL*RO(NZ)*EVAT(NZ)*(TI(NZ)-TOO)
735           vxy2=DL(NZ)*(PSII(KL)-PSII(MM))/(2*DELZ)
736           VXY=vxy1+vxy2
737           TI(KL)=TI(MM)-2*DELZ*VXY/LAMDA(NZ)
738
739           DO 40 I=3,NZ
740             ABTH=ABS(THETAI(I)-THETA(I))
741             ABST=ABS(TI(I)-T(I))
742             IF(ABTH.LE.EPTH.AND.ABST.LE.EPST)GO TO 40
743             GO TO 43
744    40     CONTINUE
745           do 41 i=2,nz
746              psi(i)=psii(i)
747              t(i)=ti(i)
748              theta(i)=thetai(i)
749              ff(i)=fi(i)
750    41     continue
751           GO TO 49
752    43     DO 42 I=2,NZ
753              T(I)=0.5*(TI(I)+T(I))
754              PSI(I)=0.5*(PSII(I)+PSI(I))
755   C
756              theta(i)=0.5*(thetai(i)+theta(i))
757              ff(i)=0.5*(fi(i)+ff(i))
758
759    42     CONTINUE
760   C         CALL THETRETEN(PSI,THETA,FF)
761     60   CONTINUE
762     975  WRITE(*,*)'Limits exceeded, No convergence in time step',J
763          WRITE(LUO,*)'Limits exceeded, No convergence in time step',J
764          GO TO 98
765   C  ccccccccccccccccccccccccccccccccccccccccccccccccccccccccccccc
766   C  for isotope transport
767   C  General method for time but central difference for space
768   C  0<w2<1
769
770   cccccccccccccccccccccccccccccccccccccccccccccccccccccccccccccccc
771     49   KII=0
772          DO 699 I=2,NZ
773             XIET(I)=XIF(I)*EVAT(I)
774     699  CONTINUE
775
776   C    CALCULATE FXX FUNCTION
777          I=2
778          XEVT1=2*(EVAT(I+1)-EVAT(I))
779          XEVT2=2*(EVATO(I+1)-EVATO(I))
```



```
780          XIVT1=2*(XIF(I+1)-XIF(I))
781          XIVT2=2*(XIO(I+1)-XIO(I))
782          FXX(I)=(XIF(I)-1.)*XEVT1+EVAT(I)*XIVT1
783          FXO(I)=(XIO(I)-1.)*XEVT2+EVATO(I)*XIVT2
784
785          DO 799 I=3,MM
786             XEVT1=(EVAT(I+1)-EVAT(I-1))
787             XEVT2=(EVATO(I+1)-EVATO(I-1))
788             XIVT1=(XIF(I+1)-XIF(I-1))
789             XIVT2=(XIO(I+1)-XIO(I-1))
790             FXX(I)=(XIF(I)-1.)*XEVT1+EVAT(I)*XIVT1
791             FXO(I)=(XIO(I)-1.)*XEVT2+EVATO(I)*XIVT2
792     799  CONTINUE
793
794          I=NZ
795          XEVT1=2*(EVAT(I)-EVAT(I-1))
796          XEVT2=2*(EVATO(I)-EVATO(I-1))
797          XIVT1=2*(XIF(I)-XIF(I-1))
798          XIVT2=2*(XIO(I)-XIO(I-1))
799          FXX(I)=(XIF(I)-1.)*XEVT1+EVAT(I)*XIVT1
800          FXO(I)=(XIO(I)-1.)*XEVT2+EVATO(I)*XIVT2
801
802   C  solve for the relative isotope conc. dal
803          I=2
804          AID1A=w2*DI(I)
805          AID1B=W2*DELZ/2*XIET(I)
806          AID1(I)=AID1A-AID1B
807
808          AID2A=(1-w2)*DIO(I)
809          AID2B=(1-W2)*DELZ/2*XIETO(I)
810          AID2(I)=AID2A-AID2B
811
812          CID1A=w2*SQRT(DI(I)*DI(I+1))
813          CID1(I)=CID1A+AID1B
814          CID2A=(1-w2)*SQRT(DI(I)*DI(I+1))
815          CID2(I)=CID2A+AID2B
816
817          THTF=W2*THETA(I)+(1-W2)*THETAO(I)
818          BID1A=THTF/RATIO
819          BID1B=W2*DELZ/2*FXX(I)
820          BID1C=AID1A+CID1A
821          BID1(I)=BID1A-BID1B+BID1C
822
823          BID2B=(1-W2)*DELZ/2*FXO(I)
824          BID2C=AID2A+CID2A
825          BID2(I)=-BID1A-BID2B+BID2C
826
827          DID1(I)=BID1B
828          DID2(I)=BID2B
829
830          DO 641 I=3,MM
831            AID1A=w2*SQRT(DI(I)*DI(I-1))
832            AID1B=W2*DELZ/2*XIET(I)
833            AID1(I)=AID1A-AID1B
834
835            AID2A=(1-w2)*SQRT(DIO(I)*DIO(I-1))
836            AID2B=(1-W2)*DELZ/2*XIETO(I)
837            AID2(I)=AID2A-AID2B
838
839            CID1A=w2*SQRT(DI(I)*DI(I+1))
840            CID1(I)=CID1A+AID1B
841            CID2A=(1-w2)*SQRT(DI(I)*DI(I+1))
842            CID2(I)=CID2A+AID2B
843
844            THTF=W2*THETA(I)+(1-W2)*THETAO(I)
845            BID1A=THTF/RATIO
846            BID1B=W2*DELZ/2*FXX(I)
847            BID1C=AID1A+CID1A
848            BID1(I)=BID1A-BID1B+BID1C
849
850            BID2B=(1-W2)*DELZ/2*FXO(I)
```

```
851           BID2C=AID2A+CID2A
852           BID2(I)=-BID1A-BID2B+BID2C
853
854           DID1(I)=BID1B
855           DID2(I)=BID2B
856
857    641  CONTINUE
858         I=NZ
859         AID1A=w2*SQRT(DI(I)*DI(I-1))
860         AID1B=W2*DELZ/2*XIET(I)
861         AID1(I)=AID1A-AID1B
862
863         AID2A=(1-w2)*SQRT(DIO(I)*DIO(I-1))
864         AID2B=(1-W2)*DELZ/2*XIETO(I)
865         AID2(I)=AID2A-AID2B
866   C
867                CID1A=w2*DI(I)
868                CID1(I)=CID1A+AID1B
869
870                CID2A=(1-w2)*DI(I)
871                CID2(I)=CID2A+AID2B
872
873                THTF=W2*THETA(I)+(1-W2)*THETAO(I)
874                BID1A=THTF/RATIO
875                BID1B=W2*DELZ/2*FXX(I)
876                BID1C=AID1A+CID1A
877                BID1(I)=BID1A-BID1B+BID1C
878
879                BID2B=(1-W2)*DELZ/2*FXO(I)
880                BID2C=AID2A+CID2A
881                BID2(I)=-BID1A-BID2B+BID2C
882
883                DID1(I)=BID1B
884                DID2(I)=BID2B
885
886   C    Calculate entries of HI
887              DO 65 I=2,NZ
888              HI(I-1)=AID2(I)*DALO(I-1)-BID2(I)*DALO(I)+CID2(I)*DALO(I+1)
889        &+DID2(I)+DID1(I)
890     65        CONTINUE
891               HI(1)=HI(1)+AID1(2)*DAL(1)
892
893   C    bottom bc incorporated DAL(kl)=DAL(MM)
894               HI(MM)=HI(MM)+CID1(NZ)*DAL(KL)
895
896              DO 66 I=1,MM
897                 A(I)=-AID1(I+1)
898                 B(I)=BID1(I+1)
899                 C(I)=-CID1(I+1)
900     66        CONTINUE
901
902   C       Solve the NZ simultanuous equations
903              CALL TRIDIA(MM,HI)
904              DO 67 I=2,NZ
905                 DAL(I)=X(I-1)
906     67        CONTINUE
907               DAL(KL)=DAL(MM)
908
909   C      Calculate DAL(1) at the end of time step
910              CALL ALFSUB(ALFA1,T(1))
911              DAL(1)=1/ALFA1*(DALA+1.0)-1.0
912   ccccccccccccccccccccccccccccccccccccccccccccccccccccccccccccccccc
913
914
915   C      Control test for output
916            Emm(j)=EVAT(2)*3600*24*10.
917            zefx(j)=zef
918            NBC=J/KODEN
919            CBC=NBC*KODEN
920            IF(CBC.EQ.J)THEN
921               TIM=(J*DELT)/24.+TIM1
```



```
922               WRITE(LUO,*)'      '
923               WRITE(LUO,*)'JULIAN DATE =',TIM
924               TIMX=J*DELT
925               WRITE(LUO,*)'TIME (hr) =',TIMX
926
927               WRITE(LUO,*)'NUMBER OF ITERATIONS = ',KI
928               DO 63 I=1,NZ
929                  EV(I)=EVAV(I)*3.6D3
930                  EL(I)=EVAL(I)*3.6D3
931                  ET(I)=EVAT(I)*3.6D3
932     63        CONTINUE
933         write(luo,*)'  '
934   C     Flow rates inside the soil profile (cm/hr)
935               WRITE(LUO,*)'Upward flow rates in the soil profile (cm/hr)|
936        &humidity'
937               WRITE(LUO,*)'depth|moist. cont.|vapor flow rate and fraction|liquid f
      low
938        &rate | humidity '
939
940               IF(KODEY.EQ.1)THEN
941                WRITE(LUO,*)' '
942                theta(1)=theta(2)
943                DO 91 I=1,NZ
944                   XTHETA=THETA(I)*100.
945                   XDAL=DAL(I)*1000.
946                   WRITE(LUO,234)Z(I),XTHETA,T(I),XDAL,XIF(I),EV(i),
947        &FRV(I),EL(I),SRH(I)
948      91          CONTINUE
949               ENDIF
950              ENDIF
951   C     Control test for DRIENESS OF THE PROFILE
952       94      IF(THETA(M2).LE.0.03.AND.THETA(NZ).LE.0.03)GO TO 97
953
954       95    CONTINUE
955             WRITE(LUO,*)'JULIAN DAY  TIME  EVAPORATION RATE  DEPTH OF ZEF'
956             do 96 j=1,nj
957               TIM=(J*DELT)/24+TIM1
958               TIMX=J*DELT
959               WRITE(LUO,117)TIM,TIMX,Emm(j),zefx(j)
960       96    continue
961
962
963             GO TO 98
964       97    WRITE(LUO,*)'WARNING - - -> PROFILE DRIED TO THE BOTTOM <- - - -'
965       98    TIM=(J-1)*DELT/24.+TIM1
966             WRITE(*,*)'TIME(hr) AT TERMINATION OF PROGRAM=',TIM
967
968   C   Formats used ..
969        100 FORMAT(A)
970        102 FORMAT(8X,'Input numerical data',//,1x,'simulation time (hr)',
971           &F15.5,/,' time increment (hr)',F15.5,/,1x,/,'depth of soil profile under
      study (cm
972           &)',F15.5,/,1x,'number of space nodes',I5,/,1x,'size of depth incre
973           &ment (cm)',F15.5,/,1x,'number of soil layers',I5,/,1x,'epsilon of
974           &moisture content ',F15.5,/,1x,'epsilon of temperature',F15.5,/,//)
975        104  FORMAT(1X,'The output will be printed every',F12.2,'  hours')
976        105  FORMAT(1X,'time (hr) ',2X,'surface temperature(deg C)',2X,
977           &'relative humidity %',2X,'DAL of atmos. vapor(per mil)')
978        106  FORMAT(F6.2,8X,F10.2,18x,F9.2,16x,F12.3)
979        109  FORMAT(1X,//,11x,'  Listing of initial conditions',//,5X,'Z  ',12X,
980           &'THETA ',8x,10x,'T ',17x,'DAL ',/,3x,'(cm)',12x,'( % )',10x,
981           &'(deg C)',10x,'(per mil)',//)
982        110  FORMAT(I4,2F10.5)
983        111  FORMAT(2F10.5)
984        112  FORMAT(F10.4)
985        115  FORMAT(4F16.2)
986        117  FORMAT(2F8.3,3X,E14.5,F10.5)
987        200  FORMAT(2F10.5)
988        234  FORMAT(F6.2,3F12.4,F10.5,3E14.4,F10.5)
989   C end of format
990
```

```
991    99   STOP
992         END
993
994
995
996   C .. Subroutines
997   *****************************************************************
998   *     num.f
999
1000        SUBROUTINE TRIDIA(M,F)
1001  C     Solves a matrix equation with a tridiagonal coefficient matrix
1002  C     using the THOMAS ALGORITHM
1003  C     THE SOLUTION IS CONTAINED IN THE X ARRAY
1004        IMPLICIT REAL*8(A-H,O-Z)
1005        PARAMETER(NN=205)
1006        COMMON/TRI/A,B,C,X
1007        DIMENSION A(NN),B(NN),C(NN),X(NN),F(NN)
1008        DIMENSION ALPHA(NN),BETA(NN),Y(NN)
1009        ALPHA(1)=B(1)
1010        BETA(1)=C(1)/ALPHA(1)
1011        Y(1)=F(1)/ALPHA(1)
1012        DO 201 I=2,M
1013           ALPHA(I)=B(I)-A(I)*BETA(I-1)
1014           BETA(I)=C(I)/ALPHA(I)
1015           Y(I)=(F(I)-A(I)*Y(I-1))/ALPHA(I)
1016   201      CONTINUE
1017  C     BEGIN BACKWARD SUBSTITUTION FROM LAST ROW
1018        X(M)=Y(M)
1019        NU=M-1
1020        DO 203 I=1,NU
1021           J=M-I
1022           X(J)=Y(J)-BETA(J)*X(J+1)
1023   203  CONTINUE
1024        RETURN
1025        END
1026
1027
1028  *****************************************************************
1029  *  hyd.f
1030
1031  C  2) Hydraulic subroutines
1032
1033        SUBROUTINE  PSWKS
1034        IMPLICIT REAL*8(A-H,O-Z)
1035        PARAMETER(R=4.6199D+6,GR=980.665D0)
1036        PARAMETER(NN=205)
1037        COMMON/PROS/POR
1038        COMMON/DTKP/THWK
1039        COMMON/WK/PSWK
1040        COMMON/XSAT/KSAT
1041        COMMON/KWSK/KSTHR
1042        COMMON/RETD/AD1,THR1,VNU
1043        COMMON/GAGA/GAMA,GAMA2,BD2X,AD1X
1044        COMMON/VANGN/AD2,BD2,THR2
1045        COMMON/CWHR/RHWC
1046        real*8 POR(NN),KSTHR,KSAT
1047        BD2X=1/BD2
1048        GAMA=1-1/BD2
1049        GAMA2=-1/GAMA
1050        TX=273.16+25
1051        VNU=2.3026*R*TX/GR
1052        SE=(THWK-THR2)/(POR(1)-THR2)
1053        PSWK=-(SE**GAMA2-1)**BD2X/AD2
1054        RHWC=EXP(PSWK*GR/(R*TX))
1055        AD1X=1/(RHWC-AD1)
1056  C     this following stat. is variation from Van Genuchten
1057  C     thr=thwk
1058        thr=thr2
1059        SE=(THR-THR2)/(POR(1)-THR2)
1060        SEG=(1-(1-SE**(1/GAMA))**GAMA)**2.
1061        KSTHR=KSAT*SE**.5*SEG
```



```
1062        RETURN
1063        END
1064
1065
1066
1067        SUBROUTINE SRHSUB
1068  C     This subroutine calculates the relative humidity of soil
1069  C     using the Kelvin relation.
1070        IMPLICIT REAL*8(A-H,O-Z)
1071        PARAMETER(NN=205)
1072        PARAMETER(R=4.6199D+6,GR=980.665D0)
1073        COMMON/NDKL/NZ
1074        COMMON/SOILRH/SRH
1075        COMMON/ZXY/Z
1076        COMMON/FEZ/ZEF
1077        COMMON/TTT/T
1078        COMMON/isp/psi
1079        COMMON/WK/PSWK
1080        COMMON/KWT/TWK
1081        COMMON/RETD/AD1,THR1,VNU
1082        COMMON/GAGA/GAMA,GAMA2,BD2X,AD1X
1083        DIMENSION SRH(NN),Z(NN),PSI(NN),T(NN)
1084  C   Find ZEF from moisture content data close to the surface
1085        CALL ZEFSUB
1086        RHWK=EXP(PSWK*GR/(R*TWK))
1087        DO 27 I=2,NZ
1088           IF(Z(I).LT.ZEF)THEN
1089             SRH(I)=SRH(1)+Z(I)/ZEF*(RHWK-SRH(1))
1090           ELSE
1091             TK=T(I)+273.16
1092             SRH(I)=EXP(PSI(I)*GR/(R*TK))
1093           ENDIF
1094   27   CONTINUE
1095   28   RETURN
1096        END
1097
1098
1099        SUBROUTINE ZEFSUB
1100  C     This subroutine calculates the depth of the evapo. front
1101        IMPLICIT REAL*8(A-H,O-Z)
1102        PARAMETER(NN=205)
1103        COMMON/NDKL/NZ
1104        COMMON/DTKP/THWK
1105        COMMON/FEZ/ZEF
1106        COMMON/ZLED/DELZ
1107        COMMON/thtt/theta
1108        COMMON/KWT/TWK
1109        COMMON/TTT/T
1110        COMMON/ZXY/Z
1111        DIMENSION THETA(NN),T(nn),Z(NN)
1112        DO 22 I=2,NZ
1113          IF(THETA(I).LT.THWK)THEN
1114             GO TO 22
1115          ELSE
1116             PCC=THWK-THETA(I-1)
1117             SED=PCC/(THETA(I)-THETA(I-1))
1118             GO TO 23
1119          ENDIF
1120   22        CONTINUE
1121   23   ZEF=Z(I-1)+SED*DELZ
1122        TWK=T(I)+273.16
1123        RETURN
1124        END
1125
1126        SUBROUTINE PSRET
1127  C     calculates the unsaturated water potential PSI
1128  C     corresponding to liquid moisture content for all nodes
1129  C     using the interpolating cubic spline program (given above)
1130  C     and the retention table provided in 2nd input data file.
1131        IMPLICIT REAL*8(A-H,O-Z)
1132        PARAMETER(NN=205)
```

```
1133          COMMON/NDKL/NZ
1134          COMMON/thtt/theta
1135          COMMON/isp/psi
1136          COMMON/DTKP/THWK
1137          COMMON/WK/PSWK
1138          COMMON/CWHR/RHWC
1139          COMMON/FFFF/FF
1140          COMMON/RETD/AD1,THR1,VNU
1141          COMMON/GAGA/GAMA,GAMA2,BD2X,AD1X
1142          COMMON/VANGN/AD2,BD2,THR2
1143          COMMON/PROS/POR
1144          DIMENSION THETA(NN),PSI(NN),FF(NN),POR(NN)
1145          DO 15 I=2,NZ
1146             XO=THETA(I)
1147             xn=xo-.002*xo
1148             xp=xo+.002*xo
1149             IF(XO.LT.THWK)THEN
1150                SE=(XO-THR1)/(THWK-THR1)
1151                ADS=AD1+SE*(RHWC-AD1)
1152                PSI(I)=VNU*(LOG10(ADS))
1153             ELSE
1154                SE=(XO-THR2)/(POR(I)-THR2)
1155                PSI(I)=-(SE**GAMA2-1)**BD2X/AD2
1156             ENDIF
1157             IF(XN.LT.THWK)THEN
1158                SEN=(XN-THR1)/(THWK-THR1)
1159                ADSN=AD1+SEN*(RHWC-AD1)
1160                PSN=VNU*(LOG10(ADSN))
1161             ELSE
1162               SEN=(XN-THR2)/(POR(I)-THR2)
1163               PSN=-(SEN**GAMA2-1)**BD2X/AD2
1164             ENDIF
1165             IF(XP.LT.THWK)THEN
1166                SEP=(XP-THR1)/(THWK-THR1)
1167                ADSP=AD1+SEP*(RHWC-AD1)
1168                PSP=VNU*(LOG10(ADSP))
1169             ELSE
1170                SEP=(XP-THR2)/(POR(I)-THR2)
1171                PSP=-(SEP**GAMA2-1)**BD2X/AD2
1172             ENDIF
1173  C       correct psi for temp. will cancel taking DTL in equations and DT=DTV
1174  C          psi(i)=psc*exp(-ck*(T(i)-20))
1175  C          psp=psp*exp(-ck*(T(i)-20))
1176  C          psn=psn*exp(-ck*(T(i)-20))
1177  C       correct psi for temp. will cancel taking DTL in equations and DT=DTV
1178  C          psi(i)=psc*exp(-ck*(T(i)-20))
1179  C          psp=psp*exp(-ck*(T(i)-20))
1180  C          psn=psn*exp(-ck*(T(i)-20))
1181             ff(i)=(xp-xn)/(psp-psn)
1182    15    CONTINUE
1183          RETURN
1184          END
1185
1186
1187          SUBROUTINE THETRETEN(PS,THET,F)
1188  C       calculates the liquid moisture content corresponding to water potential
1189          IMPLICIT REAL*8(A-H,O-Z)
1190          PARAMETER(NN=205)
1191          COMMON/NDKL/NZ
1192          COMMON/DTKP/THWK
1193          COMMON/WK/PSWK
1194          COMMON/PROS/POR
1195          COMMON/RETD/AD1,THR1,VNU
1196          COMMON/VANGN/AD2,BD2,THR2
1197          COMMON/GAGA/GAMA,GAMA2,BD2X,AD1X
1198          DIMENSION THET(NN),PS(NN),POR(NN),F(NN)
1199          ck=6.8D-3
1200          DO 15 I=2,NZ
1201  C       correct psi for temp. will cancel taking DTL in equations and DT=DTV
1202  C             psC=ps(i)*exp(ck*(T(i)-20))
1203                psC=ps(i)
```



```
1204                psn=psC-0.001*abs(psC)
1205                psp=psC+0.001*abs(psC)
1206                if (psC.ge.-1.0)then
1207                   psC=-1.0
1208                endif
1209                IF(PSC.LT.PSWK)THEN
1210                   PCC=PSC
1211                   SE1=AD1X*(10**(PCC/VNU)-AD1)
1212                   THET(I)=SE1*(THWK-THR1)+THR1
1213                ELSE
1214                   SX1B=ABS(AD2*PSC)
1215                   SE1B=(SX1B)**BD2
1216                   SE2B=(1+SE1B)**(-GAMA)
1217                   THET(I)=SE2B*(POR(i)-THR2)+THR2
1218                ENDIF
1219                IF(PSN.LT.PSWK)THEN
1220                   PCN=PSN
1221                   SE1N=AD1X*(10**(PCN/VNU)-AD1)
1222                   THETN=SE1N*(THWK-THR1)+THR1
1223                ELSE
1224                   SX1N=ABS(AD2*PSN)
1225                   SE1N=(SX1N)**BD2
1226                   SE2N=(1+SE1N)**(-GAMA)
1227                   THETN=SE2N*(POR(i)-THR2)+THR2
1228                ENDIF
1229                IF(PSP.LT.PSWK)THEN
1230                   PCP=PSP
1231                   SE1P=AD1X*(10**(PCP/VNU)-AD1)
1232                   THETP=SE1P*(THWK-THR1)+THR1
1233                ELSE
1234                   SX1P=ABS(AD2*PSP)
1235                   SE1P=(SX1P)**BD2
1236                   SE2P=(1+SE1P)**(-GAMA)
1237                   THETP=SE2P*(POR(i)-THR2)+THR2
1238                ENDIF
1239                F(I)=(THETP-THETN)/(PSP-PSN)
1240    15       CONTINUE
1241             do 17 i=2,nz
1242                if(thet(i).le.thr1)then
1243                   thet(i)=thr1
1244                endif
1245    17       continue
1246          RETURN
1247          END
1248
1249
1250          SUBROUTINE LDENS
1251  C       calculate liquid water density using the relation given by Finlayson
1252  C       et al.(1978).
1253          IMPLICIT REAL*8(A-H,O-Z)
1254          PARAMETER(NN=205)
1255          COMMON/DNS/RO
1256          COMMON/NDKL/NZ
1257          COMMON/TTT/T
1258          DIMENSION RO(NN),T(NN)
1259           DO 10 I=2,NZ
1260             X3=T(I)
1261             RO(I)=1.D0+1.45D-5*X3-5.15D-6*X3**2.D0
1262    10    CONTINUE
1263          RETURN
1264          END
1265
1266
1267          SUBROUTINE VISCOS(T)
1268  C       calculates dynamic viscosity coefficient (Ref. Finlayson et al. 1978)
1269          IMPLICIT REAL*8(A-H,O-Z)
1270          PARAMETER(NN=205)
1271          COMMON/NDKL/NZ
1272          COMMON/VISCO/MU
1273          REAL*8 MU(NN),T(NN)
1274          DO 10 I=2,NZ
```

```
1275            X4=T(I)
1276            Y1=SQRT(8078.4+(X4-8.435)**2.)
1277            Y2=2.1551*(X4+Y1)-138.54
1278            MU(I)=1/Y2
1279     10   CONTINUE
1280          RETURN
1281          END
1282
1283          SUBROUTINE SVDENS
1284     C    calculates saturated vapor density using the relation given
1285     C    by Childs and  Halstaff (1982).
1286          IMPLICIT REAL*8 (A-H,O-Z)
1287          PARAMETER(NN=205)
1288          COMMON/SATVD/SVD
1289          COMMON/NDKL/NZ
1290          COMMON/TTT/T
1291          COMMON/EITSUB/EITA
1292          DIMENSION SVD(NN),T(NN),EITA(NN)
1293          DO 10 I=1,NZ
1294             X5=T(I)
1295             Y5=X5+273.16
1296             Z5=X5+237.3
1297             SVD(I)=EXP(17.294*X5/Z5)*1323D-6/Y5
1298             EITA(I)=SVD(I)*(-1./Y5+4104/Z5**2)
1299     10   CONTINUE
1300          RETURN
1301          END
1302
1303
1304          SUBROUTINE DTKPSV
1305     C    calculates the vapor thermal diffusion coefficient DTV and
1306     C    the isothermal water vapor conductivity KPSIV.
1307          IMPLICIT REAL*8 (A-H,O-Z)
1308          PARAMETER(NN=205)
1309          PARAMETER(R=4.6199D+6,GR=980.665D0)
1310          COMMON/DTKP/THWK
1311          COMMON/TORT/TORV
1312          COMMON/DIFWV/DAWV
1313          COMMON/EITSUB/EITA
1314          COMMON/PROS/POR
1315          COMMON/DNS/RO
1316          COMMON/SATVD/SVD
1317          COMMON/SOILRH/SRH
1318          COMMON/NDKL/NZ
1319          COMMON/thtt/theta
1320          COMMON/TTT/T
1321          COMMON/VISPK/KPSIV
1322          COMMON/VTD/DTV
1323          REAL*8 KPSIV(NN)
1324          DIMENSION DTV(NN),DAWV(NN),SRH(NN),SVD(NN),THETA(NN),
1325         &POR(NN),RO(NN),EITA(NN),T(NN)
1326     C    Calculate saturated vapor density SVD and the derivative of
1327     C    saturated vapor density with respect to temperature EITA
1328              CALL SVDENS
1329     C    Calculate atmospheric water vapor diffusivity DAWV
1330              CALL WVD
1331
1332              DO 31 i=2,NZ
1333              IF(THETA(I).LE.THWK)THEN
1334                 FTHAK=1.0
1335              ELSE
1336                 FTHAK=(POR(I)-THETA(I))/(POR(I)-THWK)
1337              ENDIF
1338              PF=POR(I)-THETA(I)+FTHAK*THETA(I)
1339              DTAO=1/POR(I)
1340              DTV(I)=DAWV(I)*PF*SRH(I)*DTAO*EITA(I)/RO(I)
1341              ABC=GR/(R*(T(I)+273.16))
1342              KPSIV(I)=DAWV(I)*TORV*(POR(I)-THETA(I))*ABC*SVD(I)*
1343         &SRH(I)/RO(I)
1344     31       CONTINUE
1345              RETURN
```



```
1346              END
1347
1348
1349          SUBROUTINE  KTOTL
1350     C    calculate the total water conductivity
1351          PARAMETER(NN=205)
1352          COMMON/NDKL/NZ
1353          COMMON/KKK/K
1354          COMMON/VISPK/KPSIV
1355          COMMON/ISPK/KPSI
1356          REAL*8 KPSI(NN),KPSIV(NN),K(NN)
1357          DO 33 i=2,NZ
1358             KPSI(I)=KPSIV(I)+K(I)
1359     33   CONTINUE
1360          RETURN
1361          END
1362
1363
1364          SUBROUTINE FLOW
1365          IMPLICIT REAL*8(A-H,O-Z)
1366          PARAMETER(NN=205)
1367          COMMON/Nfl/rinfl
1368          COMMON/NDKL/NZ
1369          COMMON/SATVD/SVD
1370          COMMON/SOILRH/SRH
1371          COMMON/DIFWV/DAWV
1372          COMMON/PROS/POR
1373          COMMON/KKK/K
1374          COMMON/VISPK/KPSIV
1375          COMMON/ZLED/DELZ
1376          COMMON/ISPK/KPSI
1377          COMMON/isp/psi
1378          COMMON/VTD/DTV
1379          COMMON/FVAP/FRV
1380          COMMON/XFVAP/XFRV
1381          COMMON/TTT/T
1382
1383
1384          COMMON/EVP/EVAV,EVAL,EVAT
1385          REAL*8 K(NN),KPSI(NN),KPSIV(NN)
1386          DIMENSION T(NN),DTV(NN),PSI(NN),EVAV(NN),EVAL(NN),EVAT(NN),
1387         &FRV(NN),POR(NN),SVD(NN),SRH(NN),DAWV(NN),XFRV(NN)
1388     C    Calculate water fluxes EVAL, EVAV,and EVAT at all nodes in the profil
1389     C    (cm/s)
1390
1391     C    EVAPORATION FROM SURFACE
1392          i=1
1393          DV=0.5*(DAWV(i)+DAWV(i+1))*POR(i+1)
1394          EVAPS=DV*(SRH(i+1)*SVD(i+1)-SRH(i)*SVD(i))/DELZ
1395          EVAV(i)=EVAPS
1396          if(rinfl.eq.0)then
1397             EVAL(I)=0.0
1398          else
1399             eval(I)=-1*rinfl
1400          endif
1401          EVAT(i)=EVAV(i)+EVAL(i)
1402          FRV(i)=EVAV(i)/EVAT(i)
1403          I=2
1404          EVAV(I)=DTV(I)*(T(I+1)-T(I))/DELZ+
1405         &KPSIV(I)*(PSI(I+1)-PSI(I))/DELZ
1406          EVAL(I)=K(I)*((PSI(I+1)-PSI(I))/DELZ-1.D0)
1407          EVAT(I)=EVAV(I)+EVAL(I)
1408          FRV(I)=EVAV(I)/EVAT(I)
1409          XV=ABS(EVAV(I))
1410          XL=ABS(EVAL(I))
1411          XT=XV+XL
1412          XFRV(I)=XV/XT
1413          DO 37 I=3,NZ-1
1414             EVAV(I)=DTV(I)*(T(I+1)-T(I))/(DELZ)+
1415         &KPSIV(I)*(PSI(I+1)-PSI(I))/(DELZ)
1416             EVAL(I)=K(I)*((PSI(I+1)-PSI(I))/(DELZ)-1.D0)
```

```
1417            EVAT(I)=EVAV(I)+EVAL(I)
1418            XV=ABS(EVAV(I))
1419            XL=ABS(EVAL(I))
1420            XT=XV+XL
1421            XFRV(I)=XV/XT
1422            FRV(I)=EVAV(I)/EVAT(I)
1423   37     CONTINUE
1424          I=NZ
1425          EVAV(1)=DTV(I)*(T(I)-T(I-1))/(DELZ)+
1426         &KPSIV(I)*(PSI(I)-PSI(I-1))/(DELZ)
1427          EVAL(I)=K(I)*((PSI(I)-PSI(I-1))/(DELZ)-1.D0)
1428          XV=ABS(EVAV(I))
1429          XL=ABS(EVAL(I))
1430          XT=XV+XL
1431          XFRV(I)=XV/XT
1432          EVAT(I)=EVAV(I)+EVAL(I)
1433          FRV(I)=EVAV(I)/EVAT(I)
1434          RETURN
1435          END
1436
1437
1438
1439
1440          SUBROUTINE KUNSAT
1441          IMPLICIT REAL*8(A-H,O-Z)
1442          PARAMETER(NN=205)
1443          COMMON/DNS/RO
1444          COMMON/VISCO/MU
1445          COMMON/TTT/T
1446          COMMON/DTKP/THWK
1447          COMMON/KWSK/KSTHR
1448          COMMON/PROS/POR
1449          COMMON/NDKL/NZ
1450          COMMON/thtt/theta
1451          COMMON/KKK/K
1452          COMMON/XSAT/KSAT
1453          COMMON/RETD/AD1,THR1,VNU
1454          COMMON/GAGA/GAMA,GAMA2,BD2X,AD1X
1455          COMMON/VANGN/AD2,BD2,THR2
1456          REAL*8 K(NN),MU(NN),POR(NN),ksat,KSTHR
1457          DIMENSION THETA(NN),T(NN),RO(NN)
1458   C      Calculate liquid dynamic viscosity MU
1459          CALL VISCOS(T,MU)
1460          A1=1
1461   C      The following statment is a modification of
1462   C      Van Genuchten Hyd. condc  model
1463          A1=0.0
1464   CCCCCC
1465          THR=A1*THR2+(1-A1)*THWK
1466
1467          DO 22 I=2,NZ
1468             THET=THETA(I)
1469             IF(THET.lt.THR)then
1470               K(i)=0
1471             ELSE
1472               SE=(THET-THR)/(POR(I)-THR)
1473               SEG=(1-(1-SE**(1/GAMA))**GAMA)**2.
1474               K(I)=KSAT*SE**.5*SEG
1475             ENDIF
1476   C ..  Temperature Adjustment of K-unsaturated based on Tref=20 C
1477               K(I)=K(I)*1.0D-2*RO(I)/MU(I)
1478    22    CONTINUE
1479          RETURN
1480          END
1481
1482
1483          SUBROUTINE WVD
1484   C      Calculates the diffusion coefficient of water vapor
1485          IMPLICIT REAL*8(A-H,O-Z)
1486          PARAMETER(NN=205)
1487          COMMON/NDKL/NZ
```



```
1488          COMMON/TTT/T
1489          COMMON/DIFWV/DAWV
1490          DIMENSION DAWV(NN),T(NN)
1491   C      Refere to the following formula in Kimball et al.,1976.
1492          DO 28 I=1,NZ
1493             DAWV(I)=.229*(1.0D0+T(I)/273.16D0)**1.75
1494    28    CONTINUE
1495          RETURN
1496          END
1497
1498
1499          SUBROUTINE DLSUB
1500   C      Calculates the coupling coefficient for heat transfer Dl
1501          IMPLICIT REAL*8(A-H,O-Z)
1502          PARAMETER(NN=205)
1503          COMMON/NDKL/NZ
1504          COMMON/LATHT/HVAP
1505          COMMON/DNS/RO
1506          COMMON/TTT/T
1507          COMMON/VISPK/KPSIV
1508          COMMON/PROS/POR
1509          COMMON/LD/DL
1510          REAL*8 KPSIV(NN)
1511          DIMENSION DL(NN),HVAP(NN),POR(NN),RO(NN),T(NN)
1512   C      Calculate latent heat of evaporation coefficient HVAP
1513             CALL LHVAP
1514          DO 32 I=2,NZ
1515             DL(I)=RO(I)*HVAP(I)*KPSIV(I)
1516    32    CONTINUE
1517          RETURN
1518          END
1519
1520
1521          SUBROUTINE HCAPT
1522   C      calculates the volumetric heat capacity of the soil at all nodes
1523   C      as function of moisture content and organic matter.
1524          IMPLICIT REAL*8(A-H,O-Z)
1525          PARAMETER(NN=205)
1526          COMMON/NDKL/NZ
1527          COMMON/thtt/theta
1528          COMMON/ORG/VO
1529          COMMON/PROS/POR
1530          COMMON/CCC/CC
1531          DIMENSION POR(NN),VO(NN),THETA(NN),CC(NN)
1532          DO 10 I=2,NZ
1533             CC(I)=.46D0*(1.D0-POR(I))+.14D0*VO(I)+THETA(I)
1534    10    CONTINUE
1535          RETURN
1536          END
1537
1538
1539          SUBROUTINE THCOND
1540   C      calculates the thermal conductivity as a function of liquid moisture
1541   C      content for all nodes using the cubic spline program and table of
1542   C      thermal conductivity provided in 2nd input data file.
1543          IMPLICIT REAL*8 (A-H,O-Z)
1544          PARAMETER(NN=205)
1545          COMMON/THC/ALA,BLA
1546          COMMON/NDKL/NZ
1547          COMMON/THC/LAMDA
1548          COMMON/thtt/theta
1549          REAL*8 LAMDA(NN),THETA(NN)
1550          DO 10 I=2,NZ
1551             X6=THETA(I)
1552             LAMDA(I)=ALA+BLA*X6
1553    10    CONTINUE
1554          RETURN
1555          END
1556
1557
1558          SUBROUTINE LHVAP
```

```
1559  C     calculates the latent heat of vaporization of water.
1560  C     Reference : Duane Hampton, 1989.
1561        IMPLICIT REAL*8(A-H,O-Z)
1562        PARAMETER(NN=205)
1563        COMMON/NDKL/NZ
1564        COMMON/TTT/T
1565        COMMON/LATHT/HVAP
1566        DIMENSION HVAP(NN),T(NN)
1567        DO 10 I=2,NZ
1568           X7=T(I)
1569           HVAP(I)=597.5-0.58*X7
1570   10   CONTINUE
1571        RETURN
1572        END
1573
1574
1575  C  ISOTOPIC BLOCK SUBROUTINES
1576  ******************************************************
1577  *    < LIST OF VARIABLES >
1578  *
1579  * ALFA         isotopic fractionation factor
1580  * DI           total diffusivity of isotopic species
1581  * DIRV         diffusivity of isotopic species in vapor
1582  * DIS          diffusivity of isotopic species in liquid water
1583  * KODEI        numerical input code =1(Deuterium),2(Oxygen-18)
1584  * TORL         cofficient of tortuosity for liquid flow
1585  ******************************************************
1586        SUBROUTINE ISOTOPE
1587        IMPLICIT REAL*8(A-H,O-Z)
1588        PARAMETER(NN=205)
1589        PARAMETER(TORL=0.667)
1590        PARAMETER(SIGMAD=1.02511,SIGMAO=1.02849)
1591        COMMON/DIPA/adifO,bdifO,adifD,bdifD
1592        COMMON/NDKL/NZ
1593        COMMON/DNS/RO
1594        COMMON/SATVD/SVD
1595        COMMON/DIFWV/DAWV
1596        COMMON/SOILRH/SRH
1597        COMMON/PROS/POR
1598        COMMON/ALKDI/KODEI
1599        COMMON/TORT/TORV
1600        COMMON/XIXI/XIF
1601        COMMON/FVAP/FRV
1602        COMMON/XFVAP/XFRV
1603        COMMON/thtt/theta
1604        COMMON/TTT/T
1605        COMMON/ID/DI
1606        DIMENSION T(NN),THETA(NN),DIS(NN),DI(NN),
1607       &SVD(NN),SRH(NN),RO(NN),ALFA(NN),DVS(NN),DIRV(NN),
1608       &DAWV(NN),POR(NN),XIF(NN),FRV(NN),XFRV(NN)
1609
1610  C     Calculate the diffusivity of isotope in liquid water DIS
1611  C     The relation between T and DIF was established for this code
1612  C     based on data form Langsworth,L.G, 1954 and Wang et al., 1953.
1613        if(kodei.eq.1)then
1614           adif=adifD
1615           bdif=bdifD
1616        else
1617           adif=adifO
1618           bdif=bdifO
1619        endif
1620
1621        DO 5 I=2,NZ
1622           X=T(I)
1623           DIF=adif+bdif*X
1624           DIS(I)=TORL*THETA(I)*DIF*(1-XFRV(I))
1625    5   CONTINUE
1626        DO 10 I=1,NZ
1627          CALL ALFSUB(ALFA(I),T(I))
1628   10   CONTINUE
1629
```



```
1630  C     Calculate the diffusivity of isotopic species in vapor DIRV
1631        DO 15 I=2,NZ
1632          DVS(I)=DAWV(I)*TORV*(POR(I)-THETA(I))
1633          IF(KODEI.EQ.1)THEN
1634             SIGMA=SIGMAD
1635          ELSE
1636             SIGMA=SIGMAO
1637          ENDIF
1638          DIRV(I)=SRH(I)*SVD(I)/RO(I)*ALFA(I)/SIGMA*DVS(I)
1639    15  CONTINUE
1640
1641  C    Calculate the total isotope diffusivity DI
1642        DO 20 I=2,NZ
1643           DI(I)=DIS(I)+DIRV(I)
1644    20  CONTINUE
1645
1646  C   Calculate the xi function
1647        DO 21 I=1,NZ
1648        XIF(I)=1-FRV(I)*(1.-ALFA(I)/SIGMA)
1649    21  CONTINUE
1650        RETURN
1651        END
1652
1653        SUBROUTINE ALFSUB(ALF,XT)
1654        IMPLICIT REAL*8(A-H,O-Z)
1655        COMMON/ALKDI/KODEI
1656  C     Calculate the fractionation factor alfa
1657          TK=XT+273.16
1658          IF(KODEI.EQ.1)THEN
1659             R=2.4844D7/(TK**2.D0)-7.6248D4/TK+5.2612D1
1660          ELSE
1661             R=1.137D6/(TK**2.D0)-.4156D3/TK-2.0667D0
1662          ENDIF
1663          RS=-R/1.D3
1664          ALF=EXP(RS)
1665          RETURN
1666          END
1667
1668
1669
1670
1671
1672
1673
1674
1675
1676
1677
1678
1679
1680
1681
```

```
1     2
2     -.0822 -.0151
3     .70 .7
4     252. 1.0  100. .5  1 .05 2e-6  1000 1.2e-4
5     1 1 1
6     10
7          129.000 24.725  35.2500 0.000
8          130.000 24.825  34.5000 0.000
9          131.000 24.825  34.5000 0.000
10         132.000 24.825  34.5000 0.000
11         133.000 24.825  34.5000 0.000
12         134.000 33.488  26.0000 0.000
13         135.000 25.938  25.7500 0.000
14         136.000 27.050  25.1250 0.000
15         137.000 25.588  25.5000 0.000
16         138.000 25.410  25.5000 0.000
17    24.0
18       0.500       2.0500       1.2000      -3.5000  28.370  23.970  19.290  33.640
       36.550
19       1.000       2.6002       8.0455      -1.5768  28.490  24.430  20.170  32.790
       36.550
20       1.500       3.0614      14.8978       0.3816  28.435  24.775  20.850  31.835
       36.280
21       2.000       3.5227      21.7500       2.3399  28.880  25.620  22.030  31.380
       36.510
22       2.500       4.0713      26.1575       3.6444  28.805  26.080  22.550  30.620
       35.980
23       3.000       4.6200      30.5650       4.9490  28.730  26.540  23.070  29.860
       35.450
24       3.500       4.6969      30.8796       5.1585  28.380  26.730  23.190  29.035
       34.570
25       4.000       4.7738      31.1941       5.3680  28.030  26.920  23.310  28.210
       33.690
26       4.500       4.8507      28.9485       4.8920  27.750  27.025  23.395  27.610
       32.975
27       5.000       4.9276      26.7030       4.4160  27.470  27.130  23.480  27.010
       32.260
28       5.500       5.0046      23.8659       3.7801  27.300  27.195  23.595  26.645
       31.765
29       6.000       5.0815      21.0287       3.1443  27.130  27.260  23.710  26.280
       31.270
30       6.500       5.1584      18.1297       2.4875  27.045  27.295  23.840  26.100
       30.950
31       7.000       5.2353      15.2307       1.8308  26.960  27.330  23.970  25.920
       30.630
32       7.500       5.3572      12.4400       1.1955  26.935  27.345  24.105  25.875
       30.425
33       8.000       5.4791       9.6493       0.5602  26.910  27.360  24.240  25.830
       30.220
34       8.500       5.7195       7.1372      -0.0114  26.915  27.370  24.365  25.860
       30.080
35       9.000       5.9600       4.6250      -0.5830  26.920  27.380  24.490  25.890
       29.940
36       9.500       6.0141       4.5895      -0.5815  26.930  27.390  24.590  25.950
       29.805
37      10.000       6.0681       4.5540      -0.5800  26.940  27.400  24.690  26.010
       29.670
38      10.500       5.9948       4.5185      -0.5785  26.935  26.115  25.395  27.670
       29.483
39      11.000       5.9216       4.4830      -0.5770  26.930  24.830  26.100  29.330
       29.295
40      11.500       5.8258       4.4475      -0.5755  26.900  26.170  25.500  27.735
       29.108
41      12.000       5.7300       4.4120      -0.5740  26.870  27.510  24.900  26.140
       28.920
42      12.500       5.6943       4.3765      -0.5725  26.825  27.545  24.915  26.140
       28.690
43      13.000       5.6585       4.3410      -0.5710  26.780  27.580  24.930  26.140
       28.460
44      13.500       5.6770       4.3055      -0.5690  26.725  27.625  24.925  26.125
       28.210
```



```
45      14.000       5.6955       4.2700      -0.5670  26.670  27.670  24.920  26.110
       27.960
46      14.500       5.7404       4.2345      -0.5655  26.600  27.710  24.905  26.085
       27.700
47      15.000       5.7853       4.1990      -0.5640  26.530  27.750  24.890  26.060
       27.440
48      15.500       5.8286       4.1635      -0.5625  26.460  27.790  24.865  26.020
       27.180
49      16.000       5.8720       4.1280      -0.5610  26.390  27.830  24.840  25.980
       26.920
50      16.500       5.8860       4.0925      -0.5595  26.320  27.860  24.810  25.935
       26.670
51      17.000       5.9000       4.0570      -0.5580  26.250  27.890  24.780  25.890
       26.420
52      17.500       5.8661       4.0215      -0.5565  26.175  27.915  24.755  25.840
       26.190
53      18.000       5.8322       3.9860      -0.5550  26.100  27.940  24.730  25.790
       25.960
54      18.500       5.7694       3.9505      -0.5535  26.035  27.950  24.710  25.735
       25.755
55      19.000       5.7065       3.9150      -0.5520  25.970  27.960  24.690  25.680
       25.550
56      19.500       5.6431       3.8795      -0.5505  25.910  27.955  24.690  25.630
       25.380
57      20.000       5.5797       3.8440      -0.5490  25.850  27.950  24.690  25.580
       25.210
58      20.500       5.5442       3.8085      -0.5475  25.805  27.920  24.705  25.530
       25.085
59      21.000       5.5087       3.7730      -0.5460  25.760  27.890  24.720  25.480
       24.960
60      21.500       5.5293       3.7375      -0.5445  25.730  27.845  24.760  25.440
       24.890
61      22.000       5.5500       3.7020      -0.5430  25.700  27.800  24.800  25.400
       24.820
62      22.500       5.6433       3.6665      -0.5410  25.690  27.725  24.870  25.370
       24.815
63      23.000       5.7365       3.6310      -0.5390  25.680  27.650  24.940  25.340
       24.810
64      23.500       5.8708       3.5955      -0.5375  25.685  27.555  25.030  25.320
       24.855
65      24.000       6.0051       3.5600      -0.5360  25.690  27.460  25.120  25.300
       24.900
66      24.500       6.1368       3.5245      -0.5345  25.705  27.350  25.225  25.285
       24.975
67      25.000       6.2686       3.4890      -0.5330  25.720  27.240  25.330  25.270
       25.050
68      25.500       6.3543       3.4535      -0.5315  25.740  27.120  25.435  25.260
       25.150
69      26.000       6.4400       3.4180      -0.5300  25.760  27.000  25.540  25.250
       25.250
70      26.500       6.4492       4.0851      -0.5335  25.780  26.885  25.640  25.245
       25.350
71      27.000       6.4583       4.7522      -0.5370  25.800  26.770  25.740  25.240
       25.450
72      27.500       6.4130       5.3321      -0.5400  25.780  26.660  25.820  25.235
       25.535
73      28.000       6.3677       5.9120      -0.5430  25.761  26.550  25.900  25.230
       25.620
74      28.500       6.3029       6.4098      -0.5490  25.726  26.445  25.960  25.220
       25.675
75      29.000       6.2381       6.9076      -0.5550  25.690  26.340  26.020  25.210
       25.730
76      29.500       6.1890       7.3284      -0.5555  25.654  26.250  26.055  25.200
       25.765
77      30.000       6.1400       7.7492      -0.5560  25.618  26.160  26.090  25.190
       25.800
78      30.500       6.1326       8.0982      -0.5595  25.582  26.080  26.100  25.185
       25.815
79      31.000       6.1251       8.4471      -0.5630  25.547  26.000  26.110  25.180
       25.830
80      31.500       6.1485       8.7293      -0.5665  25.529  25.930  26.105  25.170
```

	25.820							
81	32.000	6.1718	9.0115	-0.5700	25.511	25.860	26.100	25.160
	25.810							
82	32.500	6.2060	9.2321	-0.5730	25.476	25.795	26.080	25.145
	25.790							
83	33.000	6.2402	9.4526	-0.5760	25.440	25.730	26.060	25.130
	25.770							
84	33.500	6.2657	9.6166	-0.5795	25.404	25.675	26.025	25.120
	25.730							
85	34.000	6.2912	9.7806	-0.5830	25.368	25.620	25.990	25.110
	25.690							
86	34.500	6.3002	9.8932	-0.5860	25.332	25.570	25.940	25.095
	25.635							
87	35.000	6.3092	10.0058	-0.5890	25.297	25.520	25.890	25.080
	25.580							
88	35.500	6.3053	10.0722	-0.5925	25.261	25.475	25.830	25.065
	25.515							
89	36.000	6.3014	10.1385	-0.5960	25.226	25.430	25.770	25.050
	25.450							
90	36.500	6.2889	10.1637	-0.5995	25.190	25.390	25.705	25.035
	25.380							
91	37.000	6.2764	10.1888	-0.6030	25.154	25.350	25.640	25.020
	25.310							
92	37.500	6.2594	10.1778	-0.6060	25.118	25.315	25.565	25.005
	25.230							
93	38.000	6.2425	10.1669	-0.6090	25.083	25.280	25.490	24.990
	25.150							
94	38.500	6.2257	10.1250	-0.6125	25.047	25.245	25.410	24.975
	25.065							
95	39.000	6.2089	10.0832	-0.6160	25.011	25.210	25.330	24.960
	24.980							
96	39.500	6.1974	10.0156	-0.6190	24.976	25.180	25.250	24.940
	24.895							
97	40.000	6.1858	9.9479	-0.6220	24.940	25.150	25.170	24.920
	24.810							
98	40.500	6.1845	9.8595	-0.6255	24.904	25.125	25.090	24.905
	24.725							
99	41.000	6.1833	9.7711	-0.6290	24.869	25.100	25.010	24.890
	24.640							
100	41.500	6.1973	9.6671	-0.6320	24.834	25.070	24.930	24.870
	24.555							
101	42.000	6.2113	9.5631	-0.6350	24.800	25.040	24.850	24.850
	24.470							
102	42.500	6.2454	9.4487	-0.6385	24.750	25.015	24.775	24.830
	24.390							
103	43.000	6.2794	9.3342	-0.6420	24.700	24.990	24.700	24.810
	24.310							
104	43.500	6.3307	9.2143	-0.6455	24.650	24.960	24.630	24.790
	24.240							
105	44.000	6.3820	9.0945	-0.6490	24.600	24.930	24.560	24.770
	24.170							
106	44.500	6.4402	8.9745	-0.6520	24.555	24.900	24.490	24.745
	24.100							
107	45.000	6.4984	8.8544	-0.6550	24.510	24.870	24.420	24.720
	24.030							
108	45.500	6.5529	8.7392	-0.6585	24.465	24.845	24.355	24.700
	23.965							
109	46.000	6.6073	8.6240	-0.6620	24.420	24.820	24.290	24.680
	23.900							
110	46.500	6.6474	8.5188	-0.6655	24.375	24.790	24.230	24.655
	23.835							
111	47.000	6.6874	8.4135	-0.6690	24.330	24.760	24.170	24.630
	23.770							
112	47.500	6.7028	8.3233	-0.6675	24.290	24.730	24.115	24.605
	23.715							
113	48.000	6.7182	8.2330	-0.6660	24.250	24.700	24.060	24.580
	23.660							
114	48.500	6.7078	8.1595	-0.6595	24.210	24.675	24.005	24.555
	23.605							
115	49.000	6.6974	8.0860	-0.6530	24.170	24.650	23.950	24.530
	23.550							

116	49.500	6.6690	8.0279	-0.6470	24.135	24.620	23.900	24.505
	23.505							
117	50.000	6.6406	7.9698	-0.6410	24.100	24.590	23.850	24.480
	23.460							
118	50.500	6.6025	7.9256	-0.6350	24.060	24.560	23.805	24.455
	23.415							
119	51.000	6.5645	7.8814	-0.6290	24.020	24.530	23.760	24.430
	23.370							
120	51.500	6.5250	7.8495	-0.6225	23.985	24.505	23.715	24.405
	23.325							
121	52.000	6.4854	7.8176	-0.6160	23.950	24.480	23.670	24.380
	23.280							
122	52.500	6.4526	7.7965	-0.6100	23.915	24.450	23.630	24.350
	23.245							
123	53.000	6.4197	7.7755	-0.6040	23.880	24.420	23.590	24.320
	23.210							
124	53.500	6.3970	7.7638	-0.5975	23.850	24.390	23.555	24.295
	23.170							
125	54.000	6.3743	7.7521	-0.5910	23.820	24.360	23.520	24.270
	23.130							
126	54.500	6.3610	7.7483	-0.5850	23.790	24.330	23.485	24.240
	23.100							
127	55.000	6.3477	7.7444	-0.5790	23.760	24.300	23.450	24.210
	23.070							
128	55.500	6.3427	7.7468	-0.5730	23.730	24.275	23.415	24.180
	23.040							
129	56.000	6.3377	7.7492	-0.5670	23.700	24.250	23.380	24.150
	23.010							
130	56.500	6.3399	7.7564	-0.5605	23.670	24.220	23.350	24.120
	22.985							
131	57.000	6.3420	7.7636	-0.5540	23.640	24.190	23.320	24.090
	22.960							
132	57.500	6.3503	7.7741	-0.5480	23.615	24.160	23.290	24.060
	22.935							
133	58.000	6.3587	7.7846	-0.5420	23.590	24.130	23.260	24.030
	22.910							
134	58.500	6.3721	7.7968	-0.5355	23.560	24.100	23.235	24.005
	22.890							
135	59.000	6.3855	7.8090	-0.5290	23.530	24.070	23.210	23.980
	22.870							
136	59.500	6.4029	7.8215	-0.5230	23.505	24.045	23.190	23.945
	22.850							
137	60.000	6.4203	7.8340	-0.5170	23.480	24.020	23.170	23.910
	22.830							
138	60.500	6.4406	7.8452	-0.5110	23.455	23.990	23.145	23.880
	22.815							
139	61.000	6.4609	7.8564	-0.5050	23.430	23.960	23.120	23.850
	22.800							
140	61.500	6.4831	7.8649	-0.4985	23.410	23.930	23.100	23.820
	22.785							
141	62.000	6.5053	7.8733	-0.4920	23.390	23.900	23.080	23.790
	22.770							
142	62.500	6.5282	7.8774	-0.4860	23.365	23.875	23.065	23.760
	22.760							
143	63.000	6.5512	7.8815	-0.4800	23.340	23.850	23.050	23.730
	22.750							
144	63.500	6.5739	7.8798	-0.4735	23.320	23.820	23.030	23.700
	22.735							
145	64.000	6.5966	7.8781	-0.4670	23.300	23.790	23.010	23.670
	22.720							
146	64.500	6.6179	7.8691	-0.4610	23.280	23.760	22.995	23.635
	22.710							
147	65.000	6.6392	7.8601	-0.4550	23.260	23.730	22.980	23.600
	22.700							
148	65.500	6.6582	7.8422	-0.4490	23.240	23.705	22.970	23.570
	22.695							
149	66.000	6.6771	7.8244	-0.4430	23.220	23.680	22.960	23.540
	22.690							
150	66.500	6.6925	7.7961	-0.4365	23.200	23.650	22.945	23.510
	22.685							
151	67.000	6.7079	7.7679	-0.4300	23.180	23.620	22.930	23.480

	22.680							
152	67.500	6.7188	7.7279	-0.4310	23.160	23.595	22.920	23.445
	22.670							
153	68.000	6.7296	7.6878	-0.4320	23.140	23.570	22.910	23.410
	22.660							
154	68.500	6.7358	7.6356	-0.4395	23.120	23.540	22.900	23.380
	22.660							
155	69.000	6.7421	7.5833	-0.4470	23.100	23.510	22.890	23.350
	22.660							
156	69.500	6.7443	7.5194	-0.4545	23.080	23.485	22.880	23.315
	22.655							
157	70.000	6.7465	7.4554	-0.4620	23.060	23.460	22.870	23.280
	22.650							
158	70.500	6.7455	7.3805	-0.4690	23.045	23.430	22.860	23.250
	22.645							
159	71.000	6.7446	7.3057	-0.4760	23.030	23.400	22.850	23.220
	22.640							
160	71.500	6.7412	7.2205	-0.4840	23.010	23.375	22.840	23.190
	22.640							
161	72.000	6.7377	7.1354	-0.4920	22.990	23.350	22.830	23.160
	22.640							
162	72.500	6.7326	7.0406	-0.4995	22.975	23.325	22.820	23.125
	22.635							
163	73.000	6.7275	6.9459	-0.5070	22.960	23.300	22.810	23.090
	22.630							
164	73.500	6.7214	6.8422	-0.5145	22.940	23.270	22.805	23.060
	22.630							
165	74.000	6.7154	6.7385	-0.5220	22.920	23.240	22.800	23.030
	22.630							
166	74.500	6.7091	6.6265	-0.5295	22.905	23.215	22.790	22.995
	22.630							
167	75.000	6.7029	6.5146	-0.5370	22.890	23.190	22.780	22.960
	22.630							
168	75.500	6.6972	6.3950	-0.5445	22.875	23.165	22.775	22.930
	22.625							
169	76.000	6.6915	6.2754	-0.5520	22.860	23.140	22.770	22.900
	22.620							
170	76.500	6.6872	6.1489	-0.5595	22.840	23.115	22.760	22.870
	22.620							
171	77.000	6.6829	6.0224	-0.5670	22.820	23.090	22.750	22.840
	22.620							
172	77.500	6.6806	5.8897	-0.5745	22.805	23.065	22.740	22.810
	22.615							
173	78.000	6.6783	5.7570	-0.5820	22.790	23.040	22.730	22.780
	22.610							
174	78.500	6.6784	5.6186	-0.5895	22.775	23.015	22.725	22.745
	22.610							
175	79.000	6.6786	5.4803	-0.5970	22.760	22.990	22.720	22.710
	22.610							
176	79.500	6.6810	5.3370	-0.6045	22.740	22.965	22.710	22.680
	22.605							
177	80.000	6.6833	5.1938	-0.6120	22.720	22.940	22.700	22.650
	22.600							
178	80.500	6.6879	5.0463	-0.6195	22.705	22.915	22.690	22.620
	22.595							
179	81.000	6.6925	4.8988	-0.6270	22.690	22.890	22.680	22.590
	22.590							
180	81.500	6.6990	4.7477	-0.6345	22.670	22.865	22.670	22.560
	22.585							
181	82.000	6.7056	4.5966	-0.6420	22.650	22.840	22.660	22.530
	22.580							
182	82.500	6.7141	4.4427	-0.6500	22.635	22.815	22.650	22.500
	22.575							
183	83.000	6.7226	4.2887	-0.6580	22.620	22.790	22.640	22.470
	22.570							
184	83.500	6.7329	4.1325	-0.6655	22.600	22.770	22.625	22.440
	22.560							
185	84.000	6.7432	3.9763	-0.6730	22.580	22.750	22.610	22.410
	22.550							
186	84.500	6.7552	3.8186	-0.6805	22.560	22.725	22.600	22.380
	22.540							

187	85.000	6.7672	3.6608	-0.6880	22.540	22.700	22.590	22.350
	22.530							
188	85.500	6.7807	3.5021	-0.6955	22.525	22.675	22.575	22.320
	22.520							
189	86.000	6.7942	3.3434	-0.7030	22.510	22.650	22.560	22.290
	22.510							
190	86.500	6.8091	3.1845	-0.7105	22.490	22.630	22.545	22.265
	22.500							
191	87.000	6.8241	3.0257	-0.7180	22.470	22.610	22.530	22.240
	22.490							
192	87.500	6.8403	2.8673	-0.7255	22.450	22.590	22.515	22.210
	22.480							
193	88.000	6.8565	2.7088	-0.7330	22.430	22.570	22.500	22.180
	22.470							
194	88.500	6.8735	2.5515	-0.7405	22.410	22.545	22.485	22.155
	22.460							
195	89.000	6.8906	2.3942	-0.7480	22.390	22.520	22.470	22.130
	22.450							
196	89.500	6.9076	2.2387	-0.7555	22.370	22.500	22.455	22.100
	22.435							
197	90.000	6.9245	2.0832	-0.7630	22.350	22.480	22.440	22.070
	22.420							
198	90.500	6.9405	1.9302	-0.7705	22.330	22.460	22.425	22.045
	22.405							
199	91.000	6.9565	1.7771	-0.7780	22.310	22.440	22.410	22.020
	22.390							
200	91.500	6.9708	1.6271	-0.7855	22.290	22.415	22.390	21.990
	22.375							
201	92.000	6.9850	1.4772	-0.7930	22.270	22.390	22.370	21.960
	22.360							
202	92.500	6.9966	1.3311	-0.8005	22.250	22.370	22.355	21.935
	22.345							
203	93.000	7.0081	1.1850	-0.8080	22.230	22.350	22.340	21.910
	22.330							
204	93.500	7.0161	1.0433	-0.8155	22.210	22.330	22.320	21.885
	22.310							
205	94.000	7.0242	0.9017	-0.8230	22.190	22.310	22.300	21.860
	22.290							
206	94.500	7.0279	0.7652	-0.8305	22.170	22.290	22.280	21.835
	22.275							
207	95.000	7.0316	0.6287	-0.8380	22.150	22.270	22.260	21.810
	22.260							
208	95.500	7.0299	0.4980	-0.8455	22.130	22.250	22.240	21.785
	22.240							
209	96.000	7.0283	0.3673	-0.8530	22.110	22.230	22.220	21.760
	22.220							
210	96.500	7.0206	0.2431	-0.8605	22.090	22.210	22.200	21.735
	22.205							
211	97.000	7.0129	0.1189	-0.8680	22.070	22.190	22.180	21.710
	22.190							
212	97.500	6.9983	0.0019	-0.8720	22.045	22.170	22.160	21.685
	22.170							
213	98.000	6.9837	-0.1152	-0.8760	22.020	22.150	22.140	21.660
	22.150							
214	98.500	6.9644	-0.2249	-0.8760	22.000	22.135	22.120	21.635
	22.130							
215	99.000	6.9452	-0.3346	-0.8760	21.980	22.120	22.100	21.610
	22.110							
216	99.500	6.9265	-0.4370	-0.8760	21.960	22.100	22.080	21.585
	22.090							
217	100.000	6.9079	-0.5395	-0.8760	21.940	22.080	22.060	21.560
	22.070							

Mar 28 1994 22:23:03 **work/datwhB** Page 1

```
1      .667
2      .2 .013
3      .024 .021  .005 .09  2.75
4      1.05D-5  5.33D-7  1.5D-5  7.D-7
5      .351  0.
6      5E-4  2.75e-2
7
8
9
10
11
```

This dissertation is accepted on behalf of the faculty of the Institute by the following committee:

Fred M Phillips
Adviser

H Hendrickx

Andrew Campbell

John L Wilson

25 April '94
Date

I release this document to New Mexico Institute of Mining and Technology.

Shunbaji 25 April 1994

Students Signature Date